# TOWARDS CHEMICAL PROFILING AT THE CELLULAR LEVEL

A Thesis Submitted for the Degree of
Doctor of Philosophy by

C. Logan Mackay

School of Chemistry
College of Science and Engineering
University of Edinburgh

July 2003

"Can one infer the construction of a grand piano from the sound heard when it crashes from a tenth storey window?"

S. Meyerson, Mass Spectrometry and Real Life, *Chemtech*, **1979**, 5, 60

## Abstract

Traditional methods for the analysis of cellular components have focused on 'grid and find' assays that provide quantitative information from a large population of cells, often as many as a million cells. The results of these studies are often presented only as the percentage of the dry weight of the cells and not the concentration within individual cells. The research presented in this thesis is concerned with the development and application of methods for single cell sampling and analysis (SiCSA) from fungal cells that overcomes this deficit. The methods developed offer the potential to investigate the intra-cellular concentration of biologically relevant molecules within selected cells of a heterogeneous population. The instruments and techniques for this work are described along with an overview of the fundamental principles behind this methodology.

The model organism studied in this work was the filamentous fungi, *Neurospora crassa*, the orange bread mould. It is the best characterised of all the filamentous fungi, a group of organisms that are critically important to agriculture, medicine and the environment. Capillary electrophoresis electrospray mass spectrometry (CE-ESI-MS) was used to measure the intra-cellular concentration of disaccharides, in particular trehalose. In *Neurospora crassa* this molecule is synthesised in response to environmental stress, and has been reported to accumulate at concentrations as high as 10 mM, based on measurements using bulk cell populations. The value of 1.3 mM for the intra-cellular concentration of disaccharide measured in the single cell sampling experiments described in this thesis is in good agreement with this previously published maximum concentration.

Following topical application of a commercially relevant fungicide, azoxystrobin, to cell cultures of *Neurospora crassa*, the intra-cellular concentration of the fungicide was measured. For cells treated with azoxystrobin at a concentration of 14.8 μM (the saturation concentration of azoxystrobin in water), the intra-cellular concentration was shown to reach 9.9 μM within 5 minutes. It is likely that the high surface to volume ratio of the fungal hyphae facilitats the rapid diffusion of these large hydrophobic molecules across the cell membrane.

The development of novel instrumentation applicable to the analysis of ultra-low volume samples is presented, encompassing microsampling, transfer, ionisation and detection. Their utility in comparison with competing techniques is discussed, along with suggestions as to the expected development of this technique and possible directions for future work.

## Acknowledgments

I would like to thank all those people who made the completion of this thesis possible. Special thanks must go to my supervisor Pat Langridge Smith and Sandy Yates; without their initial persuasion, I would not have started this work, and since then, they have been, both a constant source of support, and of advice.

Thanks must also go to Syngenta International, who funded the research, provided a number of extra pieces of critical equipment and supported my attendance at international conferences. I would especially like to thank Dr Frank Moffatt who maintained his interest and support throughout the research, and to the laboratory staff at Jealotts Hill Research Station, who allowed me instrument time and made my visits to the company enjoyable, in particular Mike Jessop.

Thanks must also go to Richard Goodwin, and the rest of the inmates of the EMSG, both past and present, each of whom contributed in their own special ways to the running of the asylum and made my time in the group special. I guess it will be I that switches off the lights and locks the door after all.

And finally I must thank my family for their supported, especially my wife, Caroline and my Granddad, without whom I would never have got this far.

## Table of Contents

# 1 Introduction

Traditional methods for the analysis of cellular components have focused on 'grid and find' assays that provide quantitative information from a large population of cells, often as many as a million cells. The results of these studies are often presented only as the percentage of the dry weight of the cells and not the concentration within individual cells. The research presented in this thesis is concerned with the development and application of single cell sampling and analysis (SiCSA) of fungal cells that overcomes this deficit. It was the upshot of a collaboration between a fungal microscopy group and a physical chemistry group, and was funded by Syngenta International.

The research focused on the development of novel single cell sampling and analysis methods, using microsampling and mass spectroscopic analysis techniques, as a means of determining and quantifying the concentration of endogenous biologically relevant molecules and the uptake of externally applied growth inhibitors. The techniques developed are based on the use of a device commonly referred to as the plant pressure probe, and on-line capillary electrophoresis (CE) electrospray ionisation (ESI) mass spectrometry (MS). The plant pressure probe was originally developed as a tool for measuring the turgor pressure in plant cells. Samples were aspirated using this device then transferred to the CE capillary and subsequently to the mass spectrometer for analysis.

In the remainder of this chapter the history of single cell sampling and analysis techniques will be outlined. In Chapter 2, a brief review of electrophoresis and CE is presented; emphasis is placed on the methods used to quantify separation performance. In Chapter 3 an outline of the development of liquid interfaces used in mass spectrometry is presented, focusing in particular on electrospray ionisation sources for capillary electrophoresis. This is then followed by a description of the mass spectrometer used in this work. A full description of the equipment and techniques used in this work for the acquisition and analysis of picolitre and nanolitre biological samples from single fungal cells is given in Chapter 4. Microscopy, micromanipulation and microsampling are discussed in the context of single cell

analysis, together with an explanation of the development of small volume sample transfer and column loading. The techniques developed to prevent sample contamination and loss are also discussed.

In Chapter 5, the fungal model under investigation, *Neurospora crassa*, is introduced along with a description of carbohydrate uptake. An extensive characterisation of the technique developed for single cell analysis is presented along with the complex series of internal and external controls that were required to minimise contamination of the sample. The results of experiments to measure the intra-cellular concentration of disaccharides within fungal cells of *Neurospora crassa* are also be presented

The development and action of fungicides are discussed in Chapter 6. The results of experiments to measure the concentration of a particular fungicide, azoxystrobin, within fungal cells *Neurospora crassa* are also reported. In Chapter 7, results of preliminary investigations into the use of novel devices for the analysis of ultra low volume samples are presented. Of particular interest was the use of a novel droplet on demand (DOD) liquid interface. Finally, an overall conclusion, along with a discussion of future work is presented in Chapter 8.

## 1.1 Single cell sampling and analysis

Until the second half of the twentieth century, traditional 'grind and find' assays were the only method of cell analysis available to the biological, chemical and medical sciences [1]. It then became apparent that such fields would benefit from a better understanding of how specific cells functioned in a heterogeneous population [2]. For example, analysis of a sample taken from a large population of cells will result in a value that is an average; this is then extrapolated to give the amount contained in one cell. Unfortunately, the assumption that this average measurement is indicative of the analyte concentration from each individual entity in the population is not always valid, especially in situations where only a few cells exhibit marked chemical differences. It has been shown that even closely opposed, morphologically similar cells may differ widely in the concentrations of certain key molecules [3]. By investigating the activities of individual cells, in relation to space, time and environment, it is possible to gain an understanding of the whole organism that could not be achieved with biochemical approaches that use tissue homogenates

Due to the high chemical complexity and limited quantities of analyte, the analysis of single cells presents an analytical challenge. The difficulty of cell isolation and the sacrifice of the subject animals add further to the significance of the sample. Together, these attributes often make the sample scarce, rare, and precious and the analysis limited to a single measurement.

Certain techniques have been devised to address the problem of localising a particular compound or compounds to certain cells; these include *in-situ* hybridisation [4], ion selective fluorescent probes [5], ion selective micro-electrodes [6], X-ray analysis ([7], immunocytochemistry [8], and nuclear magnetic resonance imaging [9]. Often these techniques lack the quantitative precision and wide chemical species range necessary for true single cell analysis.

Single cell studies can clearly benefit clinical diagnosis and treatment. In regular blood tests, hundreds of thousands of cells are homogenised to provide sufficient amounts of analytes for quantification. In the early stages of disease or carcinogenisis, only a few cells may carry the specific chemical or biological

markers indicative of infection. Unfortunately, such markers are likely to be completely masked by the average contents of the overabundant healthy cells. If cells are examined individually, the chances of recognising abnormal cells are substantially better [10].

It was clear that techniques that would enable the manipulation, analyte selectivity and detection sensitivity to make measurements directly from individual cells would be highly beneficial. The past thirty years has seen numerous scientific advances in the development of miniaturised analytical instrumentation to enable the analysis of smaller samples at higher spatial resolution. These discoveries have led to the analysis of metals, inorganic compounds and a number of organic molecules at the single cell level. However, the analysis of these trace molecules still remains a formidable analytical challenge. The difficulties presented by the analysis of any molecule by conventional biochemical methods are amplified by the complexity of the cell and the limited sample volume available. A substance at a concentration of 1 μM in a large cell with a volume of 1 nL will yield only 1 fmol for analysis if the content of the entire cell could be collected. The sample removed from the cell will also contain many compounds, some in high concentration, which may interfere with the measurement of the analyte. Any method chosen for the analysis of single cells must therefore be suitable for dealing with the complexity of the cellular contents and have the sensitivity required for small samples. In the ideal world, this technique would also make it possible to determine a wide variety of compounds in one analysis, even if their concentrations vary over a wide range, give qualitative and quantitative information, and be non-destructive to the cell. Despite the difficulties discussed above, interest in the chemistry of a single cell has been such that a number of analytical methods have been developed.

The earliest reference to single cell analysis was made in 1953, when RNA was isolated from single neurones [11]. Until that time, the best analytical techniques required 100 to 1000 μg of RNA; a typical neuronal cell contains a maximum of 200-1000 pg RNA [12]. As was to become a common trend in the field of single cell sampling and analysis, a new technique had to be devised. In this case, copper silk

thread electrophoresis was able to provide sensitivity a million times greater than conventional detection techniques. The silk was soaked in buffer, and then stretched across a glass microscope slide. The RNA sample was digested with ribonucleases then placed directly onto the slide using microscopy combined with micromanipulation. A voltage was then applied along the length on the fibre and the RNA bases separated by ionophoresis. The fibre could then be investigated photometrically and the absolute amount of each base computed. This research introduced a number of the key issues that would have to be resolved in the development of any technology applicable to single cell sampling and analysis (SICSA) [13]. Before any analysis can take place, the cells of interest must be either dissected out or cultured from a larger population. The environment the cells are exposed to must duplicate the natural environment, as any stress placed on them, either osmotically, chemically or by altering the temperature was likely to affect the balance of the molecules under investigation. The physical act of microsampling required a good quality inverted microscope, micromanipulation equipment, a device that allows the content of the cell to be collected, and a skilled operator. The analytical technique employed to investigate the sample often had to be designed from scratch or highly modified from existing technology.

In 1965, micro-electrophoresis was again used to separate genetically different haemoglobin mixtures from single red blood cells [14]. Micro-spectrophotometric techniques had been shown to be able to separate and quantify haemoglobin F from haemoglobin A [15], but not other haemoglobins, including $A_2$, S, C and J, present in differing amounts in normal and diseased cells. Since the heterogeneity of the cell preparations prevented the analysis on a large scale, analysis of single cells was necessary. Cellulose fibres, proved to be unsuitable due to difficulties in placing the cells on the thin fibre and an inability to separate haemoglobin A from $A_2$. A new elaborate micro-electrophoresis device was developed that instead of a silk fibre used polyacrylamide as the supporting medium. The erythrocytes were embedded in a polyacrylamide fibre and electrophoresis was conducted in a special chamber. Attempts at staining were unsuccessful, but analysis was possible by direct detection due to the nature of haemoglobin.

## 1.2 Capillary electrophoresis

The turning point for SiCSA came with the investigation of large neurones (>100 μm length) from the land snail, *Helix aspersa* [16,17,18]. The unique characteristics of capillary electrophoresis (CE) have made possible the analysis of biological systems and compartments that previously posed intractable problems. CE, described fully in Chapter 2, was the breakthrough that realised the feasibility of detecting molecules present in lower concentrations and in smaller volume cells. It has proven an attractive technique for SICSA due to its favourable characteristics. The sample volume requirements are very small and has direct compatibility with biofluids. CE is a particularly appropriate method for the analysis of the complex mixture of chemicals that make up cytoplasm. The presence of DNA and membranes results in a very viscous liquid that would quickly lead to the blockage of packed chromatography columns. The complex chemical make up of the cell extract would also result in poisoning of the column, as molecules present bind irreversibly to the stationary phase. This adherence of molecules to the capillary walls does occur in CE, but can easily be rectified by the flushing with weak sodium hydroxide [19]. The technique was used to separate and identify amino acids, di-peptides and amines. CE was shown to provide highly efficient separations with upwards of one million theoretical plates [20].

The improvements in the instrumentation are most pronounced in the development of automation, sample handling capabilities and detection strategies. The sampling strategies employed are dependent on the desired type of sample. Both cytoplasmic sampling and whole cell sampling have been used [16,17,18,21,22]. Cytoplasmic sampling involves the direct removal of an aliquot from an immobilised cell and the subsequent analysis of that sample. Whole cell sampling, as the name suggests, involves the analysis of the entire cell and may result in the inclusion of some of the extra-cellular matrix the cell is growing in.

Injection of the cell, or cell aliquot, into the capillary is typically performed under a microscope using micromanipulation (Chapter 4) and has been achieved with both electrokinetic and hydrostatic techniques. Cell cytoplasm aliquots can be injected directly onto the separation column, but whole cells require an intermediate step to lyse the cells prior to separation. Hydrostatic based cell extract injection systems use a vacuum attached to the outlet end of the capillary. The microsampling device is used to remove a sample of cytoplasm from the cell. The device is then moved close to or into the inlet of the capillary. As the sample is ejected from the needle, a slight vacuum is applied to the outlet, using a gas tight syringe attached to a sealed buffer reservoir, and the suction pulls the sample into the capillary. For whole cells, the technique is similar. The capillary inlet must be placed close to the cells of interest and again a slight vacuum is applied to the outlet of the capillary and the cell is drawn in. This technique has been refined slightly by the use of optical tweezers to hold the cell prior to injection into the capillary [23,24,25]. It is especially useful for small cells, where there is difficulty in selectively injecting single cells due to their random movements [26].

Once in the capillary, whole cells must be lysed prior to separation. For cells with weak membranes, lysis can be achieved simply by the application of the separation voltage. This causes the cell to burst due to the applied potential, or the change in the ionic strength between the isotonic sample plug and the running buffer. To aid this technique, injections of a non-isotonic buffer solution can also be made to induce lysing. For particularly rugged cells, lysis can be achieved by aiming a laser at the capillary wall or by the use of a Tesla coil [27,28].

Attempts have been made to improve the injection of cells and cell extracts into the electrophoresis capillary. Etching of internal and external tapers onto the capillaries with hydrofluoric acid (HF) has been successfully used to facilitate the insertion into the cell for sampling cell extract and whole cell sampling, respectively [29,30]. More desirable, tapered capillaries have made by hand pulling the capillaries in a flame [31]. These tips taper to a smooth point, unlike the jagged tips created with HF, and allow whole cells of a diameter larger than that of the capillary opening to

be drawn up. This also reduces the risk of rupture, especially when sampling from prokaryotic cells that commonly exhibit high turgor pressure.

### 1.2.1 Detection strategies

Due to the small sample volumes and concentrations of any particular analyte in the cell sample to be analysed, SICSA development has been led by improvements in the detection strategies employed. In commercially available CE instruments detection is achieved by UV absorbance. This offer satisfactory sensitivity when dealing with large samples and high concentrations and has been used successfully for certain SICSA applications [32,33,34]. When the samples are ultra low volume and low concentration, the short path length dictated by the narrow fused silica capillary renders the UV absorbance detector useless. Other strategies have been successfully implemented. Electrochemical detection, operating in the amperometric [35] voltametric modes [16], and laser induced fluorescence (LIF) [36] [37,38,39] (discussed in Chapter 4), are the most widely used detection techniques for single cell applications. As will be discussed later, and forming the basis of this research, electrospray ionisation mass spectrometry (ESI-MS) has also been implemented successfully [40].

## 1.3 Matrix assisted laser desorption ionisation mass spectrometry

An interesting development in SiCSA is the use of matrix assisted laser desorption ionisation (MALDI). MALDI has several features that make it attractive for the analysis of samples derived from single cells. It is compatible with crude mixtures, requires minimal sample clean up, employs simple instrumentation and offers high sensitivity [10,41]. On the downside, quantification is very hard to achieve.

MALDI is a mass spectrometric ionisation technique whereby a sample is co-crystallised onto a stage with a chemical that strongly absorbs the appropriate wavelength of light, typically 337 nm (Figure 1.1). The stage is placed into the source region of the mass spectrometer. A pulsed laser beam is then aimed at the sample causing part of the illuminated substrate to vaporise. A rapidly expanding plume carries some of the analyte into the vacuum with it and aids in the ionisation process.

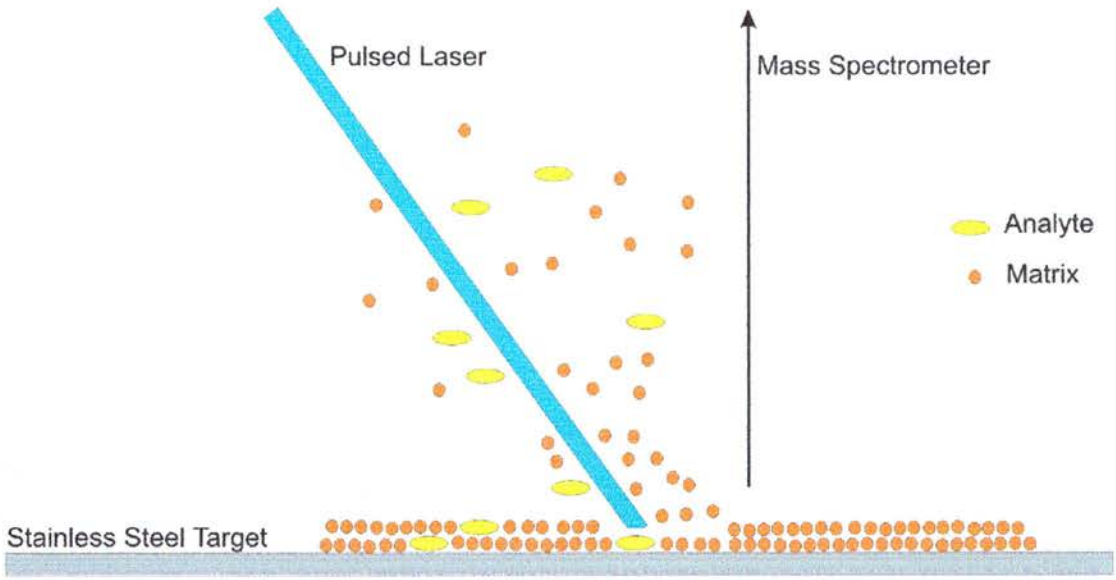


Figure 1-1 Illustration of matrix assisted laser desorption ionisation process

Once the sample molecules are vaporised and ionised they are transferred electrostatically into the analysis region of the mass spectrometer where they are separated and detected.

Although MALDI is well known for its wide dynamic range of analysis, the chemical complexity and the range of concentrations encountered in cellular samples often result in problems with analyte suppression. This problem can often be circumvented by careful sample preparation, the most important step in MALDI. Numerous studies have reported on varying preparation protocols [42,43,44,45,46,47,48,49]. Most single cell MALDI studies have used 2,5-dihydroxybenzoic acid (DHBA) as a matrix as it appears to have a role in stabilising membranes, deactivating endogenous proteolytic enzymes and reducing the effects of high salt concentrations improving spectral quality. MALDI has been successfully used to investigate neuropeptides in *Aplysia californica* [50,51,52,53], peptides in *Xenopus laevis* [54,55], as well as peptides and proteins in rat cells [49,56].

An interesting technique was to grow the cells directly onto the MALDI target [57]. When compared with the results from cells added to the target just prior to analysis, it was found that spectra resulting from the cells grown on the target exhibit greater ion abundance. This strategy provided the possibility of studying intact cells while keeping them in contact with other cells and substrates. It also eliminated complicated sample handling, making the technique applicable to routine analysis by biotechnologists and cell biologists.

The elaborate combination of CE, nanovial microsampling and MALDI was used to analyse cells isolated from *Aplysia californica* [58]. Cells were isolated, lysed and transferred to a nanovial. The sample was then injected into the CE column by gravity. The eluent from the column was collected directly onto the MALDI target. The complex mixture of the crude sample was thereby separated so reducing signal suppression; the CE eluent is salt free and MALDI friendly. The technique was also combined with $^{35}S$ radionuclide detection to aid quantification.

A method of simplifying the microsampling step has been to use a PixCell II (Axion, USA) laser capture microdissection device (Figure 1.2) combined with MALDI mass spectrometric analysis [50]. It is possible to quickly and accurately isolate pure cell populations from healthy and diseased tissues.

Figure 1-2 PixCell II laser capture microdissection system

Human and mouse histological sections were mounted on glass slides. The PixCell II system was used to isolate samples of approximately 200 to 2000 cells, which were then transferred to a MALDI target plate for analysis by time-of-flight mass spectrometry (TOF-MS). No proteins were identified in the samples, but the work did highlight that laser capture microdissection is a fast and reliable method to acquire protein profiles from specific cell populations.

The examples of MALDI mass spectrometric analysis of single cells offered above demonstrate that although MALDI does offer a convenient and rapid method of qualitative analysis, the difficulties involved in providing quantifiable results reduce the potential applications of the technique.

## 1.4 Cell types investigated

### 1.4.1 Mollusc neurones

The neurons from molluscs were chosen as a target for early single cell analysis primarily because they were large heterogeneous cells, which were distinguishable by chemical analysis. The cells are large, often greater than 100 μm in diameter, and can reproducibly be found in the same location from organism to organism. The presence of neurotransmitters such as dopamine and epinephrine which could be easily oxidised, allowed amperometric detection, while the presence of amino acids provided components which are either natively fluorescent or could be tagged for fluorescent detection.

Whole cells from the land snail *Helix aspersa* were analysed with single cell techniques [59]. In this experiment, the cells of interest were micro-dissected away from the organism and transferred to micro vials. The neuron was homogenised and the primary amines derivatised with naphthalene-2,3-dicarboxaldehyde. The supernatant was then transferred by pneumatic injection into a capillary for separation. Two detection systems were used; the first was a carbon-fibre microelectrode operating in a voltametric mode. The detector is a fine carbon fibre 1 mm in length and 5 to 10 μm in diameter. It is placed in the outlet end of the capillary and acts as both the working and sensing electrode. The microelectrode

was held at a constant voltage and the varying current caused by the oxidation and reduction of eluting molecules measured. The second detection system employed was laser induced fluorescence (LIF) using a helium-cadmium laser as the excitation source. The work revealed that relatively few compounds could be oxidised or reduced, limiting the applicability of amperometric detection. LIF detection was used to successfully identify a number of labeled amino acids. However, no attempts were made at quantification.

An interesting adaptation of single cell analysis was to aspirate cytoplasm directly from the cells. This was performed by Wallingford *et al.* using neurons of the land snail *Helix aspersa* [60]. A microinjection tip was attached to the inlet of the electrophoresis capillary which was inserted into the neuron, and electrokinetic injection used to draw the sample from the cell. Electrochemical detection was used to generate an electropherogram of several unidentified peaks. The technique removed the requirement for a separate microsampling device and also reduced the number of sample handling operations, thereby limiting the risk of sample loss or contamination.

Whole cell injection of the dopamine neuron of *Planorbis corneus* was used to investigate the efficacy of various on-column lysing techniques [61]. Three cell lysing processes were compared: lysing on column with non–physiological buffer for 60 s, lysing on column with non-physiological buffer for 300 s, and cell pre-treatment with reserpine, a vesicle depleting agent, prior to on-column lysing for 60 s. Electrochemical detection operating in amperometric mode was again employed. The resulting electropherogram revealed that only 24% of the dopamine present in the cell is located in the cytoplasm and the rest in vesicles.

### 1.4.2 Erythrocytes

The early research on mollusc cells clearly illustrated that it was within the scope of the technology available to begin to investigate the content of smaller mammalian cells. Initially this attention was directed to the non-nucleated erythrocytes. These have been investigated for a variety of analytes by laser induced fluorescence (LIF). Erythrocytes are biconcave, in shape, 7-8 μm across, 1-2 μm thick, and have an

estimated volume of 87 fL. The cell's shape is maintained by a cytoskeleton composed of spectrin and actin, but normal cells must be very flexible as they become deformed when flowing through capillaries and narrow slits in the splenic circulation.

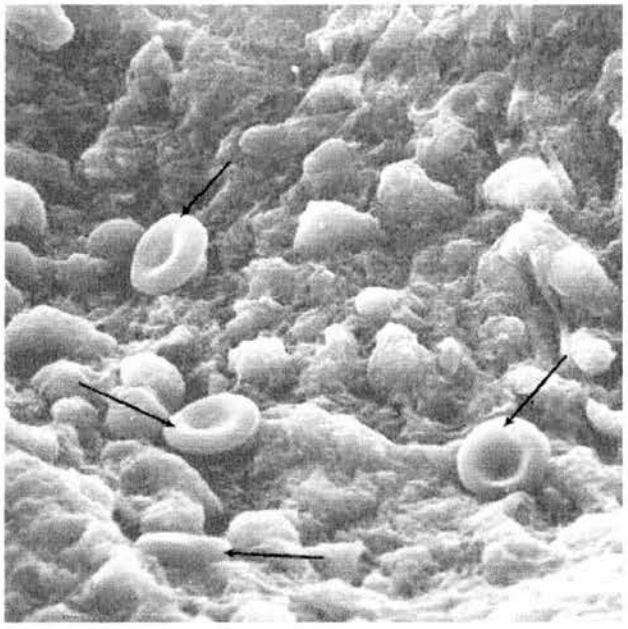

Figure 1-3 Scanning electron microscope image of erythrocytes. Reproduced from reference [62].

The first reported investigation of erythrocytes (Figure 1.3), in 1992, used a whole cell sampling technique whereby the chosen cell was drawn into the capillary using a vacuum pulse [63]. Once in contact with the capillary, the cell adhered to the capillary wall and was lysed upon contact with the running buffer. An argon laser operating at 275 nm was used as an excitation source and indirect fluorescence was used to detect the concentration of $Na^+$ and $K^+$ within the cells.

In 1996, haemoglobin from human erythrocytes was investigated using capillary electrophoresis interfaced with a 7 Tesla Fourier transform ion cyclotron mass

spectrometer (FT ICR-MS) [40]. The combination of CE with electrospray ionisation (discussed fully in Chapter 4) and FTICR mass spectrometry may provide the ideal combination for single cell sampling and analysis due to the inherent sensitivity of the technique and the enhanced information content available from high-resolution and high-precision mass measurement. The results revealed that it was possible to detect hemoglobin in as few as five cells drawn into the capillary.

### 1.4.3 Plant cells

The investigation of plant cells by SICSA techniques introduced the further complication of tough cell walls and turgor pressure [1]. The microsampling needles required for these cells must have an extremely sharp and narrow outer diameter to the tip, or the cell will rupture spilling the content. The ascorbic acid concentration within parenchymatous cells from citrus fruit was investigated using gravity induced hydrodynamic injection and UV absorbance detection [64]. Samples from wheat epidermal cells have also been analysed for the levels of inorganic cations and anions [34]. The research presented an intricate method whereby samples were collected from cells using the turgor pressure, and then ejected in a Petri dish of silicone oil. The samples could then be stored for analysis at a later date. It also proved possible to add internal standards, derivatising agents and, more importantly, the samples could be divided such that a number of analyses could be performed on each sample.

### 1.4.4 Sub-cellular analysis

At the present time, the state of the art in microsampling and analysis techniques is the analysis of sub-cellular components [65]. The first report of this was the investigation of vesicles obtained from the atrial gland of *Aplysia californica* [31]. The vesicles studied were 30-200 nm in diameter with volumes of zeptolitres to low femtolitres. Optical trapping was used to immobilise the vesicles and aid sampling. The sampled vesicles were derivatised with on-column labeling with naphthalene-2,3-dicarboxaldehyde and detected using LIF. The analysis of sub-cellular components has been repeated a number of times by other groups, with animal and plant cells [66].

The sampling and analysis of these very small volumes of complex biological material represent one of the most challenging goals facing cellular biologists. The development of the sampling techniques, modification of CE techniques and the enhancement in detection strategies have facilitated the progress of single cell analysis from the early studies, using relatively large invertebrate neuronal cells, to the investigation of sub-cellular organelles. Single cell sampling and analysis can be expected to contribute significantly to our general and quantitative understanding of the interactions between individual cells. This will be of particular interest in fields such as cancer research where it may be a single cell within a general population that expresses an unusual phenotype.

## 2 Theoretical aspects of capillary electrophoresis

The separation of individual components from complex mixtures is vitally important in the chemical and biochemical sciences. If it were possible to identify or quantitatively determine any element or compound by simple measurement, no matter what its concentration or the complexity of the matrix, separation techniques would have no value. Without the ability to obtain a pure sample of an analyte it becomes difficult to provide structural and functional information on the substance in question, and the techniques commonly used in separation science have been developed alongside the technology they serve. From medieval times until the early twentieth century, the only techniques available to the separation scientist were filtration, distillation, precipitation and crystallisation. Now with the increasing complexity of the systems under investigation, particularly in the field of biochemistry, there has been a demand for the rapid development of new analytical and preparative separation technologies. In comparison with the separation of purely chemical systems, biological mixtures pose further problems. Due to the idiosyncratic characteristics, inherent to bio-molecules, the separation technologies must be amenable to the strict pH and temperature requirements. This is necessary to offset the often unstable nature, both structural and functional, the extremely complex nature of crude samples (where the desired component is usually a minor percentage of the total), and the ability to distinguish the desired component among other structurally similar components. The development of separation technologies, is still aimed at exploiting the differences in physio-chemical properties between the various components of the molecules of interest. The most useful in this respect are volatility, solubility, charge, molecular size, shape and polarity. The techniques that exploit these properties can be categorised as involving either chromatography (in the gaseous or liquid phase) or electromigration. Important factors to consider with separation methods are the variation in properties of the analytes to be separated, the number of components that can be resolved and the efficiency of the separation provided [67].

## 2.1 Electrophoresis

In 1909, Michaelis discovered that it was possible to separate proteins based on their isoelectric points and coined the phrase 'electrophoresis' [68]. Although early experiments demonstrated the potential of electrophoresis to separate biological molecules based on size and charge, the experiments were limited by the incomplete separation of the proteins, the relatively large sample volumes required and the necessity of relatively low electric fields due to the convection currents generated by Joule heating, even in the presence of dense sucrose solutions [69].

In the following years, research was directed towards the development of anti-convective media for electrophoresis [70]. Paper [71], starch and agarose [72] were all shown to be appropriate for the analysis of peptides, proteins and oligonucleotides. Later, in the 1960s, polyacrylamide gels were developed, allowing high resolution separation of both native and denatured proteins [73]. Due to the speed of the technique, resolving power and cost, polyacrylamide gel electrophoresis (PAGE) quickly became popular and can now be found in virtually every biochemistry laboratory.

### 2.1.1 Electrophoresis theory

Electrophoresis (Figure 2.1) is defined as the migration of charged electrical species when dissolved, or suspended, in an electrolyte through which a current is passed. Cations will experience a force causing them to accelerate towards the negatively charged electrode (cathode) and anions towards the positively charged electrode (anode). Neutral solutes experience no force. This can be shown theoretically,

$$F = qE \qquad \text{Equation 2.1}$$

where $F$ is the magnitude of the force, $q$ is the charge on the ion and $E$ is the applied electric field.

As these ions are present in a viscous medium, they will continue to accelerate until this force is balanced by an equal in magnitude but opposing force due to the

frictional force, $F_{fr}$, exerted by the surrounding fluid. For a spherical ion this can be calculated from the following equation,

$$F_{fr} = -6\pi\eta r v_e \qquad \text{Equation 2.2}$$

where $r_h$ is the Stokes' radius of the particle, $\eta$ is the viscosity of the buffer and $v_e$ is the electrophoretic migration velocity. The electrophoretic migration velocity of a charged particle depends on its electrophoretic mobility, $\mu_e$, and on the applied electric field, $E$:

$$v_e = \mu_e E \qquad \text{Equation 2.3}$$

where

$$\mu_e = q/6\pi\eta r_h \qquad \text{Equation 2.4}$$

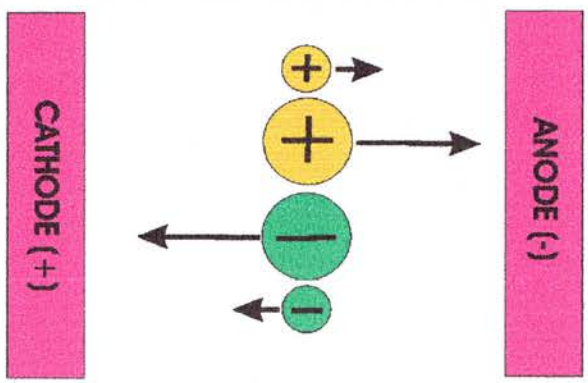


Figure 2-1 Diagram illustrating electrophoresis. Cations will experience a force causing them to accelerate towards the negatively charged electrode (cathode) and anions towards the positively charged electrode (anode). Larger ions will experience more drag and hence move more slowly than smaller ions.

## 2.2 Capillary electrophoresis

The development of capillary electrophoresis was pioneered by Hjertén, who built his first functional CE instrument based on large bore (3 mm) borosilicate tubes in 1959, and over the next eight years investigated a wide range of molecules, from small inorganic molecules to large proteins [73]. By the 1970s the 3 mm bore had been reduced to 0.2 mm eliminating the convection problems associated with the wide bore and simplifying the instrument's design. During the late 1970's and early 1980s, as detector design was improved and high-quality fused silica tubing became available, there was a rapid growth of interest in CE, culminating in the first commercial instruments in 1989 [74,75].

### 2.2.1 Electroosmotic flow

The observation that with CE, all species (positive, negative and neutral) eventually pass the detector indicates that a force other than electrophoretic mobility is involved. If the applied field was the only force acting on the ions, net positively charged molecules would pass the detector, neutral components would remain static and negatively charged species would be driven out of the capillary at the cathode (Figure 2.1). This additional force is electroosmosis or electroendoosmosis flow and originates at the capillary wall, giving rise to electroosmotic flow (EOF), crucial to many forms of CE. A good review can be found in a number of references [76,77]. The silica surface becomes charged when in contact with aqueous solution, with the magnitude of this charge being pH dependent. The walls of a fused silica capillary contain acidic silanol groups that ionise as $SiO^-$ at pH values higher than the isoelectric point (pI) of silica. The value of the pI of silica is still under debate, with the value being placed between 1 and 4 [78]. The pH of the buffer solution will determine the fraction of the silanol groups that are ionised. At low pH, close to the pI, the silanols are relatively uncharged, and at high pH most are charged. The net negative charge on the silanols results in electrostatic forces that attract cations from the buffer and form a number of layers close to the capillary wall. The layers formed by these molecules and their associated water molecules have a net positive charge that decreases exponentially on moving from the wall into the bulk solution. A simple model for this phenomenon was proposed by both Gouy [79] and Chapman

[80] (Figure 2.2). It assumes that the ions can be regarded as point charges and that they are distributed in solution close to the surface according to Boltzmann distribution.

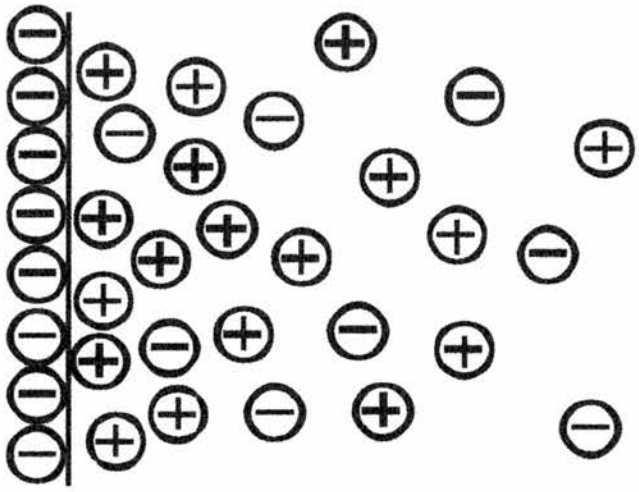

Figure 2-2 Schematic representation of the Gouy-Chapman model of the diffuse double layer for an anionic surface.

Using the Poisson-Boltzmann distribution and the Debye-Hückel approximation, it is possible to derive the variation in potential, $\psi$ with distance from the surface,

$$\psi = \psi_0 \exp(-\kappa x) \qquad \text{Equation 2.5}$$

where $\psi_0$ is the potential at the surface, $x$ is the distance from the surface and $\kappa$ is defined in the equation:

$$\kappa = \left( \frac{2F^2 I}{\varepsilon_0 \varepsilon_r RT} \right)^{1/2} \qquad \text{Equation 2.6}$$

where $F$ is the Faraday constant, $I$ is the ionic strength of the solution (mol $m^{-3}$), $\varepsilon_0$ is the permittivity of a vacuum, $\varepsilon_r$ is the relative dielectric constant of the solution, $R$ is the gas constant and $T$ is the temperature.

The double layer thickness ($\delta$) can be calculated as the inverse of $\kappa$ and is defined as the distance over which $\psi_0$ decays by a factor of $e$. As there has to be overall electrical neutrality, the potential at the surface, $\psi_0$, can be related to the charge density at the surface, $\sigma_0$,

$$\sigma = \varepsilon_0 \varepsilon_r \kappa \psi_0 \qquad \text{Equation 2.7}$$

This model was further improved by Stern, by considering not just the ions free to move, but also the ions held tightly to the surface by absorption (Figure 2.3) [81]. These behave differently and must therefore be treated in a different manner. This was achieved by utilising the potential, $\zeta$, at the sheer plane between mobile and immobile ions instead of $\psi_0$. The plane that separates this electrical double layer is located roughly one hydrated ion radius from the surface. The potential falls linearly between the surface and the Stern plane and then exponentially into the bulk solution. It is possible to calculate $\zeta$ experimentally, but not the potential at the Stern layer, $\psi_d$ [78]. The slip plane is the interface between the hydrated capillary surface and the bulk solution and the electrical potential that exists at this point is termed the zeta potential, $\xi$. The zeta potential can be calculated from the equation,

$$\xi = 4\pi\sigma d / D \qquad \text{Equation 2.8}$$

where $d$ is the thickness of the electric double layer, $\sigma$ is the electrical charge on the Stern layer and D is the dielectric constant.

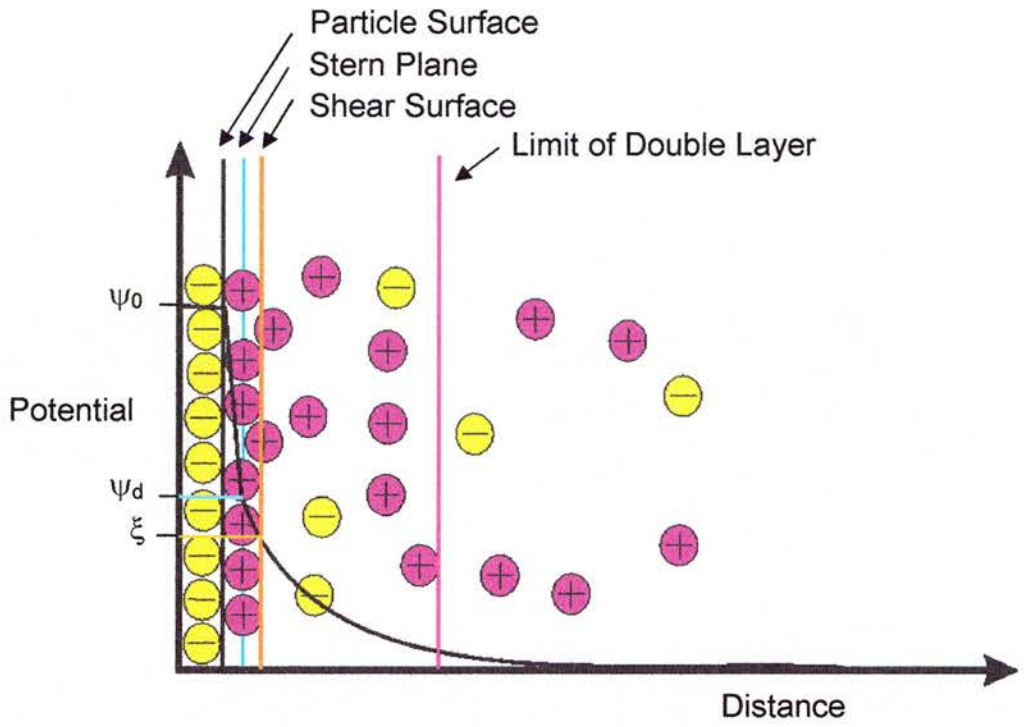


Figure 2-3 Electric double layer according to Stern's theory

The application of a high potential along the capillary causes these loosely bound cations to migrate towards the cathode, and carries the associated water molecules osmotically in the same direction. This results in EOF, as the entire buffer solution is dragged towards the cathode due to the hydrogen bonding of the water of hydration molecules and the bulk water molecules. The velocity of EOF ($\mu_{eo}$) at an infinite distance from the surface can be described by the Smoluchowski equation:

$$\mu_{eo} = \frac{\varepsilon_0 \varepsilon_r \zeta E}{\eta} \qquad \text{Equation 2.9}$$

It has been shown by Rice and Whitehead [82] that this expression is valid only when the value of $\kappa a$ is large. In the case of cylindrical capillaries, $a$ refers to the internal radius. At low values of $\kappa a$, there is significant deviation from plug flow, while at high values the flow profile is flat except right at the surface, with

Smoluchowski velocity developed across the majority of the capillary diameter (Figure 2.4). Plug flow has been determined to be acceptable at values of $\kappa a$>5 [83].

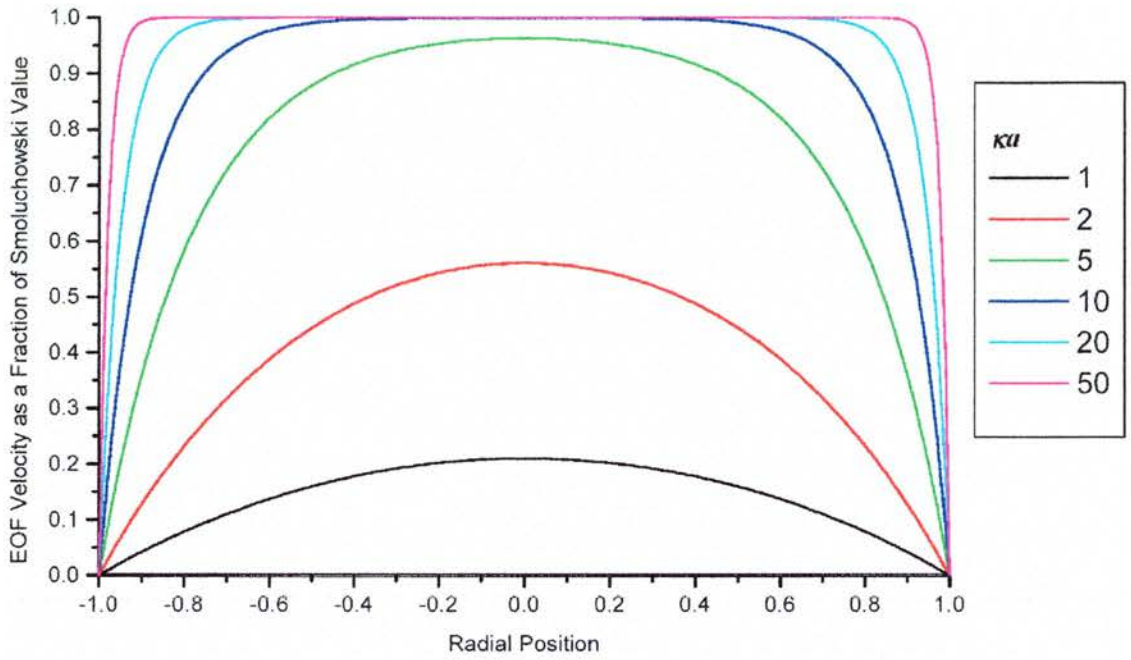


Figure 2-4 Diagram showing the variation in EOF velocity profile as a function of the value of the parameter $\kappa a$. Reproduced from reference [120].

The level of EOF is highly dependent upon electrolyte pH as the zeta potential is largely governed by the ionisation of the acidic silanols on the capillary wall. Below pH 4 the ionisation is small and the EOF flow rate is negligible, at pH9 and above the silanols are fully ionised and the EOF is strong. The level of EOF also increases as the electrolyte concentration is reduced and the zeta potential reduces.

### 2.2.2 Pressure flow

As discussed above, the EOF is generated along the entire length of the capillary and the flow rate is constant throughout the capillary. The resulting flow profile of the EOF is plug-like with the solutes travelling at the same rate across the diameter of

the capillary. This is an advantage of CE over pumped systems such as high performance liquid chromatography (HPLC) and open tube liquid chromatography (OTLC) where the solution is pushed from one end of the column, resulting in the solution at the edges of the column travelling at slower speeds than in the middle. The peaks therefore become broader as they travel along the column.

The velocity of a viscous liquid moving through a capillary would vary from zero at the walls to a maximum along the centre of the vessel.

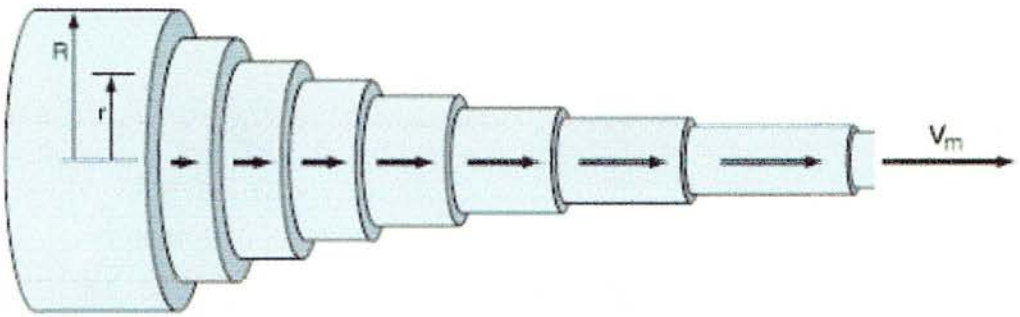


Figure 2-5 Diagram illustrating the variation of fluid velocity across a pressure driven capillary.

The velocity profile as a function of radius is given by the expression,

$$u_r = \frac{1}{4\eta}\frac{\Delta P}{L}(r_i^2 - r^2) \qquad \text{Equation 2.10}$$

where $u_r$ is the fluid velocity at any radial point $r$, $\Delta P$ is the pressure drop across the tube, $L$ is the length of the tube and $r_i$ is the internal radius of the tube. The higher flow rate seen at the centre of the capillary results in a parabolic velocity profile which leads to the band broadening problems seen in pressure driven separation techniques (Figure 2.5). EOF as a driving force for separation techniques offers superior flow characteristics that reduce band dispersion (Figure 2.6).

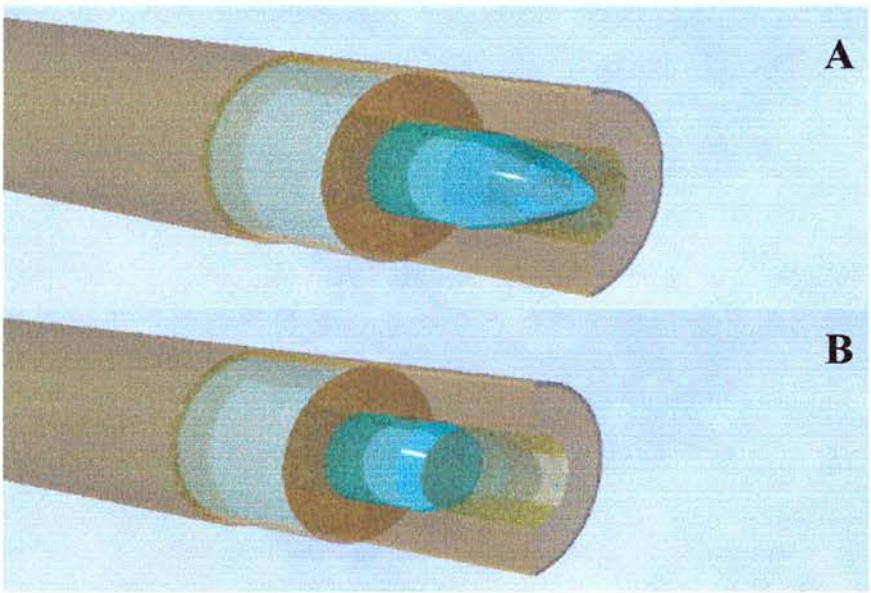


Figure 2-6 Comparison of: (A) pressure driven flow, (B) EOF driven flow

### 2.2.3 Combined electrophoretic and electroosmotic flow velocities

The migration velocities of cations and anions depend on their electrophoretic mobilities, EOF and, obviously, the applied voltage and capillary length. All neutral species migrate at the same velocity as the EOF, in a single band. When the mobility of the analyte and the EOF are combined, the migration velocity can be calculated using the equation,

$$v = \frac{(\mu_{eo} + \mu_e)V}{L} \qquad \text{Equation 2.11}$$

where $\mu_{eo}$ is the EOF mobility and $\mu_e$ is the electrophoretic mobility of the analyte, $V$ is the potential and $L$ is the capillary length. This is illustrated in Figure 2.7, where initially all molecules are introduced into the capillary at the same location. Molecules of varying size are carried forward by the bulk flow, and ions either outpace or fall behind the bulk flow. Electrophoresis will give small anions a larger velocity towards the cathode than large anions of like charge, meaning that small anions will fall further behind the bulk flow than large anions. Similarly, small cations will outpace larger cations of like charge, all outpacing the bulk flow.

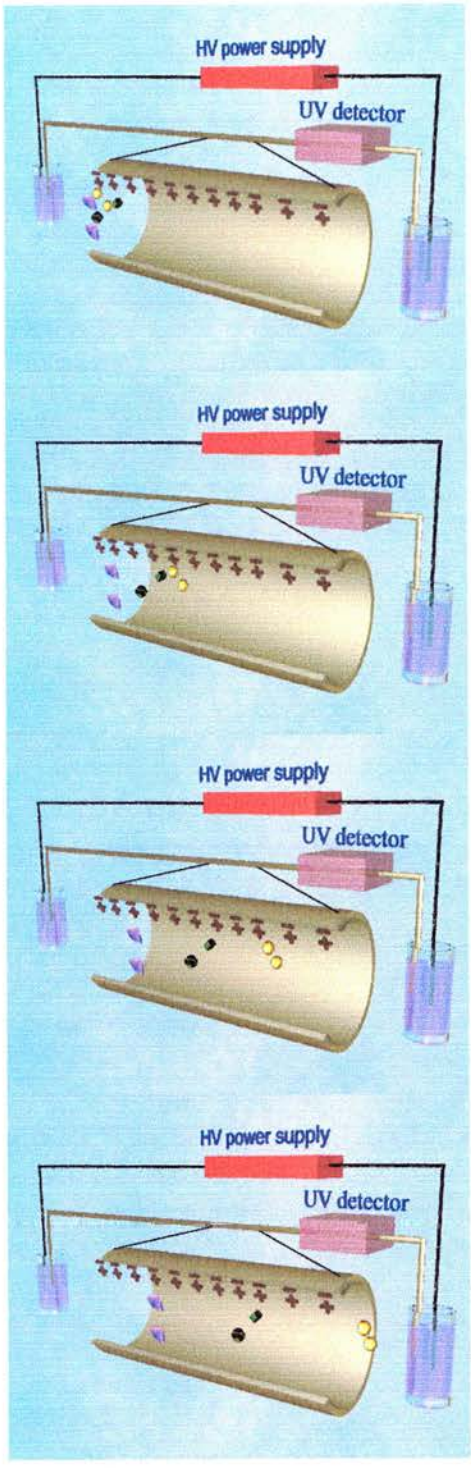


Figure 2-7 Schematic representation of a basic capillary electrophoresis instrument. Yellow spheres represent cations, green cyliders represents uncharged molecules carried with the flow front, and pink cones represents anions.

Although the rate of analyte migration is an important factor in the design of CE experiments, the control of band spreading is equally important. Analyte bands start the separation with a width, determined by the injection volume and method, that spreads as they pass along the capillary. It would not be possible using non-discriminating detection techniques (e.g. UV absorption) to detect bands that result from analytes with such similar migration times, or that band spreading has resulted in a single wide unresolved peak. Therefore, for successful separation, the conditions must be carefully controlled to optimise migration rate differences and band broadening. Obtaining narrow peaks is often of prime importance, as altering the relative migration rates will simply rearrange the peaks. High performance in electro-driven separation systems can be limited by self-heating. The electric current passing thorough the electrolyte and the capillary itself, gives rise to Ohmic heat. An equilibrium will be reached, where heat generation equals heat lost. However, as heating exists in the whole capillary, heat is lost only through the capillary surface. This leads to a parabolic temperature profile across the bore of the capillary, resulting in distortion of the solute bands and loss of resolution. [84,85,86]. It was concluded by Knox that heating will not affect performance if

$$Ed_c C^{1/3} < 1500 \qquad \text{Equation 2.12}$$

where $E$ is the potential gradient ($kVm^{-1}$), $d_c$ is the capillary ID (μm) and $c$ is the concentration in moles per litre. This predicts that with a voltage of 25 kV across a 50 cm column and a concentration of 0.01M the maximum capillary ID should be 140 μm.

### 2.2.4 The plate model and band-broadening

Of the early attempts to explain the process of band-broadening, that by Martin and Synge was the most successful [87]. They described a plate model that made it possible to compare the peak width with retention time, whereby the column of liquid can be represented by a series of mixing cells termed plates. The model was developed from concepts originally used to describe distillation. Although not directly applicable to the physical environment in a CE column, as it describes the

interaction of mobile phase with a stationary phase, experimentation has revealed that it still offers a method of comparing separation efficiencies [88].

The model assumes that the separation capillary can be represented by a series of mixing cells, or plates. The flow of liquid through the capillary can then be visualised as all the mobile phase being removed from the final cell and being replaced with the content of the penultimate cell. The content of the previous cell is then moved to the penultimate cell and so on, finally back to the first cell, which is filled with fresh buffer. This process occurs almost simultaneously, separated only by the finite period of time taken for solutes in each cell to reach equilibrium. As detection resolution is based on the number of mixing cells, if a greater resolution of separation is required a greater number of cells are required, and more time will be taken.

The injection of a sample into the system is represented by the addition of analytes in buffer into the first cell of the model. As the contents of the cells are moved along the chain, analytes will progress from cell to cell at different rates. The characteristics of the model that will be most important are, therefore, the size and number of the mixing cells, as equilibration time is assumed to be constant regardless of cell size. When considering CE capillaries, the size and number of cells must naturally be linked to the dimensions of the capillary, although under certain conditions there will be more cells than under other conditions. As an example, if the flow rate in a capillary is increased, there will be larger cells and less of them if the equilibration time remains constant, this would result in a more rapid separation, with a lower resolution of separation.

### 2.3 Plate numbers and experimental data

The number of theoretical plates can be obtained from an electropherogram or chromatogram using the equation,

$$N = 16(t_R / w)^2 \qquad \text{Equation 2.13}$$

where $N$ is the number of theoretical plates of a column for a particular compound, $t_R$ is the retention time, and $w$ is the base line peak width measured in the same units as $t_R$ (Figure 2.8). It should be noted that $w$ is not the base width of the peak, but the width obtained from the intersection of the baseline with tangents drawn through the inflection points on each side of the peak.

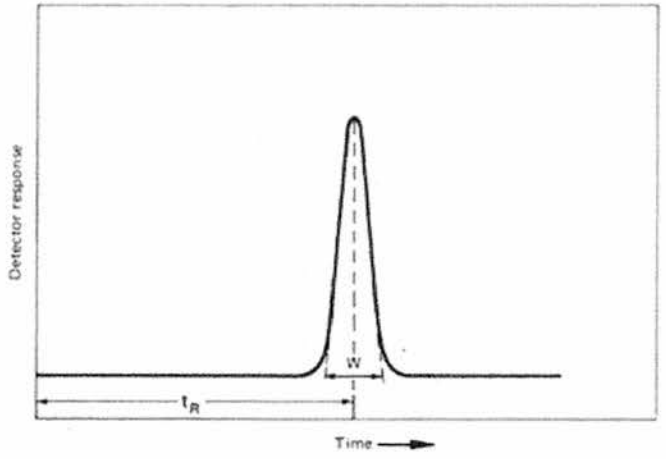


Figure 2-8 Diagram illustrating a symmetrical Gaussian chromatographic peak. The retention time is $t_R$, and $w$ is the base line peak width measured in the same units as $t_R$ . Reproduced from reference [89].

This works well for peaks that are symmetrical, have a level base line, and can be approximated by a Gaussian curve (Figure 2.8). If the peak is asymmetrical, or the base line is particularly uneven, a more appropriate method to estimate the number of theoretical plates is using the half height width $w_{1/2}$:

$$N = 8\ln 2 t_R^2 / w_{1/2}^2 = 5.545\left(\frac{t_R}{w_{1/2}}\right)^2 \qquad \text{Equation 2.14}$$

To aid comparison, it is often of more use to quote the theoretical plate number as the number of plates per meter of column, or to quote the height equivalent to a

theoretical plate (HETP). This is the length of a column divided by the number of theoretical plates.

If it is assumed that molecular diffusion is solely responsible for band broadening, then the spatial variance $\sigma_L^2$ can be calculated by,

$$\sigma_L^2 = 2Dt \qquad \text{Equation 2.15}$$

where $D$ is the molecular diffusion coeffient of the solute zone and $t$ is the time required for a zone to migrate the length ($L$) of the capillary. $t$ can be calculated by,

$$t = L/v = L^2\mu_e V \qquad \text{Equation 2.16}$$

where $V$ is the applied voltage, and $\mu_e$ is the electrophoretic mobility of the analyte.

Substituting the expression for time from equation 2.16 into equation 2.15 yields the following equation,

$$\sigma_L^2 = 2DL^2/\mu_e V \qquad \text{Equation 2.17}$$

Substituting this expression $\sigma_L$ into the following definition of the number of theoretical plates, $N$,

$$N = L^2/\sigma_L^2 \qquad \text{Equation 2.18}$$

gives,

$$N = \mu_e V/2D \qquad \text{Equation 2.19}$$

From this equation, a number of interesting observations can be made. The separation efficiency ($N$) is proportional to the applied voltage and is independent of the capillary length and the elution time. $N$ is proportional to the ratio of the electrophoretic mobility to the diffusion coefficient; both factors are intrinsic to the analyte and therefore difficult to affect. It would therefore appear that the optimum

route to optimise the separation efficiency would be to apply the highest voltage possible to the shortest capillary possible. It must be noted that this is limited by Ohmic heating.

### 2.3.1 Injection volume

An important factor influencing band broadening in CE is the length of the injection volume, which may be a few millimetres in length. This is a significant length given that the total length of the capillary may be only 250 mm and in the case of UV absorbance detection, the detection window may be only 0.1 mm in length. The starting zone length of the sample injection can be reduced by utilising a process called stacking (Figure 2.9) [90]. This stacking reduces the width of the sample zone prior to separation and results in improved sensitivity and increased peak efficiency. Stacking occurs when the sample is dissolved in a lower ionic strength buffer than that of the separation electrolyte. Under these circumstances, the field strength is higher in the sample zone than in the rest of the capillary. The sample ions move forward rapidly in the sample zone until they encounter the electrolyte boundary, where they experience a lower applied field and their migration rate slows down. In this way, the sample zone is focused and can lead to up to a ten fold reduction in the starting peak width. This process is optimised if the sample is dissolved in pure water, or a one in ten dilution of the electrolyte.

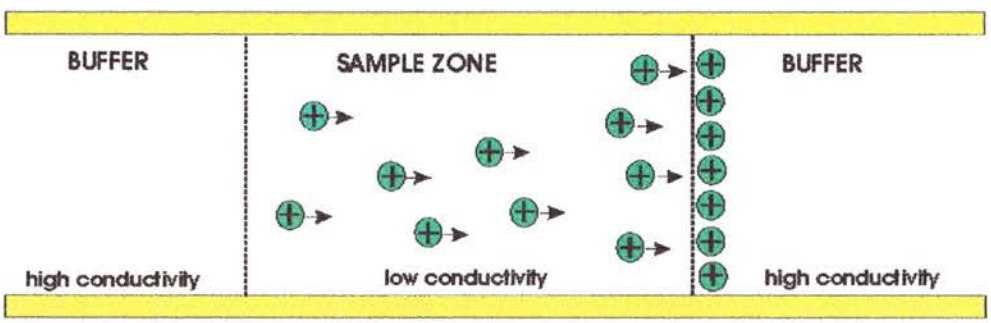


Figure 2-9 Schematic representation of Sample stacking.

### 2.3.2 Peak resolution

Another measure of separation efficiency is peak resolution (Figure 2.10). The resolution ($R_s$) between two peaks is given by,

$$R_s = \frac{2\Delta Z}{W_A + W_B} = 2\frac{[(t_R)_A - (t_R)_B]}{W_A + W_B} \qquad \text{Equation 2.20}$$

where $\Delta Z$ is the separation between peaks $A$ and $B$; and $W_A$ and $W_B$ are the widths at the base of peaks $A$ and $B$, respectively. An acceptable $R_s$ is of the order of one with baseline resolution between two peaks.

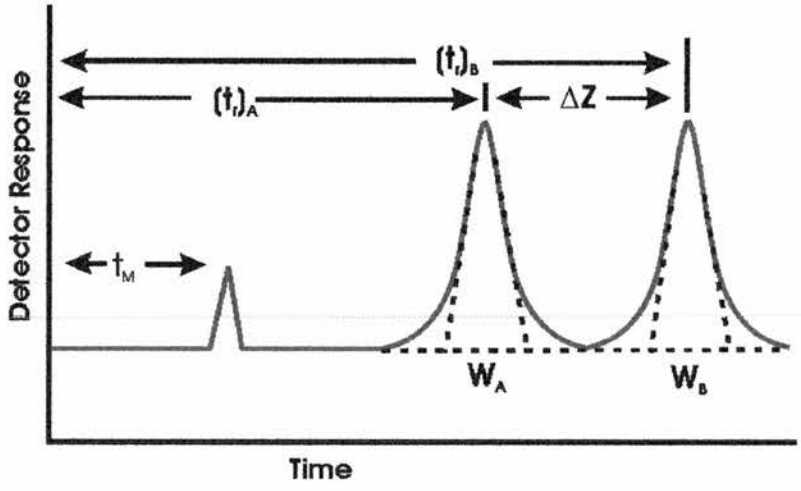


Figure 2-10 Diagram illustrating the measurements necessary for the calculation of the peak resolution for Gaussian peaks. Reproduced from reference [91].

### 2.3.3 Peak asymmetry

The normal dispersion of component molecules, as they move through a separation system, is represented by a bell-shaped Gaussian peak. However, if some molecules are more strongly retained by the capillary surface, or stationary phase in the case of chromatographic separations, these molecules will lag behind the main band and will

form a tail on the main peak (Figure 2.11). Fronting can also occur when some of the analytes move ahead of the main band. This may be due to too large a sample being introduced onto the capillary such that the capacity is exceeded. Overloading leads to broader peaks, a decrease in resolution and inaccurate elution times.

The modern definition of peak asymmetry, $A_s$, is derived from the work of Dal Nogare and Chiu published in 1962 [92]. Peak asymetry cab be calculated from the baseline cut out by the two peak tangents drawn to the inflection points of the peak (Figure 2.11). This length, $w_b$ is divided into two parts by the perpendicular drawn to the peak maximum,

$$w_b = f + b \qquad \text{Equation 2.21}$$

where $f$ is the front width and $b$ is the back width. In a case where the peak is not Gaussian symmetrical, the two values will not be equal. $A_s$ can be calculated from,

$$A_s = \frac{w_b}{w_b - \Delta w} \qquad \text{Equation 2.22}$$

where $\Delta w$ is equal to $b$ minus $f$.

For a symmetrical, Gaussian peak, $A_s$ is equal to 1.0 and $A_s$ is greater than 1.0 for a tailing peak.

A more straightforward method that is now accepted, is to measure the peak width at 13.4% of the peak height, as it is known that this width is the same as the value of $w_b$ for a Gaussian peak (see Figure 2.11). To simplify matters further, 10% of the peak height is used instead of 13.4%. This valve represents a 7% difference compared with the true peak width at base.

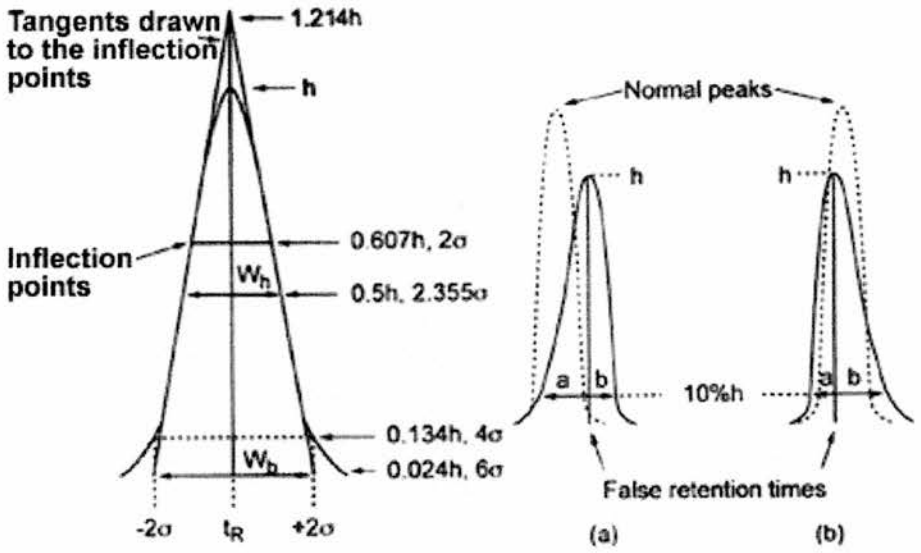


Figure 2-11 Diagram illustrating the measurements necessary for a simplified method of calculation of the peak resolution. Reproduced from reference [93].

# 3 Mass spectrometry

In this chapter, a review of the development of liquid interfaces for mass spectrometry applicable to single cell samples will be presented. The theory of quadrupole and time-of-flight mass spectrometry will also be discussed.

## 3.1 Liquid phase interfaces for mass spectrometry

Over the last 30 years, a great deal of attention has been focused on the interfacing of liquid separation techniques with mass spectrometry. A liquid phase mass spectrometry interface is, as the name suggests, the connection between a mass spectrometer and a flow of liquid. The source of the liquid flow can vary from, in its simplest form a syringe pump device providing a homogeneous flow of sample, to the eluent from a liquid chromatograph system that would provide multiple discrete bands of analyte. The various liquid sources also generate differing flow rates, from capillary electrophoresis (~100 nL/min) to HPLC (~1 ml/min). Over the years, many types of interface have been constructed, some of which will be presented in this chapter to give an introduction and history of liquid interface techniques. Particular attention will be paid to electrospray ionisation techniques.

The critical problem with coupling a liquid flow to a mass spectrometer is that maintaining a high vacuum within the mass spectrometer in difficult. In the case of gas chromatography mass spectrometry (GC-MS), the gas flow entering the mass spectrometer is in the range of 0.5-2 $cm^3$/min. This can be compared with a typical gas flow 1000 $cm^3$/min that would result from a liquid interface with a water flow of 1 mL/min [94]. To maintain a suitable vacuum within a mass spectrometer (~$10^{-5}$ mbar) a pumping rate of ~75,000 L/s would be required. Another critical factor in the case of liquid interfaces is the need to vaporise the eluent prior to ionisation.

To make progress, several fundamental problems had to be addressed: the volume of solvent eluting from the upstream device, the composition of the mobile phase and the nature of the analytes. These problems have been solved in a number of different ways and a wide variety of literature exists that reviews these developments [95].

### 3.1.1 Continuous flow fast atom bombardment

Fast atom bombardment (FAB) was developed as a method for generating protonated molecules for mass spectrometry (Figure 3.1) [96] [97]. In its most simple form, the

analyte is dissolved (or suspended) in a non-volatile liquid matrix such as glycerol, placed within the instrument, and bombarded with a beam of atoms. The atom beam is obtained by ionising argon or less commonly xenon; these fast ions are then accelerated and focused towards a collision chamber [98]. The fast ions are then collided with slow argon atoms to generate fast moving atoms and slow moving ions. Any remaining ions are eliminated from the beam as it exits the collision chamber by a pair of electrodes. The fast atom beam then continues on to collide with the sample. It was always thought that if ions were used in the incident beam, charging of the sample stage would occur, degrading the signal strength. This has now been disproved with the publication of work involving caesium ion beams.

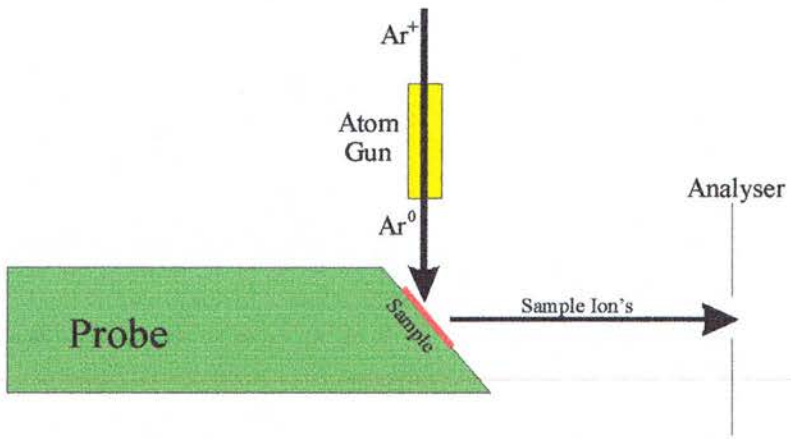


Figure 3-1 Schematic diagram of fast atom bombardment interface.

The continuous flow FAB interface operates in a similar way to the interface described above, with the exception that the sample is constantly replenished. A capillary links the separation technique outlet with the centre of the FAB sample probe [99,100]. Buffers used in this technique typically have 1-5 % glycerol added and flow rates vary from 1 to 5 μL/min. The solvent quickly evaporates from the tip of the FAB probe leaving the analyte and the glycerol that acts as a FAB matrix. The atoms again collide with the sample solution and induce a shock wave that ejects ions and molecules from the solution. The resulting ions are accelerated by an electrostatic gradient towards the analyser.

### 3.1.2 Electrospray and nanospray

Electrospray has become the most widely used LC-MS interface technique in modern mass spectrometry (Figure 3.2). It is a versatile method for the production of gas phase analyte ions from solutions and is almost ideal for biological analytes. The method was first investigated in the late 1960s [101], but it was not until the mid 1980's that its use as an interface for mass spectrometry was demonstrated by Fenn and the power of the technique was revealed [102,103]. Its development was credited with a Nobel Prize for Chemistry in 2002.

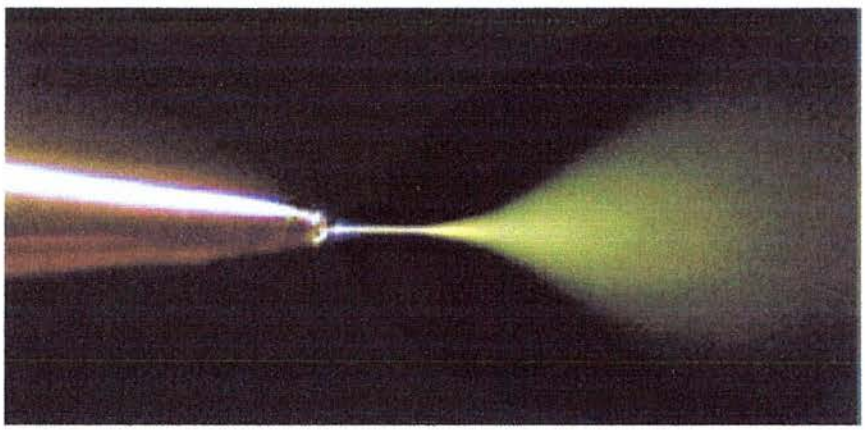

Figure 3-2 Photograph showing nano electrospray ionisation, the outcome of which, is the transfer of analyte species, generally ionised in the condensed phase, into the gas phase as isolated entities. Reproduced from reference [104].

The principal outcome of the electrospray process is the transfer of analyte species, generally ionised in the condensed phase, into the gas phase as isolated entities (Figure 3.3). This is achieved using, as the name suggests, an electric potential gradient rather than the more traditional pneumatic method of forming atomised droplets.

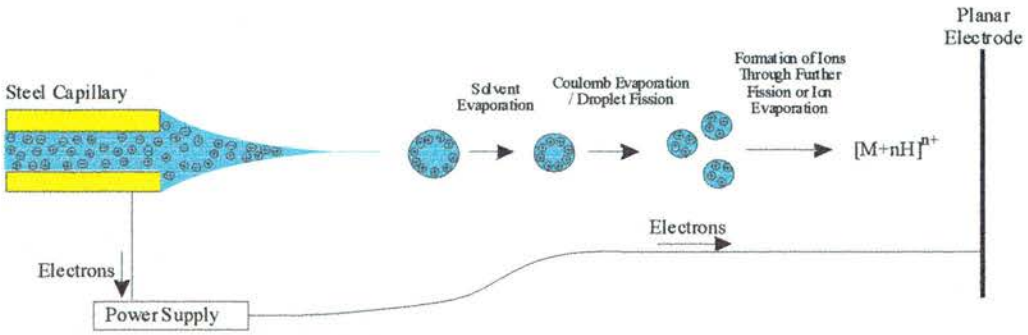


Figure 3-3 Schematic representation of the electrospray electrolytic cell.

There are four key processes in electrospray ionisation: the generation of charged droplets from electrolyte dissolved in a solvent, the evaporation and repeated explosion of the droplets leading to highly charged small droplets capable of producing gas phase ions, the mechanism of gas phase ion production, and secondary processes by which gas phase ions are modified by various processes in the atmospheric region of the mass spectrometer.

In the schematic representation of an ESI interface (Figure 3.3) the analyte dissolved in buffer is passed through a metal capillary held at high electrical potential (3 to 5 kV) and placed 1-2 cm away from a planner counter electrode. The narrow capillary tip leads to a high electric field strength, $E$. The magnitude of the capillary electric field, $E_c$, can be calculated as follows,

$$E_c = \frac{2V_c}{r_c}\ln(\frac{4d}{r_c}) \qquad \text{Equation 3.1}$$

where $r_c$ is the capillary radius, d is the distance to the planar counter electrode and $V_c$ is the potential applied to the capillary. For an applied potential of 2000 V, a capillary radius of 0.2 mm and a distance to the counter electrode of 2 cm, the electric field magnitude would be $3.3 \times 10^6$ V/cm. The imposed field $E_c$ also penetrates the liquid in the capillary tip, such that when the applied potential is positive, some positive ions will migrate towards the liquid surface and some negative ions will migrate away from it until the imposed field inside the liquid is essentially removed by charge redistribution. The accumulation of positive charges

at the surface can then lead to a destabilisation of the liquid, with the surface of the liquid being drawn out down the potential gradient towards the counter electrode. This continues until a sharp cone is formed, the Taylor cone. At a sufficiently high field, the tip of the cone becomes unstable and a jet of liquid, enriched with positive ions, is formed. At a distance downfield, the liquid jet breaks up to form discrete drops in which an excess of positively charged ions exists [105].

The efficiency of electrospray is dependent on the desolvation of the charged droplets formed as the filament breaks up and the optimisation of the yield of gas phase ions. The droplets formed in the process described above tend to have radii in the region of 1 – 1.5 μm and a charge of $\approx 10^{-14}$ C.

Once individual droplets have been formed, solvent evaporation quickly causes the droplet to shrink. As the volume of the droplets decreases, the charge density approaches the Rayleigh limit, the point where the charge is sufficient to overcome the surface tension that hold the droplet together, defined by,

$$Q_R^2 = 64\pi^2 \varepsilon_o \gamma R_R^3 \qquad \text{Equation 3.2}$$

where $Q$ is the charge, $\varepsilon_o$ is the permittivity of the vacuum and $\gamma$ is the surface tension.

In droplets with a radius of approximately 1 μm, fission takes place slightly below ($\approx$ 80%) the Rayleigh limit. Investigation of the fission event reveals that the droplet does not suddenly split evenly into smaller droplets of even charge, but are observed to vibrate alternately from oblate to prolate shapes. These vibrations appear to stimulate the loss of droplets as a tail, much like the tip of the Taylor cone forming a filament. The daughter droplets emitted vary little in size, with a radius of approximately 10% of the parental droplets radius. They carry only 2% of the parental mass, but 15% of the original charge [106].

This 'uneven' fission event leads to approximately 10 daughter droplets for every fission event, all carrying a far higher charge-to-mass ratio. These daughter droplets then desolvate further until they also reach $\approx$ 80% of the Rayleigh limit when they also undergo fission. This process is repeated several times. Each cycle, the time

taken for the droplet to reach its critical charge to mass ratio decreases. It is the later generation droplets that would be expected to evolve gas phase ions. The time required to reach a droplet charge-to-mass ratio where gas phase ions may be evolved is in the region of many 100 μs, which is a substantial percentage of the total time spent in the atmospheric region of the interface, thought to be 1 – 2 ms.

The evolution of gas phase ions from the highly charged daughter droplets is a contentious issue in which solution chemistry plays an important role. A number of theories exist based on very different mechanisms. The earliest clear description was the charge-residue model (CRM). It depended on the formation of extremely small radius (r=1 nm) droplets containing one ion. These droplets would then desolvate leaving the ions in the gas phase [107,108]. Further investigation refined this theory and titled it the single ion in droplet theory (SIDT) [109].

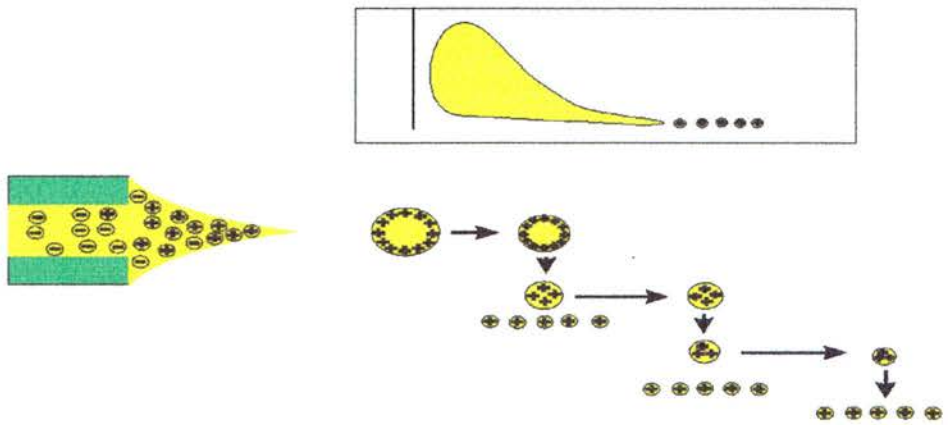

Figure 3-4 Schematic diagram of the charged residue model.

A second mechanism, the ion evaporation model (IEM), assumed that ions would evaporate from small highly charged droplets [110]. The conditions under which the droplet will emit ions are close to the Rayleigh limit (r= 8 nm and 70 charges). In these circumstances, fission will not take place, but instead gas phase ions are emitted. Droplet conditions may be maintained at levels close to the Rayleigh limit, as the droplet will desolvate as well as losing charges. In this way ion emission will be maintained and very small initial droplets are not required as a starting point.

A final mechanism, has been proposed by Siu *et al.* [111] whereby the ions are not formed from the droplets at all, but are emitted directly from the Taylor cone tip. It is a radical proposal and as yet has few followers, and the experimental evidence presented is contentious. It is certainly an interesting theory, and will be discussed further in Section 3.1.4.

Ignoring the mechanism proposed by Siu *et al.* there is now a general agreement by many authors that neither the CRM nor the IEM models account for all the experimental observations. It is speculated that the two models describe different aspects of the observed process of gas phase ion formation [112]. For small ions

(e.g. salt ions), the IEM is thought to be applicable, and for macro ions (e.g. proteins) the CRM is more likely [106].

### 3.1.3 Nanospray

The development of nanospray (nESI), has shed further light on the generation of charged gas phase ions from dispersed charged liquid droplets [113]. Initial investigations revealed, surprisingly, that when conventional ESI is replaced with nESI, a number of clear differences are observed:

- ion signal intensities are equal or even higher than with ESI
- there is increased tolerance to salt contamination

As the droplet fission processes themselves are not expected to differ in the two techniques, the difference is likely to exist in the dispersion of the liquid into charged droplets. In conventional ESI, with μL/min forced-flow rates, the droplets formed are in the μm range. In contrast for nESI, where the ESI outlet is replaced with a tapered glass needle with a small orifice (~5 μm) and forced flow is abandoned, the resulting flow rate is ~50 nL/min and the droplet diameter has been estimated at 180 nm [113]. The high salt tolerance of nESI can be explained by the theory that the formation of droplets with a diameter one order of magnitude smaller means that less fission events are necessary before ions are released, and each additional fission event results in an increase in salt concentration. It has also been observed that with smaller initial droplets, less analyte is lost as a lowly charged residue (wet salt crystal). Again this is the result of fewer fission events and the resulting lower salt concentration in the offspring droplets.

From the observations summarised above, it can be assumed that different predominant fission pathways within the fission cycle lead from disperse liquid charged droplets to ions in the gas phase [114].

### 3.1.4 Droplet ESI

A novel development that was originally designed to investigate the electrospray process but resulted in an interface for mass spectrometry is the droplet electrospray source (dESI) [115]. A high-pressure pump is used to create a jet that is broken into

discrete droplets by a piezoelectric 'buzzer' upstream of the orifice. A high potential (3 kV) electrode can be positioned either distant from the droplet stream or close to the stream (20 μm). When distant, a corona discharge was observed to acts on the droplets and resulting ions exhibit properties that match those resulting from atmospheric pressure chemical ionisation (APCI). When the electrode is close to the droplet stream, the ions formed exhibit properties associated with electrospray.

It was observed that in the case of dESI, coulombic fission events occurred at a droplet charge $Q$ that is lower than $Q_R$, the Rayleigh limit. As the Rayleigh stability limit only hold for spherical droplets, deformation from spherical geometry induced by the piezoelectric buzzer destabilises the droplets and will lead to uneven fission. The formation of fine daughter droplets was also visualised; a fine jet was observed leaving the droplet after charging and a signal was detected with the mass spectrometer. As discussed in Section 3.1.2, Siu *et al.* proposed that gas phase ions were emitted directly from the Taylor cone and not from the highly charged small droplets. In this work, electrospray type mass spectra were obtained from charged droplet fission in the absence of a Taylor cone. This would further suggest that research is far from providing a clear definition of the electrospray process and as with many topics in science, the final answer may be that all the mechanisms discussed above occur in certain situations.

## 3.2 Mass spectrometry fundamentals

Although the instrument used predominately in the research presented in the following chapters was a hybrid quadrupole time-of-flight mass spectrometer, it would be of advantage to discuss the fundamentals of quadrupole and time-of-flight mass analysers separately.

## 3.3 Electrostatic quadrupole mass analysers

Mass separation in a quadrupole mass filter is achieved by creating a stable trajectory for ions of specific m/z values in a hyperbolic electrostatic field (Figure 3.5). A great deal of information is available in the literature, and a good review was written by Wollnik [116]. A ideal quadrupole mass filter would consists of four high-precision rods with a hyperbolic cross section, located precisely in an orthogonal array through which the ions with an energy-to-charge ratio of a 1-2 eV may be passed [117].

However, it is now common for cylindrical rods to be used. Diametrically opposing rod pairs are electronically connected to form pairs of rods with a 180° phase shift. One pair has an RF voltage superimposed on a positive DC voltage, while the other pair has a DC and RF voltage with a 180° phase shift applied. Typically, the poles have a fixed DC (~10 V) and alternating RF voltage (~MHz and ~400V peak to peak) applied to them. RF only quadrupoles act as a high-pass mass filter that could eliminate all low mass ions. By adding the DC voltage, it is possible to destabilise both high and low mass ions to create a mass filter for a narrow range of ion masses. The potential $\phi_o$ applied to the opposing pairs of rods is given by:

$$\pm\phi_0 = U + V\cos\varpi t \qquad \text{Equation 3.4}$$

where $U$ is the DC voltage. $V\cos\omega t$ is the time-dependent RF voltage in which $V$ is the RF amplitude and $\omega$ the RF frequency.

For ions entering the quadrupolar field with given values of $U$, $V$ and $\omega$, only those with certain m/z values will be resonant with the field and have a stable trajectory through the quadrupole. Non-resonant ions will develop unstable trajectories (large amplitudes in x or y directions) and be lost. It has been shown that the range of stable trajectories of trapped ions and their relationship with the electrostatic field can be modelled by a version of the Mathieu equation [117].

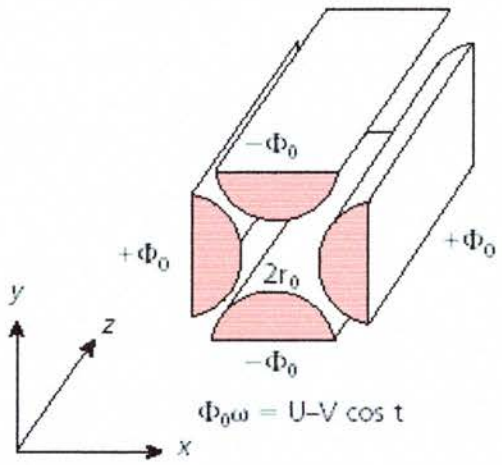


Figure 3-5 Schematic diagram of a quadrupole mass analyser. Reproduced from reference [118].

By altering the both the DC offset and the RF voltage it is possible to scan the range of m/z values that are transmitted through the mass filter. As the resolving power of a quadrupole mass filter increases with the number of cycles the ions experience within the RF field, and ions with higher m/z have a lower velocity, the resolution will increase with increasing m/z. However, the transmission efficiency will decrease, due to the longer time that ions of higher masses spend in the quadrupole.

### 3.4 Time-of-flight mass analysers

Time-of-flight mass spectrometry (TOF-MS) was first developed fifty years ago, with the first commercial instrument being marketed by the Bendix Corporation in 1955 based on a design by Wiley and McLaren [119]. In the last 15 years, there has been a rapid increase in the interest in TOF-MS, led by the success of matrix-assisted laser desorption ionisation (MALDI) and hybrid quadrupole and TOF instruments.

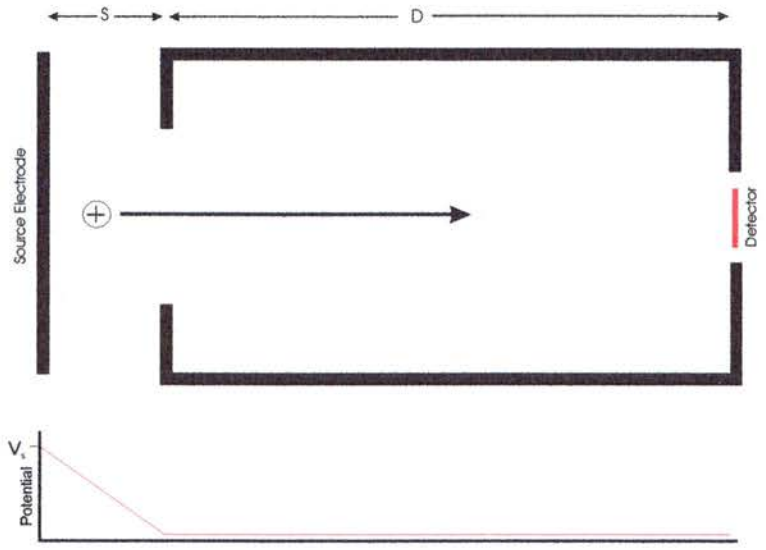


Figure 3-6 Schematic diagram of a linear time-of-flight mass spectrometer

Time-of-flight mass analysers are characterised by their pulse analysis technique rather than a continuous scanning technique such as quadrupoles described above. In its simplest form (Figure 3.6), a time-of-flight (TOF) analyser consists of a field free drift region, D, which is held at constant electrical potential, and a source region, S, where a gradient in electrical potential exists, $V_s$. Ions present in the short source region are accelerated into the drift region by the action of the electric field, $E$. Analysis is based on the principle that ions of different m/z values will have been accelerated to the same kinetic energy, $E_K$, in the source,

$$E_K = zeEs \qquad \text{Equation 3.5}$$

where $e$ is the charge on an electron in coulombs and $z$ is the number of charges. However, ions of different mass will exhibit different velocities ($v$),

$$v = (2zeEs/m)^{1/2} \qquad \text{Equation 3.6}$$

where $m$ is the mass of the ion. The time, $t$, taken for ions to traverse the length, $d$, of the drift region is also dependent on the mass of the ions,

$$t = \left(m/2zeEs\right)^{1/2} d \qquad \text{Equation 3.7}$$

Thus, the time that is required for each ion traverse the drift region is different: high masses take longer to reach the detector than low mass ions. The basic formula by which the time spectrum can be converted to a mass spectrum is given by the equation:

$$m/z = 2eEs(t/d)^2 \qquad \text{Equation 3.8}$$

In an ideal instrument, ions would be created instantaneously in the source region, all initially located at the same point and having the same velocity. For a reliable mass spectrum, the time of ion extraction must be known to a high degree of accuracy. This problem is usually addressed by the used of a pulsed ionisation technique such as L2MS [120] or gated and deflector techniques as found on the Micromass Q-ToF [121].

### 3.4.1 Resolution in time-of-flight mass spectrometry

A major limitation in achieving high resolution is the consequence of the spread in time, space and kinetic energy of the initial ion packet. It must be assumed for the purposes of calculation that all the ions will be accelerated from the same position and have the same $K_E$. Unfortunately this isn't true and there are four potential causes of inaccuracy associated with ion formation and acceleration [122].

The time difference in the selection of two ions of the same mass and velocity will remain the same during the flight to the detector and will result the ions reaching the detector at different times.

Ions that are not formed in the same plane perpendicular to the electric field, due to the width of the ion beam, will be accelerated to different kinetic energies. Ions accelerated from the rear of the source region will be accelerated across a larger electrical potential to a higher kinetic energy than an ion present close to the drift region.

Ions with variations in initial velocity and direction, but the same mass and position, will also leave the source with different $K_E$. This is due to ions with velocities

opposing the accelerating field having to be decelerated and then accelerated in the correct direction.

One solution to the resolution problem was proposed by Wiley and McLaren [119]. They attempted to compensate for the spatial and kinetic distribution through the development of a dual stage extraction source. Variations in initial kinetic energy were corrected for by the introduction of a delay between ion formation and extraction (time lag focusing). Spatial focusing was achieved with the use of two extraction regions, at different field strengths. It was possible, by adjusting the lengths and field strengths to focus the ion packet onto the detector. Although the design was successful in improving mass resolution, it was not possible to correct for spatial and kinetic energy distributions simultaneously. Also conditions had to be altered for different masses.

### 3.4.2 Reflectron mass analysers

An alternative method to correct for dispersion in the kinetic energy distribution is the reflectron mass analyser, first described in 1973 (Figure 3.7) [123]. It provides a method by which ions that have different initial kinetic energies, but the same *m/z* values will reach the detector at the same time. The reflectron is positioned as the end of the field free drift region, opposite to the source. It consists of a series of electrodes, running from the potential of the drift region up to a potential slightly higher than the source potential. Incoming ions penetrate the reflectron until they exchange all kinetic energy for potential energy, at which point they reverse and are accelerated back through the reflectron emerging with the same kinetic energy as they entered. Ions with greater kinetic energy will penetrate the reflectron further and will therefore have a longer flight path. This means that ions having different velocities will reach the detector at the same time. If the reflectron is set at a small angle with respect to the axis of the drift region, the ions exiting the reflectron will not follow the same flight path as incoming ions and the detector can be placed adjacent to the source. The reflectron does not affect the kinetic energy spread of the ions, but does correct for the effects of this variation on the arrival times.

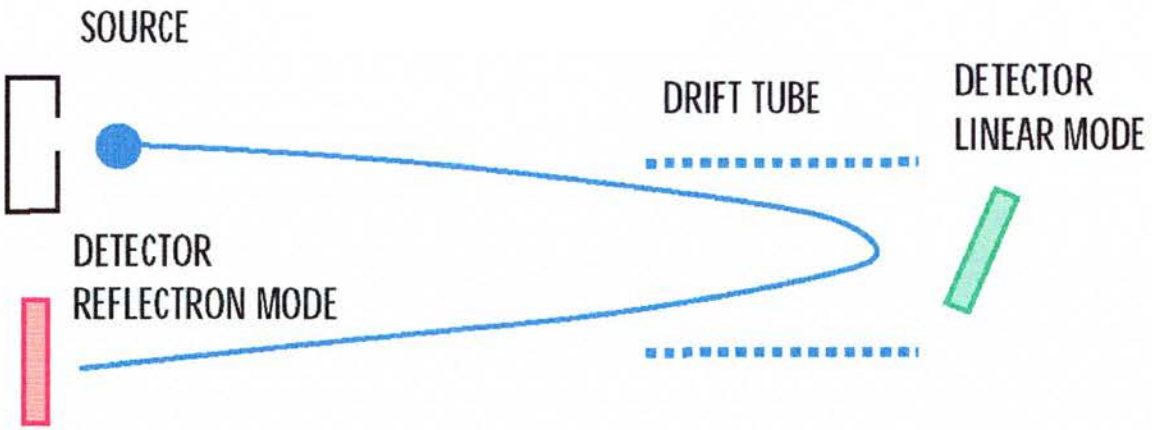


Figure 3-7 Schematic diagram of a reflectron time-of-flight mass analyser. Reproduced from reference [124]

### 3.5 Orthogonal acceleration/ time-of-flight (oa-TOF) mass analysers

Instruments, such as the Q-ToF (Micromass, UK) used in this work, employ a technique termed orthogonal acceleration. The technique, originally pioneered in the 1960s was developed to permit TOF analysers to be used with constant ionisation sources such as ESI [121,125]. The early work was rediscovered and perfected in the late 1980s and early 1990s, by two independent groups, and is now the basis of a number of commercial instruments [125]. In the case of the Q-ToF, ions are formed and introduced into the instrument, as in a conventional quadrupole mass spectrometer. The voltages applied to the quadrupole are set such that they do not scan, but act as an m/z filter. Ions of interest proceed through the instrument as an ion beam. At a point, analogous with the source region in the previous examples, the ion beam is acted on by a deflector plate such that a packet of ions is accelerated orthogonally into the field free drift region. This ion packet is then analysed as in a conventional reflectron TOF instrument. The efficacy of this style of analyser was reduced as it exhibited a mass discrimination effect; that is, ions with lower m/z values possessed higher velocities in the direction of ion formation, such that a separation of ions occurred across the deflector region. This separation continued post acceleration and could lead to ions not hitting the detector if their m/z value was

too high or too low. The introduction of higher pressure quadrupole regions (~90 mBar) such that ions are thermalised to low eV kinetic energies by collisional cooling, has reduced but not removed this effect.

## 3.6 Tandem mass spectrometry

Tandem mass spectrometry is a process whereby analyte ions of a particular m/z value may be selected and fragmented. This is followed by the analysis of these newly formed fragment ions. Only a brief summary will be presented as a great deal of attention has been paid to the technique in the literature and a number of good reviews are available [126]. Tandem in space instruments, such as the Q-ToF, require more than one analyser. The first is required for analyte isolation. The ions then pass through a collision cell where they are then fragmented by collisions with gas molecules, and an analyser is used for detection of the fragment mass to charge ratios. Quadrupole mass filters work well when used as a precursor ion selector as ToF analysers do not scan and consequently detect the fragment ions efficiently. It can therefore be seen that oa-ToF mass spectrometers make very sensitive instruments for product-ion tandem mass spectrometry.

### 3.6.1 Modes of acquisition

Full scan analysis is the plot of the sum of the ion abundance in each MS scan plotted as a numerical value. It is typically performed over a wide m/z range that encompasses all the ions of interest. Compounds of every mass are plotted on the same spectrum such that identifying the compound of interest can be difficult as many have the same m/z values. Full scan analysis if often confused with total ion current (TIC) plot. TIC refers to a plot of the mass scan data collected over time and does not specify a scan mass range or a type of MS experiment. It is possible to have a TIC plot of a full scan analysis, selected ion monitoring or a single reaction monitoring experiment.

### 3.6.2 Selected ion monitoring

When the mass spectrometer is set to selected ion monitoring (SIM), a spectrum is returned of a very small mass range, typically one Thomson. Therefore only compounds with the selected mass are reported. The SIM plot can look very different from a full scan analysis, as the ions revealed as peaks may be only very

minor components of the overall mixture. A SIM plot, although identifying ions with similar m/z values, may not provide a unique identification of the compound, as many components in a complicated mixture, as found in cell extracts will have the same m/z value.

### 3.6.3 Selected reaction monitoring

Selected reaction monitoring (SRM) is a method by which it is possible to achieve a unique identifying fragment ion for the precursor ion of interest in the midst of a complicated matrix. SRM plots commonly contain a single peak corresponding to the fragment ion of interest. The technique is achieved by specifying the precursor ion mass, performing MS/MS to cause fragmentation then monitoring for a single fragment ion. The specific experiment is commonly known as a 'transition' and is written as (parent mass $\rightarrow$ fragment ion) for example (534 $\rightarrow$ 375).

# 4 Instrumentation

In this chapter, a full description of the instrumentation used in this research is presented. The development of the techniques used for microsampling from fungal cells and the methods used to transfer the samples to the CE capillary are discussed. This is followed by a description of how the separation instrumentation was used, both in its standard form and modified specifically for SiCSA. This is followed by a description of the mass spectrometric interface that was used in this work. Together with details of the Micromass Q-ToF mass spectrometer that was used for all the SiCSA experiments described later in Chapters 5 and 6.

At the outset of this research, it was thought that it would be possible to perform the cell culture, microscopy and sampling in a dedicated microscopy facility, and then transfer the samples to a dedicated analytical laboratory. After some early experiments into the feasibility of transferring the samples, it was determined that it was critical that all equipment required was located in the same laboratory, and as close to each other as was feasible.

## 4.1 Microscopy

### 4.1.1 The modern inverted microscope

The modern inverted microscope is based on a design by Le Chatelier in 1888 [127]. As the name suggests, an inverted microscope is upside down compared with a conventional microscope. The light source and condenser are positioned above the stage pointing down. The objective lenses and turret are below the stage pointing up.

The sample is placed on the stage as on a conventional microscope, but is observed from the underside, rather than from above. The design has the primary advantage that samples can be easily examined when they are far too large to fit within the confines of an upright microscope and micromanipulation of the sample is possible. Most importantly for SICSA, only the side facing the objective lens is required to be optically flat.

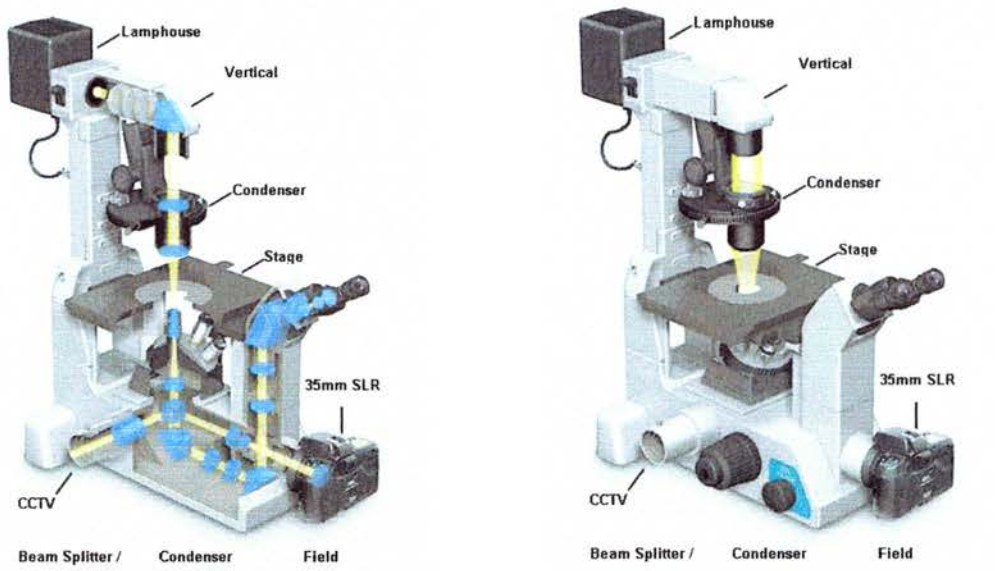


Figure 4-1 The Nikon TE200 inverted light microscope. The design has the primary advantage that samples can be easily examined when they are far too large to fit within the confines of an upright microscope and micromanipulation of the sample is possible. Reproduced from reference [128].

For a sample to be observed on a traditional microscope, it is requires that the specimen be placed on a glass slide and a cover slip is pressed on top to provide an optically flat surface. To achieve this, a small sample must be removed from the bulk culture and placed in an artificial environment created by the slide and cover slip. As a result, the temperature and oxygen content of the sample may change quickly from those of the culture. The sample will also quickly dry out unless repeatedly replenished with water. The loss of water by evaporation and the periodic replenishment may change the salinity of the sample frequently. These changes can impose severe stress on the organisms that can affect their behaviour and in extreme cases cause their death. In the case of the inverted microscope, only the underside of

the sample, facing the objective lenses is required to be optically flat. As a result large samples can be examined without being removed from the bulk population.

### 4.1.2 Imaging system

In order to perform measurements and provide an accurate record of the microsampling experiments, a charged coupled device (CCD) camera (JVC, UK) [129] was mounted onto the microscope. Due to the large size of video data files (1 Gb/minute), it was necessary to record the video data onto a mini digital video cassette (Sony, JP) [130] using a digital video camera (DCR-TRV20E) (Sony, JP) equipped with a facility to record data from an external source. Video processing and measurement were achieved by importing the data into a desktop computer equipped with Premiere (Adobe, USA) [131].

### 4.1.3 Micromanipulation

The use of micromanipulation systems in microscopy has had a long history; since the development of the first microscopes in the 17$^{th}$ century biologists have desired the ability to manipulate the specimens they observed. The earliest record of a microdissection system has been attributed to Dujardin, who reported in 1835 a description of the microdissection of protozoan. A cotton fibre was placed under a cover slip and used to cut off sections of cytoplasm. The design overcame several technical issues that had affected previous designs. These included, single control, freedom from vibration, freedom from play (backlash or lost motion), variable sensitivity of control, limitation of movement to the field of view, robustness and price.

The development of micromanipulation diverged to satisfy the wide-ranging needs of an expanding scientific field, namely the differences between high and low resolution micromanipulators and microdissectors. One of the disciplines that was enabled by these developments was *in vitro* fertilisation (IVF). The first artificial fertilisation of a mammalian egg (mouse) by microinjection was reported by Lin and Clarke in 1966 [132]. The first human report came from Metka *et al.* [133] who injected single sperm into nine human oocytes, and the first human pregnancy after micromanipulation was reported by Ng [134].

A hydraulic system developed by Narishige was the style used in this work. The manipulators consist of a pair of 3 way low drift actuators equipped with coarse control (Figure 4.2), that were mounted to the left and right side of the microscope above the sample stage. The actuators were linked to the bench mounted fine control units by liquid filled capillaries. It was possible to mount a number of different devices onto the manipulators, including capillary holders, holding needles and the microsampling needle.

Figure 4-2 Photographs of Narishige micromanipulators. Reproduced from reference [135].

## 4.2 Cell culture techniques

Malt extract solid media (MES) as summarised in Table 4.1, were used in this work for the culture of fungal cells. Fungal strains, described fully in Chapter 5, were cultured using two plate types; the standard 9 cm Petri dish and a ultra-thin film dish.

Table 4.1 Components of malt extract solid media

| Compound | Quantity | |
|---|---|---|
| Malt extract | 2g | (2%) |
| Agar number 3 | 2g | (2%) |
| Distilled $H_2O$ | To 100 mL | |

### 4.2.1 Traditional culture technique

9cm Petri dishes were 30% filled with liquid media that were allowed to set under aseptic conditions, sealed with parafilm and stored at 4°C until required. Prior to use, the plates were warmed to room temperature and then inoculated with either spores or by sub-culturing, i.e. the transfer of a small agar block from an existing colony to the new plate. These plates were then inverted and incubated at 30°C for 24 hours.

### 4.2.2 Ultra-thin film culture technique

Traditional cell culture techniques could not be used with the inverted microscope, as the agar layer was too thick to view the cells through, and under prolonged periods of observation the cells became dehydrated. A humidity chamber culture technique based on common weigh boats (Fisher, UK) was used which resolved this problem. A weigh boat, with the centre of the base removed, was placed on a large glass microscope cover slip, heated slightly to allow it to flatten, then both were removed from the heat. When cool, the boat was dipped into a pool of liquid medium and then placed back onto the glass cover slip. This resulted in an agar film approximately 400 μm thick (Figure 4.3).

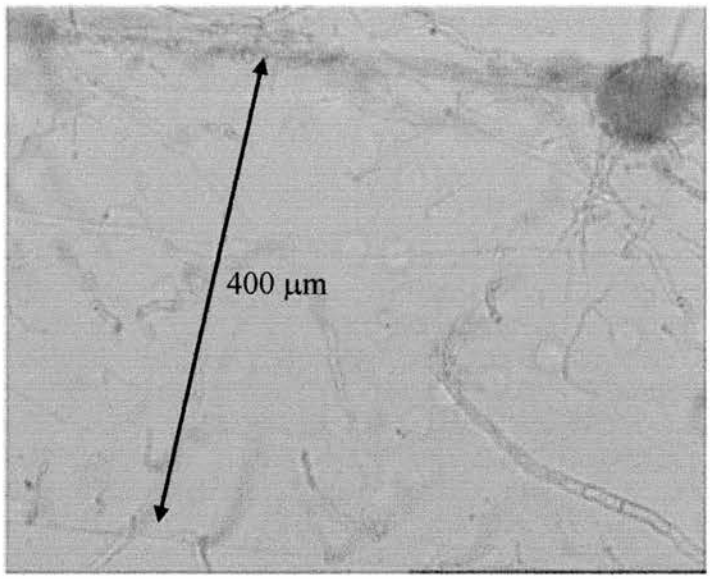


Figure 4-3 Cross section of ultra thin malt extract solid agar film. The fungal colony can be seen growing on the upper surface and penetrating into the agar.

Fungal cultures were then introduced to these plates by the addition of a small cube of agar containing traditionally cultured fungi. The plates were then placed into a 9cm Petri dish along with a disk of filter paper (Whatman, UK) moistened with distilled water. Incubation was then performed as described in Section 4.2.1.

### 4.3 Development of a microsampling system

Microsampling as a technique required the delicate combination of a number of pieces of equipment; the micromanipulators described above had to be appropriate for the size of cells under investigation, the microsampling needle had to be designed to allow the cell to be penetrated without rupturing and yet still allow material to be removed from the cell, and a device had to be attached to the needle whereby a positive or negative relative pressure could be applied to the needle in a controlled, rapid and accurate manner without causing vibrations in the manipulators and microscope. The common modern microsampling techniques have been developed from devices originally designed for use as microinjectors.

### 4.3.1 Sampling devices

Many different devices have been reported that are appropriate for use in microsampling research [65]. It is important to note that the instrumentation must be tailored to the properties of the specific cells of interest. These properties include, size, turgor pressure and culture conditions. During the course of this research, a number of devices were investigated. As discussed below, no appropriate microsampling device was available commercially and considerable development was required. It should be noted that microsampling from fungi required the use of micropipettes with a smaller tip OD than would be used for mammalian cells, due to the turgor pressure present within the cells. This had a knock on effect, in that a greater negative relative pressure had to be generated to compensate for the smaller tip OD. It was therefore not possible to use devices devised for sampling from mammalian cells without modification.

### 4.3.2 The galinstan system

The first device investigated was a galinstan based microinjection system, which used the heat-induced expansion of the liquid alloy, galinstan [136]. This alloy, a mixture of gallium, indium and tin, is placed in a glass capillary sealed at one end and tapered at the other to provide a pipette for microsampling. A tungsten heating element is coiled around a glass capillary, through which a constant flow of air is pumped (Figure 4.4, 4.5). The exit of this glass capillary is angled such that the gas passes over the galinstan filled pipette. By controlling the current in the heating element, it is possible to accurately control the temperature of the gas and thereby the volume of the galinstan. It was hoped that this could be used to aspirate cytoplasm from the cells.

It did prove possible to generate increased and decreased relative pressures that could have been used to draw and eject sample to and from the needle. It was also possible to show that the temperature could be accurately controlled. The device did, however suffer from a number of problems. It proved very hard to manufacture the needles; it could take an hour or more to fabricate a single needle and there was a high failure rate. A more important failing of the system was the slow reaction time

of the system. It could take almost twenty seconds after application of current to the heating coil for a full reaction to be seen in the pipette and, more importantly for its use as a microsampling device, it would take up to one minute for the sampling pipette to cool after removal of the heat source and the galinstan to contract. The device also suffered from problems associated with the low swept volume of the system.

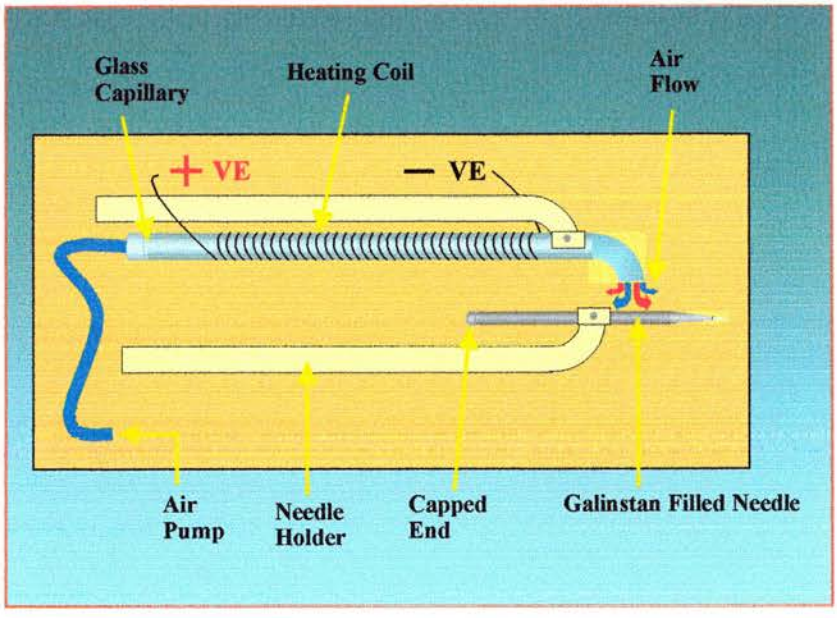


Figure 4-4 Schematic diagram of the galinstan microsampling device. A tungsten heating element is coiled around a glass capillary, through which a constant flow of air is pumped. The exit of this glass capillary is angled such that the gas passes over the galinstan filled pipette. Reproduced from reference [137].

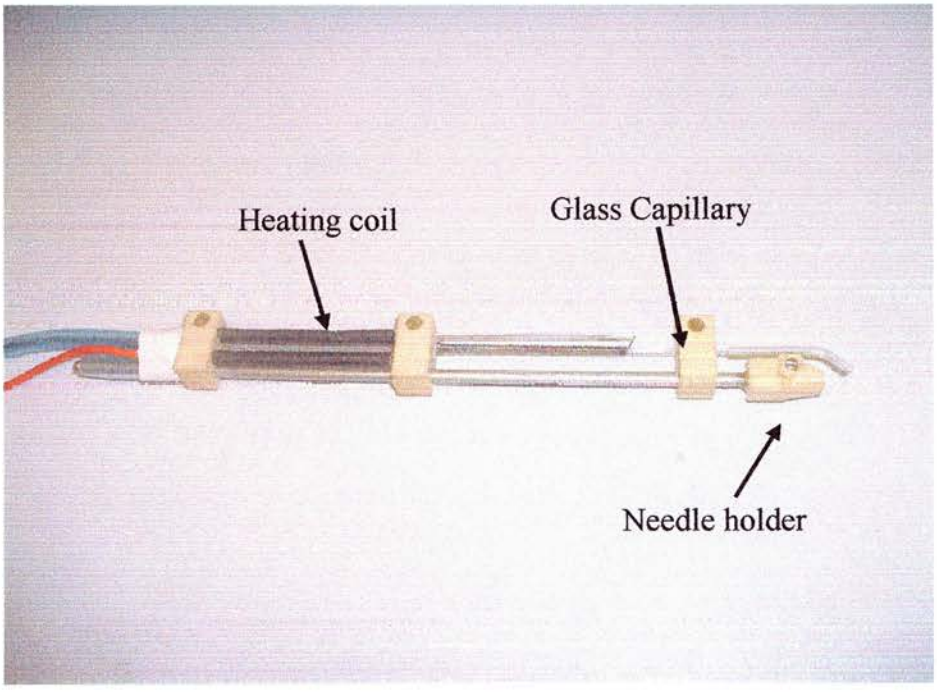


Figure 4-5 Photograph of the galinstan microsampling device

### 4.3.3 The UltraMicroPump-II

The UltraMicroPump-II (WPI, USA) consists of a computer controlled electro-mechanical syringe pump that was connected to a pulled microsampling needle by an oil filled length of Teflon tubing and an aluminium needle holder. The motorised pump could be controlled by a computer, whereby the syringe plunger is moved by set distances, producing negative or positive relative pressures, at a level determined by the diameter of the syringe. The greater the diameter of the syringe, the greater the change in the pressure produced per step.

The system suffered from a lack of precision. The steps that the pump could be moved through were too crude to be applicable to fine microsampling.

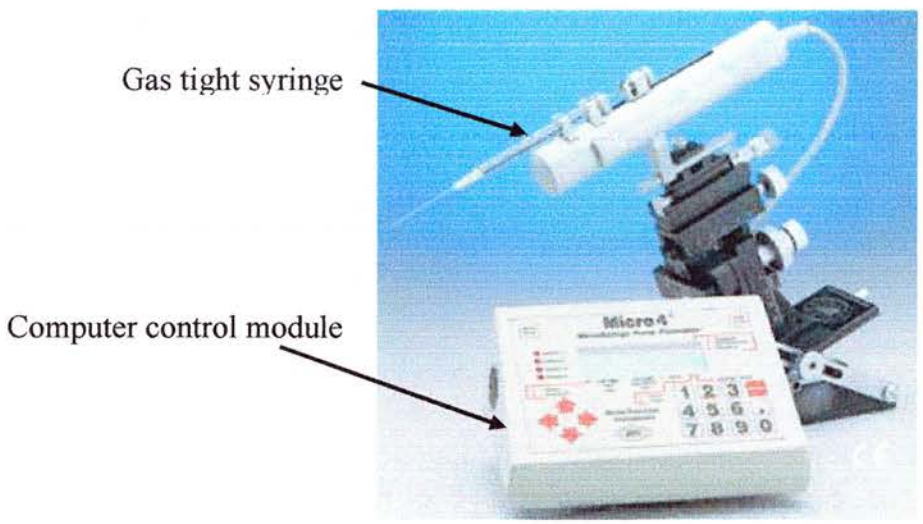


Figure 4-6 Photograph of the computer controlled syringe system. Reproduced from reference [138].

### 4.3.4 The plant pressure probe

The plant pressure probe, previously mentioned in Chapter 1, once modified, was used throughout this research [139]. It was originally developed as an instrument to measure and manipulate the intra-cellular hydrostatic pressure of plant cells and was

used to map cell turgor pressure in space and time in response to water stress [140]. The earliest reference to a pressure probe device describes a water and air filled glass capillary that could be used to measure the turgor pressure in giant algae cells by relating the compression of an air bubble to cell hydrostatic pressure [141]. The device was improved by replacing the air bubble with an electronic pressure sensor, attached to an oil-filled capillary and a piston that could by varied to affect of the intra-cellular turgor pressure [142]. Since then it has been successfully modified for the measurement of hydrostatic pressure in different plant environments, including roots, leaf cells and xylem. A schematic diagram showing the various components of a typical pressure probe is given in Figure 4.7.

The first description of the use of the device for microsampling was in 1989 [143], when it was used to remove cell sap from individual plant cells for analysis. The reported smallest sample that has been aspirated from a cell using this device was 0.5 pL which was analysed for mannitol and hexos [144].

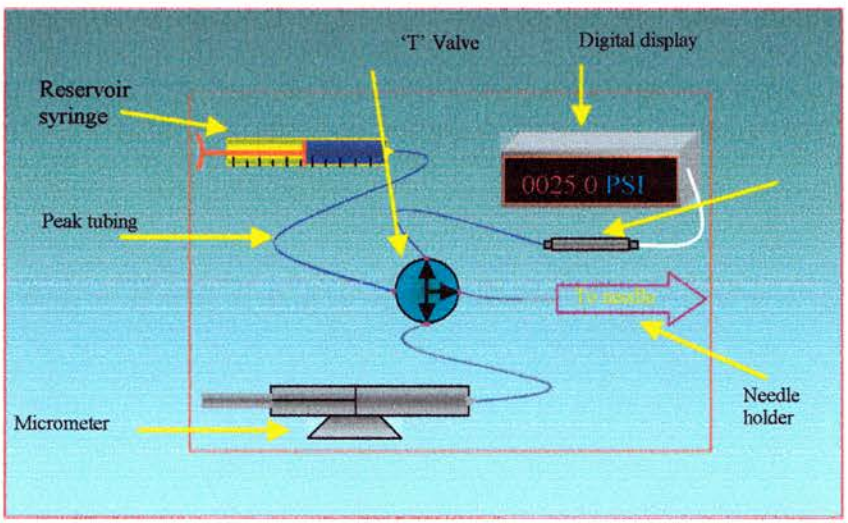


Figure 4-7 Schematic diagram of the plant pressure probe. Reproduced from reference [137].

In the pressure probe used in this work a high precision micrometer (Narishige, JP) [135] was employed, that acted on a 250 μL gas tight syringe (SGE, AU) [145]. The syringe was connected to the rest of the system by a 4-way valve, whereby the syringe could be alternately connected to either a reservoir of oil, to allow refilling of the syringe, or the needle holder and microsampling needle. Irrespective of the position the valve is in, a pressure transducer (Druck, DE) [146] is in contact with the column of oil. The resulting display of the relative pressure within the system could be used to aid microsampling by providing a warning of possible extremes of pressure. A photograph of the modified version of the pressure probe used in this work is given in Figure 4.8.

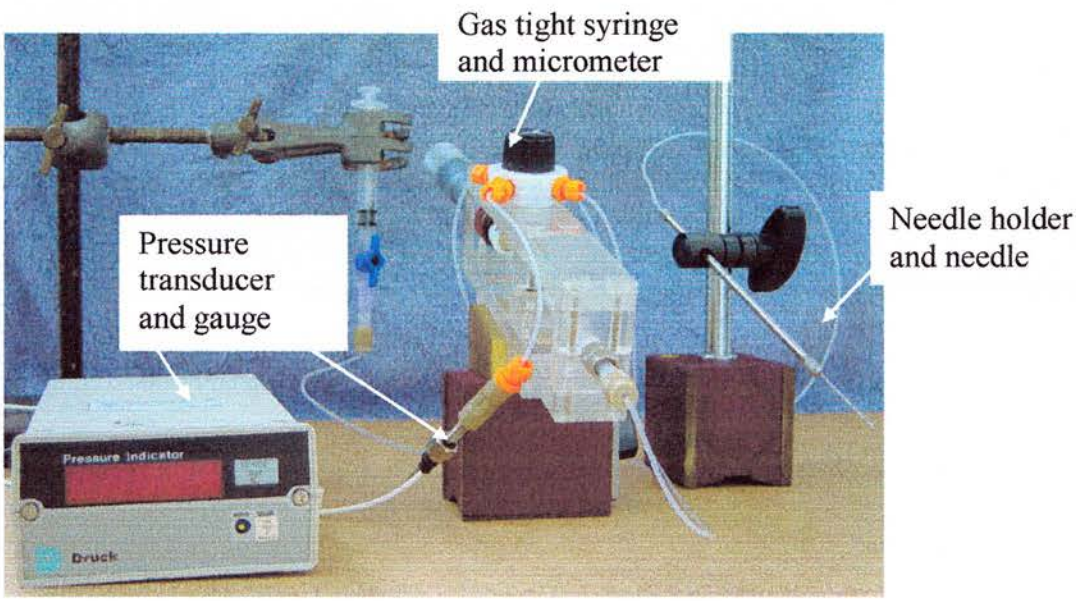


Figure 4-8 Photograph of the modified pressure probe.

It was necessary to further modify the device to meet the requirement of this project. It was found that the silicone oil (BDH 200 100cs silicone fluid) used in the pressure probe restricted the application of negative relative pressures, as gas present in the oil tended to exsolve, forming gas bubbles in the capillary. The formation of these

bubbles then further restricted the application of negative relative pressures through expansion. Degassing the oil, by vacuum, prior to filling the system, improved the situation, but did not cure it. Flushing and refilling of the system was also required prior to each experiment. The silicone oil's viscosity also caused a slow reaction time between the change in pressure at the piston, and the reaction at the capillary tip. Following experimentation with a number of fluids, it was decided that fluorinert FC-77 (3M, USA) offered the best properties and appeared to resolve the problems. This fluid did not exsolve gas, and therefore did not require degassing, and it was possible to apply far greater negative pressures than were possible with silicone oil, even when degassed. The oil also exhibited reduced viscosity and improved the system's response to pressure changes induced by the syringe.

### 4.3.5 Microsampling needles

The early micropipettes were originally developed for use in neurophysiology research and provided the technical basis for major advances [147]. Improvement of these early needles was hindered by limitations in microelectrode fabrication techniques; as a result, the study of systemic intra-cellular environments was confined almost entirely to the study of large cells. These early needles were fabricated using simple instruments whereby a weight was suspended under a mounted borosilicate capillary. The capillary was then locally heated causing it to be pulled into a pair of needles. A breakthrough came with the development of a micropipette puller that was to become the forerunner of most modern instruments [148]. The innovation of this electrode/needle puller, that is still crucial for today's pullers, was that it could produce very fine tips, accurately and reliably. It was the incorporation of features, such as air-cooling of the capillary, to produce shorter needle tips [149], and the two-stage horizontal puller, providing a smooth and consistent pull, that provided the reliability of this instrument. The pullers in use today still follow this design, with the only significant improvement being the addition of a computerised control to allow multi-stage pulls.

The micropipettes suitable for microsampling vary widely depending on the organism under investigation. Mammalian cells, lacking both cell walls and turgor

pressure present less of a problem for microsampling. The needles can have wide tip ID and a bevel that is used to create a sharp tip to penetrate the external cell membrane. This design of needle was inappropriate for plant and fungal cells, where the cell wall maintains a cell turgor pressure. Suitable needles would have a narrow outside diameter (OD) (4 μm) and no bevel, to avoid rupturing the cell.

The most reliable method found to create suitable microsampling needles for use in this work was to use the Sutter Flamin/Brown (Linton Instruments, UK) Model P-97 programmable microprocessor controlled needle puller (Figure 4.9) in conjunction with borosilicate capillaries (Harvard Apparatus Ltd, Kent, UK) of dimensions 1.17 mm ID and 1.5mm OD. This instrument allows the precise control of the pulling parameters, hence allowing the design of specific needles for use as microsampling and holding pipettes. Features that enable highly reproducible needles to be made include an environmental chamber with programmable air pressure, self-contained air filtration system and humidity control.

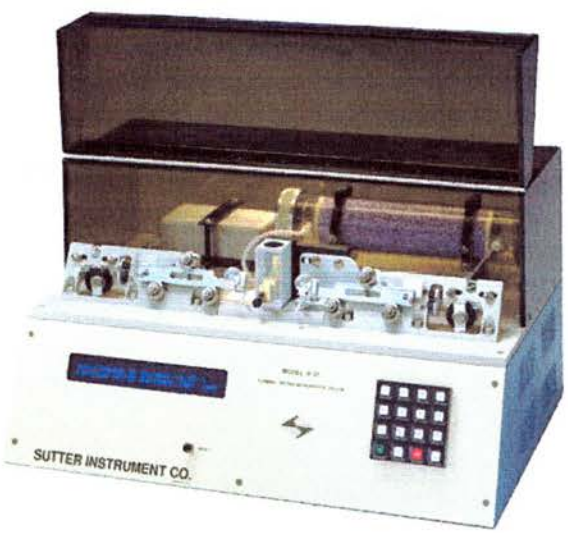


Figure 4-9 Sutter Flaming/Brown Model P-97 programmable microprocessor controller needle puller. Reproduced from reference [150].

### 4.3.6 Microsampling pipette fabrication

Needles were pulled using a multistage program. This increased the ability to refine the parameters of the needle and resulted in needles of the form shown in Figure 4.10. The key requirements for the needles were a narrow tip OD and a shallow angle of expansion of the needle OD. The only method for developing a needle shape was by empirical experimentation, that is, to pull a needle, test it and then modify a variable in the program. This was repeated until a suitable needle was found. On a day-to-day basis, the instrument was found to provide a high level of reproducibility between batches as well as between individual needles. It should be noted that it was necessary to modify the program occasionally, for example when the heating element aged and particularly after it was replaced, as the needle shape produced would vary slightly.

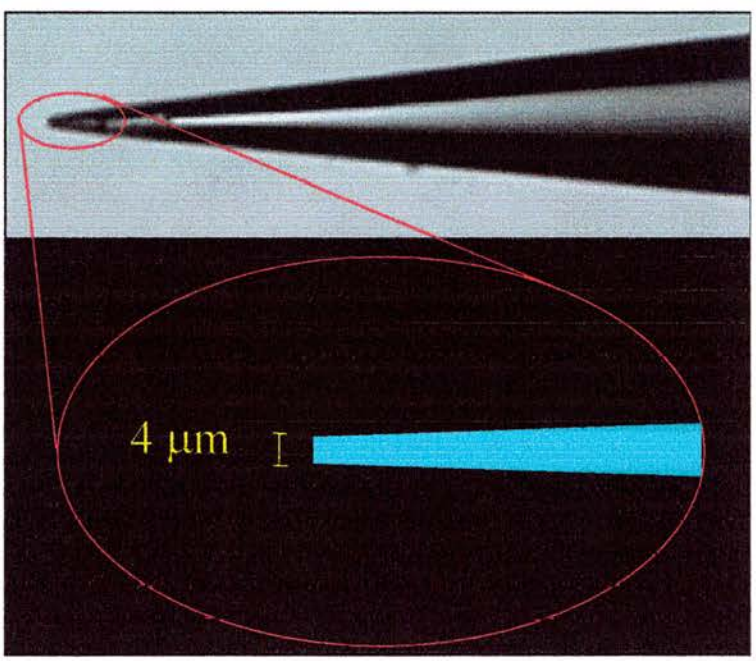


Figure 4-10 Photomicrograph of microsampling pipette.
(Above) microscope image of microsampling pipette.
(Below) magnified schematic of the tip region of the pipette.

### 4.3.7 Calibration of the microsampling pipettes

One aim of this research was to develop a quantitative technique, in terms of volume of cell sap and not the percentage of dry mass, for the determination of the levels of various target molecules in small volume of cell extract derived from fungal cells. In order to perform this task, it was of particular importance that the volume of cytoplasm aspirated from the cells was calculated accurately.

To this end, a method by which the volume of the sample collected in the microsampling pipette could be determined by observation with the microscope and imaging system was devised. The easiest method was to determine a correlation between the external volume of the pipette and the volume it contained. This was achieved by filling the pipette with random volumes of water, then dispensing its content into a reservoir of silicone oil (Figure 4.12). The liquid formed a perfect sphere from which the volume could be calculated by measuring the sphere diameter. The sphere volume could then be related to the height (A) of the liquid in the pipette (Figure 4.11 and Table 4.2, Figure 4.13). Taking the wall thickness (C-D) of the pipette into account significantly improved the accuracy of the calculation. The results of these experiments were used to plot a calibration curve that related the volume of the sample to the geometry of the needle as viewed under the microscope. This was performed following every change to the needle pulling program and following the instillation of a new filament in the puller, as both affect the internal and external dimensions of the needle. This allowed the volume of the sample to be directly compared to the geometry as the needle as viewed under the microscope.

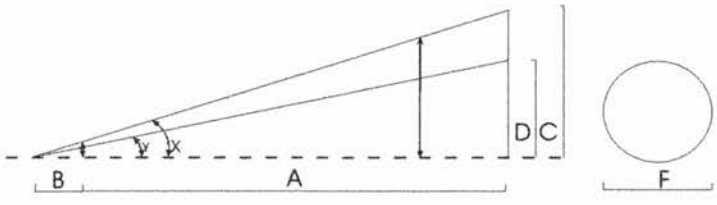


Figure 4-11 Diagram of the dimensions of a microsampling pipette.

Table 4.2 Example of calibration data relating dimensions of a microsampling pipette to the sampling volume

| Micropipette dimensions | | | | | | Volume of sample (nL) | Volume of sphere (nL) | Error (%) |
|---|---|---|---|---|---|---|---|---|
| A+B (μm) | A (μm) | B (μm) | C (μm) | D (μm) | F (μm) | | | |
| | | | | | | | | |
| 733.00 | 720.00 | 13.00 | 50.50 | 48.29 | 150.20 | 1.77 | 1.77 | -0.14 |
| 665.00 | 652.00 | 13.00 | 46.00 | 44.00 | 135.74 | 1.33 | 1.31 | 1.55 |
| 644.00 | 631.00 | 13.00 | 44.55 | 42.61 | 130.77 | 1.21 | 1.17 | 3.01 |
| 631.00 | 618.00 | 13.00 | 43.65 | 41.75 | 128.36 | 1.13 | 1.11 | 2.36 |
| 626.00 | 613.00 | 13.00 | 43.31 | 41.42 | 127.32 | 1.11 | 1.08 | 2.37 |
| 555.00 | 542.00 | 13.00 | 38.39 | 36.72 | 111.49 | 0.77 | 0.73 | 5.48 |
| 524.00 | 511.00 | 13.00 | 36.25 | 34.67 | 105.59 | 0.64 | 0.62 | 4.03 |
| 480.00 | 467.00 | 13.00 | 33.21 | 31.76 | 96.73 | 0.49 | 0.47 | 3.13 |
| 464.00 | 451.00 | 13.00 | 32.10 | 30.70 | 92.34 | 0.44 | 0.41 | 6.64 |
| 444.00 | 431.00 | 13.00 | 30.72 | 29.38 | 89.10 | 0.38 | 0.37 | 3.40 |
| 347.00 | 334.00 | 13.00 | 24.00 | 22.96 | 67.17 | 0.17 | 0.16 | 9.21 |
| 322.00 | 309.00 | 13.00 | 22.28 | 21.30 | 61.91 | 0.13 | 0.12 | 8.47 |
| 269.00 | 256.00 | 13.00 | 18.61 | 17.80 | 50.06 | 0.07 | 0.07 | 7.99 |

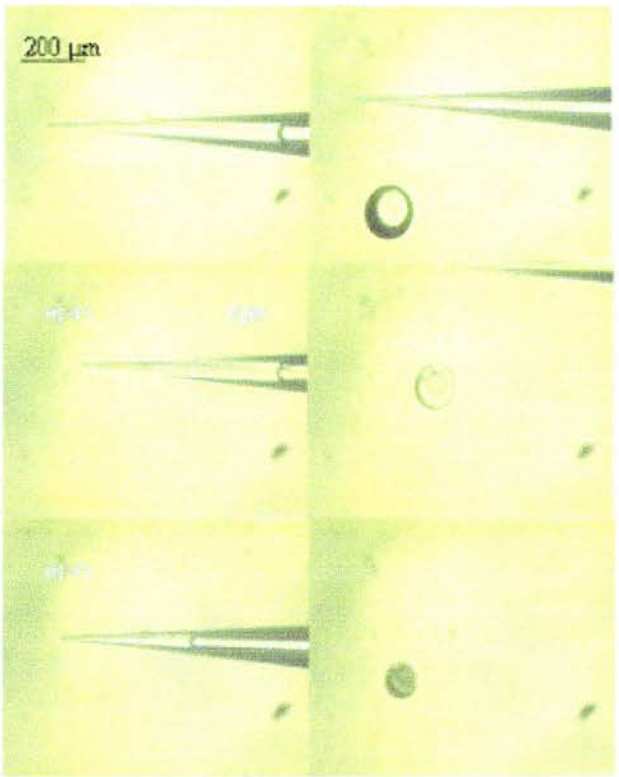


Figure 4-12 Series of video images showing filled micropipettes and the volume of droplets dispensed under oil.

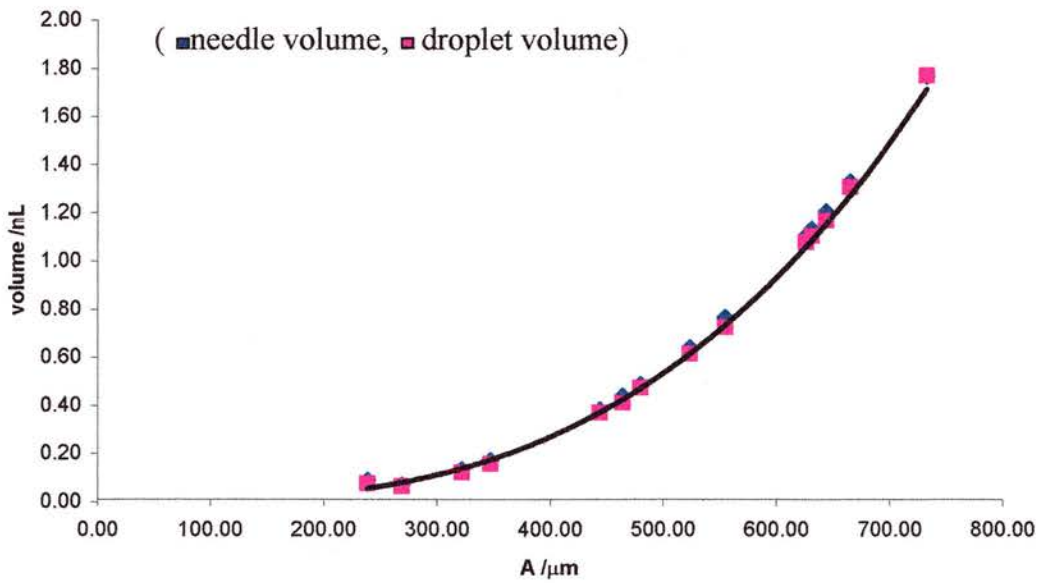


Figure 4-13 Typical calibration graph of sample volume versus observed height (A) of liquid in micropipette.

## 4.4 Microsampling technique

The microsampling technique used in this work was performed on the Nikon TE200 inverted microscope (Section 4.1.1) using the Narishige micromanipulators (Section 4.1.3). The modified pressure probe was, after extensive testing, found to be the most appropriate device to generate the negative relative pressures required for extracting intra cellular samples and a number of microsampling needle designs were tested before an optimum shape was chosen (Section 4.3.6).

By applying a thin covering of silicone oil into the modified culture vessel, the risk of desiccation during long periods of observation and micromanipulation was prevented. The growth rate and properties of the fungal colonies for the strains used (Chapter 5) did not appear to be affected by the use of these techniques even during prolonged observation with a low power visible light source (20-30 min). An additional advantage of the silicone oil was that it was found to be immiscible with the fungal samples and the FC-77 Fluorinert oil that was used in the microsampling apparatus. As a result, if silicone oil was drawn into the sampling needle, it could be clearly distinguished from the Fluorinert, CE running buffer and cell extract, allowing corrections to be made. The differing densities of the oils also meant that when Fluorinert was ejected from the needle tip, it quickly sank and did not interfere with the microsampling.

Prior to performing a sampling event, the relative pressure in the microsampling system was adjusted to be slightly positive relative to atmospheric pressure. This was to reduce the possibility of the uptake of any extra cellular matrix into the pipette prior to penetration of the cell. Microsampling was performed by identifying the target cell compartment using the microscope, then by altering the focus of the microscope to slightly above the cells of interest. The oil filled microsampling needle and a holding pipette could be positioned above the cell on either side without the risk of colliding with the cell or agar. The focus was then returned to the target cell and the holding pipette moved to be touching the cell directly opposite the proposed microsampling site. The microsampling needle was then moved into position alongside the cell and, as smoothly as possible, moved to penetrate the cell.

Figure 4.4 shows a series of video images for microsampling from a single hyphal compartment of the wild type of *Neurospora crassa*. The turgor pressure of the cell would often initially force cell content into the microsampling pipette. This process was then aided by reducing the relative pressure in the microsampling system so as to draw further sample into the pipette. Once a suitable volume was aspirated, the pipette was withdrawn and lifted above the cells.

### 4.5 Fungal extract transfer techniques

Although the three steps (sampling, transfer and analysis) required for any SiCSA technique are described and discussed in separate sections, it was shown to be critical that the individual steps are continuous. The most important step was the transfer of the sample from the microsampling needle to the separation capillary. Exposure of the sample to the atmosphere leads to increased problems associated with evaporation and contamination. Samples of 50 pL exposed to the atmosphere can be seen to evaporate within a fraction of a second (Figure 4.15). To limit this effect, the sample, once acquired from the cell was immediately transferred to the CE capillary for separation prior to mass spectrometic analysis without ever being exposed to the atmosphere. The small volume and relatively low concentration of analytes also meant that any contamination resulting from unclean equipment could lead to erroneous results.

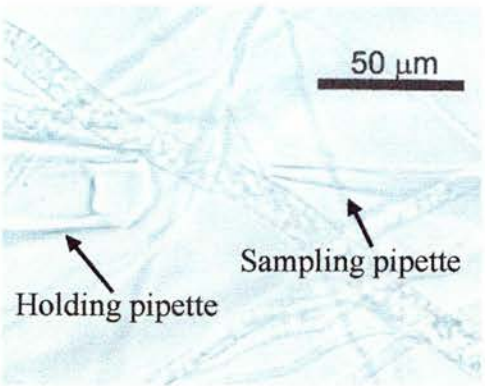


Holding needle is positioned opposite microsampling needle.

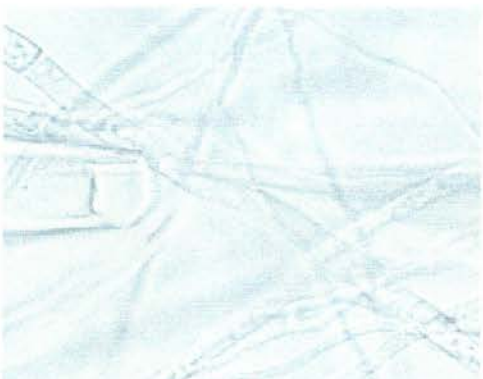

Hyphae braced by holding needle as stabbing motion of micromanipulators is used to penetrate the hyphal compartment.

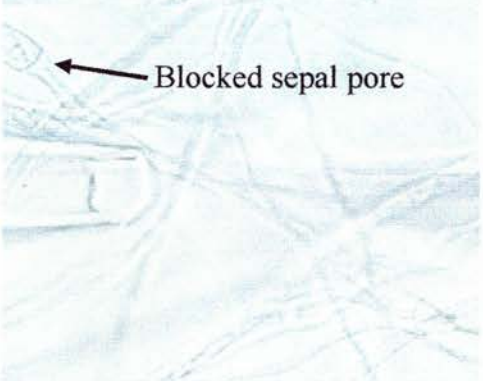


As compartment is penetrated, the septal pores are blocked and cytoplasmic streaming is stopped.

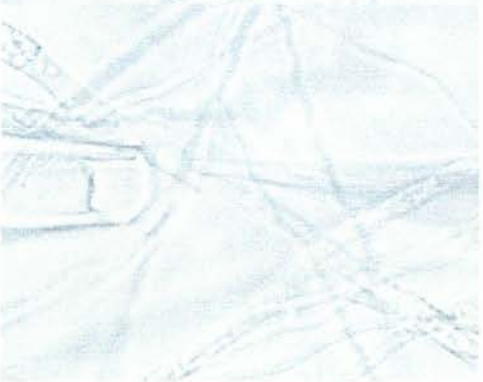

Reducing the relative pressure in the pressure probe allows the entire contents of the compartment to be aspirated. The walls of the compartment are drawn together.

Figure 4-14 Series of video images illustrating microsampling from a single hyphal compartment of *Neurospora crassa* (wild type).

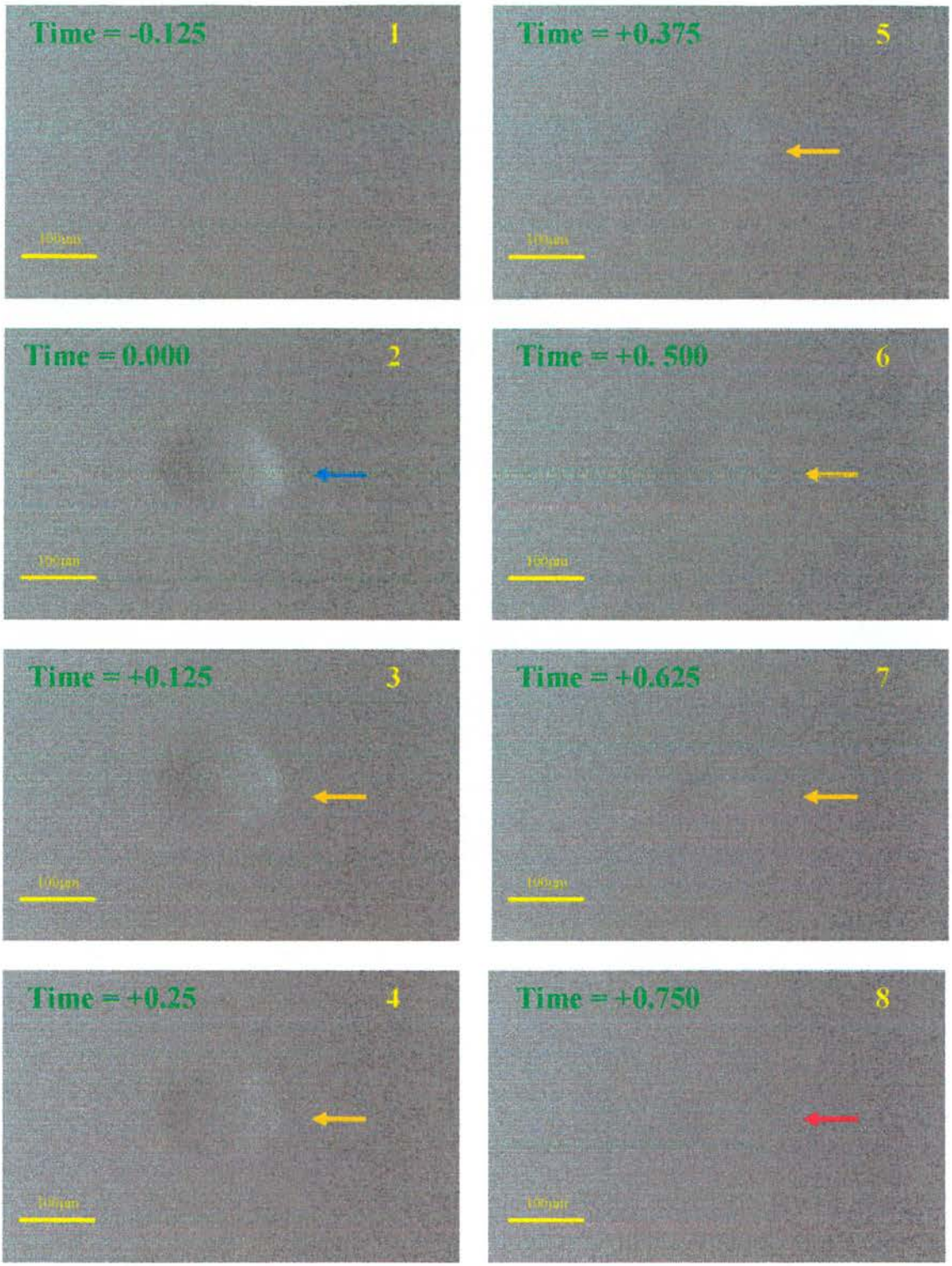


Figure 4-15 Series of video images illustrating the evaporation of a 56 pL water droplet on a glass slide at 22°C.

The transfer of cell extract from the microsampling pipette to the separation capillary was performed in the silicone oil bath under the microscope. Transfer of the sample above the culture vessel, in the atmosphere was investigated but was found to be unreliable. As the silicon oil was not found to affect the following CE separation, it was decided to perform all extract transfers under oil. Many previously published techniques that relied on UV absorbance and other on-capillary detection strategies were able to employ a slight negative relative pressure at the outlet reservoir of the separation capillary [66,36,33,39]. This method of drawing a sample into the capillary was not possible in the current work where ESI MS was used as a detection strategy, since the capillary terminates in atmosphere at the mass spectrometer interface. It was, however, possible to create a slight pressure gradient across the capillary by lifting the capillary inlet slightly (~2 cm) above the level of the capillary outlet.

Transfer was achieved by replacing the holding pipette used during microsampling with the separation capillary. It was found that the condition of the cut face of the capillary was critical, as an uneven face made accurate positioning of the microsampling pipette relative to the capillary inlet unreliable. The tip of the microsampling pipette containing the sample was positioned directly in front of the inlet of the separation capillary. A slight positive pressure was applied to the pipette forcing the sample out of the pipette and onto the face of the capillary. Figure 4.16 shows a series of video images illustrating this sample transfer procedure. The slight pressure difference across the capillary caused by the variation in heights of the inlet and outlet draws the sample into the capillary. The variation in height across the separation capillary was found to be critical. If the entrance to the capillary was too low relative to the exit, the sample would not be drawn into the capillary and could result in mobile phase leaking from the capillary into the oil bath. If too high, silicone oil surrounding the capillary would be drawn in before the sample was ejected into the capillary entrance, requiring the capillary to be flushed with fresh running buffer.

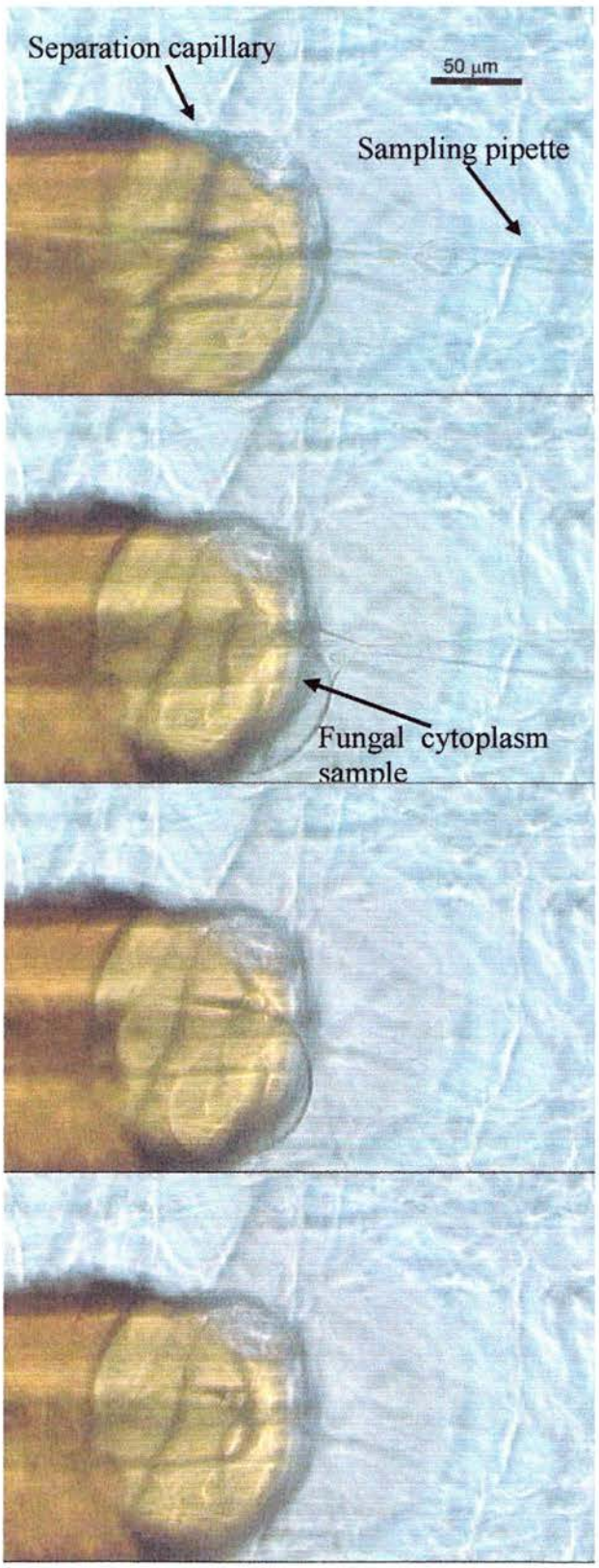


Microsampling pipette containing sample is brought close to the capillary

By increasing the relative pressure in the pressure probe, sample can be ejected into the entrance of the capillary.

Surface tension draws the sample into the capillary

Sample is loaded and the capillary is then transferred to the inlet reservoir (not shown).

Figure 4-16 Video images illustrating the sample transfer procedure

Early sample transfers were performed in the layer of silicone oil directly above the fungal cells. Although this was a more reliable technique, as samples were often lost as the pipette is lifted from the oil, the problems associated with the risk of sample contamination from the extra cellular matrix ruled out this method. Instead, the sampling pipette containing the aspirated cell extract was transferred to a fresh reservoir of silicone oil and the transfer was performed as described above. Following transfer, the capillary could be removed from the micromanipulator and the inlet placed in the mobile phase reservoir.

## 4.6 Separation

### 4.6.1 Properties of fused silica capillaries

The fused silica capillaries used in this work were purchased from Composite Metal Services (Worcester, UK). Although several experiments were performed using square cross section tubes, little advantage was found to compensate for the additional cost and limited selection of sizes. Therefore, the majority of the work was performed in circular cross section tubes [151,152]. The capillaries are commonly supplied with a coating of polyimide, but a less robust transparent Teflon coating is also available. (The majority of the separation work was performed using 50 ±0.3 μm ID and 192 ±0.6 μm OD. These offered advantages for CE-MS, which will be discussed in Section 4.8.2.)

Fused silica is inert to the majority of chemical attack, and provides good electrical insulation and temperature stability (Table 4.3). Although as supplied, with its coating of polyimide, it is very robust, if scratched moisture can reach the bare fused silica and it can become brittle [153,154]. In addition, over time the ends of the tubing exposed to the atmosphere also become brittle and must be discarded.

Table 4.3 Table of the characteristics of fused silica [155].

| | |
|---|---|
| Electrical resistivity | $2x10^4$ ohm cm at 20 °C |
| Optical transmission range | 0.18 to 3.5 μm |
| Chemical resistance | Inert to most elements and compounds.<br>No reaction with acids at any temperature except phosphoric which reacts at 200°C and hydrofluoric which reacts at all temperatures<br>Slow reaction with alkalis at normal temperatures |
| Homogeneity | Completely homogeneous and free from the addition of fluxes or foreign material. |
| Pressure tolerance in capillaries | Pressures of $10^5$ psi ($0.69 x10^9$ Pa) |

### 4.6.2 Mobile phases suitable for CE-ESI-MS

The choice of mobile phase used in capillary electrophoresis is critical for obtaining successful separation of the analytes. The list of electrolytes and additives that could be used is extensive [156]. When choosing a mobile phase that is suitable for a CE separation where the detection will be performed by ESI mass spectrometry, the list is more limited. The use of a liquid sheath flow greatly increases the range of buffers that can be employed, due to the effective dilution of the low CE elution flow (50 nL/min) by the much larger volume of liquid from the sheath (230 nL/min). It was possible to employ either aqueous or mixed aqueous /organic buffer solutions. However, in this work the most successful approach involved the use of aqueous buffers provided that an organic buffer was supplied via the sheath flow to aid the electrospray process. The most widely used CE separation buffer and the one chosen for the majority of the experiments presented in this thesis was ammonium acetate although an investigation of the use of ammonium bicarbonate was also performed. The decision to use these buffers was made primarily due to their volatility and their compatibility with biological matrices. Although buffer concentrations up to 0.1M have been reported, the optimum sensitivity was achieved by minimizing the concentration and an optimum was found to be 10 mM ammonium acetate. The use of surfactants, although common practice in stand-alone CE which uses UV

detection, was avoided in this work as they result in intense non-analyte signals in both positive and negative ion ESI.

Formic acid was used as a proton source in the sheath flow. This was chosen over acetic acid, as early investigations revealed a broad range of background ions that were associated with the use of acetic acid.

The separation capillary used in the SiCSA experiments was substantially longer than is typical for CE-MS, due to the requirement for the capillary to extend to the microscope stage for sample loading. A number of experiments used laser induced fluorescence (LIF) detection for extra-cellular markers. The use of this technique also required the capillary length to be extended to incorporate the detector. Typically, CE is performed at potential gradient of 500 $Vcm^{-1}$. Unfortunately due to the length of capillary required for the SiCSA experiments and the limitations of the available power supply, a potential gradient of only 290 $Vcm^{-1}$ could be applied. As a result, the separation time increased to nearly forty minutes compared with ten minutes for a typical CE-MS run. As it was not possible to increase the voltage with our instrument past 25 kV, it became important to maximize the EOF. This was achieved by increasing the pH of the mobile phase with the addition of ammonia resulting in a buffer pH of 8.5. This significantly increased the EOF and reduced the analysis time to approximately ten minutes.

### 4.6.3 Separation instrumentation

The 3850 Capillary Electropherograph (Isco, USA) employed in these experiments was designed to be used as a stand-alone CE device offering tuneable absorbance detection. It originally possessed all the components of a stand-alone CE instrument; a tuneable (190 to 360 nm) absorbance detector, a high voltage power supply, some means of standardizing sample injection and method of flushing the capillary. The power supply was originally capable of generating electrical potentials of between -30 and +30 kV. In reality the power supply was incapable of producing over 25 kV in either +ve or –ve modes due to internal electrical discharge.

Sample introduction would normally have been performed by either electrokinetic or vacuum injection. The injection timing apparatus allowed the instrument to provide

accurately timed electrokinetic injections at a potential of 5 kV with a rise time of approximately 1 s.

Capillary flushing was performed manually, by connecting the inlet to a gas tight syringe and pushing 0.1M NaOH through the capillary. The Isco absorbance detector capillary guides were designed to function accurately with a 360 μm OD capillary. The use of 192 μm OD capillaries, in this work, dramatically reduced the reliability of the detector. The reduced path-length of the 50 μm ID capillary also reduced the sensitivity of the detector. The detector was capable of performing single channel absorbance detection in the range from 190 to 360 nm (deuterium lamp). Absorbance data was output as an analogue signal, with a full range of either 10 mV or 1 V. Electronic smoothing of the output was performed, with a time constant of 0.8 s commonly used.

### 4.6.4 Modification of the capillary electropherograph for use in SiCSA

In an effort to limit the length of separation capillary between the microscope and the mass spectrometer, it was found that it was best to position the Isco CE farthest from the microscope and perform CE on a small polythene stage located between the microscope and the mass spectrometer (Figure 4.17). The electrical supply from the Isco was connected to a platinum electrode that could be dipped into either a sample or mobile phase by a length of high voltage electrical cable. In later experiments, a laser induced fluorescence detector was positioned close to the mass spectrometer interface.

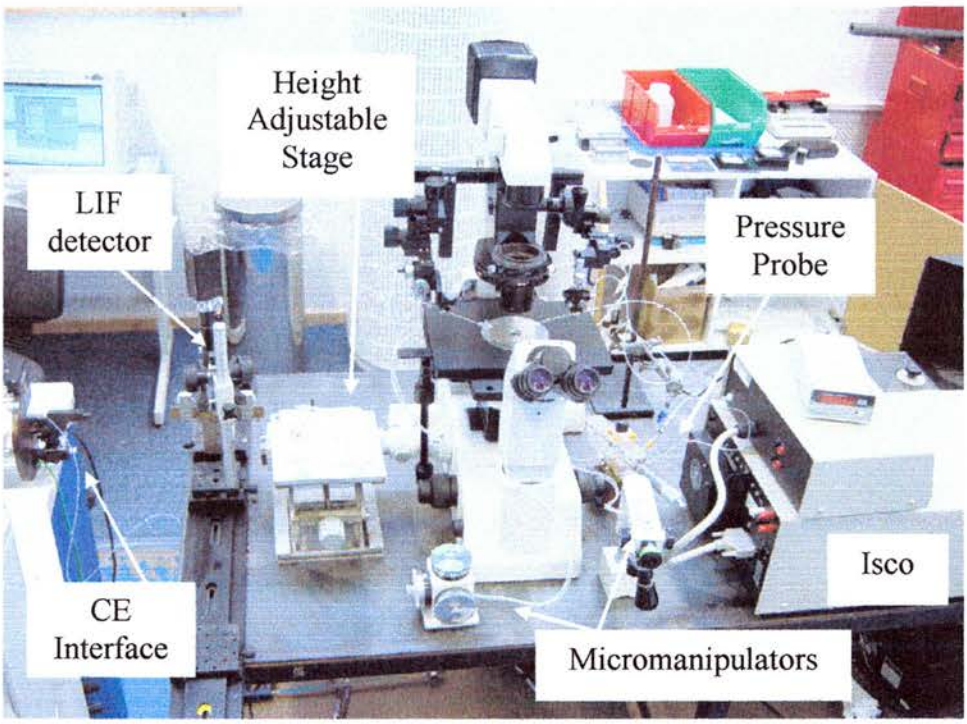


Figure 4-17 Photograph of apparatus used to perform SiCSA experiments

This style of interface although allowing the shortest possible length of capillary to be used, posed significant risk of electrocution. Every effort was taken to limit the risk by placing insulating barriers between live components and the operators. The apparatus was never left unattended when running.

A typical CE run would be performed in a fused silica capillary of internal diameter 50 μm, external diameter of 192 μm and a total length of 860 mm (from the inlet to outlet at the mass spectrometer). All new capillaries were conditioned by rinsing for 30 min with 0.1 M NaOH solution, to etch the inner surface of the capillary, exposing more silanol groups and cleaning poisoned surfaces to increase the EOF. It was often noted that there would be a significant increase in the EOF over a period as the capillary was repeatedly etched. Between runs, the capillary was washed for two minutes with 0.1 M NaOH, one minute with water and finally two minutes with running buffer. All standards, described in the following chapters, were loaded by electrokinetic injection (5 s at 5 kV) resulting in an injection volume of 2.93 nL. CE separation was carried out using a potential of 20 kV. Although the Isco instrument

was capable of performing vacuum injection, when used for CE-MS this style of injection is not feasible as it is not possible to apply the vacuum to the capillary outlet. All experiments were performed with positive polarity (inlet anodic).

A make up flow (50:50 (v:v)methanol:water 1% formic acid) was supplied to the CE-MS interface at a flow rate of 0.23 μL/min by syringe pump. Nitrogen desolvation gas was applied axially to the sample and an electrospray voltage of 4.5 kV was used. The interface, discussed later in Section 4.8.2, was positioned orthogonally to the inlet of the mass spectrometer.

## 4.7 Laser induced fluorescence

Laser induced fluorescence (LIF) is a visible light emission produced by molecules on absorption of electromagnetic radiation. A photon of energy is supplied by an external source, in this case by a laser. The photon is absorbed by the molecule, promoting it to an excited electronic state. The molecule then decays from this excited state in a finite length of time (know as the excited state lifetime). During emission, photons are emitted and a lower molecular energy state, commonly the electronic ground state is attained. Due to energy dissipation during the excited-state lifetime, resulting from internal relaxation amongst the different rotational and vibrational levels within the excited state, the energy of the photons produced is lower, and therefore of longer wavelength than the excitation photon.

A key disadvantage of this technique is that not all molecules fluoresce. Conversely, the advantages of using LIF as a detection technique include its low background reading compared with signal strength, high sensitivity, high speed (excited-state lifetimes are commonly in the region of $1\times10^{-9}$ to $1\times10^{-10}$ s), and the unlikelihood that the molecule under investigation will be affected or destroyed by the technique.

### 4.7.1 LIF instrumentation

Excitation was performed using a 543 Argon Ion laser (Omnichrome, USA). A 'window', 20 mm in length, was burned in the polyamide coating of the capillary, leaving the transparent silica capillary visible, held in a specially constructed 'clamp' device. A microscope (Prior Scientific, USA) and a PE2015 CCD camera (Pulnix, USA) were positioned above the window (Figure 4.18). An OG550 glass filter (Schott, USA) was placed in front of the CCD camera to block out the excitation

wavelength, which would interfere with the observation of the fluorescence of the rhodamine 6G analyte. The camera was then positioned so as to provide as sharp an image of the capillary as possible. The resultant images were recorded using a digital video recorder and converted into sequences of bitmap files, showing both the progression of the fluorescent 'plug' in the capillary and also the shape of the solute band (Figure 4.19 and 4.20).

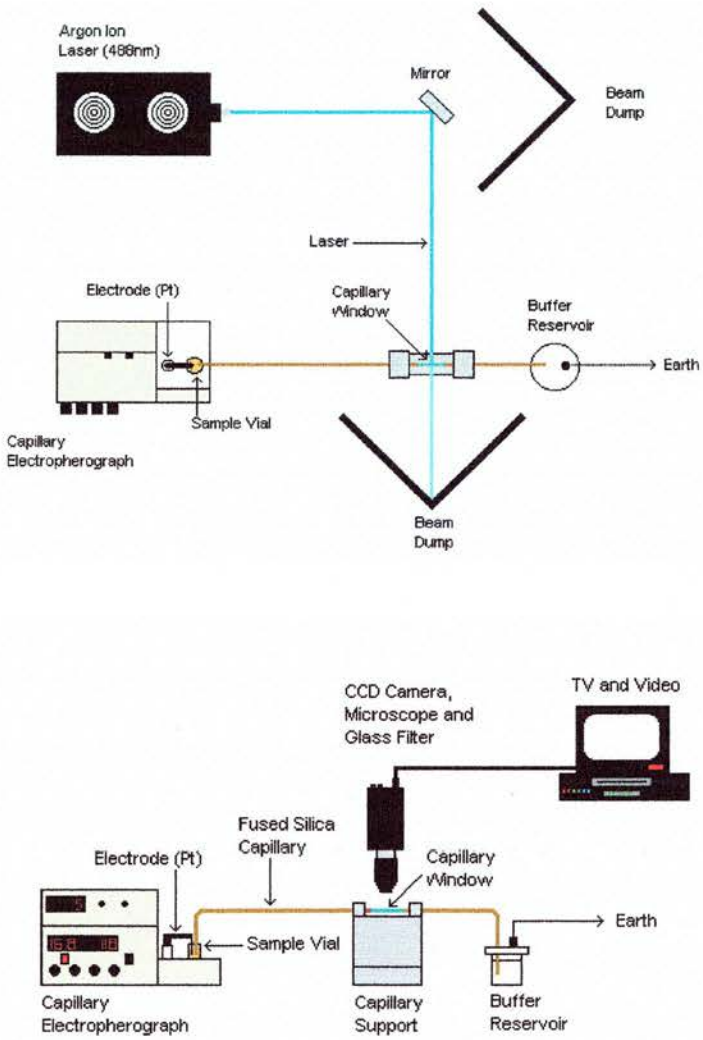


Figure 4-18 Upper: Schematic diagram of the LIF excitation apparatus.
Lower: Schematic diagram of the LIF detection apparatus.

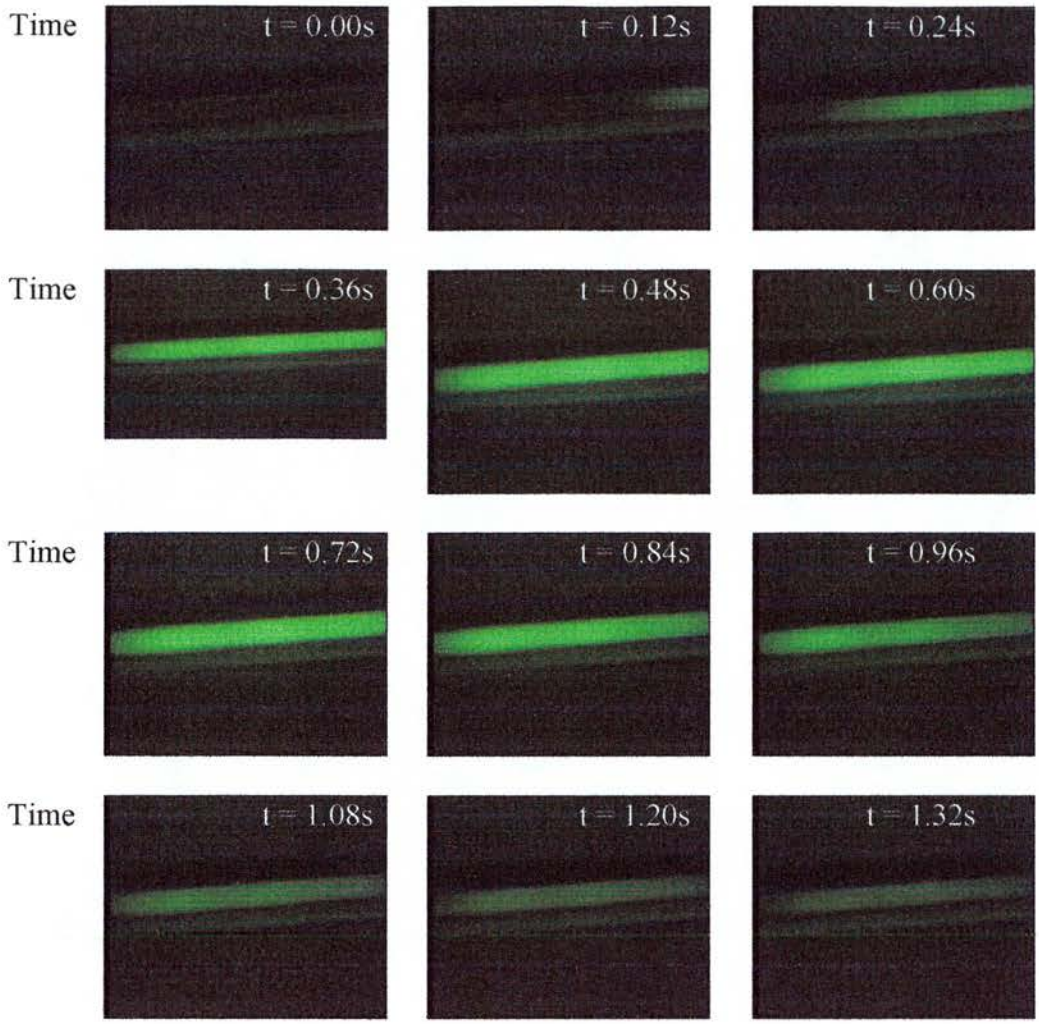


Figure 4-19 A series of video images showing an example of CE-LIF detection using rhodamine 6G. The capillary diameter is 50 μm.

Figure 4-20: A series of three negative video images, each separated by around 0.5s, showing the progression of the fluorescent solute band in the capillary. Note the flat front of the band in all 3 pictures, characteristic of electroosmotic flow. The capillary diameter is 50 μm.

### 4.7.2 Pretty picture integrator program

The pretty picture integrator (PPI) was a custom written LabView (National Instruments, USA) program that was designed to take an average of the intensity over the entire area of each frame. Video processing was achieved by importing the relevant video clip onto a computer equipped with Adobe Premier. The individual frames are then exported as sequentially numbered bitmap files. The pretty picture integrator imports and analyses each bitmap file individually, assigning a value to the sum of the total intensity of all the pixels in the image. A screen shot of the pretty picture integrator is shown in Figure 4.21. The resulting chromatogram is then displayed on the screen and exported to Excel (Microsoft) (Figure 4.22). As there are 24 frames per second, a 4 minute movie would results in 6000 bitmap files, and a huge amount of memory consumption (6 Gb).

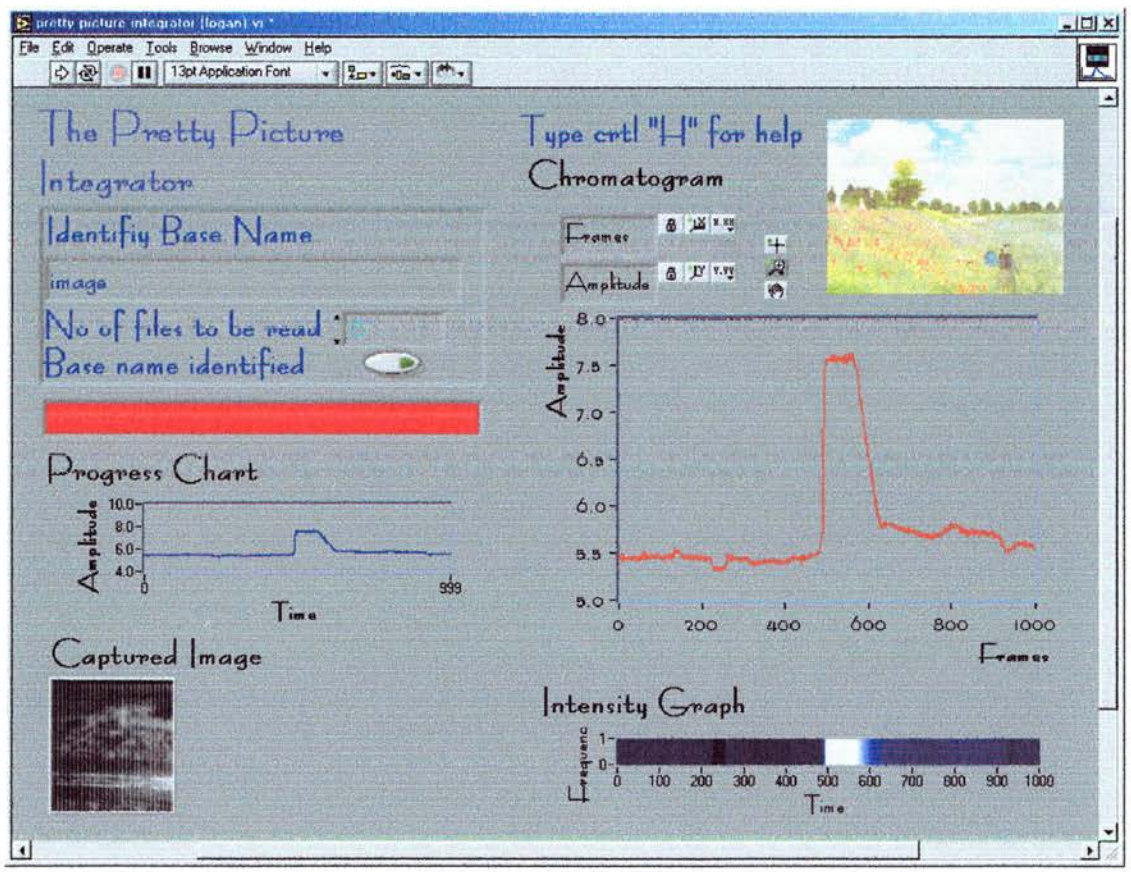

Figure 4-21 Typical screenshot of the PPI program.

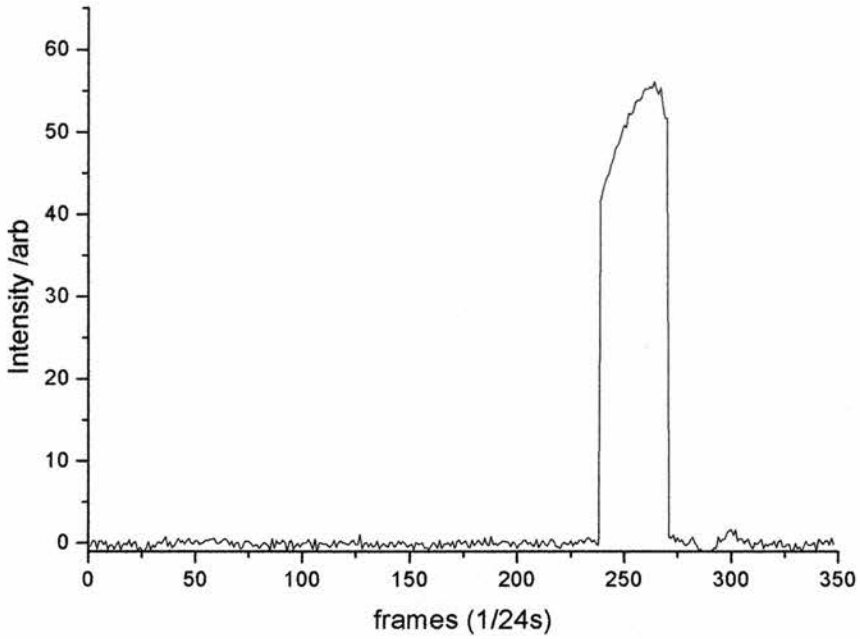


Figure 4-22 Typical output from PPI program.

## 4.8 Mass Spectrometric Instrumentation

### 4.8.1 CE-MS interface development

When considering the various detection strategies that have been employed for capillary electrophoresis, mass spectrometry provides the greatest potential. The advantages of this technique include the capability for determining the mass to charge ratio (m/z) of the analytes, as well as in some cases providing structural information. The use of MS as a method of detection also offers the ability to resolve co-eluting analytes on the basis of their m/z values. This is of particular interest when highly complicated samples such as those derived from crude cell extracts are investigated. This can be simply illustrated by comparing a CE chromatogram acquired with an on-column UV absorbance detector with the corresponding CE-MS chromatogram obtained for the group of compounds (Figure 4.23 and Figure 4.24).

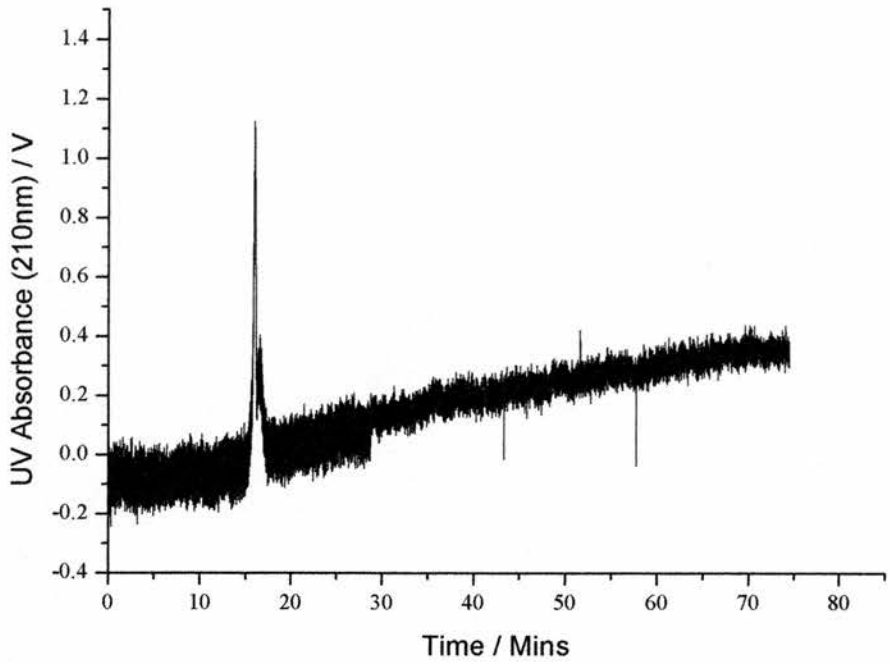


Figure 4-23 CE chromatogram using 210 nm UV absorbance for the detection of glucose, maltose and azoxystrobin.

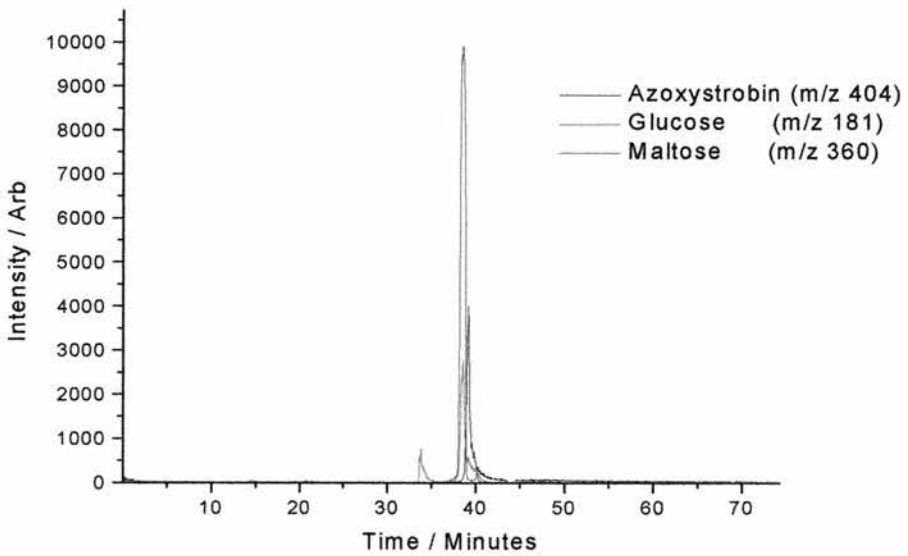


Figure 4-24 Combined CE-MS SIM chromatogram for same sample as Figure 5.23. (Displayed in SIM mode by selection of m/z 404, m/z 181 and m/z 360).

A sample containing azoxystrobin (0.1 mg/mL), glucose (0.1 mg/mL) and trehalose (0.1 mg/mL) was electrokintically injected at 5 kV for 5 s. UV absorbance detection was performed at 210 nm. It is clear that in this particular experiment, the use of MS facilitates the identification of a number of co-eluting compounds. This is a significant advantage when the compounds under investigation, as described in the following chapters, are expected to elute at very similar times.

The hyphenation of capillary electrophoresis and mass spectrometry (CE-MS) was an obvious development considering the limits imposed by traditional detection strategies. The interfaces for CE-MS bear little similarity to those developed for LC-MS, as the flow rates are dramatically reduced and electrical continuity is critical. In LC-MS, flow rates are typically in excess of 100 μL/minute; in CE-MS typically 50-100 nL/minute. As a result, to maintain the electrospray process, the spray tip design must be optimised for this low flow rate, or a sheath flow must be provided.

For on-line CE-MS experiments, the capillary outlet has to be removed from the waste reservoir and positioned in front of the mass spectrometer inlet; this opens the electrical circuit and terminates the CE process. To rectify this situation, the electrical connection that provides the electrospray voltage can also function to maintain the CE electrical continuity [157,158]. In this case, to protect the sensitive electrical components of the mass spectrometer a 100 MΩ resistor is placed in-line with the electrospray electrical connection.

The vertical displacement of the column inlet, relative to the outlet is of particular importance, as even a few millimetres can lead to a severe reduction in separation performance. The negligible backpressure offered by the capillary also places certain constraints on any interface design, as any flow restriction imposed by the interface could reverse the flow of buffer up the centre of the capillary resulting in a break in the electrical continuity of the buffer and collapse of the flow. Although many groups have overcome the problem, by the use of pressurised inlet reservoirs, the application of pressure must be used sparingly or the separation can be greatly compromised.

The interface must also be designed to maintain the separation resolution of CE; peaks generated by CE may be as narrow as a 3 s, and considering the low flow rate,

any significant dead volumes would degrade the separation. This rules out the use of zero dead volume connectors (ZDV) as they are not truly zero dead volume, and if a sheath flow is used the mixing volume at the tip of the emitter should also be minimised.

In the earliest reference to CE-MS the separation was performed in the traditional manner, with the capillary inlet dipped into a vial containing mobile phase, except that the capillary outlet was surrounded by a stainless steel sheath and placed in front of the mass spectrometer inlet (Figure 4.25) [159]. Running potentials of up to 60 kV could be applied to the inlet vial, while potentials of up to 5 kV could be applied to the sheath. In this case, the sheath acted as both the CE cathode and the electrospray capillary. A nitrogen gas nebuliser, flowing counter to the ESI was used to aid desolvation.

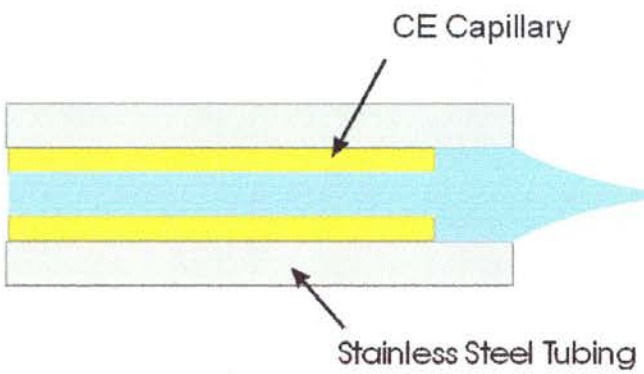


Figure 4-25 Schematic diagram of earliest CEMS interface [159].

The use of the stainless steel sheath created a large dead volume at the tip of the CE capillary and resulted in a reduction in the chromatographic resolution. A stable electrospray proved hard to maintain with this design of interface, and could easily be perturbed by stray electric fields, mechanical perturbations (e.g. vibrations), or minute variations in flow that cause increasingly severe oscillations in performance as the flow rate was affected. The interface design also limited the range of buffer compositions that could be used. For example, aqueous solutions or buffers with a concentration lower than $10^{-2}$ M could not be used, as they could not support electrospray.

The interface design was significantly improved by the addition of a flowing liquid sheath (Figure 4.26) [160]. This addition of the liquid sheath resulted in a number of improvements over the previous interface. The key advantage is a much broader range of CE operating conditions that may be adapted to mass spectrometric detection. For example, the sheath flow can be controlled to allow the operation of CE at flow rates previously too low for stable ESI performance. The dead volume was also dramatically reduced, leading to a reduction in the degradation of the chromatographic resolution caused by the interface. The sheath flow also reduced the analyte contact with the stainless steel surfaces, thought to affect the signal strength. When the CE capillary was retracted into the stainless steel sheath, analyte signals were lost, even though the ESI is unperturbed. This loss of signal is though to result from the loss of ions due to an electrochemical process at the stainless steel capillary. Through the sheath liquid, electrical connection was still maintained. The sheath liquid can be the same as the CE buffer, but it is often advantageous to use another liquid to improve electrospray performance. With the earlier interface design, aqueous buffers could not be electrosprayed; the buffers used were; water buffers (50:50 (v:v)) with a small amount of electrolyte added. In this design, methanol, acetonitrile or propanol could be used as a sheath electrode liquid allowing aqueous CE buffers to be used with concentrations up to at least 0.2 M.

A key advantage of the sheath liquid electrode interface is that solutes can be added that will act to modify the electrospray process, either by manipulation of the liquid-phase chemistry related to ion desorption or, potentially, by post column derivatisation to yield an analyte providing distinctive mass spectral information or more efficient ionisation. The mixing of the sheath liquid and the CE buffer within the electrospray cone is extensive and the addition of certain components, such as acetic or formic acid, offers significant increases in ESI efficiencies.

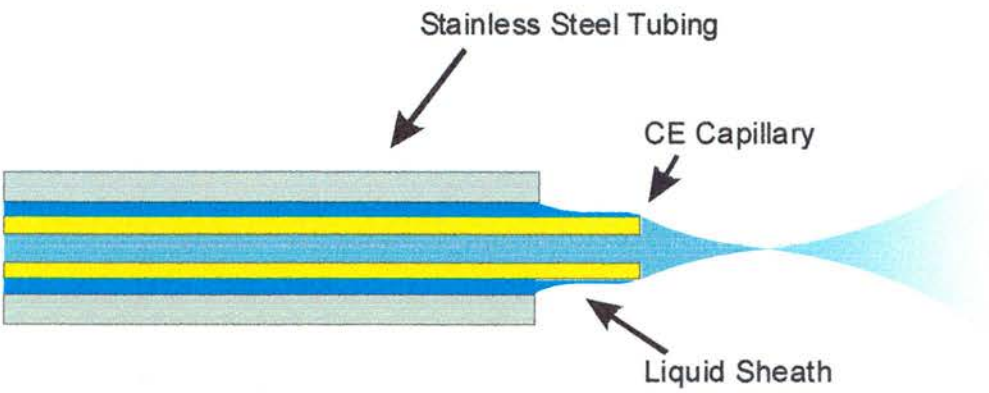


Figure 4-26 Schematic diagram of an improved CE-MS interface incorporating a liquid sheath [160].

This style of interface has been adopted by a number of companies and offers superior reliability and/or quantitation. The interface still suffers from reduced sensitivity, because since ESI is largely concentration dependent, the addition of sheath liquid reduces the ultimate sensitivity of the device.

Although a number of in-house built interface designs were tested during the course of this work), it was decided eventually to use a commercially available interface (Micromass, UK). This interface did not require a pressurised inlet reservoir, and although less sensitive resulting from large mixing volumes and high sheath flow rates, provided superior reliability and ease of use.

### 4.8.2 Micromass CE-MS interface

The interface is based closely on the design originally used by Smith and co workers [160]. It utilises both a liquid sheath and a coaxial nitrogen desolvation gas (Figure 4.27).

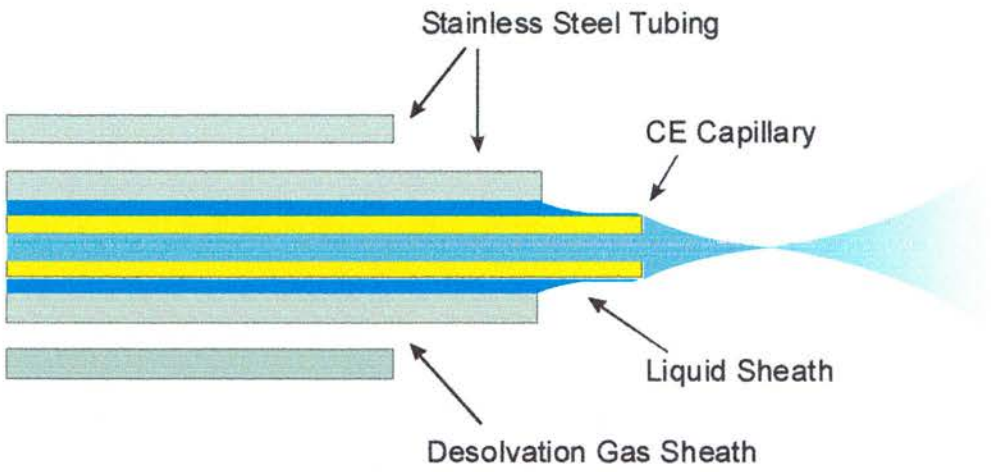


Figure 4-27 Micromass tri-axial CE interface.

The sprayer consists of a tee-piece, to allow the addition of the make-up solvent, a fused silica CE extension capillary, and a stainless steel capillary to direct the make-up liquid to the sprayer tip (Figure 4.28). At the rear of the sprayer is a capillary adjuster mechanism that allows spray stability to be optimised. The interface was designed to work most efficiently when the position of the emitter was approximately 7mm from the sample cone and about 3mm off the axis of the apex. A make up liquid of 50:50 (v:v) methanol:water 1% acetic acid, at a flow of 0.8 µl/min was recommended. The Q-ToF nebuliser gas source was used as a supply for the interface. Both the electrospray voltage and nebuliser gas were switched off during electrokinetic injection, as it was found to affect the volume injected. Once CE voltage was applied, the nebuliser gas and spray voltage were switched on. Optimum ESI was achieved by fine adjustment of the position of the interface and of the degree to which the stainless steel capillary protruded.

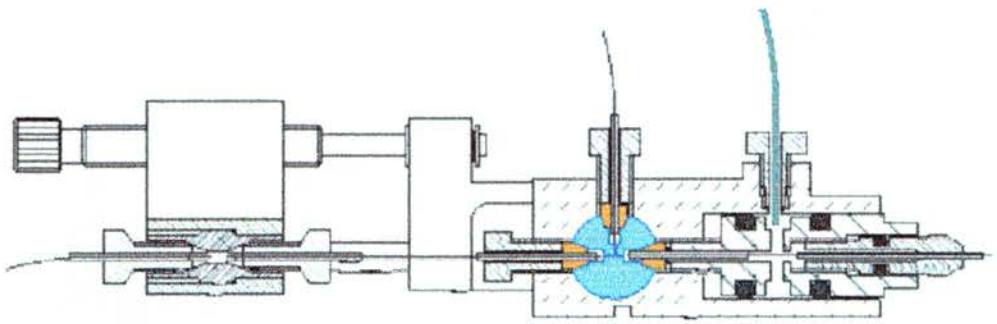

Figure 4-28 Schematic diagram of the Micromass tri-axial interface. Modified from reference [161]

### 4.8.3 Modification of the interface

Typically CE is performed in 375 μm OD fused silica capillaries. As a result, all instruments are designed such that this size of capillary can be used. These include the capillary guides used in UV absorbance detectors and auto-samplers that transfer the capillary inlet from one vial to another. The tri-axial outlet of the Micromass CE-MS interface is designed such that it requires the use of a 192 μm OD capillary. This means that a zero dead volume (ZDV) connector is normally required between the separation capillary and the capillary that passes through the interface. The presence of a ZDV is known to result in a substantial loss of peak resolution resulting from mixing in the union [120]. In the current experiments, since the length of the capillary had to kept to a minimum, it was decided that UV detection was not required and a 192 μm OD fused silica could be used throughout by simply passing the capillary through the ZDV.

As mentioned earlier, one of the problems inherent in using a sheath flow is that the dilution of the capillary eluent reduces the ultimate sensitivity of the interface. It was found that with careful tuning of the interface, it was possible to reduce the sheath flow rate from 0.8 μL/minute to 0.23 μL/minute. At this flow rate, it was still possible to maintain reliable operation of the interface.

### 4.8.4 Micromass Q-ToF mass spectrometer

The majority of the experiments presented in this research were carried out using a Q-ToF mass spectrometer, which was designed and built by Micromass (Manchester, UK) in 1994 [161]. In this section, a brief description of this hybrid quadrupole time of flight mass spectrometer is given. The Q-ToF was originally developed to address an inherent problem associated in using triple quadrupole mass spectrometers for ultra-high sensitivity tandem mass spectrometry, namely that when performing MS/MS experiments the third quadrupole is scanning for product ion detection. To compensate, the quadrupole is set to a low resolution that maximises transmission. Because of the scanning time of the third quadrupole required for data acquisition, much time is spent accessing areas of the mass range that can be devoid of data. The solution was a novel geometry quadrupole orthogonal acceleration time-of-flight mass spectrometer, which takes advantage of the high transmission and multiplexed data acquisition inherent to all TOF analysers. In the Q-ToF, the quadrupole can act as either an ion guide (MS mode) transmitting all the ions to the TOF analyser, or as an ion filter (MS/MS mode) allowing only ions in a pre-defined mass range to pass through the quadrupole. After passage through the quadrupole analyser, the filtered ions can be fragmented by collision-induced dissociation in a hexapole collision cell, prior to analysis by the TOF. A schematic diagram of the instrument is shown in Figure 4.29.

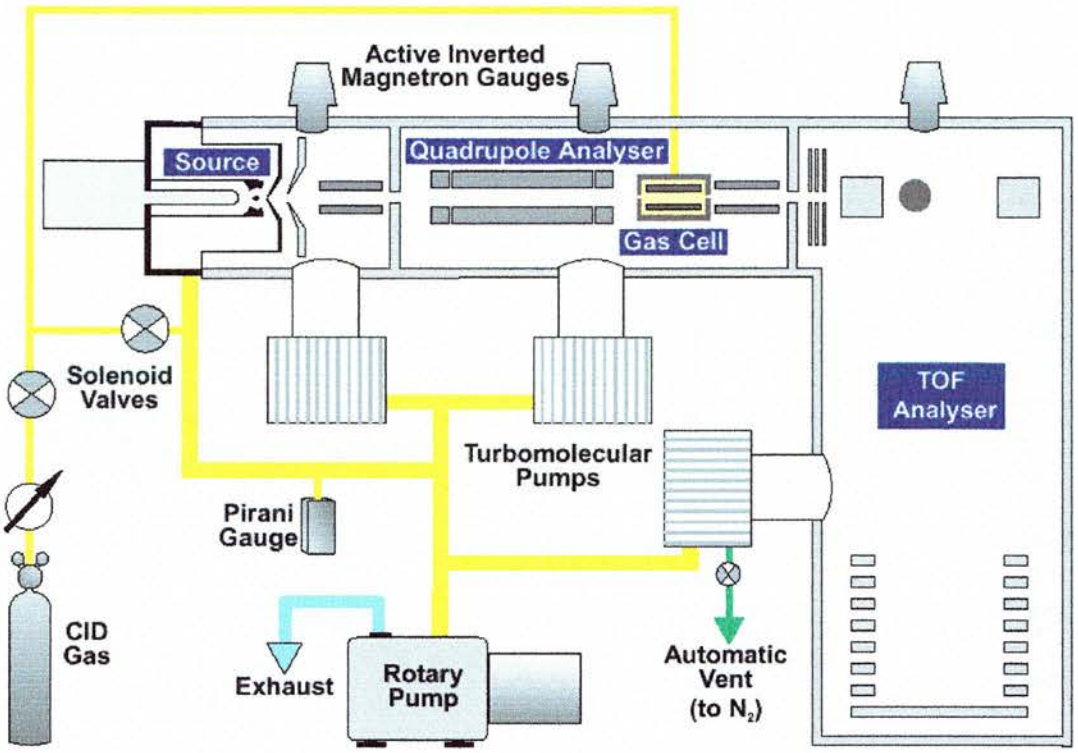


Figure 4-29 Schematic diagram of the Micromass oa-TOF (Q-ToF) mass spectrometer. Reproduced from reference [161].

### 4.8.5 The Z-spray source

Another development implemented on the Q-ToF is a dual orthogonal sampling, or Z-spray, source that limits contamination while delivering enhanced signal-to-noise ratio. The interface functions in two stages, first by directing the ESI spray perpendicularly past the sampling cone, preventing large droplets, involatile material and particulates from entering the sampling cone. In the second step transmitted ions enter the instrument orthogonally through a second aperture. This limits the volume of gas that enters the analyser region of the mass spectrometer. Therefore the orifice of the sampling cone can have a larger diameter allowing a greater volume of gas to be sampled and therefore increasing the transmission of ions. A schematic diagram of the Z-spray source is shown in Figure 4.30

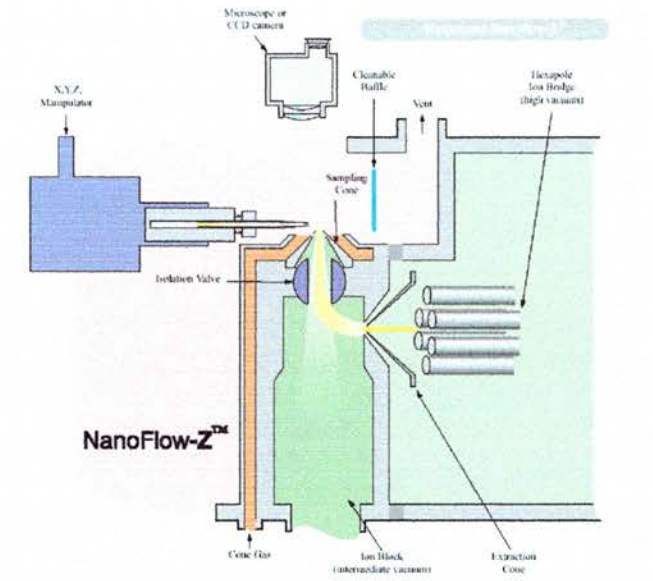


Figure 4-30 Schematic diagram of the Z-spray source.
Reproduced from reference [161].

## 4.9 Concluding remarks

The challenge of developing a technique for the sampling, transfer and analysis of ultra-low volume samples derived from single cells has been met. A number of microsampling devices were investigated. The plant pressure probe was determined to be the most appropriate, enabling samples to be rapidly and accurately aspirated from selected fungal cells. CE was chosen as the transfer technique as it simultaneously offered the capability of separation, desalting and transfer whilst protecting the sample from the atmosphere. A commercially available sheath flow CE-MS interface was chosen instead of custom-designed sheathless interfaces. This interface did result in a reduction in sensitivity over the custom designed interfaces, although this was compensated for by increased reliability. The use of LIF as an additional detection technique, that could be used on-line with CE-MS, was also investigated for the detection of fluorescent molecules.

# 5 Carbohydrate accumulation in fungi

'Fungi are a unique group of organisms, different from all others in their behaviour and cellular organisation' [162]. Traditionally they were aligned with plants in some classification systems, considered to be a subkingdom of kingdom Plantae, due to their cell wall and lack of mobility. The classification system was updated in 1866 and the two-kingdom system replaced by the three-kingdom classification system. The third kingdom, termed protista, included all microscopic life including algae, bacteria, protozoa and fungi. Following the development of the electron microscope in the 1950s the simplicity of bacterial cells was described and lead to their separation as prokaryotes, with all other organisms termed eukaryotes. Following discussion over the many fundamental differences of fungi with respect to other eukaryotes, they were assigned to a separate kingdom heralding the five-kingdom approach to classifying organisms. Monera, protista, fungi, plantae, and animalia. Phylogenetic research is now throwing the whole concept of organism classification into question.

There are a number of growth forms for fungi. The most common is mycelial, where a network of hyphae is produced. Other forms include single rounded cells or chains of cells that attach to food sources by tapering rhizoids, and unicellular yeasts that divide by either binary fission or budding. The method for growth is closely related to habitat, with some fungi able to alternate between yeast and mycelial forms depending on the environment [163,162].

## 5.1 Fungal lifecycle

Of the approximately 250,000 different species of fungi, about 75% belong to the ascomycetes (90% of which are filamentous fungi, the remainder being yeasts) and 25% are basidiomycetes (whose fruiting bodies are commonly known as 'mushrooms') [164]. As a group, the fungi have an enormous impact on the world economies: yeast is used extensively in the brewing industry, filamentous fungi are used for the production of foodstuffs and the industrial production of enzymes and chemicals, and basidiomycetes are consumed as food all over the world. Fungi are

known to infect nearly all food crops and represent the most universal and costly pathogens.

Fungi lack an embryonic stage and develop directly from spores. These spores may be of mitotic or meiotic origin and germinate into hyphae or single growing cells. The hyphae (Figure 5.1) that grow from fungal spores are tubes separated into cell-like compartments by septa (Figure 5.2). The number of nuclei increases by mitosis as the hyphae grow. Each cell compartment may contain more than one nucleus. The septa contain pores that allow the free trafficking of cytoplasm including nuclei, mitochondria and vesicles between the compartments. The hyphae have a defence mechanism against cell damage to prevent whole scale destruction of the hyphae that this trafficking could cause if a compartment were ruptured. When a compartment is ruptured, sub-cellular organelles, termed Woronin bodies lodge in the septal pores preventing further flow of cytoplasm into the damaged region. This will be discussed fully in Section 5.3.1. The yeasts, in comparison, tend to remain as single cells and do not form mycelia.

## 5.2 Hyphae and the concept of the single cell

It must be stressed that in reality, the cell cannot be considered a sac of liquid in which molecules move freely; the cell is, in fact, a highly organised unit whose structure is maintained by a complex cytoskeleton. When considering microsampling from cells, it is important to understand that any sample aspirated will be composed not only of a complex mixture of chemicals, but also relatively large structures. The presence of large quantities of DNA and membranes acts to increase the viscosity of the sample.

While higher fungi may form discrete cells that can be considered as individual entities, they also produce hyphae that are extensive structures along which considerable steaming of cytoplasm and organelles can occur in the direction of growth. A colony of filamentous fungi is composed of a three-dimensional, branched, interconnecting network of hyphae with an indefinite number of growing points. As the hyphae exhibit growth at the tips, the growing region of the mycelium moves away from the original position. Secondary differentiation occurs within the

basic framework laid down during the vegetative growth phase. The colony in the early stages of expansion is trophic, but will commonly also develop to have reproductive dispersal as a survival function [165].

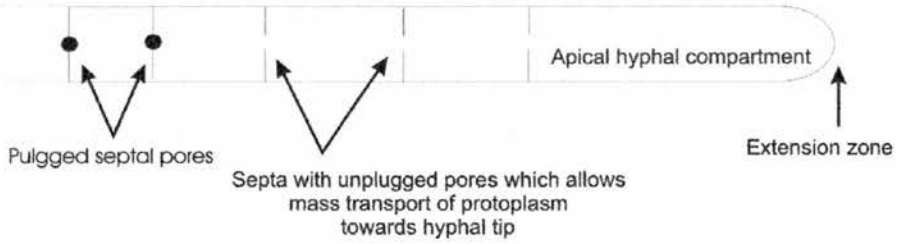


Figure 5-1 Diagrammatic representation of different regions within a hyphae.

## 5.3 *Neurospora crassa*

*Neurospora crassa*, the orange bread mould, has served as a simple model organism for genetic and biochemical studies since Beadle used it to establish the one genome enzyme model in 1941 [166]. The many ways in which *Neurospora crassa* has provided insights into biological processes have been described briefly [167], and in great detail [168]. *Neurospora crassa* is the best-characterised of the filamentous fungi, a group of organisms critically important to agriculture, medicine, and the environment. It is widespread in nature, and thus, like the fruit fly, *Drosophila melanogaster*, it is exceptionally well suited as a subject for biological research. Six decades of research on the genetics, biochemistry and cell biology of *Neurospora crassa* have established this organism as a gold mine of biological knowledge. The entire genome has now been sequenced and is available online [169].

### 5.3.1 Woronin bodies

As mentioned previously, Woronin bodies act to prevent widespread damage to the fungal hyphae when an individual compartment is ruptured. The Russian mycologist, Woronin, first reported these small organelles, in 1864, in the fungus

*Ascobolus pulceherrimus* [170]. These organells are highly refractive and are present in small numbers on either side of the septum that divides hyphal compartments. Since their discovery, Woronin bodies have been identified in more than 50 species of fungi, but appear to be restricted to ascomycotina, some of which are plant [171] and human pathogens [172]. When hyphae are damaged, the Woronin bodies act to plug the septal pores within seconds [173].

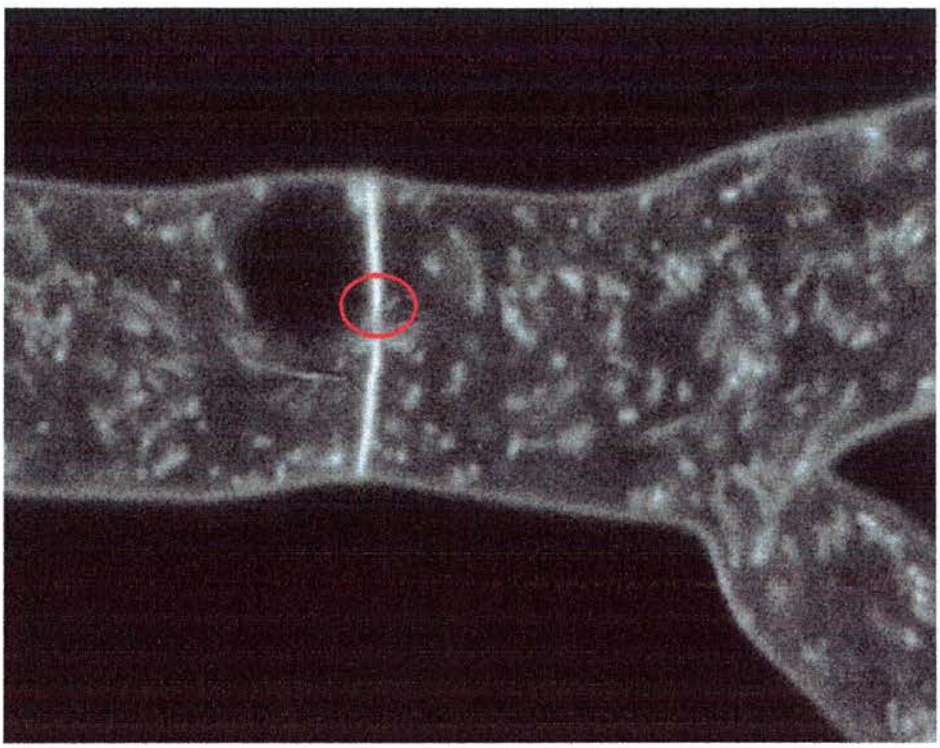

Figure 5-2 Confocal microscopy image highlighting a septal pore between two hyphal compartments of *Neurospora crassa* (stained with Dapsmi, a membrane dye).

The presence of these organelles means that even though cytoplasmic streaming occurs when a cell is pierced to remove a sample, the septal pores are quickly blocked, limiting the volume that can be removed. This can be seen when microsampling wild type cells (Figure 4.14). This situation is further complicated by the influx of water from the extra-cellular matrix [174], and has the effect of diluting the concentration of molecules in the sample obtained.

### 5.3.2 Hex-1 deletion mutant of *Neurospora crassa*

Until recently, most information concerning the Woronin bodies was obtained from light microscopic analysis. As their small size is near to the limit of resolution of the light microscope, they were described simply as refractile bodies. However, under the electron microscope they were identified as 400-700 nm electron-dense organelles, bound by a single membrane [175,176]. Woronin bodies are slightly larger than the septal pore (150-500 nm) and fall into two structural classes, spheres and hexagonal rods [177]. While the biosynthesis and biochemical function of Woronin bodies was historically hard to examine, as no molecular component of the organelle has been identified, research has now provided a fraction enriched in Woronin bodies from *Neurospora crassa* [178]. From this fraction it was possible to determine the N-terminal sequence of an abundant 19 kDa protein, and show that it was encoded by a gene deposited in GenBank (Accession Number AF001033) as a possible subunit of the vacuolar ATPase [178]. This gene, termed Hex-1, encoded the principal protein of the Woronin body and the expressed protein, HEX-1, was found to assemble into hexagonal crystals *in vitro* and when expressed in *Saccharomyces cerevisiae*. Most importantly for this research, the deletion of the Hex-1 gene in *Neurospora crassa* results in the absence of Woronin bodies and hyphae that continue to seep cytoplasm when a cell compartment is ruptured [179]. The result is that when microsampling is performed with Hex1 mutant hyphae, volumes larger than a single cell compartment can be acquired from a single aspiration, reducing the risk of contamination and dilution of the sample by components of the extra-cellular matrix (Figure 5.3).

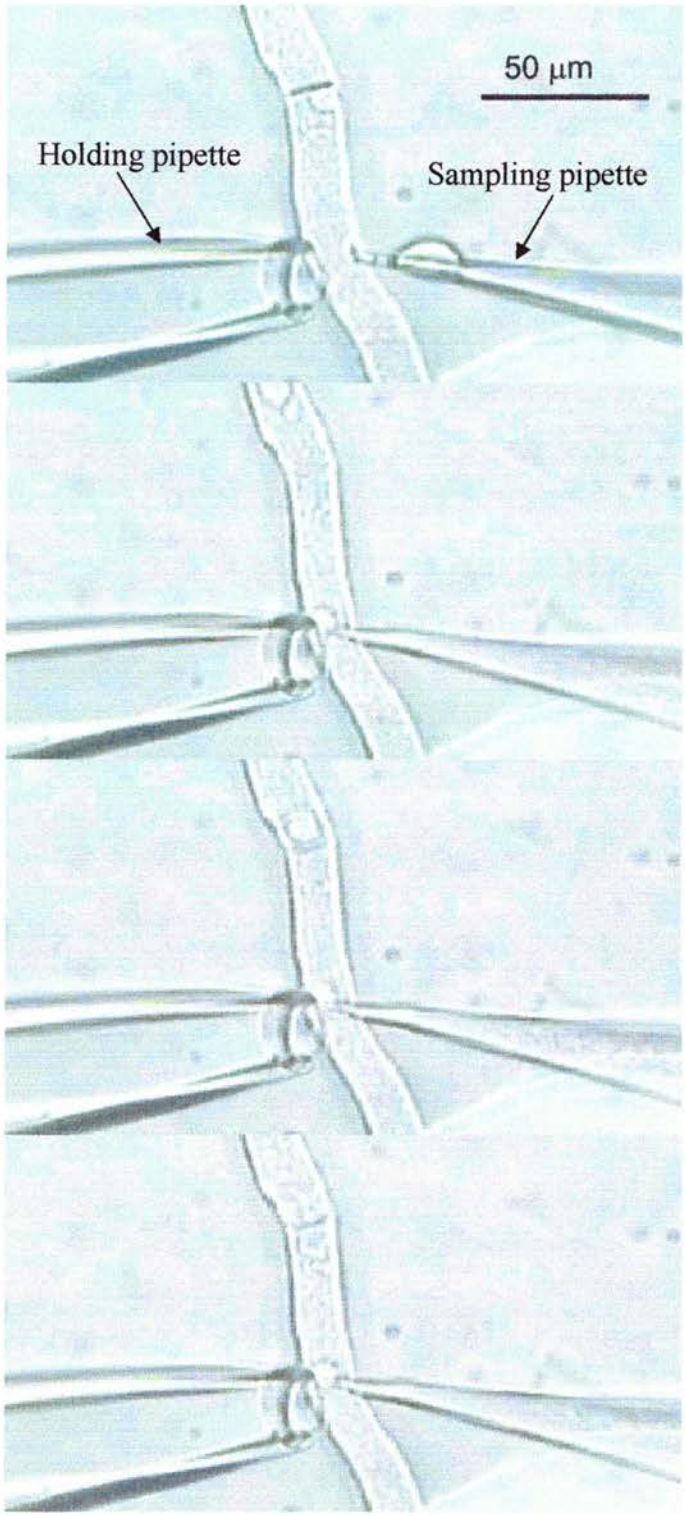


Microsampling pipette in position ready to stab cell.

Sample is drawn into pipette. No Woronin bodies to block the septal pores.

Continuation of cytoplasmic streaming clearly noticeable via passage of vacuole through open septal pore and non-collapse of punctured hyphal compartment (compare Figure 4.14).

Figure 5-3 Series of video images showing microsampling from Hex-1 mutant of *Neurospora crassa*.

### 5.4 Disaccharides and carbohydrate uptake in *Neurospora crassa*

*Neurospora crassa*, a heterotroph, is typically provided with maltose and glucose as a carbon substrate in most laboratory media. It is able to grow on a variety of other simple carbohydrates and oligosaccharides [180]. Invertase, a glycoprotein expressed by *Neurospora crassa*, is required for growth on sucrose and appears rapidly on the cell wall following germination and can sustain growth on sucrose thereafter [181]. With *Neurospora crassa*, it is generally accepted that most usable sugars enter the cell through one or more transport systems (Table 5.1), while di- and oligosaccharides are broken down by invertase outside the cell and transported in the form of glucose, galactose and fructose [182].

Table 5.1 Sugar transport in *Neurospora crassa* [183]

| **Transport System** | **Substrate** | **Type** | **Regulation** |
|---|---|---|---|
| I | Glucose (8-25mM) | Diffusional | Constitutive |
| II | Glucose (0.01-0.04 mM)<br>Galactose<br>Mannose<br>Xylose | Concentrative | Depresses with Carbon Starvation; Turnover on re-addition of glucose |
| Galactose | Galactose (400 mM) | Unknown | Depressed with carbon starvation |
| Fructose | Fructose (0.4mM) | Probably concentrative | Depressed with carbon starvation |

The predominant intra-cellular isomer of maltose is trehalose (α-D-glucopyranosyl (1-1)-α-d-glucopyranoside), a non-reducing disaccharide of glucose found in bacteria, fungi, plants and insects [184]. It is known to exhibit an extraordinary capacity to protect biological membranes and proteins both *in vitro* and *in vivo* against osmotic and heat stress [185]. In cells exposed to stress, trehalose can

accumulate to levels as high as 15% of the cell dry weight [186], although this is inconclusive as some stress conditions do not yield a correlation between cell tolerance and the accumulation of trehalose [187]. Intra-cellular biosynthesis of trehalose has been identified *in vivo* and is catalysed by a two-step process involving trehalose-6-phosphate (Tre6P) synthase and Tre6P phosphatase on a multimeric protein complex.

The values calculated from the percentages of the dry weight suffer from the problem that several assumptions have to be made in order to extract an estimate of the cellular concentration, in particular, that there is no contamination by extra-cellular trehalose and the need to extrapolate a value for the cell volume. There are a number of published techniques for quantifying the concentration of trehalose in fungal cells. These are summarised in Table 5.2, along with their limit of detection (LOD) and minimum sample volume.

Table 5.2 Measurement strategies for trehalose fungal cell concentration [188]

| **Technique** | **Limit of detection (LOD) for trehalose (nmol)** | **Minimum sample volume (mL)** |
|---|---|---|
| Colourimetric | 7-14 | 0.5 |
| Spectrophotometric | 0.2-0.40 | 1 |
| Gas liquid chromatography | 0.005 | 0.003 |

The use of gas liquid chromatography (GLC) [189] offers a 40-fold increase in the sensitivity of trehalose detection over spectrophotometry, and a 250-fold increase over colourimetric analysis [190]. Unfortunately the sample volume required for GLC (3 μL) prevents this technique from being applicable to SiCSA.

## 5.5 Investigation of various disaccharides

The SiCSA technique described in the previous chapter was developed to provide a method by which ultra-low volume samples could be aspirated from a chosen fungal cell compartment, and by means of a capillary electrophoresis system and ESI interface, analysed by mass spectrometry. Capillary electrophoresis was chosen since it permits the analysis of complex biological samples and offers high resolution separation.

The high resolution, although advantageous for analysis, results in very narrow peaks, often as small as 3 s. This is very inconvenient when tuning the mass spectrometer and analysing any standards. An alternative system capable of providing a continuous flow of analyte was required. Therefore, preliminary experiments were performed by nESI using the Q-ToF on standard samples of the common disaccharides that are present in the malt extract (which provides the carbon source in the culture medium the fungal cells are grown on). The disaccharides examined were trehalose, maltose, maltulose and sucrose (Figure 5.4).

All samples were obtained from Sigma Aldrich (UK). Solutions were prepared at a concentration of 0.01 mg/mL in 1:1 (v:v) methanol:20 mM ammonium acetate 0.2 % formic acid. This solvent mixture was chosen to approximate the chemical composition of the ESI spray during CE-MS experiments, the only difference being that methanol was substituted for acetonitrile. Each nESI spectrum was recorded in a new Econo12 borosilicate nESI needle (New Objectives, USA) using an electrospray potential of 1 kV and a source block temperature of 80°C. Spectra were recorded in both MS-TOF and MS/MS-TOF modes. With a continuous analyte source available, it was possible to adjust the cone voltage and source block temperature on the Q-ToF mass spectrometer and to vary the collision energy to obtain the optimum signal.

Trehalose

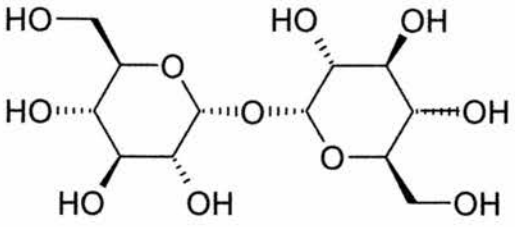

Average molecular mass: 342.3
Monoisotopic molecular mass: 342.1
Molecular formula: $C_{12}H_{22}O_{11}$

Maltose

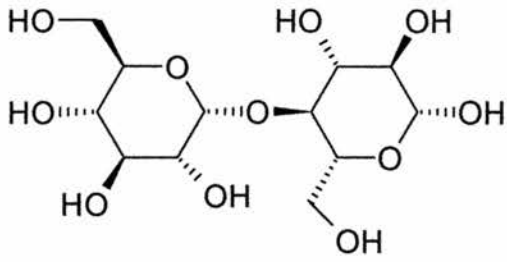

Average molecular mass: 342.3
Monoisotopic molecular mass: 342.1
Molecular formula: $C_{12}H_{22}O_{11}$

Sucrose

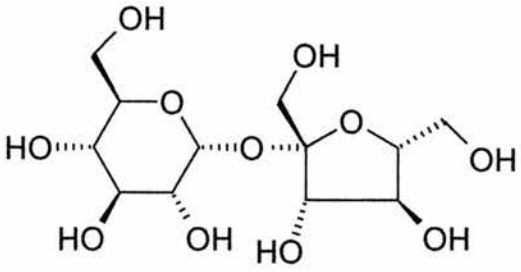

Average molecular mass: 342.3
Monoisotopic molecular mass: 342.1
Molecular formula: $C_{12}H_{22}O_{11}$

Maltulose

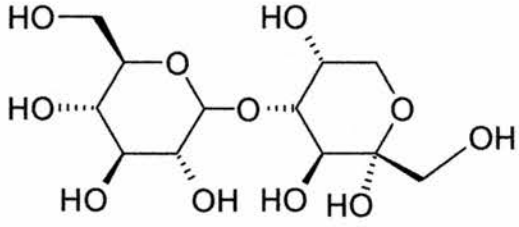

Average molecular mass: 342.3
Monoisotopic molecular mass: 342.1
Molecular formula: $C_{12}H_{22}O_{11}$

Figure 5-4 Structures of disaccharides investigated.

### 5.5.1 Development of selected reaction monitoring transition

Optimisation of the MS signal is crucial in the development of an SRM transition, as MS/MS sensitivity depends on how well the compound behaves in full MS mode. Anything that can be done to improve the full scan non-collision induced dissociation (CID) response will improve the final SRM spectra.

Figure 5.5 shows a nESI MS spectrum recorded for trehalose in positive ion mode. Interestingly, the abundance of the protonated species (expected monoisotopic peak m/z 343.1) is very low. The most common adduct ions are labelled. The ion at m/z 365.4 corresponds to the sodium adduct $[M+Na]^+$ expected monoisotopic peak m/z 365.1), the ion at m/z 360.4 corresponds to the ammonium adduct ($[MH+NH_3]^+$ expected monoisotopic peak m/z 360.2). The most abundant fragment ion at m/z 325.5 corresponds to loss of water from the protonated species ($[MH-H_2O]^+$ expected monoisotopic peak m/z 325.1). The observed peaks are all very slightly higher than the predicted monisotopic peaks due to the fact that the mass calibration of the Q-ToF was not exact.

Once the MS signal had been optimised, the collision energy and collision gas pressure were varied to give the desired level of fragmentation. Care must be taken to not provide excessive collision energy, as this can result in the dissociation of important target fragment ions. Optimisation of the degree of fragmentation was achieved by performing MS/MS at various collision energies in the hexapole collision cell (Section 4.8.8). A suitable fragment ion was chosen and its ion current was monitored while varying the collision energy and collision gas pressure.

Figure 5.6 shows a nESI MS/MS spectrum for trehalose following fragmentation induced in the hexapole collision cell. The ammonium adduct ion at m/z 360.4 shown in Figure 5.5 was selected as the precursor ion. The peak at m/z 343.5 is assigned to the protonated species. The most abundant fragment ion at m/z 325.5 corresponds to loss of water from the protonated species ($[MH-H_2O]^+$). The other two prominent fragment ions at m/z 181.8 and m/z 163.8 correspond to cleavage in the protonated species either side of the glycosidic bond ($[C_6H_{13}O_6]^+$ expected monoisotopic peak m/z 181.1; $[C_6H_{11}O_5]^+$ expected monoisotopic peak m/z 163.1).

A less abundant fragment ion can be seen at m/z 145.9. This is assigned to $[C_6H_{11}O_5\text{-}H_2O]^+$ (expected monoisotopic peak m/z 145.1).

The corresponding MS and MS/MS spectra obtained for maltose, maltulose and sucrose are shown in Figures 5.7 and 5.8, Figures 5.9 and 5.10, and Figures 5.11 and 5.12, respectively. The nESI MS spectra for each of these disaccharides are virtually identical to that of trehalose, exhibiting similar adduct and fragment ions. The nESI MS/MS spectrum for maltulose (Figure 5.10) is almost identical to that for trehalose (Figure 5.6). The nESI MS/MS spectra for maltose and sucrose are less similar. In both spectra the most abundant ion observed is at m/z 342.7. This is assigned to $[MH+NH_3\text{-}H_2O]^+$ (expected monoisotopic peak m/z 342.1). In both spectra there is also a prominent fragment ion at m/z 268.8, as yet unassigned. One noticeable difference in the spectrum for maltose is the fact that the fragment ion at m/z 181.8 is missing.

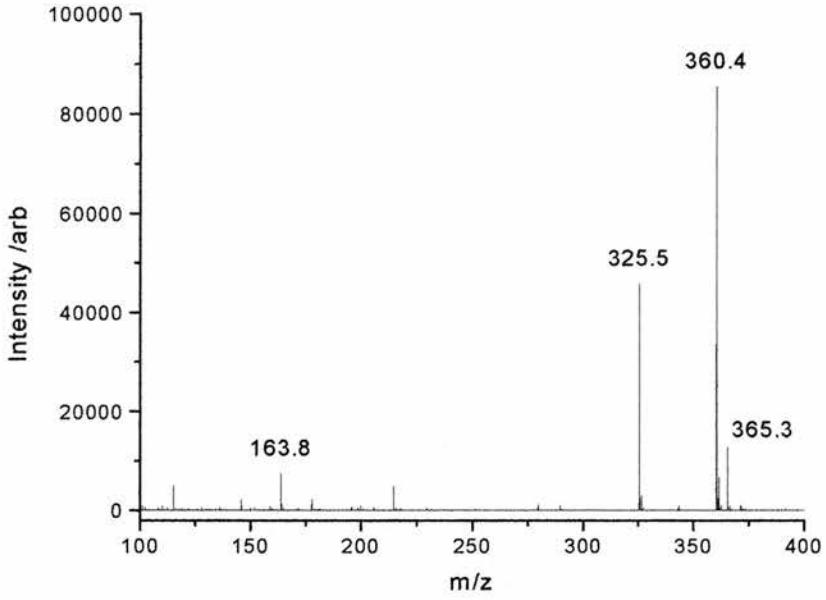


Figure 5-5 nESI MS spectrum for trehalose (0.01 mg/ml). (m/z 365.4 $[M+Na]^+$, m/z 360.4 $[MH+NH_3]^+$, m/z 325.5 $[MH-H_2O]^+$)

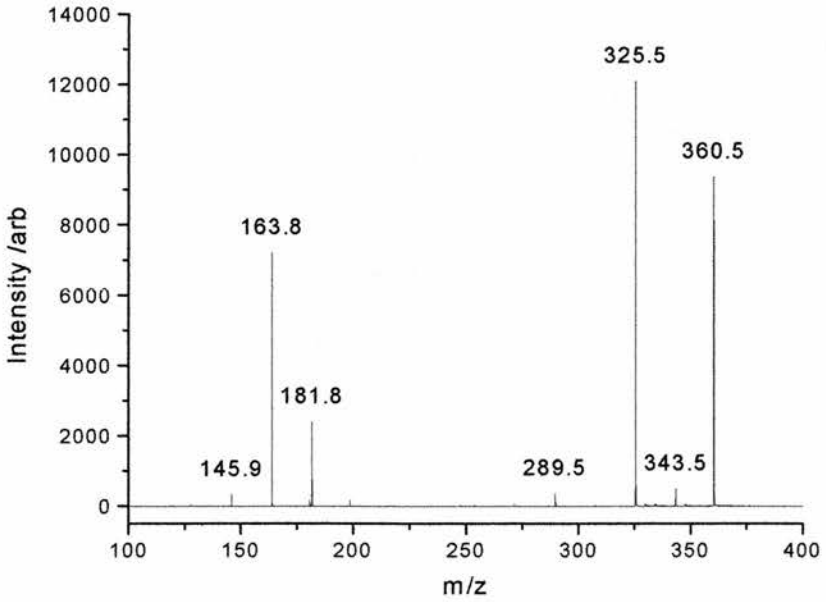


Figure 5-6 MS/MS spectrum for trehalose obtained from m/z 360 precursor ion. (m/z 360.5 $[MH+NH_3]^+$, m/z 343.5 $[M+H]^+$, m/z 325.5 $[MH-H_2O]^+$, m/z 181.8 $[C_6H_{13}O_6]^+$, m/z 163.8 $[C_6H_{11}O_5]^+$).

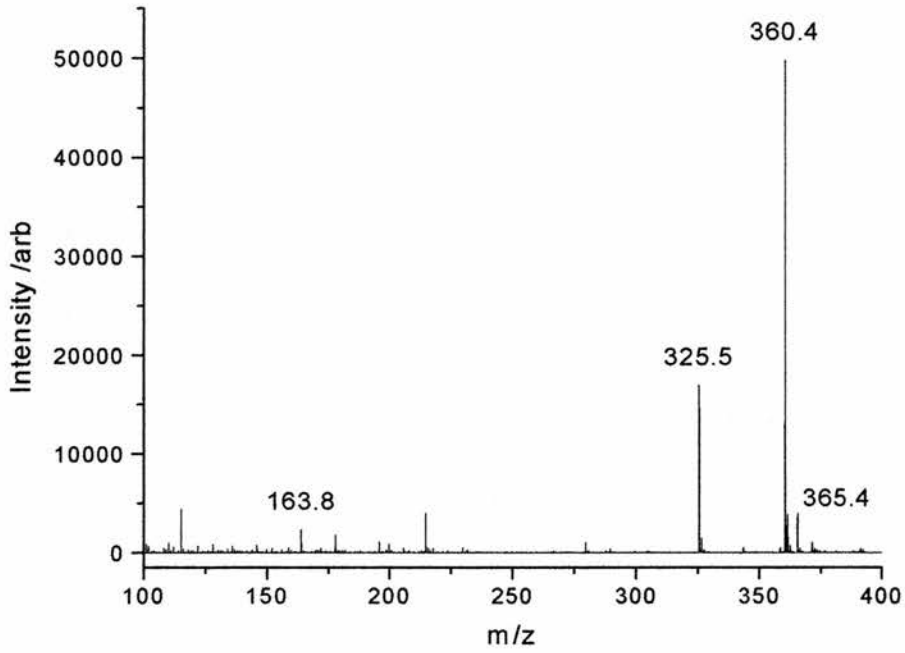


Figure 5-7 nESI MS spectrum for maltose (0.01 mg/mL).

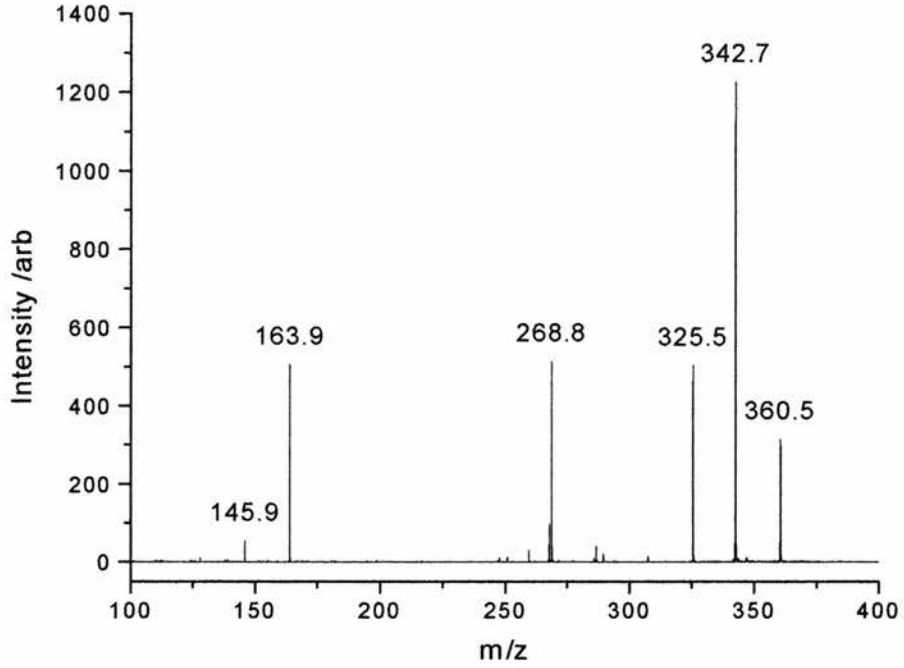


Figure 5-8 MS/MS spectrum for maltose obtained from m/z 360 precursor ion.

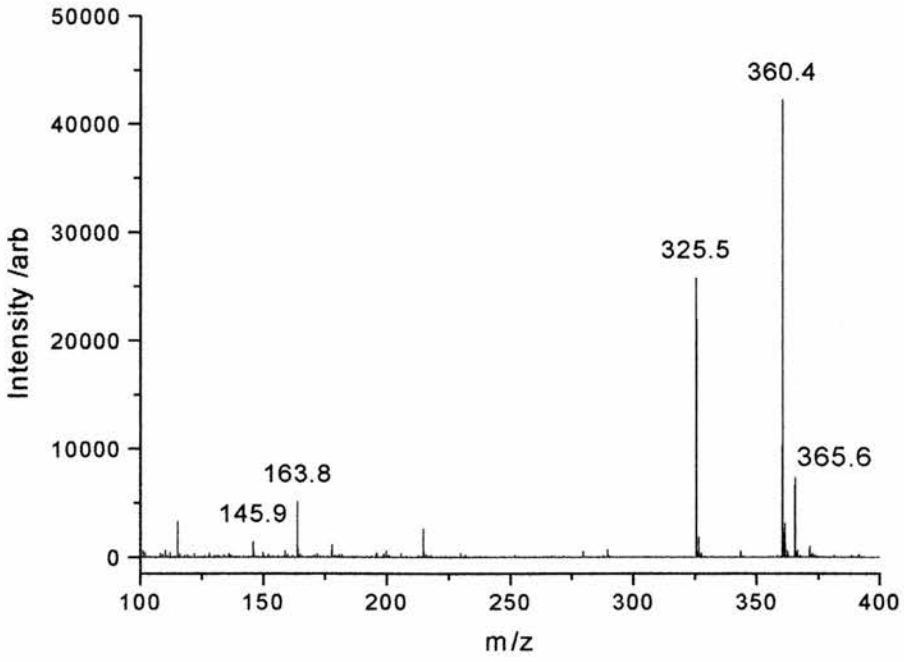


Figure 5-9 nESI MS spectrum for maltulose (0.01 mg/mL).

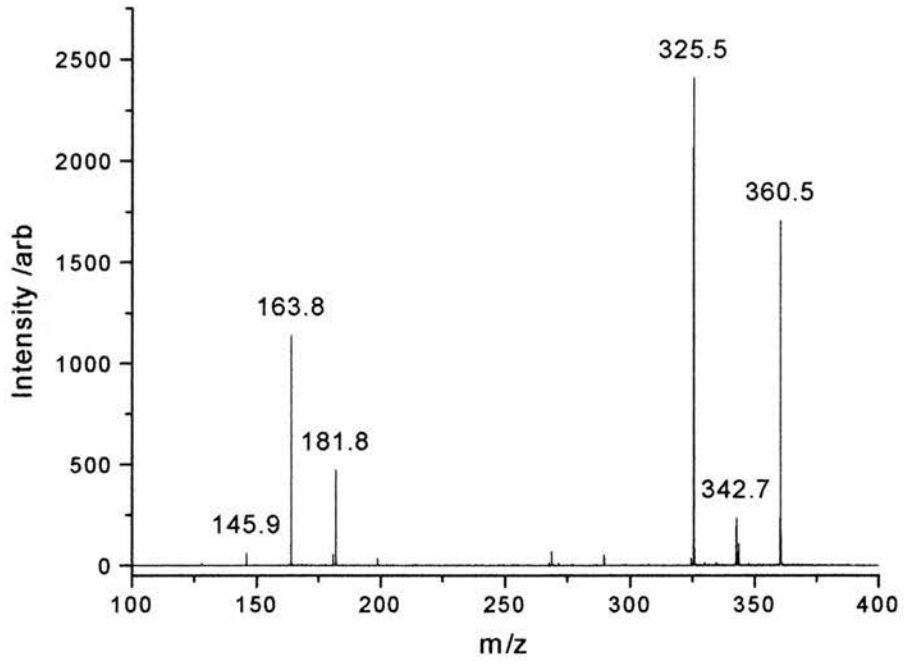


Figure 5-10 MS/MS spectrum for maltulose obtained from m/z 360 precursor ion.

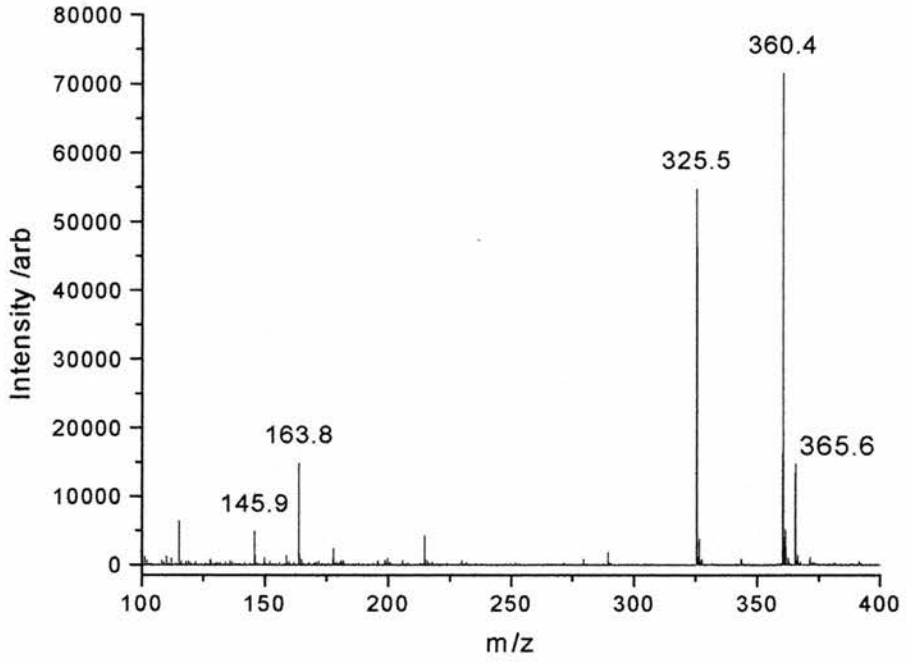


Figure 5-11 nESI MS spectrum for sucrose (0.01 mg/mL).

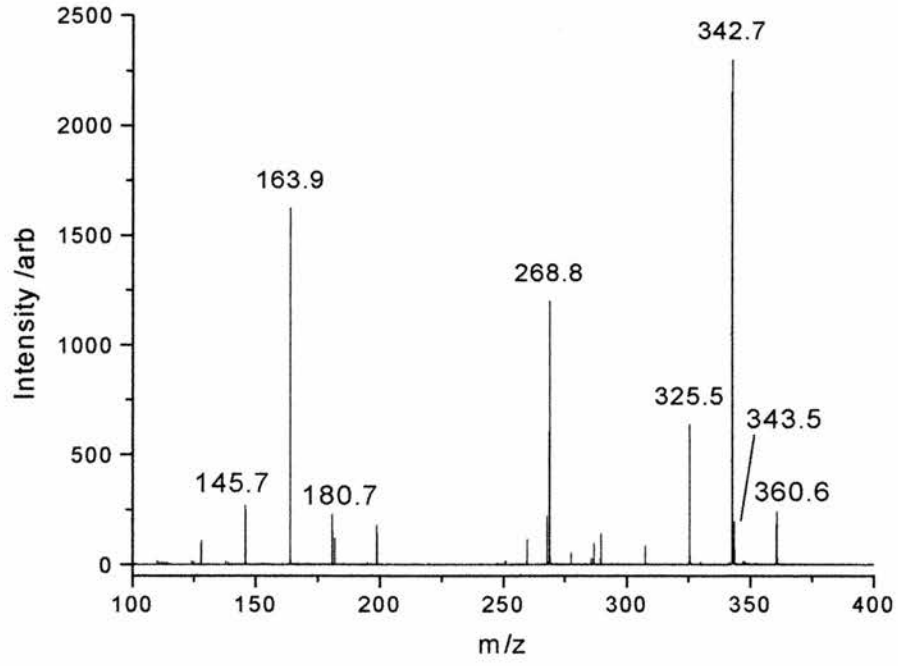


Figure 5-12 MS/MS spectrum for sucrose obtained from m/z 360 precursor ion.

MS/MS spectra can often confirm the identification of a molecule. Many compounds are isobaric, that is they have the same molecular weight. The use of collisional induced dissociation can frequently provide spectra containing a number of unique fragment ions. The combination of a precursor ion mass together with the characteristic fragment ions can be used to confirm the identity of the compound.

The MS spectra obtained for the four disaccharides trehalose, maltose, maltulose and sucrose were all extremely similar, with identical patterns of adduct ions. The fragmentation patterns for each molecule seen in the MS/MS spectra revealed little difference between trehalose and maltulose, and between maltose and sucrose. It would be difficult from these spectra to conclusively identify which specific disaccharide is present in an unknown mixture.

Published data shows that the predominant disaccharide within the fungal cells of *Neurospora crassa* is trehalose [180,188,191,192,193,194]. This molecule is synthesised by the fungi, and at enhanced levels in cells experiencing stress. The assumption was therefore made that the majority of the disaccharide present within the cells that would be microsampled was going to be trehalose; other disaccharides, including maltose would also be present, but at a much reduced concentration (<5% of trehalose concentration) [195]. The term disaccharide will from here on be used to describe this combination of trehalose and the other disaccharides.

On the basis of the MS/MS spectra, a suitable selected reaction monitoring transition for detection of trehalose (as well as other disaccharides) would be m/z ($[MH+NH_3]^+$ 360→$[MH-C_6H_{12}O_6]^+$ 163), corresponding to cleavage of the glycosidic bond.

### 5.5.2 CE-MS interface optimisation for disaccharide detection

In order to optimise and further develop the interface, a simple delivery system that would provide a constant analyte source was required, with similar characteristics to those that would be encountered when running true CE-MS experiments. The technique chosen was to spike the CE running buffer with analyte. This mimics a continually eluting analyte band and is appropriate for optimisation of the interface. This system was prone to occasional problems, although these were similar to those

that would be encountered with electrokinetic sample injection. Using this spiked running buffer the electrospray conditions could be tuned and the Q-ToF operating conditions optimised. A number of analytes were investigated, including trehalose, angiotensin I, and maltose. The electrospray sheath flow conditions and the relative linear alignment of the components of the tri-axial probe were varied and were found to be critical to the efficiency of the ionisation process and the resulting the ion abundance. Since electrospray is a concentration dependent process, a critical consideration in improving the sensitivity of detection was reducing the sheath flow rate relative to the CE flow rate. Micromass recommend a sheath flow of 0.8 μL/min. However, with careful preparation of the capillary outlet (ensuring it was square and flat), also reducing the contact between CE eluent and the stainless steel of the interface by extending the CE capillary 2 mm beyond the interface, it was possible to reduce the sheath flow to 0.23 μL/min. The position of the capillary outlet relative to the mass spectrometer source cone was also found to be critical. Prior to any experiment, the position of the interface was adjusted to optimise the signal. The height of the inlet vial relative to the outlet at the CE interface was critical to the production of a stable spray. A fall of 2 cm was found to result in a good spray and was maintained throughout subsequent experiments.

### 5.6 Development of quantifiable CE-MS for detection of disaccharides

At this stage, no capillary electrophoresis separation had yet been attempted. It was predicted (correctly) that the CE segment of the experiment might be the limiting factor in the reliability of the more elaborate and considerably more time consuming CE-MS SiCSA studies. As later discussed, once the samples had been aspirated from the cell, failure of the electrical continuity of the capillary and interface was the most common reason for an experiment to fail. Therefore, it was clearly necessary that some of these disaccharides were examined using CE-MS, prior to attempting the more complicated cell sampling experiments, to ensure that this approach could be used to quantifiably detect them.

The Isco electropherograph and modified CE-MS interface were assembled as described in Section 4.6.4. The samples were prepared at 0.01 mg/mL in running

buffer Electrophoresis was performed as described in Section 4.8.1. Samples were loaded by electrokinetic injection (5s at 5 kV) resulting in an injection volume of 2.93 nL and separation was performed using an applied potential of 20 kV. Care was taken to minimise the length of the capillary and to select a buffer solute and pH that maximised the EOF.

Mass spectrometric detection was achieved with the Q-ToF operating in MS-TOF mode. As expected, trehalose co-eluted with the solvent front, indicated by a marker for EOF, thiourea (Sigma, UK). The length of the capillary that was required to permit injection of cell extract into column under the microscope and yet still connect to the CE-MS interface on the Q-ToF was far longer than is typical for normal CE separations. This had the undesirable effect of increasing the migration time and increasing the effect of band dispersion.

The effects are quite dramatic as can be seen from a comparison of Figure 5.13 and 5.14. Figure 5.13 shows the CE-MS chromatogram obtained on the Q-ToF for trehalose, recorded in selected ion monitoring (SIM) mode using the $[MH+NH_3]^+$ adduct ion at m/z 360. This adduct ion was chosen for the SIM chromatograms as it is the most abundant in the CE-MS spectra. The data was recorded using a capillary 1500 mm in length, with an early choice of running buffer (20 mM ammonium acetate, pH 6). The elution time for trehalose of 38.6 min is extremely long and the peak resolution is rather poor (13376 theoretical plates per meter). As shown in Figure 5.14, shortening the length of the capillary (886 mm) as much as possible, together with optimisation of the buffer (10 mM ammonium acetate, pH 8.5) reduces the separation time to 8.2 min. The peak resolution also increases markedly (97237 theoretical plates per meter).

Figure 5.15 shows the integrated mass spectrum corresponding to the peak eluting at 8.2 minutes in the CE-MS chromatogram shown in Figure 5.14. In the CE-MS spectrum the adduct ions expected can be clearly seen; m/z 365.4 $[M+Na]^+$ (expected monoisotopic peak 365.1), m/z 360.5 $[MH+NH_3]^+$ (expected monoisotopic peak 360.2). The characteristic fragment ion at m/z 325.5 due to loss of water from the protonated species $[MH-H_2O]^+$ (expected monoisotopic peak 325.1), can also be

seen. Due to the fact that the mass calibration of the Q-ToF was not exact, the observed peaks are all slightly higher than the predicted monisotopic peaks.

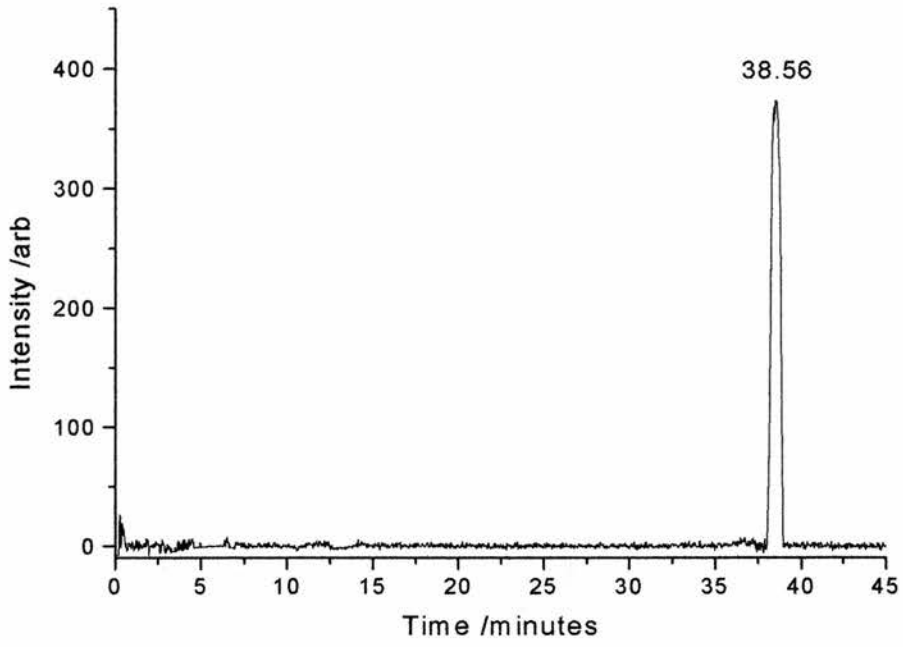


Figure 5-13 CE-MS chromatogram obtained for trehalose, recorded in SIM mode, using the adduct ion m/z 360 $[MH+NH_3]^+$. (Capillary length 1500 mm; buffer 20 mM ammonium acetate, pH 6; peak resolution 13376 TPPM).

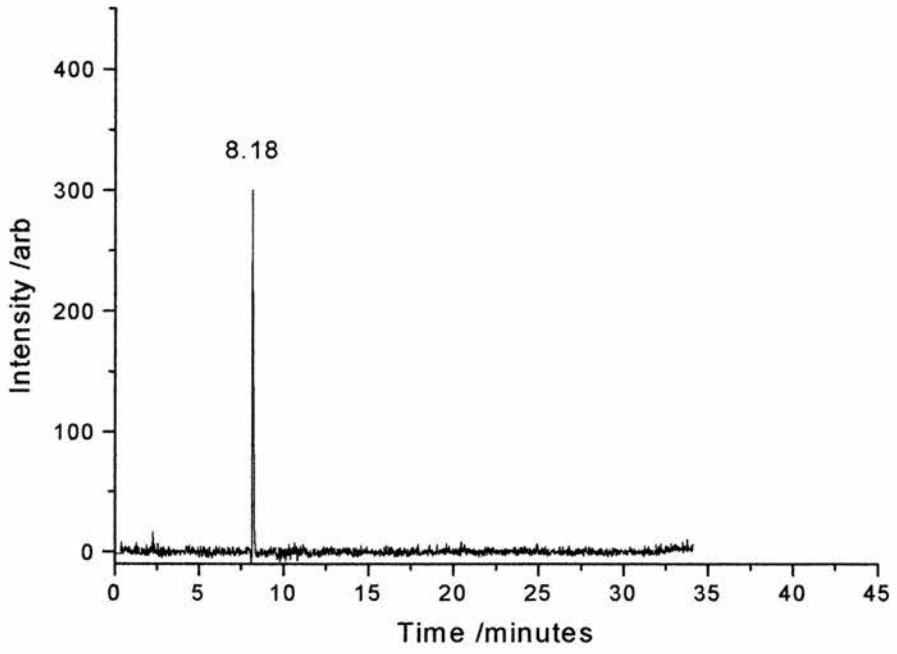


Figure 5-14 CE-MS chromatogram obtained for trehalose, recorded in SIM mode, using the adduct ion m/z 360 $[MH+NH_3]^+$. (Capillary length 860 mm; buffer 10 mM ammonium acetate, pH 8.5; peak resolution 97237 TPPM).

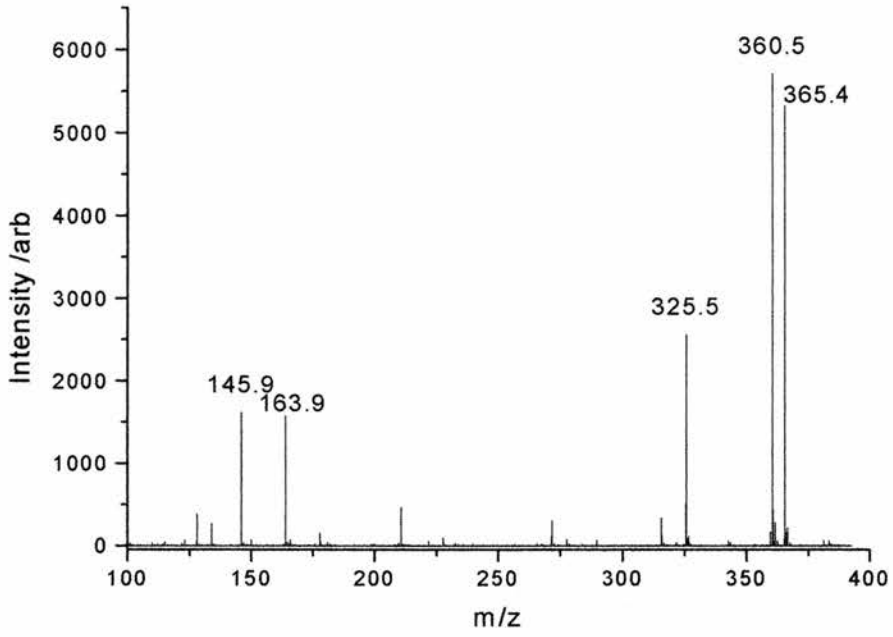


Figure 5-15 Integrated CE-MS spectrum corresponding to peak at 8.1 minutes in Figure 5.14. (m/z 365.4 $[M+Na]^+$, m/z 360.5 $[MH+NH_3]^+$, m/z 325.5 $[MH-H_2O]^+$).

### 5.6.1 Internal calibration

To further aid eventual quantitation of the level of disaccharide in microsampled fungal cells, an internal calibrant was employed. This standard was electrokinetically injected after the analyte, to compensate for run-to-run variations in the CE separation process and electrospray ionisation efficiency. In routine analysis by LC-MS, an internal standard would be mixed prior to preparation of the sample, to correct for variation in sample extraction and injection, as well as in separation and detection. Unfortunately, due to the sample volume and injection method used in this work, that approach was not possible. Therefore, extra care had to be taken to minimise errors due to variations in the sample injection procedure. Angiotensin I (A9650: Sigma Aldrich, UK) was chosen as the internal standard, as this was found to elute at a similar time to, but not co-elute with, the disaccharides. Angiotensin I

was found to provide a strong CE-MS ESI signal. (Angiotensin I is a protein with a formula weight of 1296 Da, typically observed with ESI in the 2+ charge state at m/z 648.8 (monoisotopic mass); sequence: Asp-Arg-Val-Tyr-Ile-His-Pro-Phe-His-Leu).

A concentration of 0.25 mg/mL of angiotensin I was chosen, and a bulk standard made up in running buffer (10 mM ammonium acetate, pH 8.5), aliquoted and stored at –20°C. All calibrations were performed using this reference standard. Calibrant introduction was achieved by first injecting the analyte as described previously, then transferring the capillary inlet to the reservoir containing the calibrant, and injecting a plug of calibrant solution. The capillary was then transferred to the running buffer reservoir to carry out the separation. Figure 5.16 shows a CE-MS chromatogram obtained on the Q-ToF for angiotensin I, recorded in selected ion monitoring mode, using the doubly charged ion (m/z 648.7). This data was obtained using a capillary 860 mm in length and a running buffer of 10 mM ammonium acetate, pH 8.5.

For all later CE-MS experiments the integrated peak area for the internal standard in the chromatogram was normalised to 1000 and used a correction factor for any peaks corresponding to other ions of interest. The angiotensin I calibrant performed an additional role in identifying runs where no analyte was detected due to experimental failure.

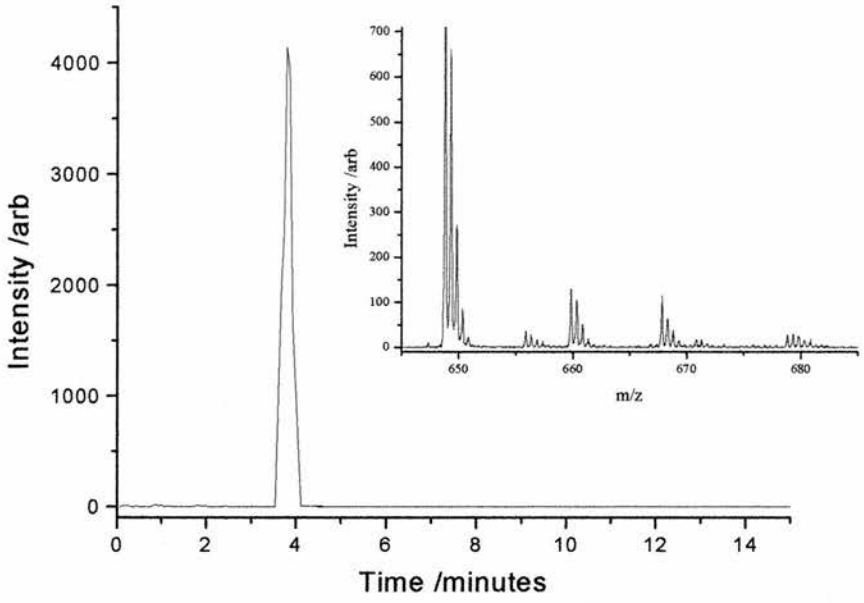


Figure 5-16 CE-MS chromatogram obtained for angiotensin I, recorded in SIM mode using the doubly charged ion (m/z 648.8). (Capillary length 860 mm; buffer 10 mM ammonium acetate, pH 8.5). The insert shows an expansion of the integrated MS spectrum corresponding to this chromatographic peak in the region of the 2+ ion.

### 5.6.2 Calibration data for the detection of trehalose by CE-MS

In order to accurately determine the concentration of disaccharides present in fungal cells, it was necessary to generate calibration data. This was carried out using trehalose, as it was predicted to be the predominant disaccharide present in the fungal cells of *Neurospora crassa*.

The reliability of a quantitative analysis depends on the precision and accuracy of the weighing, pipetting and most importantly the calibration curve. Therefore a dilution scheme was chosen, and a number of rules were observed to minimise errors during preparation of the samples. Weighing of samples of less than 1 mg was avoided as

this could introduced weighing and transfer errors. Serial dilutions were avoided as any mistake made early in the dilution series would affect all subsequent dilutions. Recently calibrated pipettes were used. Pipetting of volumes less than 10 μL was avoided as smaller volumes lead to increased error. Samples were run from lowest to highest concentration to guard against carry-over from previous samples. The CE-MS interface was placed 860 mm from the capillary inlet. Analyses were performed using the same apparatus as described in Section 4.6 with the Q-ToF operating in MS-TOF mode. CE injections were performed by electrokinetic injection (5s at 5kV).

In the resulting CE-MS SIM chromatograms the areas of the peak for trehalose (displayed in SIM mode using the $[MH+NH_3]^+$ adduct ion at m/z 360) were integrated. The integrated area of the corresponding peak for the internal standard was also measured and used to correct the data for each acquired chromatogram for any variation in the ionisation and detection efficiency. Any data points with an error of 15%, i.e. 115% or 85% of the expected value, were omitted. The calibration data is given in Table 5.3. The data points for the peak area of trehalose, both uncorrected and corrected to the normalised peak area of the internal standard, are also plotted in the form of a graph in Figure 5.17 so that the degree of linearity in the data can be more easily seen.

Table 5.3 Calibration data for detection of trehalose by CE-MS

| Mass of trehalose on column (pg) | Angiotensin I peak area | Trehalose uncorrected peak area | Trehalose corrected peak area |
|---|---|---|---|
| 375.25 | 1028.76 | 125.54 | 122.03 |
| 375.25 | 926.86 | 106.47 | 114.87 |
| 375.25 | 901.31 | 101.45 | 112.56 |
| 187.62 | 800.95 | 45.75 | 57.12 |
| 187.62 | 1169.79 | 61.73 | 52.77 |
| 187.62 | 906.09 | 57.60 | 63.57 |
| 93.81 | 982.69 | 29.21 | 29.72 |
| 93.81 | 1087.28 | 31.35 | 28.83 |
| 93.81 | 838.18 | 23.39 | 27.91 |
| 18.1 | 1403.85 | 8.03 | 5.72 |
| 18.1 | 1391.39 | 7.11 | 5.11 |
| 18.1 | 954.55 | 5.88 | 6.16 |
| 9.38 | 1451.05 | 4.15 | 2.86 |
| 9.38 | 1476.56 | 3.78 | 2.56 |
| 9.38 | 1783.78 | 3.96 | 2.22 |

Volume injected each for angiotensin I and trehalose 2.93 nL. Concentration of angiotensin I standard 0.25 mg/mL.

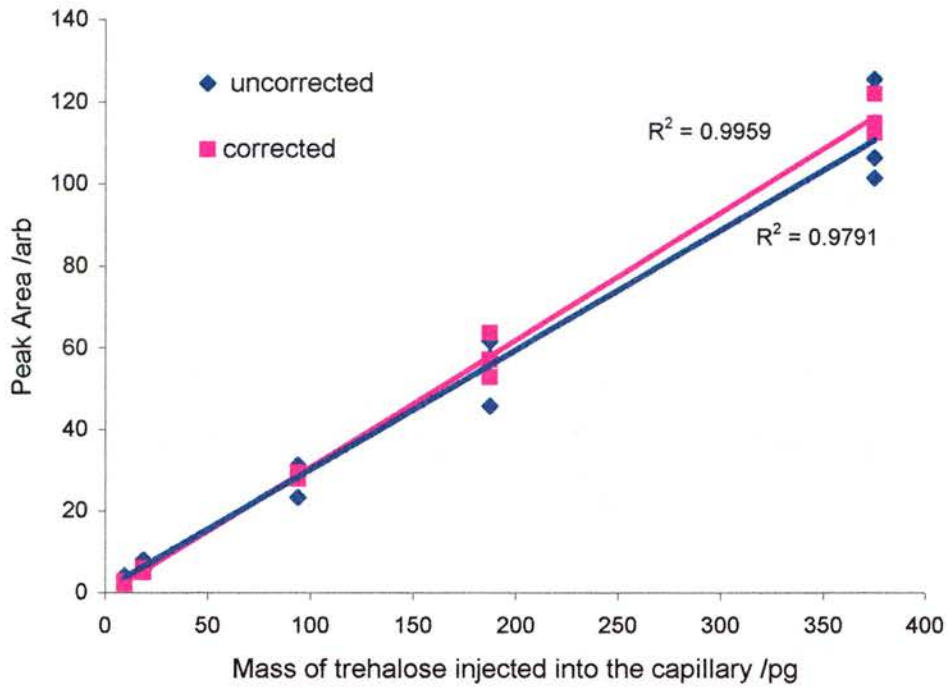


Figure 5-17 Calibration data for detection of trehalose by CE-MS. Data points shown for peak area of trehalose, uncorrected and corrected to normalised peak area of internal standard.

### 5.6.3 Limit of detection and quantification

As can be seen from Figure 5.17, correction of the detected peak areas for trehalose based on the internal standard reduced the spread of the data points at any particular concentration. This improvement was taken as positive proof that the use of internal calibration was effective in reducing variations in electrospray ionisation efficiency from run to run. Therefore, the corrected calibration data was used for all further measurements.

The limit of quantification was taken to be 6 times the standard deviation ($\sigma$) of the noise in the CE-MS SIM chromatograms and the limit of detection was taken to be $3\sigma$ of the noise. The limit of quantification for trehalose by CE-MS was determined to be 36.2 pg and the limit of detection 18.1 pg.

With the equipment used in this investigation, and the need to be able to inject sample under a microscope (this would not be possible if the capillary was manipulated by an autosampler), the sample injection reproducibility might have been affected. Other errors in the separation might have resulted from variations in the molarity of the running buffer and/or insufficient degassing. Therefore, accuracy of the calibration data was tested using a number of samples of trehalose of known concentration, and the agreement with the predicted concentrations was found to be good. This calibration data was used in all the later experiments to quantify the level of disaccharides present in the cells of *Neurospora crassa*.

### 5.7 Analysis of fungal cell extract

Fungal cell extract was aspirated from a Hex-1 mutant cell compartment and transferred into the CE capillary entrance, as described in Section 4.6. The volume of cell extract aspirated from the cell compartment was 0.85 nL. Separation was performed as described in Section 4.6. Data from the first successful analysis of fungal cell extract for disaccharides is presented in Figures 5.18-5.20.

Figure 5.18 shows the CE-MS TIC chromatogram, acquired on the Q-ToF, for this first sample of fungal extract. Separation was performed using a capillary 860 mm in length and a running buffer of 10 mM ammonium acetate, pH 8.5. The TIC chromatogram reveals very little information. Figure 5.19 shows the corresponding CE-MS chromatogram, displayed in single ion monitoring (SIM) mode, by selection of m/z 360. A peak in the data is now clearly visible at 8.2 minutes. Comparison of the data in these two figures illustrates very clearly the advantage of using the single ion monitoring mode to reduce the effects of background ions.

Figure 5.20 shows the corresponding integrated MS spectrum for the peak in Figure 5.19 at 8.2 minutes. This can be compared with the CE-MS spectrum of the trehalose standard (Figure 5.15). The adduct ions, $[M+Na]^+$ and $[MH+NH_3]^+$, which would be expected, can be seen at m/z 364.9 and 359.9, respectively. The characteristic fragment ion due to the loss of water from the protonated species can also be seen at m/z 324.9.

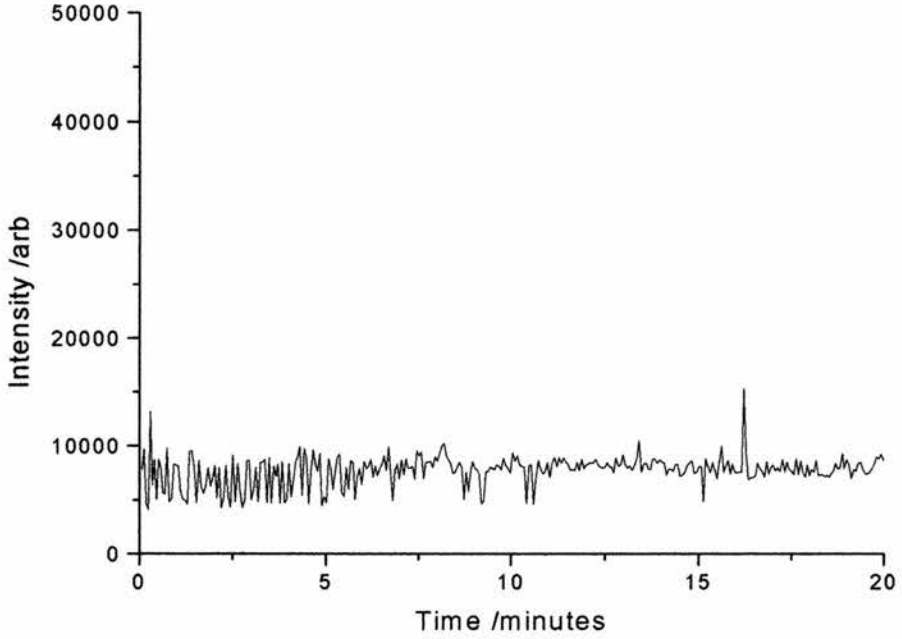


Figure 5-18 CE-MS TIC chromatogram of fungal cytoplasm from Hex-1 mutant of *Neurospora crassa*. (Sample volume 0.85 nL; CE capillary length 860 mm; buffer 10 mM ammonium acetate, pH 8.5).

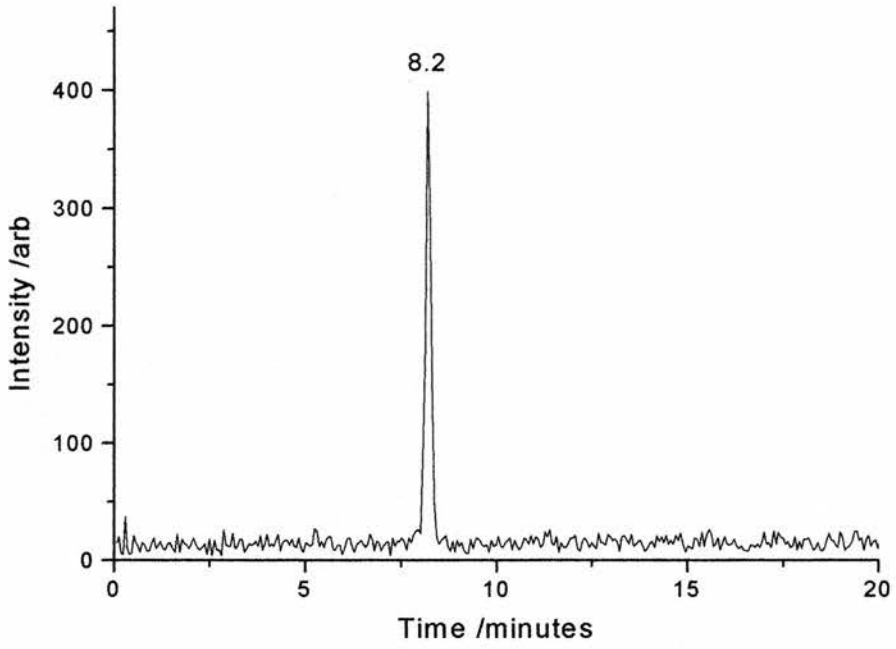


Figure 5-19 Corresponding CE-MS SIM chromatogram for same sample as Figure 5.18. (Displayed in SIM mode by selection of m/z 360).

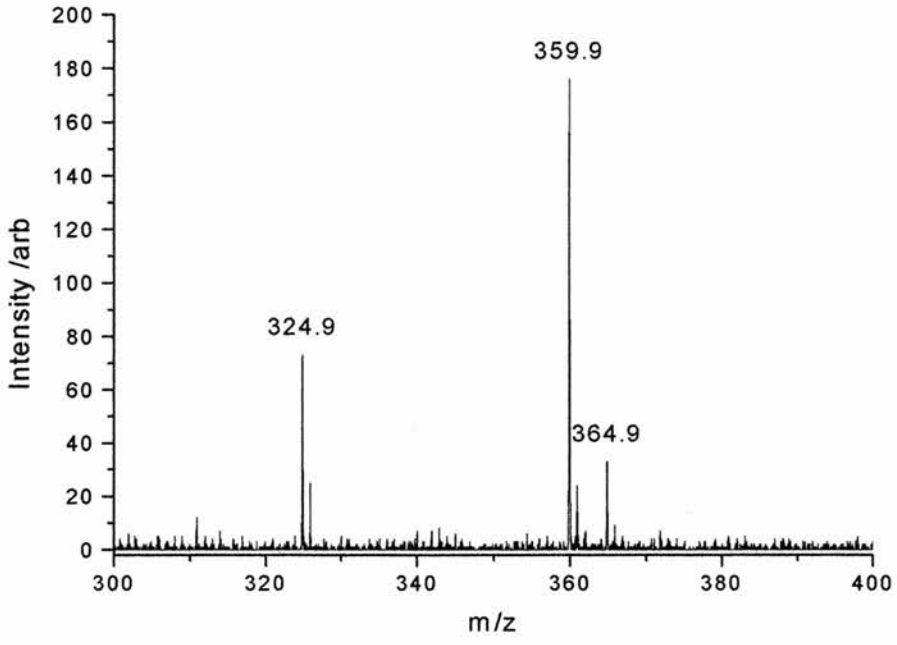


Figure 5-20 Integrated CE-MS spectrum corresponding to peak at 8.2 minutes in Figure 5.19. (m/z 364.9 $[M+Na]^+$, m/z 359.9 $[MH+NH_3]^+$, m/z 324.9 $[MH-H_2O]^+$).

The peak at 8.2 minutes visible in the selected ion monitoring chromatogram shown in Figure 5.19 matches the elution time expected for disaccharides and the corresponding integrated MS spectrum (Figure 5.20) supports this assignment. The mass of disaccharide represented by the integrated area of this chromatographic peak is 386.81 pg, implying an intra-cellular concentration of 451.66 pg/nL or 1.32 mM.

Although this value appears reasonable, based on a comparison with earlier studies sampling bulk cell mass (Section 5.8), there was a risk that however carefully the samples were aspirated, there could have be contamination from the extra-cellular matrix containing a high concentration of disaccharides. This contamination would result in an exaggerated measure of the ion abundance. This risk of contamination was reduced by the use of the Hex-1 mutant, since the streaming of cytoplasm

maintains the turgor pressure in the cell compartment when microsampling is taking place. Under these conditions, it was found that it was possible for the cell extract to leak into the extra-cellular matrix. One possible solution to the problem of contamination was to carry out the microsampling extremely quickly (~1 s). In this way, sample might be acquired and the pipette removed from the cell before contamination or dilution could occur. However, this was not a feasible practical approach. Also there would be no clear indication that contamination had taken place.

A further solution was to grow the cells on a minimal agar. This would have reduced the risk of disaccharide contamination from the media. This idea was again discounted, as cells grown on minimal media displayed substantially reduced growth rates. In fact, the hyphae barely grew beyond the limits of the agar block that was used to inoculate the agar plate and prevented microsampling. The presence of malt extract in the agar block used to inoculate the culture plate would also have presented a source of maltose contamination.

### 5.7.1 Investigation of possible contamination by extra-cellular maltose

In order to have confidence in the detected concentration of intracellular disaccharide, it was clearly necessary to investigate the effect that any possible accidental contamination from the surrounding culture medium would have on the detected intra-cellular concentration of the disaccharides of interest.

When silicone oil was added to the culture dish, a thin layer of water was observed on the surface of the agar, under the oil. The layer was suspected to be a potential source of contamination in cases where inaccurate microsampling might have led to the accidental uptake of some extra-cellular medium. This possibility was investigated by microsampling directly from this liquid layer. A somewhat larger volume of this liquid (1.8nL) than was typical for cellular microsampling was aspirated, and transferred into the separation capillary. The resulting CE-MS SIM chromatogram corresponding to selection of m/z 360 is shown in Figure 5.21. The capillary length was 860 mm and a running buffer of 10 mM ammonium acetate pH 8.5 was used. The corresponding integrated MS spectrum for the peak at 9.8 minutes

in Figure 5.21 is shown in Figure 5.22. The mass spectrum and elution time are consistent with the presence of disaccharides.

The integrated area of the peak in the CE-MS SIM chromatogram (423.69) far exceeds any of the points in the calibration data presented in Table 5.3. It is, therefore, not possible to place a firm value on the concentration or the mass of disaccharide loaded into the capillary. The value is considerably higher than was expected, since the culture media contains only 2% malt extract.

A second possibility, namely that extra-cellular media was drawn into the capillary when the capillary inlet contacts the liquid present above the culture media, was also investigated. The separation capillary inlet was dipped into the liquid present between the agar and the silicone oil, in the same way that might occur if a sample was going to be injected. It was then held in place for a period consistent with the time interval required to transfer fungal cell cytoplasm from the micropipette to the separation capillary. The capillary was then transferred to the running buffer vial and a separation performed as normal. Again, an abundant peak consistent with disaccharide was detected in the CE-MS SIM chromatogram, almost identical to that observed previously when sampling directly from the liquid layer above the agar.

This experiment demonstrated that contamination could occur simply from the act of dipping the capillary into the culture vessel and would be the most probable cause of contamination. In order to try to avoid this, transfer was attempted in air above the culture vessel but this was found to be ineffective. It was, therefore, deemed essential that sample transfer was performed in a separate pettri dish containing fresh silicone oil to minimise any possible contamination. Therefore, in all further experiments, the pipette containing the sample was lifted above the culture dish, a Petri dish containing the pure silicone oil was moved into place, and the needle lowered under the surface. The separation capillary was then moved into place and the transfer performed as described in Section 4.5.

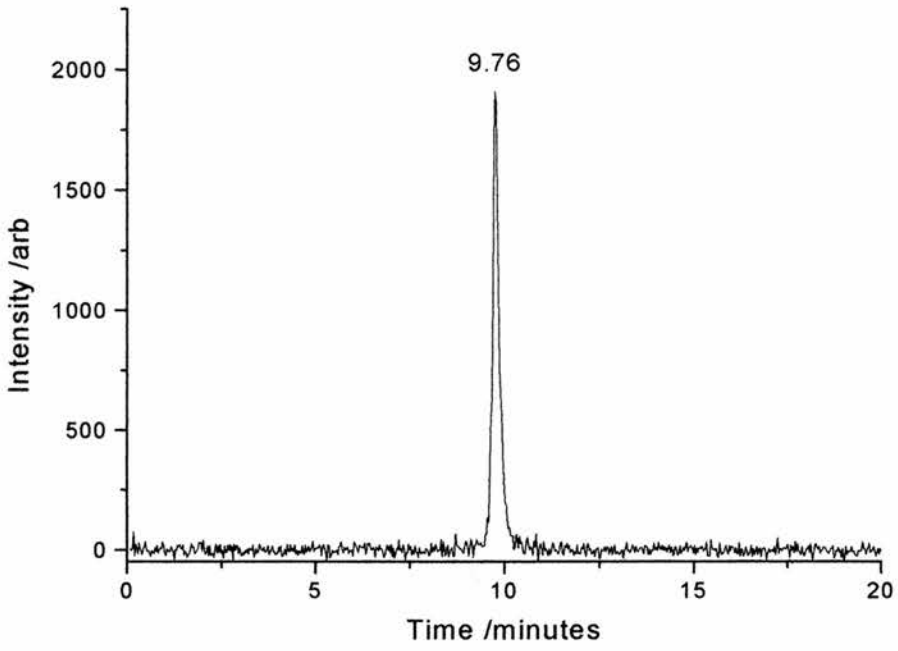


Figure 5-21 CE-MS SIM chromatogram for liquid sampled from surface of culture plate. (Displayed in SIM mode by selection of m/z 360; volume sampled 1.8 nL. Capillary length 860 mm; buffer 10 mM ammonium acetate pH 8.5).

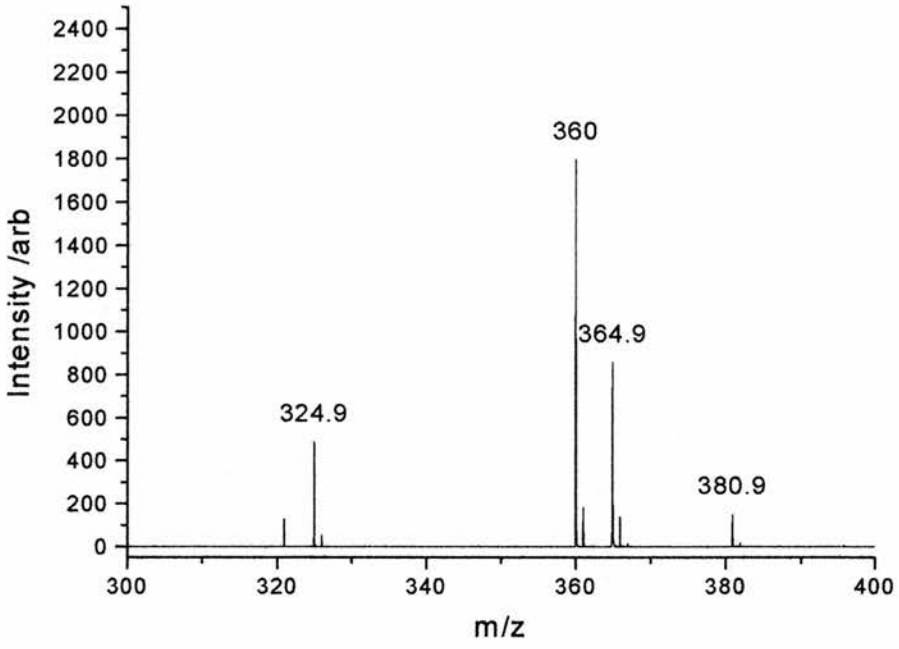


Figure 5-22 Integrated CE-MS spectrum corresponding to peak at 9.7 minutes in Figure 5.21.

### 5.7.2 Extra-cellular markers

Despite these stringent precautions it was important to have some method of detecting when any sample contamination might have occurred. The solution to this problem involved the addition of an extra-cellular marker not naturally occurring within the target cells. A number of possible markers were investigated. The ideal molecule must not occur naturally in the fungal cell, not be taken up by the cells by either active transport or simple diffusion, and must be detectable at levels similar to the disaccharides of interest. Laser induced fluorescence was chosen as the detection technique for the extra-cellular marker due to its high sensitivity [196], and its specificity. The molecule chosen as a marker was rhodamine B isothiocyanate–dextran (Molecular Probes, USA) [197] with a molecular weight of ~10,000 Da. The dextran conjugated molecules available offered good water solubility and low toxicity in plants [198]. Of the many markers available as conjugates rhodamine was chosen as it is significantly brighter and more photostable than most fluorescein dextrans. It is also not actively taken up by the cells and is not membrane impermeant [199].

Samples conataining rhodamine B isothiocyanate–dextran were prepared at a range of concentrations (Table 5.4) in running buffer (10 mM ammonium acetate at pH 8.5). The LIF detector, described fully in Section 4.7, was assembled close to the CE-MS interface, in such a way that it was not necessary to lengthen the separation capillary. Sample injection was performed electrokinetically (5s at 5 kV), and separation was carried using an applied potential of 20 kV. A typical CE-LIF chromatogram (generated using the pretty picture integrator, Section 4.7.2) is shown in Figure 4.22. The time does not relate to separation time, as only the section of video relating to the rhodamine B isothiocyanate–dextran peak was processed by the program to reduce the time taken for analysis.

The results of these experiments to determine the limit of detection of rhodamine B isothiocyanate-dextran are given in Table 5.4. Data points with an error of 15%, i.e. values above 115% and below 85% of the expected value, were discarded. The data points are also plotted in the form of a graph in Figure 5.23. The $R^2$ value of 0.96

shows that the detection strategy offers a good linear response. The limit of quantitation was taken to be 6σ of the noise in the CE-LIF chromatogram and the limit of detection was taken to be 3σ of the noise.

Table 5.4 Calibration data for detection of extra-cellular marker by CE-LIF

| Concentration of extra-cellular marker mg/mL | Injection volume (nL) | Mass of extra-cellular marker on column (ng) | Integrated fluorescence intensity |
|---|---|---|---|
| 0.5 | 2.93 | 1.46 | 1748.3 |
| 0.5 | 2.93 | 1.46 | 1817.5 |
| 0.5 | 2.93 | 1.46 | 1493.6 |
| 0.25 | 2.93 | 0.73 | 851.4 |
| 0.25 | 2.93 | 0.73 | 982.2 |
| 0.25 | 2.93 | 0.73 | 932.1 |
| 0.05 | 2.93 | 0.14 | 145.1 |
| 0.05 | 2.93 | 0.14 | 165.2 |

Extra-cellular marker: rhodamine B isothiocyanate–dextran.

The limit of detection for the extra-cellular marker was found to be 14.6 pg and the limit of quantitation 146.5 pg. As qualitative data is all that is required to determine that extra-cellular contamination has occurred, the limit of detection and not the limit of quantification, is of key importance.

The concentration of maltose in the liquid present above the agar media is expected to have a similar concentration as that of the media itself; approximately 0.02mg/mL. The limit of detection of trehalose by CE-MS was found earlier to be 18 pg. Therefore, the minimum volume of sample drawn into the capillary in which disaccharide could be detected is 0.9 nL. Consequently, as the detection limit for the extra-cellular marker is 14.6 pg, it was expected that, provided the concentration of this marker was at least 16.2 μg/mL, it would be possible to determine via LIF detection if any extra-cellular contamination had occurred. A concentration of

0.1 mg/mL was chosen. This concentration was six times the minimum required, in order to offer a suitable margin of error. The addition of this marker to the cell culture prior to commencement of microsampling could be reliably used as a control by which any SiCSA data from contaminated samples could be excluded.

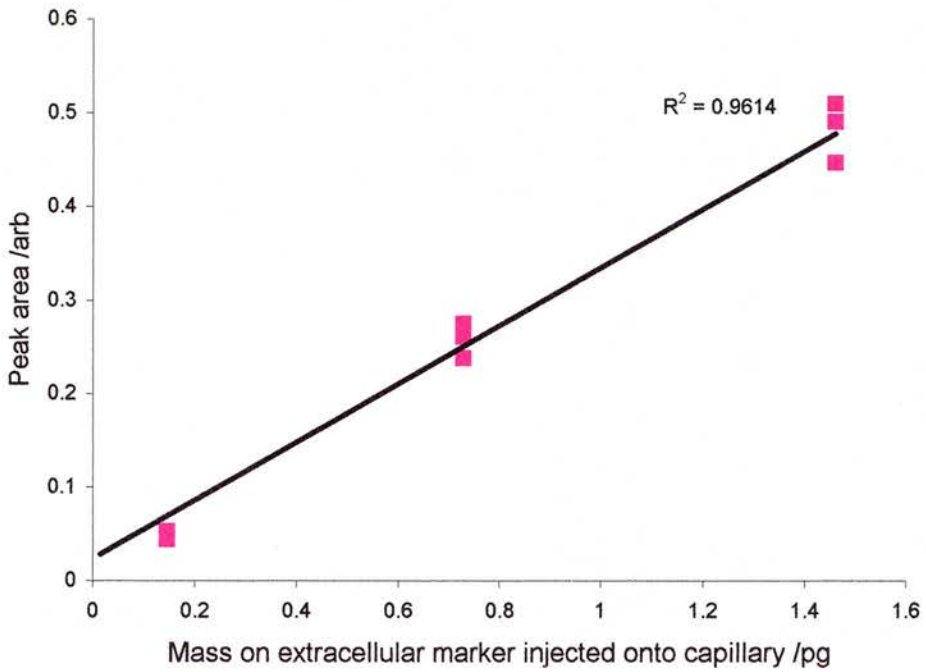


Figure 5-23 Calibration data for detection of rhodamine B isothiocyanate-dextran by CE-LIF

## 5.8 Identification of disaccharide in fungal cells

Following optimisation of the CE-MS experiment and the collection of calibration data for the internal standard (angiotensin I), extra-cellular marker (rhodamine B isothiocyanate-dextran) and trehalose, it was then possible to measure the concentration of disaccharide within the Hex-1 mutant of *Neurospora crassa*. Five minutes prior to the commencement of microsampling, a solution containing the extra-cellular marker (0.1 mg/mL) and 2% malt extract was added to the culture plate and covered with a thin layer (4mm) of silicone oil.

Samples were aspirated from fungal cells of the Hex-1 mutant of *Neurospora crassa* as previously described (Section 4.4). Transfer to the separation capillary was performed in a separate vessel containing clean silicone oil to minimise the risk of contamination from the extra-cellular matrix. Following sample transfer the internal standard (angiotensin I) was electrokinetically injected (5s at 5kV). Electrophoresis was performed in a fused silica capillary of internal diameter 50 μm, external diameter of 192 μm and a total length of 860mm. The LIF detector, which was used to confirm the presence or absence of the extra-cellular marker, was positioned 650 mm from the capillary inlet. Separation was performed as described in Section 4.6 using a running buffer of 10 mM ammonium acetate, pH 8.5.

A typical CE-MS TIC chromatogram for sampled fungal cell extract is shown in Figure 5.24. The volume sampled was 1.22 nL. The chromatogram contains a relatively large number of peaks, and it can be seen that the ion current increases dramatically after approximately 4 minutes. This increase is thought to correspond to the elution of a complex mixture of molecules present in the fungal cytoplasm.

The corresponding CE-MS chromatogram, displayed in single ion monitoring (SIM) mode, by selection of m/z 360, is shown in Figure 5.25. It shows a clear peak with a good signal-to-noise ratio (s/n 300). The elution time matches that expected for the disaccharides of interest.

The integrated CE-MS spectrum for the peak at 8.9 minutes in Figure 5.25 is shown in Figure 5.26. When compared with the CE-MS spectrum for trehalose standard (Figure 5.15) the ions match those expected both in m/z values and abundance. The ion at the ion at m/z 380.9 corresponds to $[M+K]^+$, the ion at m/z 364.9 to $[M+Na]^+$, the ion at m/z 360.0 corresponds to $[MH+NH_3]^+$ and the ion at m/z 324.9 corresponds to the loss of water from the protonated molecule$[MH-H_2O]^+$.

In order to conclusively identity the ion giving rise to the eluting peak at 8.9 minutes in the CE-MS SIM chromatogram shown in Figure 5.25, MS/MS was performed on the m/z 360 ion. Figure 5.27 shows a CE-MS/MS chromatogram obtained using selected reaction monitoring (SRM), on the transition m/z (360→163) that would be

expected for disaccharides based on the earlier nESI MS/MS spectra recorded for disaccharide standards. This CE-MS/MS chromatogram corresponds to fungal cell extract sampled in a different experiment, and because of this, the elution time varies slightly. Normally, when performing LC-MS separations, it is common to conduct MS and MS/MS scans alternately in the same experiment. However, in CE-MS the high resolution and correspondingly narrow eluting peaks means that this is very difficult. It was necessary to identify eluting species by CE-MS and then to confirm their identity with a separate CE-MS/MS experiment performed under the same conditions. It has been observed that elution times for analytes by CE commonly vary by as much as 10% [200]. This can be compared with chromatographic separations such as capLC and CEC, where elution times are highly reproducible. The signal-to-noise ratio in the CE-MS/MS SRM chromatogram (s/n 350) is similar to that in the CE-MS SIM chromatogram (Figure 5.25), although the overall ion abundance, as expected, is somewhat lower.

For completeness, Figure 5.28 shows the corresponding integrated MS/MS spectrum for the peak observed at 8.3 minutes in the CE-MS/MS SRM chromatogram shown in Figure 5.27. When compared with the nESI MS/MS spectra recorded for trehalose, maltose, maltulose and sucrose (Figures 5.6, 5.8, 5.10 and 5.12), it can be seen that that the fragment ions present and their relative abundance most closely match the data for trehalose and maltulose.

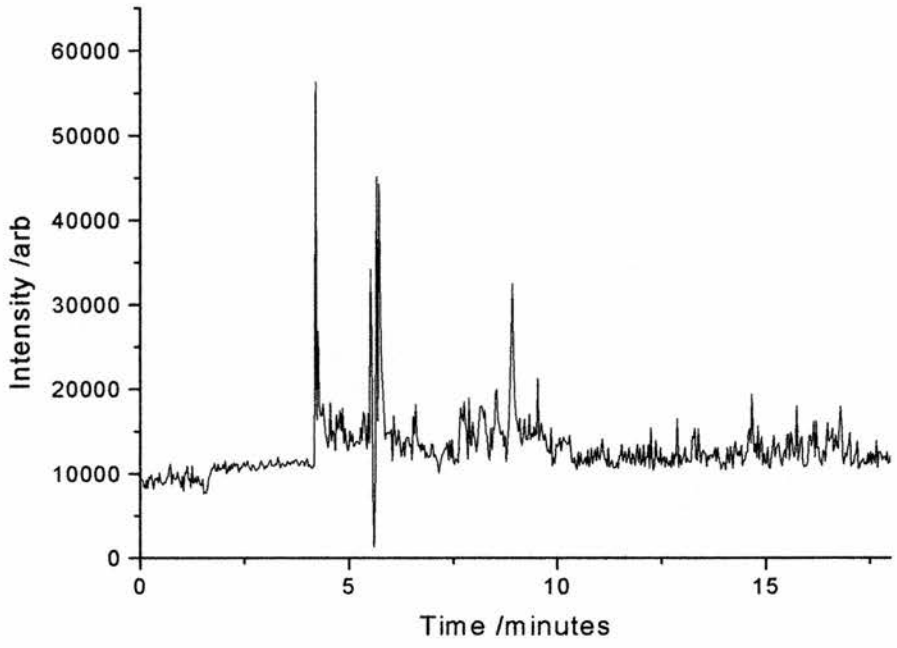


Figure 5-24 CE-MS TIC chromatogram of fungal cytoplasm from Hex-1 mutant of *Neurospora crassa*. (Sample volume 1.22 nL; CE capillary length 860 mm; buffer 10 mM ammonium acetate, pH 8.5).

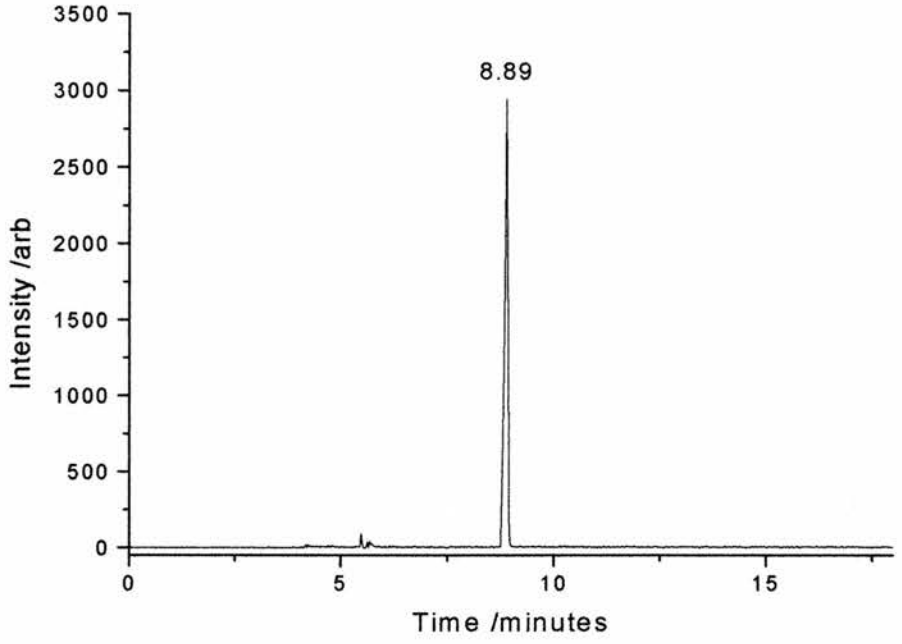


Figure 5-25 Corresponding CE-MS SIM chromatogram for same sample as Figure 5.25. (Displayed in SIM mode by selection of m/z 360)

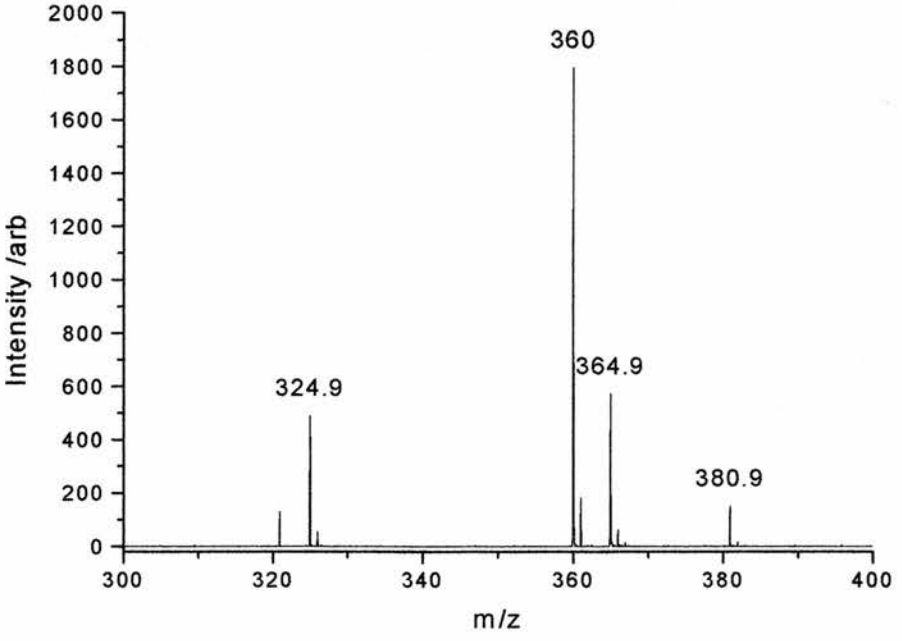


Figure 5-26 Integrated CE-MS spectrum corresponding to peak at 8.9 minutes in Figure 5.26.

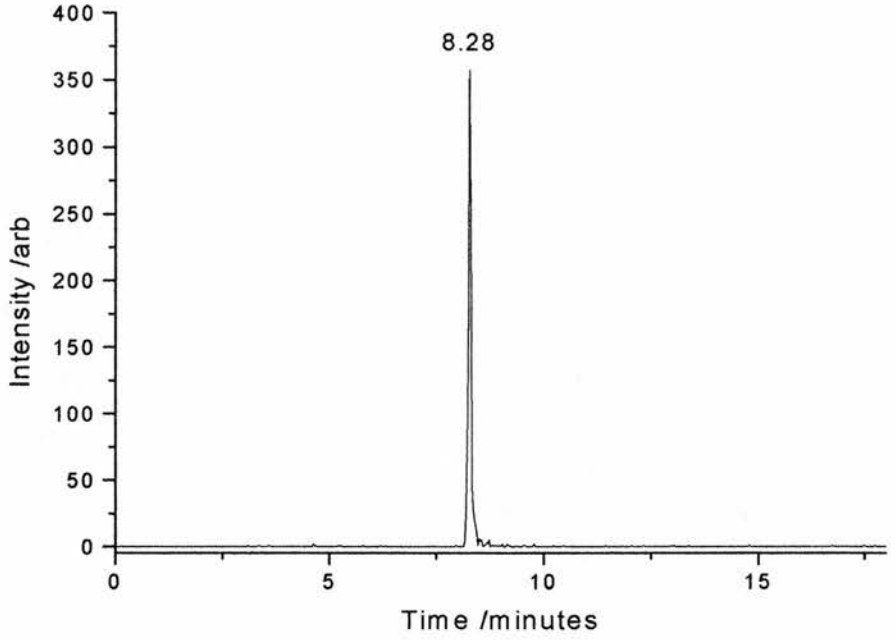


Figure 5-27 CE-MS/MS SRM chromatogram of fungal cytoplasm from Hex-1 mutant of *Neurospora crassa*. (Displayed in SRM mode by selection of the transition m/z 360→163)

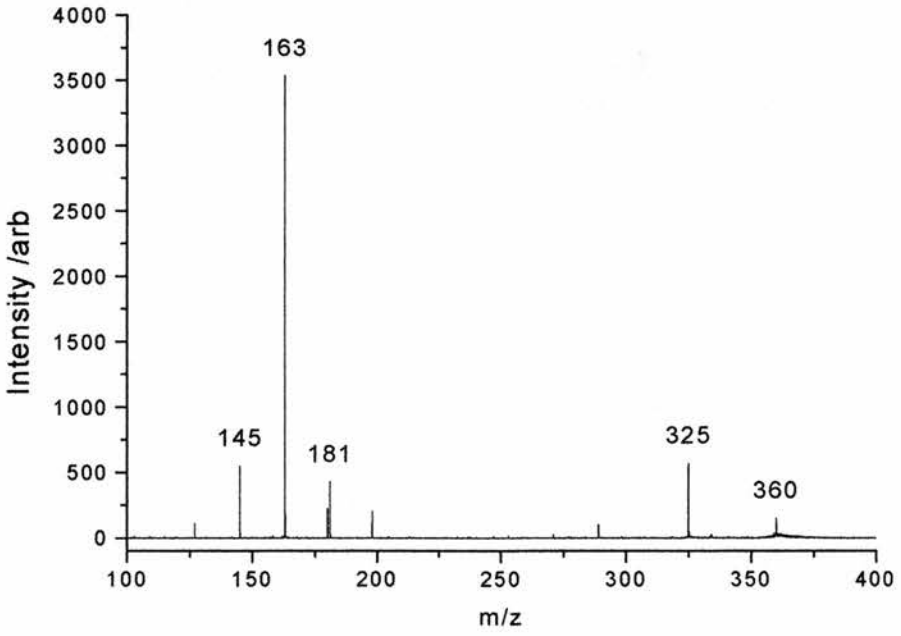


Figure 5-28 Integrated CE-MS/MS spectrum corresponding to peak at 8.3 minutes in Figure 5.28.

### 5.8.1 Quantification of intra-cellular disaccharide concentration

At the outset of this work, it had been hoped that it would be possible to determine the concentration of the disaccharides within fungal cells of the Hex-1 *Neurospora crassa* cell using CE-MS/MS. The data presented below is based on CE-MS measurements using selected ion monitoring chromatograms, which can be directly compared with the calibration data generated for trehalose.

The SiCSA CE-MS experiments required considerable operator skill and suffered from a number of problems with equipment reliability. As a result is was not possible to acquire as many results as originally hoped. In total, more than sixty separate SiCSA CE-MS experiments were carried out, not including the considerably larger number of attempts to microsample that were unsuccessful. Data from the majority of these experiments had to be discarded either because contamination was detected or because failure of electrical continuity of the CE capillary resulted in no detectable analyte. As for the calibration data recorded for trehalose (Section 5.5.4), the normalised integrated peak areas for the internal standard (angiotensin I; monitored in SIM mode as the doubly charged ion m/z 648) was used to correct the integrated peak areas detected for disaccharide (monitored in SIM mode as m/z 360).

The data resulting from those completely successful experiments that were performed is summarised in Table 5.5. It can be seen tha,t despite the limited number of experiments, there is a close correlation in the intra-cellular concentration of disaccharide measured in the fungal extract. The average concentration of disaccharide present in the cells was found to be 1.27±0.12 mM (the error represents the standard deviation of the measured values).

Table 5.5 Intra-cellular disaccharide concentration for Hex-1 mutant of *Neurospora crassa*, established by direct microsampling and CE-MS

| Sample volume (nL) | Peak area | Mass (pg) | Concentration (pg/nL) | Concentration (mM) |
|---|---|---|---|---|
| 0.856 | 120.00 | 386.80 | 451.66 | 1.31 |
| 1.122 | 161.78 | 521.10 | 464.44 | 1.35 |
| 0.915 | 105.67 | 340.74 | 372.27 | 1.08 |
| 1.242 | 176.20 | 567.45 | 456.81 | 1.33 |
| | | | | |
| | | **Average** | 436.30 | 1.27 |
| | | **Error ±** | 43.00 | 0.12 |

Error represents standard deviation in measured values.

Little previous work has been carried out to measure the concentration of disaccharides within fungal cells. This may be due to the difficulty in estimating the volumes of samples derived from bulk sampling techniques. Reported concentrations of trehalose have been based on analysis of compacted pellets comprised of large numbers of cells, and have been estimated to vary from 0.2 to 10 mM in response to stress. These estimated values correlate well with the results determined directly in this work. Although the cell will also contain a number of other disaccharides, including maltose and maltulose, these are thought to make up less than 5% of the total disaccharide present in the cell extract [195].

Gas liquid chromatography (Table 5.2) is the technique that previously offered the highest sensitivity for the estimation of the concentration of trehalose in fungal cells. This approach enables specific detection of trehalose, free from contamination from other disaccharide, but still relies on an estimation of the 'packed' cell volume in a compacted pellet and may suffer from contamination by extra-cellular trehalose. The level of detection is nevertheless two orders of magnitude less sensitive than was possible with the SiCSA CE-MS technique developed during this research; the

minimum sample volume that can be analysed is also considerably higher (Table 5.6).

Table 5.6 Comparison of techniques employed for quantification of the concentration of trehalose in fungal cells

| Technique | Limit of detection (LOD) for trehalose (nmol) | Minimum sample volume (mL) |
|---|---|---|
| Colourimetric | 7-14 | 0.5 |
| Spectrophotometric | 0.2-0.40 | 1 |
| Gas liquid chromatography | 0.005 | 0.003 |
| SiCSA CE-MS | 0.052 (fmol) | 100 (pL) |

## 5.9 Concluding remarks

A technique has been successfully developed for the analysis by CE-MS of samples aspirated from single fungal cells of *Neurospora crassa*. The risk of contamination of the sample by components present in the extra-cellular matrix has been minimised by performing sample transfer in a separate vessel, and by the use of external markers and the Hex-1 mutant of *Neurospora crassa*. The technique has been used to directly measure the intra-cellular concentration of disaccharide. The use of an internal calibrant (angiotensin I) was shown to improve quantification, by reducing variations occurring during capillary electrophoresis and subsequent electrospray ionization of eluted analyte. Use of an internal calibrant based on chemical derivatisation of the target analyte would improve quantification.

It was, unfortunately, not possible to distinguish between the various disaccharides present in the fungal cells, although it has been reported that the majority, up to 15% of the dry weight of the cell, is trehalose. Little research has been focused on the determination of the intra-cellular concentration of trehalose, although the data that does exist, extrapolated from the analysis of bulk cell populations, supports the results of the single cell sampling measurements carried out in this work.

# 6 The fungicide uptake story

It has been estimated that fungal plant pathogens are responsible for 70% of all damage caused to agricultural crops, resulting in billions of dollars of lost yield each year. This cost has driven the development of novel types of chemicals for control of plant pathogens in agriculture, worth $4.7 billion per annum in 1993 [201], rising to $5.9 billion in 1996 [202]. There is a continual need to develop new fungicidal compounds as they may offer technical advantages over existing products, by exhibiting a greater effectiveness or safety for the environment.

## 6.1 The fungicide azoxystrobin

Increasing fungal resistance and environmental controls have led to a constant requirement for materials that exhibit novel biochemical effects in the control of plant pathogens [203]. This was the goal when a class of molecules, the β-methoxyactrilates, were targeted by Zeneca. Research into this class of molecules as fungicides can be traced back to the characterisation of strobulurins, oudemansins and myxothiazols in the 1970s [204]. The strobulurins and oudemansins are found in several genera of small fungi, such as *Strobilurus tenacellus* and *Oudemansiella mucida,* commonly found on rotting wood. Myxothiazols have been isolated from various strains of the gliding bacterium *Myxococcus fulvus.*

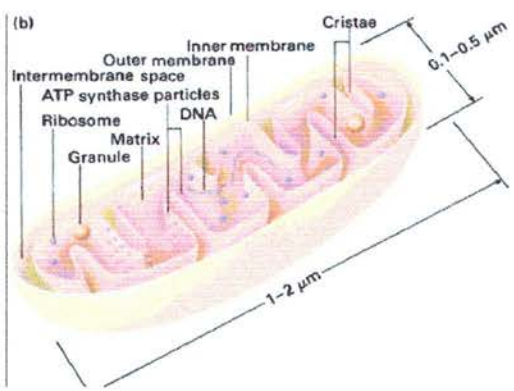


Figure 6-1 Diagram of a mitochondria. Reproduced from reference [205]

In all three classes of compounds, their fungicidal activity is a direct result of their ability to inhibit respiration in fungi. Specifically they were shown to bind to the $Q_o$ site on cytochrome b and thereby interfere with the function of the cytochrome bc1 segment of the respiratory chain located in the inner mitochondrial membrane (Figure 6.1). The bc1 complex catalyses the transfer of electrons from ubiquinol to cytochrome c and the translocation of protons across the inner mitochondrial membrane (Figure 6.2). This creates a proton gradient that in turn drives the synthesis of ATP.

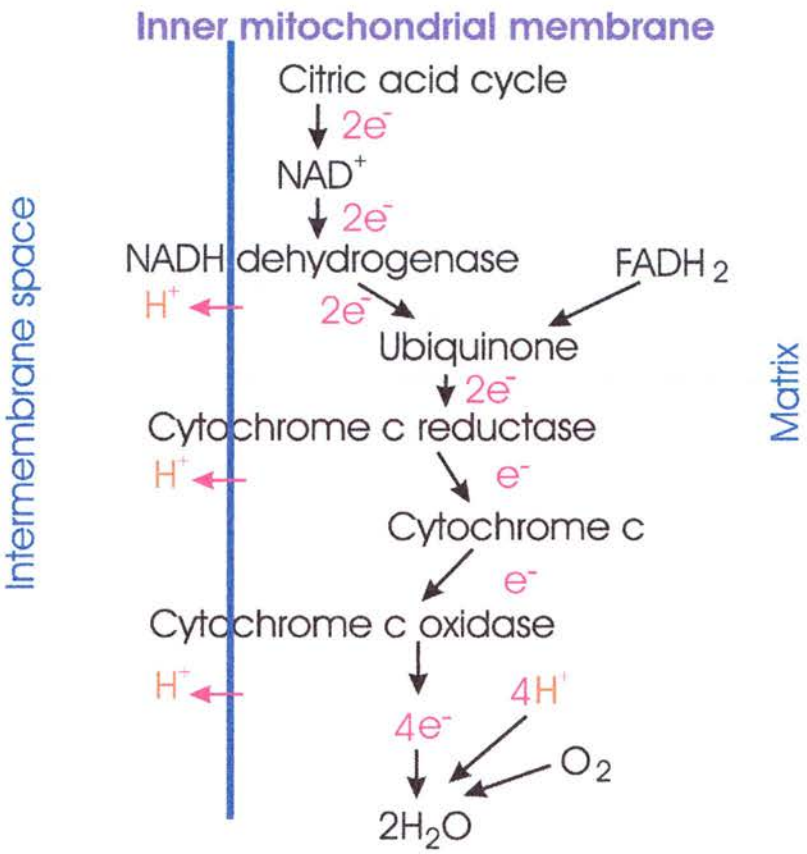


Figure 6-2 Electron transport chain.

The presence of strobulurin, oudemansin or myxothiazol does not prevent the binding of ubiquinol to cytochrome b, but is thought to result in a conformational

distortion of cytochrome b, and thereby slightly displace ubiquinol at its binding site [206]. The continuing research was centred on the strobulurins; in tests they exhibited anti-fungal activity *in-vitro*, but not in glasshouse trials. This was attributed to photoinstability and volatility. Investigation of modified molecules, retaining the β-methoxy-acrylatetoxophore, resulted in the development of a compound, azoxystrobin (Figure 6.3), which displayed good activity against plant diseases, as well as possessing photostability without exhibiting phyto-toxicity.

### 6.1.1 Azoxystrobin

Since its launch in 1998, azoxystrobin has quickly become the world's leading fungicide with worldwide sales worth $415 million (1999) [207], offering activity against many key plant pathogens including ascomycetes, basidiomycetes, deutermycetes and oomycetes.

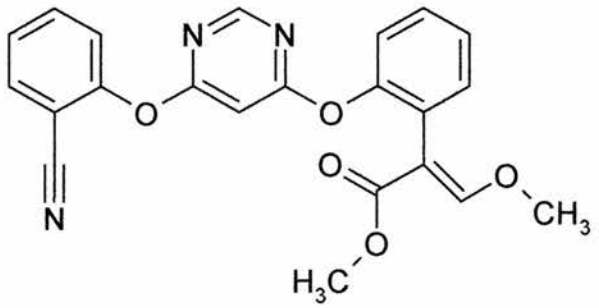


Figure 6-3 Structure of azoxystrobin:

methyl(*E*)-2-[2-[6-(2-cyanophenoxy)pyrimidin-4-yloxy]phenyl]-3-methoxyacrylate

This fungicide provides excellent disease control even in a mixed pathogen population, offering preventative, curative and eradicative activity. Treatment with azoxystrobin has been demonstrated to prevent spore germination and early stage fungal development, mycelial collapse in established fungi within 24 hours of

treatment, and anti-sporulant activity [208]. In field trials, azoxystrobin provided robust disease control on more than 60 economically important crops, including peanuts and golf course grass in the USA, bananas and tomatoes in South America, grape vines and wheat in Europe, and rice in the Far East.

### 6.1.2 Uptake into fungal cells

The cell membrane, a phospholipid bilayer, acts as a semi-permeable membrane, mediating the interchange of molecules between the intra-cellular environment, the extra-cellular matrix and other adjacent cells. It is the location of many proteins involved in cell signalling and membrane transport. These may be present entirely externally, internal to the cell membrane or they may span the membrane in the case of transmembrane proteins. For the majority of fungal species, there has been little research on the transport of low-molecular-weight nutrients and metabolites through the plasma membrane. Although an estimated 1.5 million fungal species exist, almost all knowledge stems from the species *Sacromices cerevisiae* and *Neurospora crassa.* This fact, coupled to the observation that drawing conclusions from one species and applying them to another is very uncertain [209], demonstrates how little knowledge currently exists. Fortunately, the model organism used in this research, *Neurospora crassa*, has been the focus of the majority of studies of membrane transport into fungal cells, including transport of potassium, calcium, glucose, galactose, fructose, ammonium, amino acids, nitrate, nitrite and peptides [210].

The transport of nutrients across the cell membrane is critical for growth. It has been calculated that a fungus with a dry weight of one gram must synthesise five milligrams of dry weight every minute [211]. The small diameter of the fungal hyphae results in a very high surface-to-volume ratio ($2 \times 10^6$) compared with that of typical animal cells ($2 \times 10^3$). As a consequence, large hydrophobic molecules can cross the plasma membrane in substantial amounts [212]. It is therefore very likely that azoxystrobin will pass through the lipid bilayer rapidly, and quickly achieve a similar concentration to that of the environment exterior to the cell. This is supported by the observation that fungal cell respiration can be seen to be repressed within 13 s post-treatment with azoxystrobin [213].

### 6.1.3 Original objectives of the research

At the outset of this work, the goal was to try to quantify the uptake of azoxystrobin into single fungal cells and relate this to data from an associated project, also funded by Syngenta International, in which confocal microscopy together with fluorescent imaging would be used to investigate the mechanism of azoxystrobin uptake into the fungal cell.

Syngenta International, set the original goals of this research. Their interest was in the concentration of fungicide that might accumulate in a single fungal cell. It was originally hoped that it would be possible to determine the intra-cellular concentration of azoxystrobin, and to investigate the effect of the addition of surfactants.

Based on a number of prior assumptions, the project began with the target of quantifying the intra-cellular concentration of azoxystrobin in a target fungal cell volume of 100 nL. Azoxystrobin is a hydrophobic molecule with a molecular weight of 403.4 Da, and a saturation concentration in water of 6 mg/L. Assuming that azoxystrobin passes through the cell membrane, the maximum concentration which could be achieved would be 6 mg/L. Knowing the value of the saturation concentration of azoxystrobin in water and the estimated cell volume that might be sampled, it appeared that CE-MS could provide the sensitivity required for detection and that the principal challenge would be one of microsampling and sample handling.

## 6.2 Investigation of azoxystrobin

As in the case of the SiCSA studies on disaccharides presented in Chapter 5, mass spectroscopic data for azoxystrobin was required prior to the CE-MS studies. Spectra recorded using nESI provided a convenient method to optimise the various operating parameters of the Q-ToF and to identify the predominant fragment ions. Azoxystrobin was prepared at a concentration of 10 ng/μL in a solution of 50:50 (v:v) acetonitrile:water and 0.2 % formic acid, and loaded into an Econo12 nESI emitter (New Objectives, USA). This emitter was placed orthogonally to the sample inlet of the Q-ToF and the electrospray voltage applied.

A convenient and quick way to obtain fragmentation data is by varying the skimmer cone voltage. This generally provides more gentle collision induced dissociation (CID), at least at low cone voltages, relative to CID performed in the hexapole collision cell of the Q-ToF. Moreover the extent of CID can be smoothly varied depending upon the degree of fragmentation desired. This technique has been referred to as energy-dependent electrospray ionisation mass spectrometry (EDESI-MS) [214]. The energy resolved fragmentation data can be displayed in the form of a 2D projection (collision energy versus m/z), with the ion abundance on the axis perpendicular to the paper. Breakdown graphs (a plot of percentage fragment ion abundance versus collision energy or cone voltage can be incorporated. Additionally, the data illustrated on the map can be projected onto the mass axis, the summation spectrum (shown at the top of the map), yielding a combined spectrum of ion abundance summed over all skimmer cone voltages.

Figure 6.4 shows such an EDESI mass spectrum recorded on the Q-ToF for azoxystrobin. In the summation spectrum, the protonated species $[M+H]^+$ can be seen at m/z 404, as well as a number of fragment ions at m/z 372, m/z 344, m/z 329, m/z 316 and m/z 301. The first two fragment ions observed with increasing skimmer cone voltage correspond to loss of methanol, m/z 372 $[MH-CH_3OH]^+$, and loss of methyl formate, m/z 344 $[MH-HCO_2CH_3]^+$. From the breakdown graph shown at the side of the map it can be seen that fragmentation of the protonated species to m/z 372 occurs at low cone voltages (20 V). The fragment ion m/z 344 only appears if the cone voltage is raised significantly (50 V). At higher cone voltages (60 V) the remaining fragment ions appear and the abundance of the m/z 404 and m/z 372 ions decreases significantly.

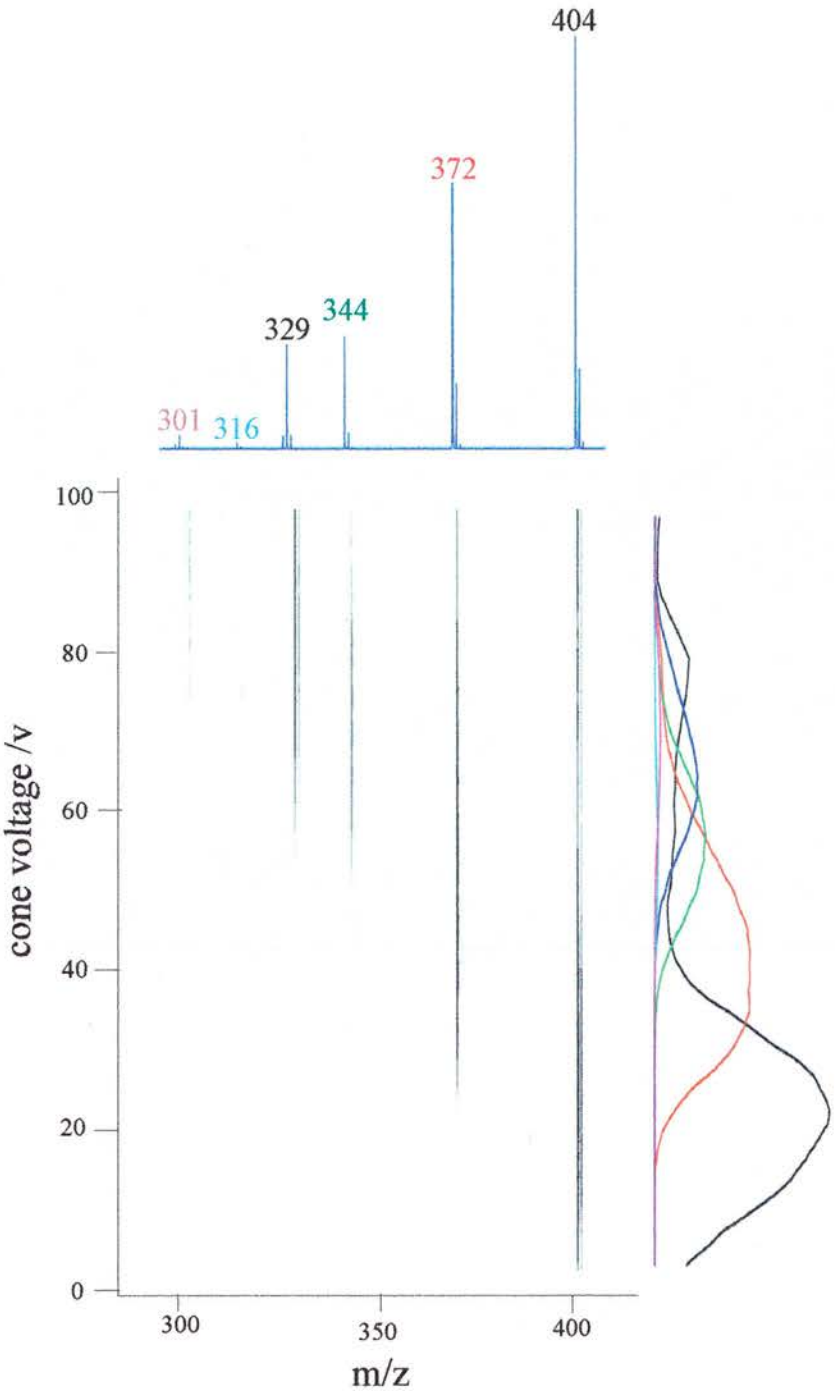


Figure 6-4 EDESI mass spectrum generated from 101 positive ion nESI MS spectra of azoxystrobin at cone voltage settings of 0-100 V. The top trace is generated by combining all 101 spectra. The side trace is a breakdown graph of all the major ions in the spectra.

### 6.2.1 Development of a selected reaction monitoring transition

Although skimmer cone voltage CID is relatively quick to perform, in order to develop a suitable selected reaction monitoring transition the Q-ToF has to be operated in MS/MS- TOF, with CID carried out in the hexapole collison cell.

For these experiments azoxystrobin was prepared at a concentration of 0.01mg/mL in 50:50 (v:v) acetonitrile:20 mM ammonium acetate with 0.2 % formic acid. This solvent mixture was chosen to mimic the chemical composition of the ESI spray during CE-MS experiments. Samples were loaded into an Econo12 nESI borosilicate needle (New Objectives, USA), which was placed orthogonal to the sample inlet of the Q-ToF and the electrospray potential applied. Figure 6.5 shows a nESI MS spectrum for azoxystrobin acquired at a cone voltage setting of 30V. A large amount of skimmer cone fragmentation can be seen of protonated azoxystrobin (expected monoisotopic peak 404.1) to the m/z 372 $[MH\text{-}CH_3OH]^+$ fragment ion (expected monoisotopic peak 372.10). Figure 6.6 shows a nESI MS/MS spectrum for azoxystrobin in which the m/z 404 $[M+H]^+$ ion was isolated and fragmented. The most abundant ions observed, as seen in the EDESI mass spectrum (Figure 6.4), correspond once again to loss of methanol, m/z 372 $[MH\text{-}CH_3OH]^+$, and loss of methyl formate, m/z 344 $[MH\text{-}HCO_2CH_3]^+$ (expected monoisotopic peak 344.10).

The m/z 404 $[M+H]^+$ ion and the m/z 372 fragment ion were chosen as the SRM transition m/z (404→372) for confirming the identification of azoxystrobin. The generation of calibration data for the detection of azoxystrobin by CE-MS, as well the subsequent SiCSA CE-MS experiments, were carried out (as for the previous study on disaccharides) using the Q-ToF in single ion monitoring (SIM) mode.. Although the use of collision induced dissociation tandem mass spectrometry (i.e operating the Q-ToF in SRM mode) probably would have provided better selectivity and increased sensitivity, the aim was to identify other compounds present in the fungal cell samples not just quantify the concentration of azoxystrobin present..

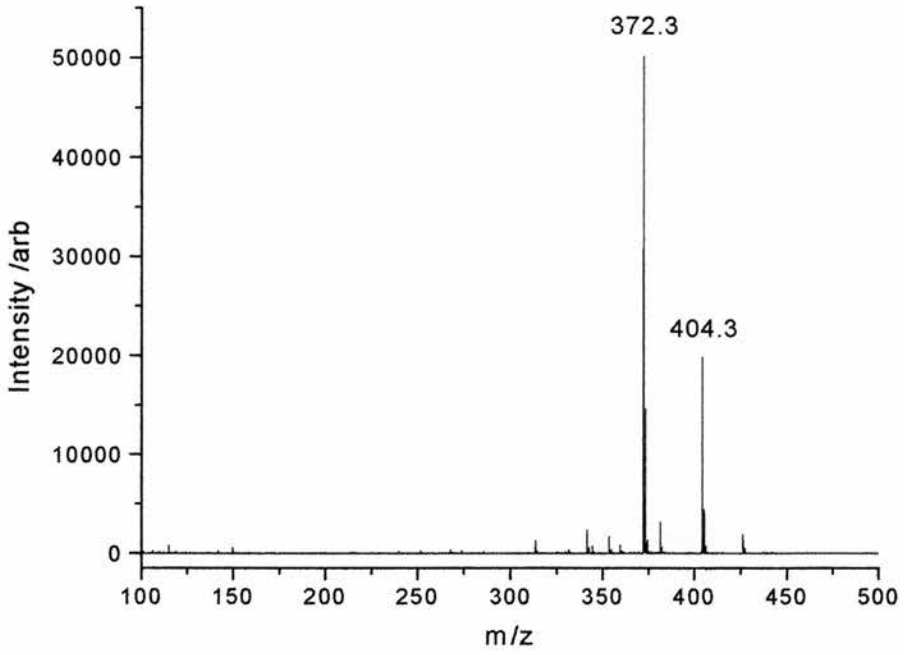


Figure 6-5 nESI MS spectrum for azoxystrobin (0.01 mg/mL). (m/z 404.3 $[M+H]^+$, m/z 372.3 $[MH-CH_3OH]^+$).

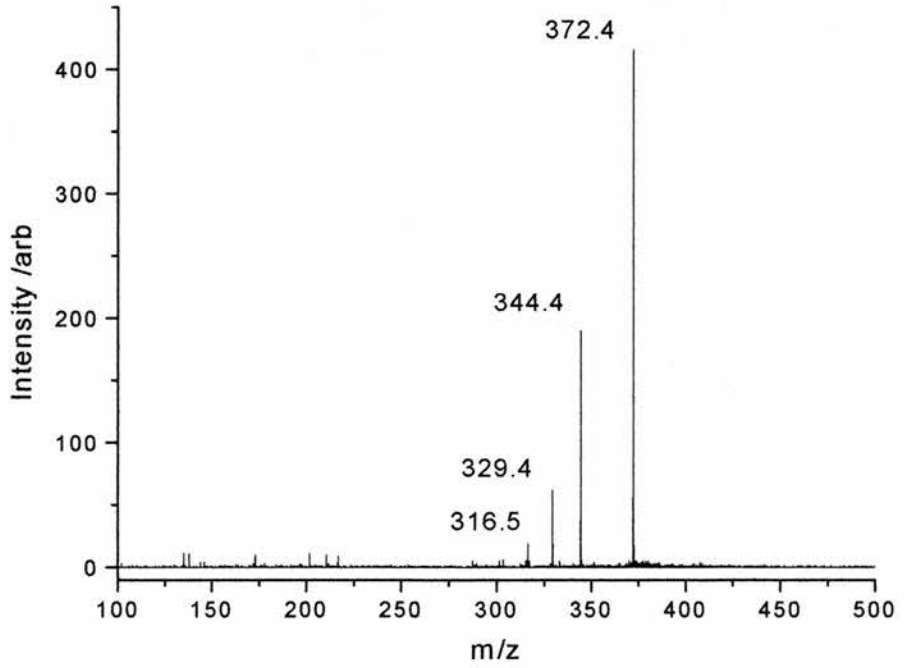


Figure 6-6 MS/MS spectrum for azoxystrobin obtained from m/z 404 precursor ion. (m/z 372.4 $[MH-CH_3OH]^+$, m/z 344.4 $[MH-HCO_2CH3]^+$).

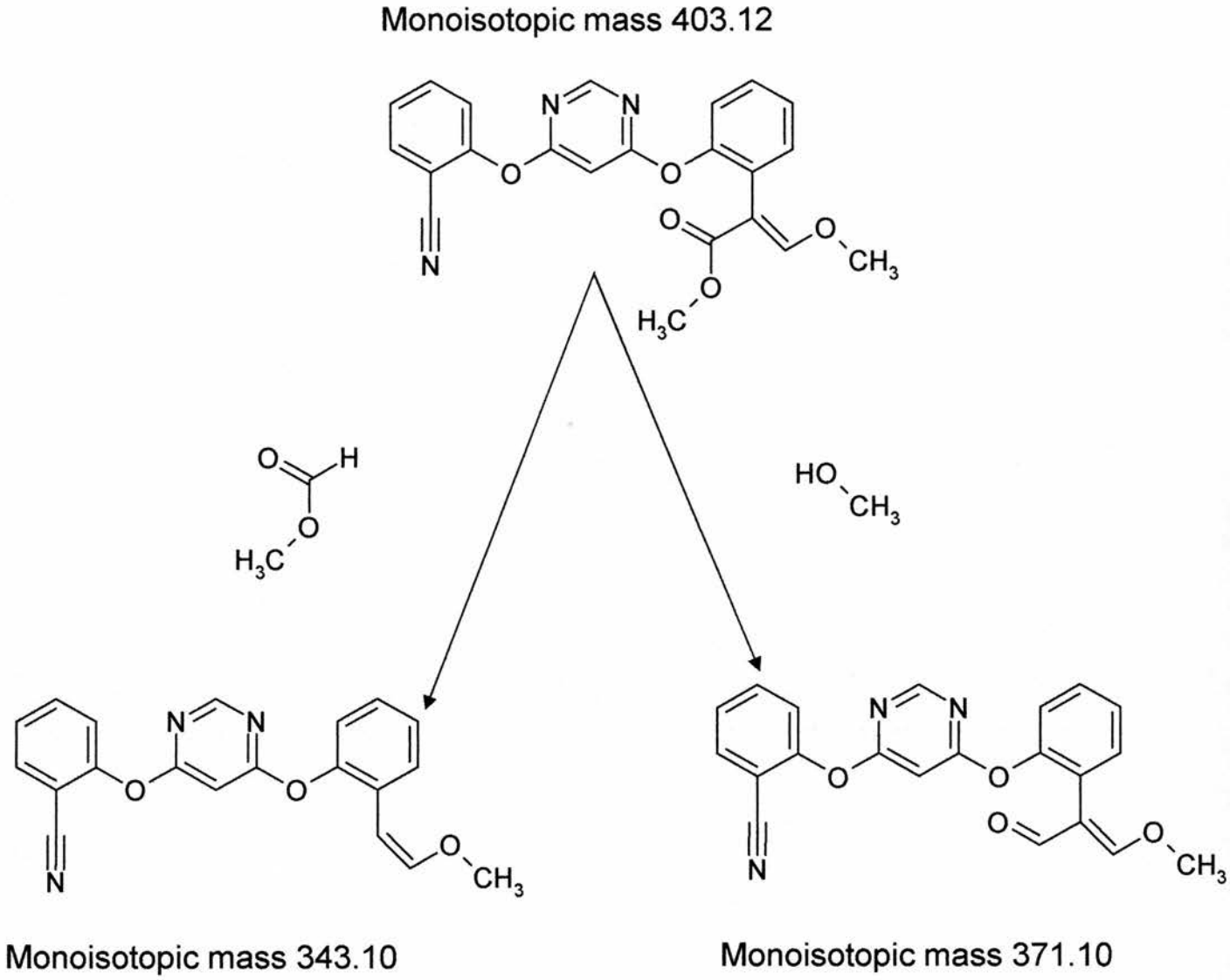


Figure 6-7 Predominant fragmentation pathways for azoxystrobin. (values given for monoisotopic mass).

## 6.3 Development of quantifiable CE-MS for detection of azoxystrobin

It was important to fully optimise the introduction of azoxystrobin to the mass spectrometer by CE-ESI. As mentioned previously, azoxystrobin is a hydrophobic compound and is not soluble in highly aqueous solutions (saturation concentration in water 6 mg/L). Therefore it was necessary to first dissolve azoxystrobin in acetonitrile, and then for each subsequent dilution, quickly reduce the concentration of acetonitrile present.

Electrophoresis was performed in a fused silica capillary of internal diameter 50 μm, external diameter of 192 μm, with a total length of 860 mm. All new capillaries were conditioned by rinsing for 30 min with 0.1 M NaOH solution. Aqueous ammonium acetate at a concentration of 10 mM and pH 8.5 was used as the running buffer. Between runs, the capillary was washed for 2 min with 0.1 M NaOH, 1 min water and finally 2 min with running buffer. As mentioned in the previous chapter, in order to optimise the electrospray and Q-ToF operating conditions, the CE running buffer was spiked with azoxystrobin, at a concentration of 0.001 mg/mL, to mimic a continually eluting analyte band. The instrument settings appropriate for azoxystrobin were found to be similar to those used for the CE-MS analysis of disaccharides described in Chapter 5.

### 6.3.1 Calibration data for the detection of azoxystrobin by CE-MS

Here again in order to accurately determine the concentration of azoxystrobin that might be present in treated fungal cells of *Neurospora crassa*, it was necessary to generate calibration data under conditions as similar as possible to those that would be employed in the SiCSA CE-MS experiments. Azoxystrobin standards at a range of concentrations were prepared in 10 mM ammonium acetate at pH 8.5. Samples were run from lowest to highest concentrations to reduce the risk of carry-over. A blank sample was run before and after each sample as well as at the end of the sample set to detect any carry-over. Analyses were performed using the apparatus already described in Section 4.6, with the Q-ToF operating in MS-TOF mode. Standards were loaded by electrokinetic injection (5s at 5kV), corresponding to an injection volume of 2.93 nL and separated using an applied potential 20 kV.

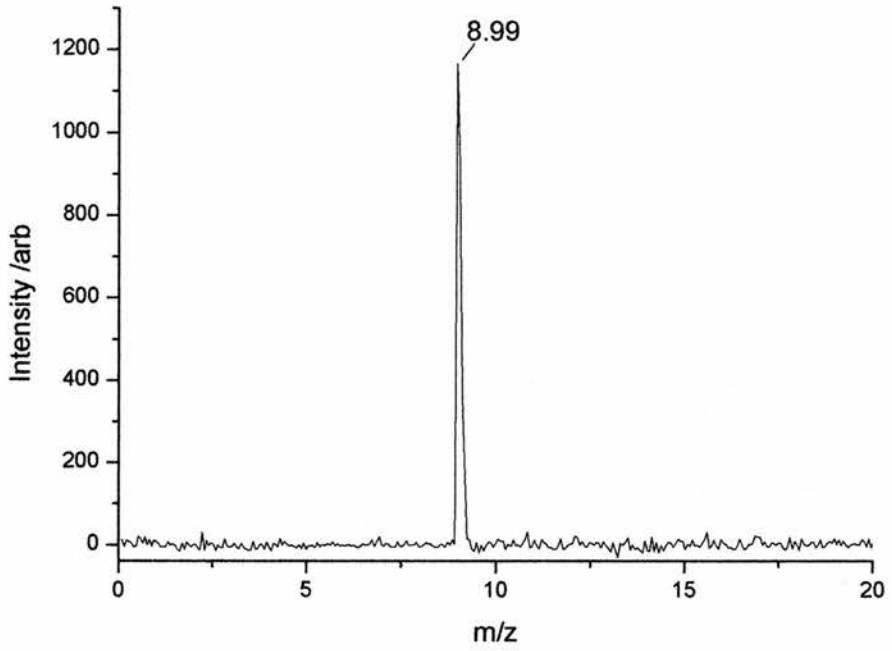


Figure 6-8 CE-MS chromatogram obtained for azoxystrobin recorded in SIM mode using the fragment ion m/z 372 $[MH\text{-}CH_3OH]^+$. (Capillary length 860 mm; buffer 10 mM ammonium acetate, pH 8.5).

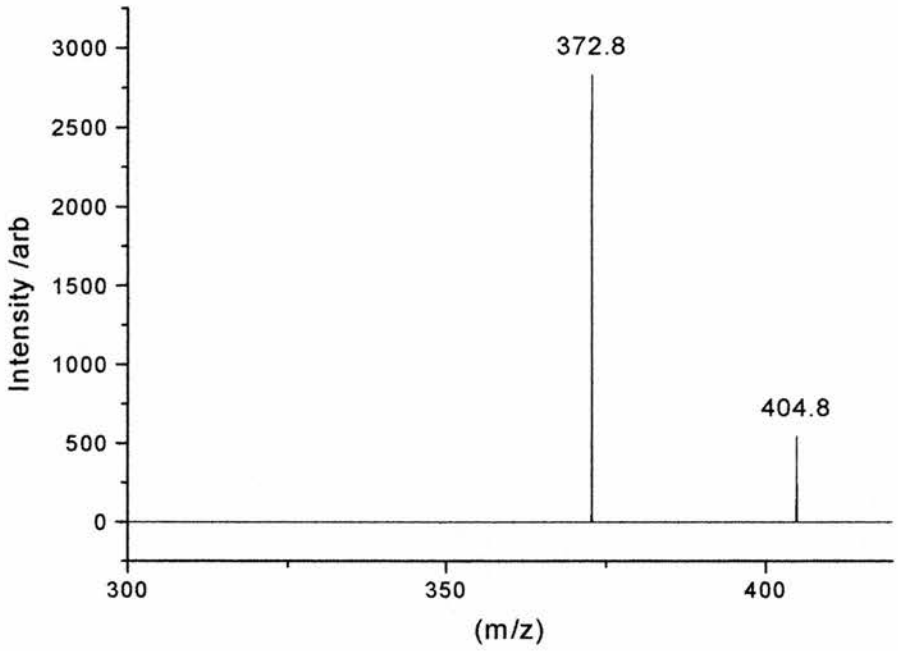


Figure 6-9 Integrated CE-MS spectrum corresponding to peak at 8.99 minutes in Figure 6.8. (m/z 404.8 $[M+H]^+$, m/z 372.8 $[MH-CH_3OH]^+$).

Figure 6.8 shows a typical CE-MS chromatogram obtained on the Q-ToF for azoxystrobin recorded in single ion monitoring (SIM) mode using the m/z 372 fragment ion. This data was recorded using a capillary 860 mm in length, with a running buffer of 10 mM ammonium acetate, pH 8.5. The elution time for azoxystrobin is 8.99 minutes, as would be expected for an uncharged molecule co-eluting with the solvent front. Figure 6.9 shows the integrated CE-MS spectrum corresponding to this peak. When compared with the nESI mass spectrum shown in Figure 6.5, it can be seen that the ions match those that would be expected for low energy CID fragmentation of azoxystrobin. The protonated species $[M+H]^+$ can be seen at m/z 404 as well as the prominent fragment ion m/z 372 $[MH-CH_3OH]^+$ selected to record the CE-MS chromatogram.

The calibration data for the detection of azoxystrobin was generated in a similar fashion to that for the trehalose standards described in Section 5.6.2. Integration was performed to measure the peak area for azoxystrobin in the CE-MS SIM chromatograms (detected in SIM mode using the fragment ion m/z 372). Angiotensin I was once again used as an internal calibrant to correct for any variation in the ionisation and detection efficiency. Data points with an error of 15%, i.e. values above 115% and below 85% of the expected value, were discarded.

The calibration data is given in Table 6.3. Correcting the measured peak areas for azoxystrobin using the normalised peak area for angiotensin I was again found to improve the linearity of the data. This can be seen more clearly in Figure 6.10 where both the corrected and uncorrected data is plotted. The limit of quantification was taken to be $6\sigma$ of the noise in the CE-MS SIM chromatogram the limit of detection was taken to be $3\sigma$ of the noise. The limit of quantification for azoxystrobin by CE-MS was determined to be 1.64 pg, corresponding to 4.06 fmol, and the limit of detection 0.82 pg. Therefore, in a 100 pL sample volume (approximately the sample volume of a single cell), the minimum concentration that could be quantifiably measured is 16.4 mg/L. Although this is higher that the hypothesised limit of detection estimated at the outset of the project, it was hoped that the larger volume of cell extract that could be aspirated due to the use of Hex-1 mutant strain of *Neurospora crassa* would compensate for any shortfall in sensitivity.

Table 6.3 Calibration data for detection of azoxystrobin by CE-MS

| Mass of azoxystrobin on column (pg) | Angiotensin I peak area | Azoxystrobin uncorrected peak area | Azoxystrobin corrected peak area |
|---|---|---|---|
| 390.00 | 937.90 | 302.20 | 322.21 |
| 390.00 | 1083.97 | 337.70 | 311.54 |
| 381.00 | 1048.12 | 354.20 | 337.94 |
| 381.00 | 869.84 | 273.20 | 314.08 |
| 381.00 | 1097.90 | 329.60 | 300.21 |
| 139.20 | 735.62 | 98.50 | 133.90 |
| 139.20 | 911.06 | 105.30 | 115.58 |
| 38.90 | 1228.12 | 42.80 | 34.85 |
| 38.90 | 869.29 | 27.60 | 31.75 |
| 38.90 | 1039.69 | 37.20 | 35.78 |
| 38.11 | 722.30 | 25.10 | 34.75 |
| 38.11 | 1232.92 | 40.60 | 32.93 |
| 38.11 | 1386.50 | 45.20 | 32.60 |
| 28.30 | 1210.58 | 33.40 | 27.59 |
| 28.30 | 828.71 | 19.40 | 23.41 |
| 28.30 | 878.14 | 22.70 | 25.85 |
| 15.80 | 1119.49 | 19.30 | 17.24 |
| 15.80 | 971.47 | 16.50 | 16.98 |
| 2.60 | 909.09 | 5.40 | 5.94 |
| 2.60 | 716.72 | 4.20 | 5.86 |
| 0.82 | 1116.63 | 4.50 | 4.03 |
| 0.82 | 922.33 | 3.80 | 4.12 |
| 0.82 | 885.19 | 3.71 | 4.19 |
| 0.63 | 927.32 | 3.70 | 3.99 |
| 0.63 | 796.02 | 3.20 | 4.02 |
| 0.63 | 1012.35 | 4.10 | 4.05 |

Volume injected each for angiotensin I and azoxystrobin 2.93 nL.
Concentration of angiotensin I standard 0.25 mg/mL.

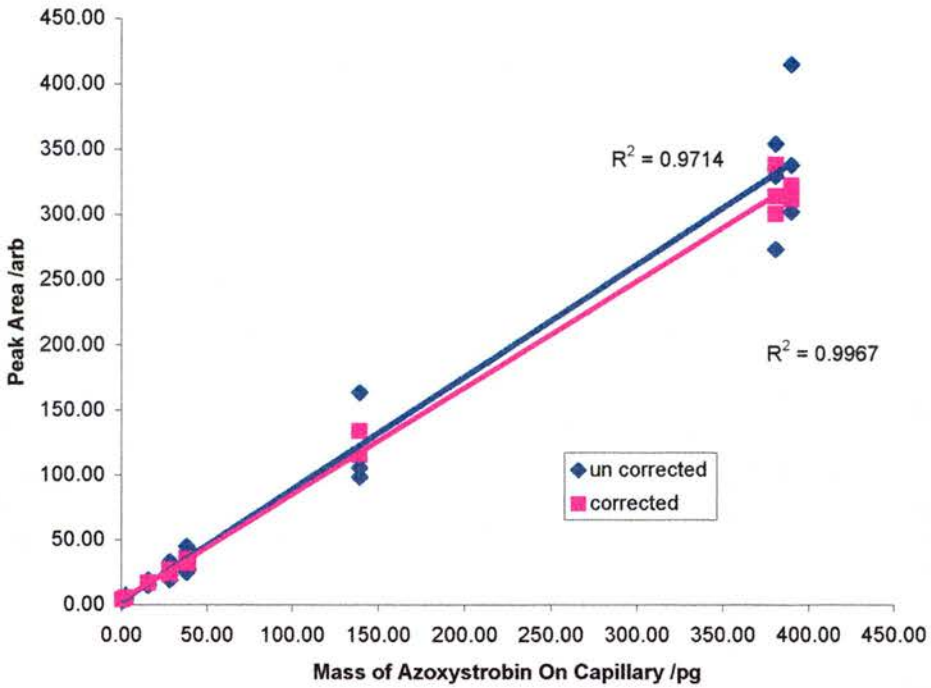


Figure 6-10 Calibration data for detection of azoxystrobin by CE-MS. Data points shown for peak area of azoxystrobin, uncorrected and corrected to normalised peak area of internal standard.

## 6.4 Method for application of azoxystrobin to cultured fungal cells

It would have been ideal to be able to simulate the agricultural type application of azoxystrobin and to determine the level of uptake of azoxystrobin by the model fungal cells. In agricultural conditions, the fungal cells are growing on and into the surface of the plant leaf; fungicide is applied as a suspension concentrate to the plants at a rate of between 50-400 g of active ingredient per hectare. The suspension concentrate is composed of 250 g/L azoxystrobin in a crystalline form, various proprietary surfactants, and a clay base. Electron microscopy performed by Syngenta International revealed that after treatment azoxystrobin is present on the plant leaves in dispersed crystals from which fungicide slowly diffuses. Previous research by Syngenta International demonstrated that the plant leaf steadily takes up azoxystrobin; the fungicide then diffuses through the leaf to reach the vascular tissue

and is transported acropetally into the transpiration stream, which results in an even distribution of fungicide molecules from the point of uptake throughout the leaf.

The field type application of azoxystrobin to fungal cells would be very hard to simulate as the model cells used in this study could not be grown on the leaf surface. It was therefore important to devise a dosing method that could closely simulate the conditions present in the field. It was also found that it was important to sample from the cells soon after treatment, as the cells quickly lost turgor pressure as respiration was suppressed. This meant that microsampling became progressively harder and the risk of contamination from the extra-cellular matrix increased.

The method chosen was to treat the fungal cells with a solution of azoxystrobin at 1 mg/mL in 2% malt extract. As this concentration is in excess of the solubility of azoxystrobin in water, a substantial quantity remained in a crystalline form. This solution (1 mL) was applied to the surface of the culture media, and the cells returned to the incubator for 5 minutes. The cells were then washed 3 times with 10 mL of 2% malt extract. The cells were then covered with silicone oil in preparation for microsampling.

### 6.5 Analysis of fungal cytoplasm for azoxystrobin

Fungal cell extract was aspirated from a chosen Hex-1 mutant cell compartment of Neurospora crassa that had been treated as described in Section 6.4, and then transferred into the CE capillary entrance, as described in Section 4.6. Separation was performed as described in Section 4.6. The volume of cell extract aspirated from the cell compartment was 1.1 nL.

Figure 6.11 shows the CE-MS SIM chromatogram for this first sample of treated fungal cell extract, displayed in single ion monitoring (SIM) mode, by selection of the $[MH\text{-}CH_3OH]^+$ fragment ion at m/z 372. Separation was performed using a capillary 1500 mm in length and a running buffer of 20 mM ammonium acetate, pH 6. The SIM chromatogram shows a very broad signal commencing at 40 minutes, with extensive tailing for over 40 minutes due to column overloading. It is clear that gross contamination of the sample occurred.

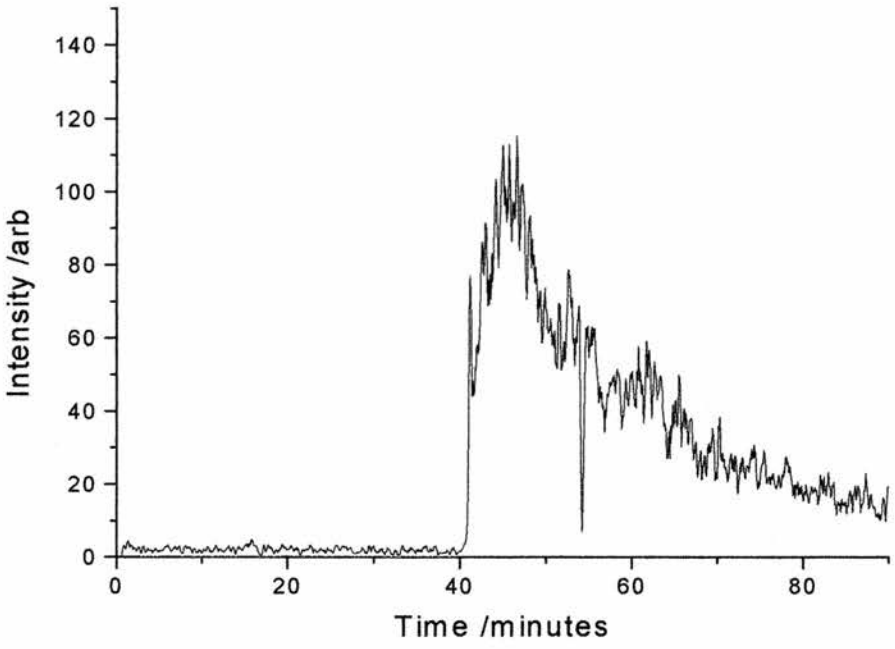


Figure 6-11 CE-MS SIM chromatogram of fungal cytoplasm from Hex-1 mutant of *Neurospora crassa*. (Displayed in SIM mode by selection of m/z 404; sample volume 1.1 nL; CE capillary length 1500 mm; buffer 20 mM ammonium acetate, pH 6)

The integrated area for this signal (2134.87) corresponds to a mass of azoxystrobin far in excess of any value used to generate the calibration data. It was clearly not possible to draw any conclusions as to the mass of azoxystrobin drawn into the separation capillary, except that a substantial amount of azoxystrobin was obviously present in the media surrounding the cells and that a significant volume of this had been drawn into the separation capillary exceeding the capillary capacity. Optimisation of the capillary column length and running buffer had not yet been performed. The experiment graphically demonstrated the need to employ a marker for extra-cellular contamination and showed that additional precautions had to be

taken when transferring samples of cell cytoplasm from the micropipette to the separation capillary.

### 6.5.1 Quantification of the intra-cellular concentration of azoxystrobin

The experimental protocol followed was similar to that developed for the SiCSA CE-MS measurement of intracellular disaccharide levels, described in the previous chapter.

Cultured cells of the Hex-1 mutant of *Neurospora crassa* cells were treated with azoxystrobin (1 mg/mL in 2% malt extract) for 5 minutes, washed 3 times (10 mL of 2% malt extract), a solution of the extra-cellular marker Rhodamine B isothiocyanate dextran (0.1 mg/ml) and 2% malt extract added, and the culture plate then covered with a thin layer (4mm) of silicone oil. Samples were aspirated from chosen fungal cells in which cytoplasmic streaming was still clearly visible. Transfer to the separation capillary was carried out in a separate vessel containing clean silicone oil to minimise the risk of contamination from the extra-cellular matrix. Following sample transfer the internal standard (angiotensin I) was electrokinetically injected (5s at 5kV). Electrophoresis was performed in a fused silica capillary of internal diameter 50 μm, external diameter of 192 μm, of total length of 860mm. The CE-LIF detector, used to confirm the presence or absence of the extra-cellular marker, was positioned 650 mm from the capillary inlet. Separation was performed as described in Section 4.6 using a running buffer of 10 mM ammonium acetate, pH 8.5. All runs where fluorescence was detected were discounted.

A typical SiCSA CE-MS selected ion monitoring (SIM) chromatogram for a sample of fungal extract from treated cells is shown in Figure 6.12. The volume sampled was 0.79 nL. The chromatogram is displayed in SIM mode by selection of the predominant fragment ion m/z 372 seen in the spectra of azoxystrobin, corresponding to the loss of methanol $[MH\text{-}CH_3OH]^+$. A well resolved peak is clearly visible with a good signal to noise ratio (s/n 10) and elution time similar to that seen for azoxystrobin standard (Figure 6.8). Figure 6.13 shows the corresponding integrated CE-MS spectrum for this eluting peak. The ions match those expected; m/z 404.53 $[M+H]^+$, m/z 372.77 $[MH\text{-}CH_3OH]^+$. The selected ion

monitoring chromatograms for the internal standard, by selection of m/z 648 corresponding to doubly charged angiotensin I, were similar to that shown in Figure 5.16.

All quantitative measurements were made from SiCSA CE-MS SIM chromatograms. However, to conclusively confirm the identity of the eluting compound a cell extract analysis was performed using the Q-ToF in MS/MS-TOF mode.

Figure 6.14 shows the CE-MS/MS chromatogram that was obtained using selected reaction monitoring on the transition m/z (404→372). Since CE-MS/MS data originates from a different experiment the elution time varies slightly. The signal-to-noise ratio in the CE-MS/MS SRM chromatogram is higher (s/n 150), although this could be due to a greater quantity of azoxystrobin having been injected into the capillary. Figure 6.15 shows the corresponding integrated MS/MS spectrum for the peak observed at 10.2 minutes in the CE-MS/MS SRM chromatogram. The predominant fragment ions that would be expected at m/z 372 and m/z 344, corresponding to loss of methanol $[MH\text{-}CH_3OH]^+$ and loss of methyl formate $[MH\text{-}HCO_2CH_3]^+$ from protonated azoxystrobin, are both clearly visible.

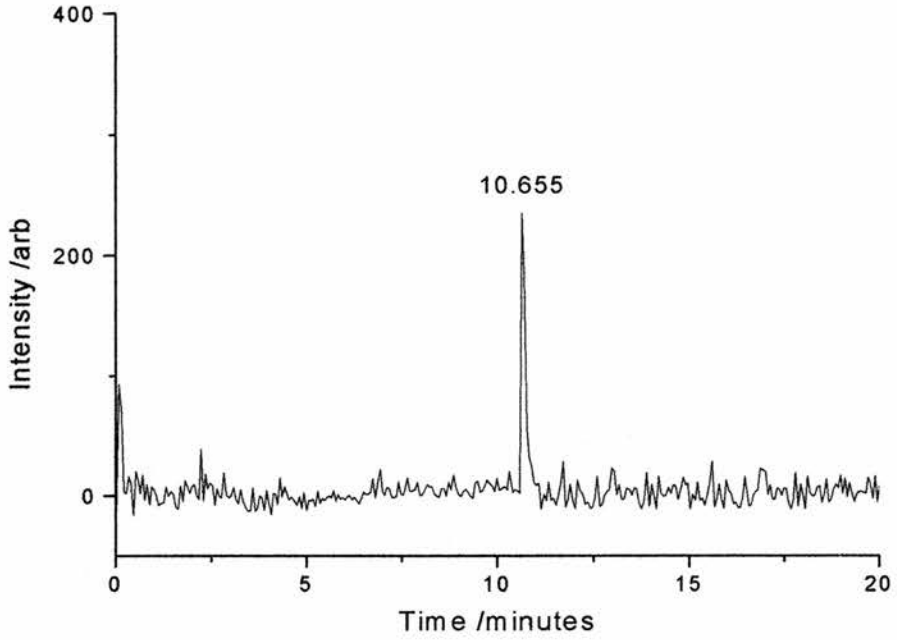


Figure 6-12 CE-MS SIM chromatogram of fungal cytoplasm from Hex-1 mutant of *Neurospora crassa*. (Displayed in SIM mode by selection of m/z 372; sample volume 1.1 nL; CE capillary length 860 mm; buffer 10 mM ammonium acetate, pH 8.5)

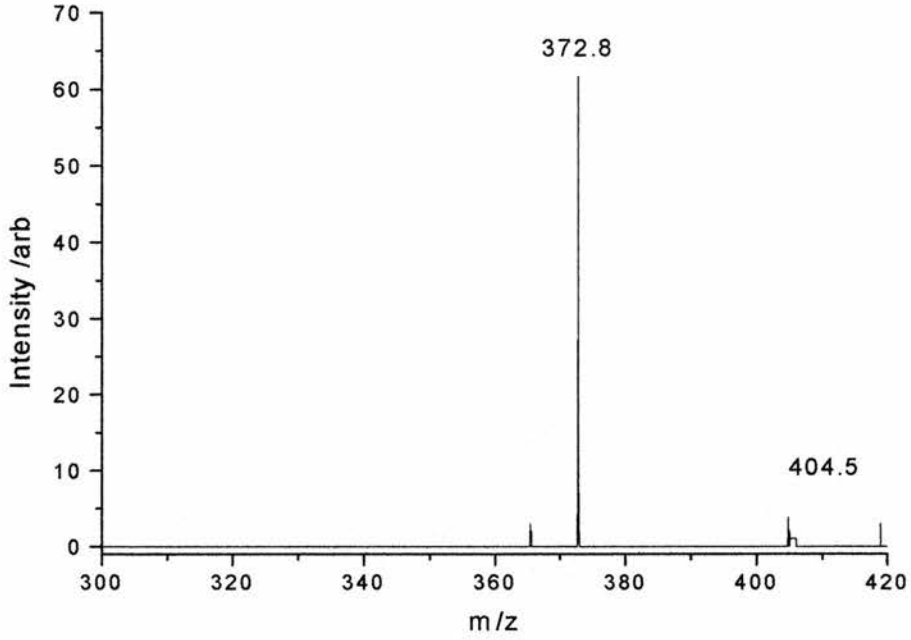


Figure 6-13 Integrated CE-MS spectrum corresponding to peak at 10.65 minutes in Figure 6.12.

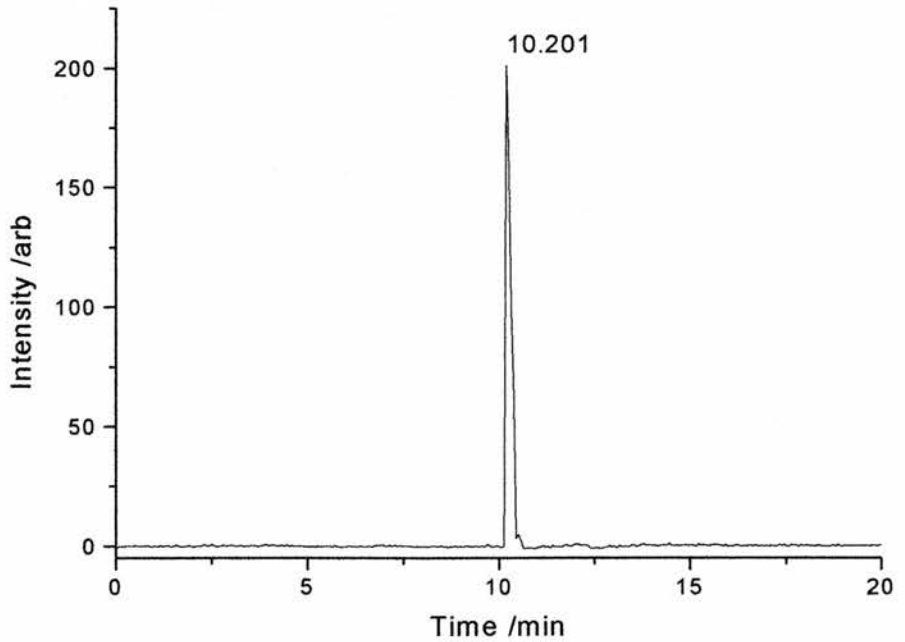


Figure 6-14 CE-MS/MS SRM chromatogram of fungal cytoplasm from Hex-1 mutant of *Neurospora crassa*. (Displayed in SRM mode by selection of transition m/z 404→372).

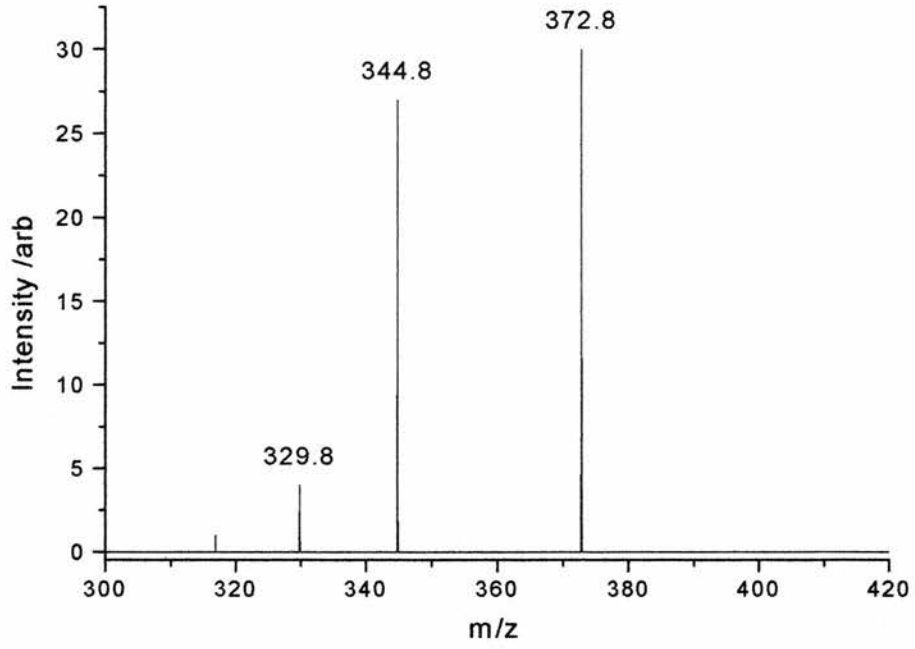


Figure 6-15 Integrated CE-MS/MS spectrum corresponding to peak at 10.2 minutes in Figure 6.14.

The data from the SiCSA CE-MS experiments that were successfully completed is presented in Table 6.4. Although more than forty experiments were carried out, data from most of them had to be discarded either because extra-cellular contamination was detected or because of broken electrical continuity of the CE capillary. For all successful runs the peak areas in the CE-MS SIM chromatograms corresponding to detected azoxystrobin were corrected using the normalised peak area for the internal standard.

Despite the limited number of successful experiments, there is good agreement between the values determined for the intra-cellular concentration of azoxystrobin detected (Table 6.4). The average concentration of the fungicide present in the cells was found to be 9.9±1.0 μM (the error represents the standard deviation of the measured values). Azoxystrobin is present in the liquid surrounding the treated cells, prior to washing, at the saturation concentration, i.e. 14.8 μM. The cells were incubated for 5 minutes following topical application of the fungicide. The concentration of fungicide that has accumulated within the cell over this time period is approximately two thirds the saturation concentration in water.

Table 6.4 Intra-cellular azoxystrobin concentration following treatment of Hex-1 mutant of *Neurospora crassa*, established by direct microsampling and CE-MS.

| **Sample volume (nL)** | **Peak area** | **Mass (pg)** | **Concentration (pg/nL)** | **Concentration (μM)** |
|---|---|---|---|---|
| 0.973 | 7.28 | 4.11 | 4.23 | 10.48 |
| 0.791 | 6.20 | 2.78 | 3.52 | 8.72 |
| 0.242 | 4.76 | 1.02 | 4.21 | 10.43 |
| | | **Average** | 3.98 | 9.9 |
| | | **Error ±** | 0.40 | 1.0 |

Error represents standard deviation in measured values.

Since the experimental protocol, operating parameters of the Q-ToF and CE separation conditions were the same as those used to determine the intracellular concentration of disaccharides, it was possible to investigate the effect that treatment with the fungicide had on the intra-cellular concentration of disaccharide. As mentioned in Chapter 5, trehalose, the predominant disaccharide in fungal cells, is synthesised at enhanced levels in *Neurospora crassa* in response to environmental stress.

SiCSA CE-MS SIM chromatograms were generated from the raw data previously acquired from treated cells. For each data set a peak corresponding to the presence of disaccharide (displayed in SIM mode by selection of the $[M+NH_4]^+$ disaccharide adduct ion) was detected. The peak area was integrated and corrected to the normalised peak area of the internal standard. The results are summarised in Table 6.5 where the mean intra-cellular concentration of disaccharide detected in treated cells is compared with the value measured for untreated cells. From the limited results available, a slightly higher level of disaccharide was present in cells that had been treated for five minutes with azoxystrobin.

Table 6.5 Effect on intra-cellular disaccharide concentration following treatment of Hex-1 mutant of *Neurospora crassa* with azoxystrobin

| **Analyte** | **Mean intra-cellular concentration of analyte (mM)** | **Error (mM)** |
|---|---|---|
| Disaccharide (untreated) | 1.25 | 0.11 |
| Disaccharide (treated) | 1.42 | 0.09 |
| Azoxystrobin | .0099 | .0010 |

Error represents standard deviation in measured values.

## 6.6 Concluding Remarks

The challenge of developing a technique applicable to quantifying the uptake of the fungicide azoxystrobin into fungal plant pathogens has been partially met. The challenge was to devise a technique whereby azoxystrobin could be topically applied to the cells and the rate of uptake and the maximum concentration within the cell determined. It was not possible to investigate fungal strains responsible for plant pathology. *Neurospora crassa*, a fungal model was chosen instead. A treatment procedure was devised that maintained sufficient turgor pressure within the cells to permit microsampling. The technique was demonstrated by the determination of the intra-cellular concentration of azoxystrobin in the Hex-1 mutant of *Neurospora crassa*.

It would have been interesting both to vary the concentration of azoxystrobin applied to the cells and to measure the uptake of azoxystrobin over time by the Hex-1 mutant of *Neurospora crassa*.

# 7 Droplet on demand interface for mass spectrometry

During the development of the experimental technique used for the analysis of fungal cell extract, described in Chapters 5 and 6, a number of alternative approaches for sample ionisation and detection were investigated which, although not employed in those studies, have the potential of being used for SiCSA experiments. In this chapter, these novel ionisation and detection strategies are described together with their application to the analysis of ultra-low volume samples.

## 7.1 The droplet on demand interface

The droplet on demand (DOD) MS interface offers an alternative to ESI for the ionisation and desolvation of target molecules at atmospheric pressure for mass spectrometry. The interface is based on a commercially available droplet on demand (DOD) dispenser (Microdrop, Germany) [215]. The DOD interface is particularly appropriate for instruments with pulsed injection mass analysers, such as time-of-flight (TOF), Fourier transform ion cyclotron resonance (FT-ICR) and ion traps, where droplet production can be synchronised with ion accumulation, prior to detection.

The piezo electric DOD dispenser produces 50 μm diameter, 65 pL droplets, on demand, at dispensing rates as high as 1000s of droplets per second. The power supply can be externally triggered using a TTL pulse. An adjustable driving voltage (~200 V) stimulates an annular piezo ceramic surrounding a pulled and ground glass capillary. Samples are placed in the sample reservoir; the transfer capillary and dispenser is then primed by lightly pressurising the reservoir with a 10 mL syringe. Once primed, the pressure is released and the dispenser is ready for use. It was important to maintain a difference in height between the tip of the dispenser and the level of liquid in the reservoir that did not exceed 10 mm, to prevent either liquid leaking from the tip or air being drawn into the capillary. It should be noted that the dispenser could operate in either a vertical or a horizontal orientation, although the latter was more appropriate in the context of this work. A pulsed light emitting diode (LED), synchronised and delayed with respect to droplet production, could be mounted onto the dispenser head and permitted visualisation of droplet formation

with the aid of a microscope equipped with a CCD camera and monitor, to enabling tuning.

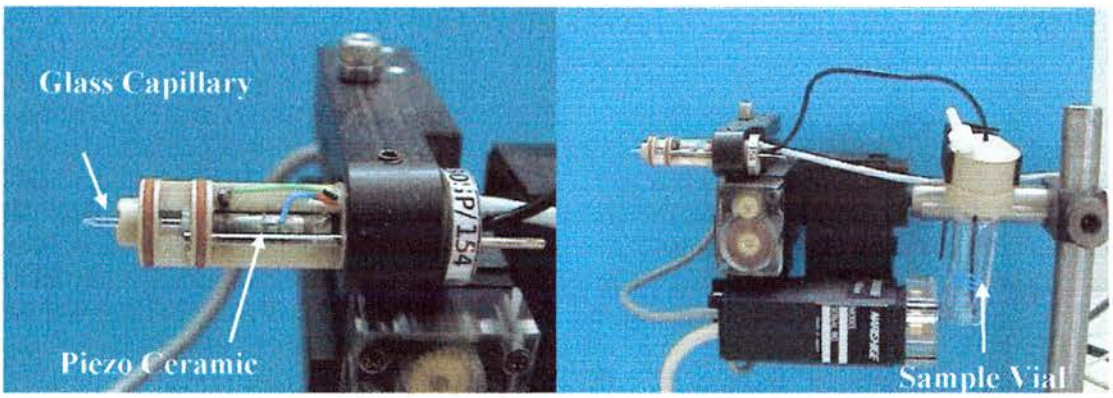


Figure 7-1 Photographs showing components of Microdrop piezo droplet dispenser and Narishige micromanipulator

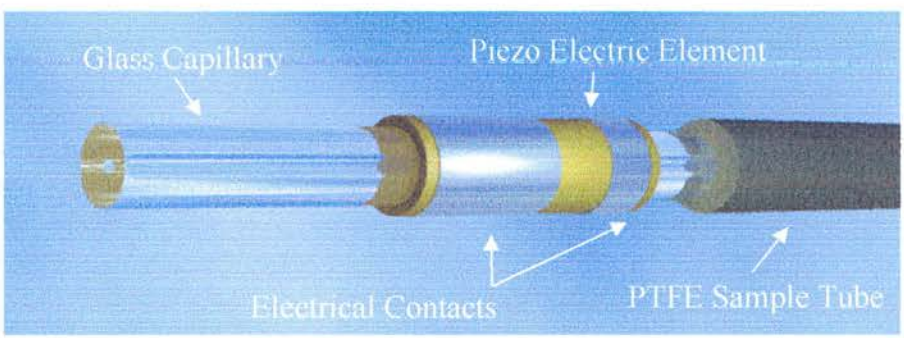


Figure 7-2 Schematic diagram of Microdrop piezo droplet dispenser

To aid in the development and evaluation of the interface, a number of compounds were chosen. The choice of chemical standards, summarised in Table 7.1 was based on their ease of ionisation by ESI and their molecular weights. They were prepared at a range of concentrations in 50:50 (v:v) methanol:water and 1% acetic acid.

Table 7.1 List of standards

| Compound | Structure | Monoisotopic mass |
|---|---|---|
| Myoglobin | GLSDGEWQQVLNVWGKVEADIAGHGQEVLI RLFTGHPETLEKFDKFKHLKTEAEMKASED LKKHGTVVLTALGGILKKKGHHEAELKPLA QSHATKHKIPIKYLEFISDAIIHVLHSKHP GDFGADAQGAMTKALELFRNDIAAKYKELG FQG | 16940.97 Da |
| Reserpine | 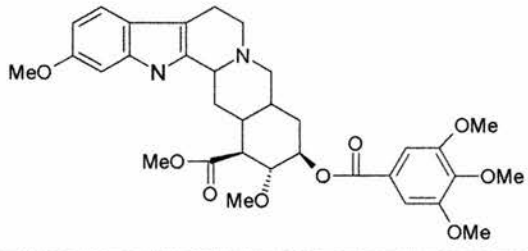 | 608.27 Da |
| Bovine Insulin B Chain | FVNQHLC(SO3H)GSHLVEALYLVC(SO3H) GERGFFYTPKA | 3493.64 Da |
| Bovin Insulin Full Chain | A Chain GIVEQCCASVCSLYQLENYCN B Chain FVNQHLCGSHLVEALYLVCGERGFFYTPKA | 5729.60Da |
| Azoxystrobin | 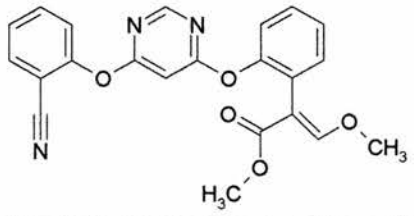 | 403.12 Da |

## 7.2 Proof of principle

The existing nano electrospray ion sources on the LCQ and Q-ToF were replaced with the droplet dispenser. The droplets were aligned with the inlet capillary on the LCQ and the sample inlet cone on the Q-ToF using electronic micromanipulators (Narishige, Japan) [135] and were observed using orthogonal CCD cameras fitted with microscope optics. A charge was induced on the droplets using a voltage applied to the reservoir by means of a platinum electrode. This voltage was applied using the normal electrospray voltage connection fitted on both instruments.

### 7.2.1 Analysis of myoglobin on the LCQ mass spectrometer

Samples of myoglobin were prepared as described in Section 7.1 at a concentration of 0.01 mg/mL. In these experiments, it was unfortunately not possible to externally trigger the droplet dispenser. As a result, the number of droplets produced per analysis is an estimate based on the frequency of production and the analysis cycle time of the mass spectrometer. Spectra acquired by nESI and DOD for the same sample are shown in Figures 7.3 and 7.4.

In both spectra extensive charge state distribution for multiply charged myoglobin ions $[M+nH]^{n+}$ is observed; from +9 to +23 in the case of the DOD spectrum and from +10 to +24 for the nESI spectrum. The relative abundance of ions corresponding to the haem group is considerably greater in the DOD spectrum. The charge series in the DOD spectrum shows a more even spread of ions centered around 1000 m/z, although may result from the higher flow rate of the DOD experiment (1.5 μL/min) relative to the nESI. flow rate (50 nL/min). The scan rate of the LCQ for these experiments was 200 ms. The DOD spectrum corresponds to a single scan while the nESI spectrum is an average of four scans. The amount of sample consumed for the DOD spectrum corresponds to 3 fmol and that for the nESI spectrum 0.4 fmol.

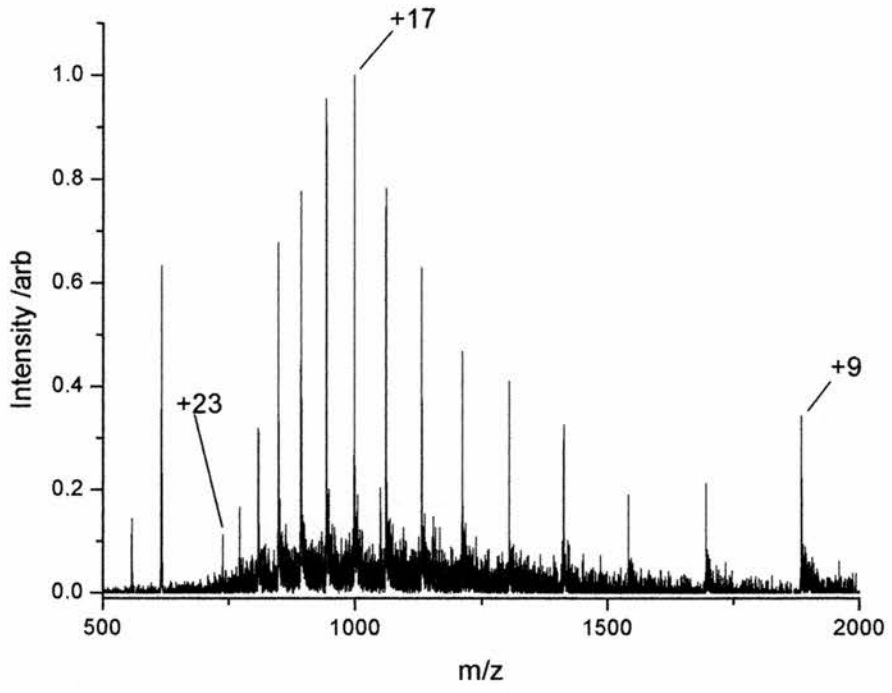


Figure 7-3 DOD MS spectrum for myoglobin (0.01 mg/mL) acquired on LCQ.

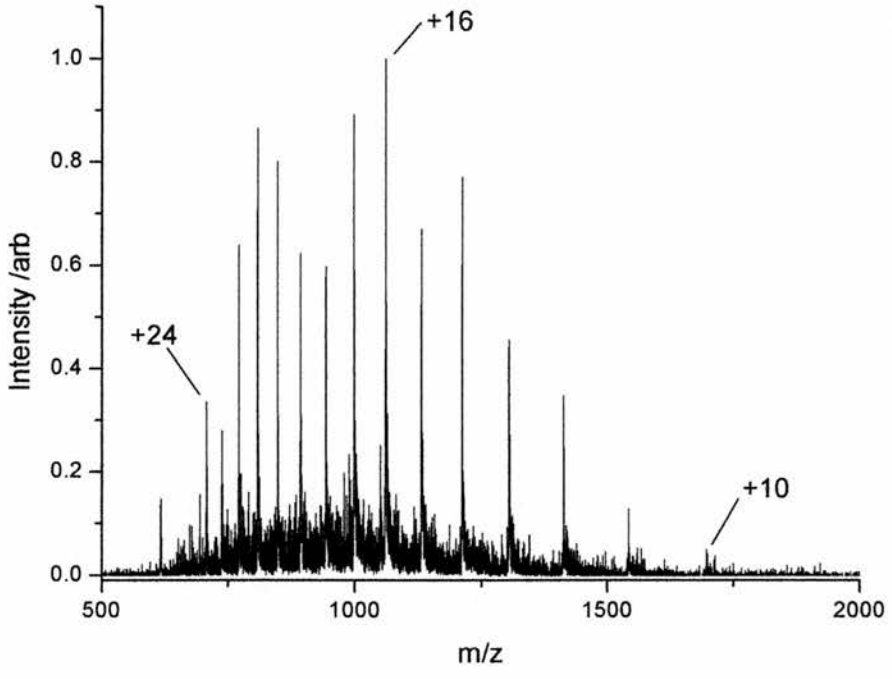


Figure 7-4 nESI MS spectrum for myoglobin (0.01 mg/mL) acquired on LCQ.

### 7.2.2 Analysis of myoglobin on the Q-ToF mass spectrometer

Similar experiments to those described above were performed on the Q-ToF mass spectrometer. Spectra acquired for myoglobin using both nESI and the DOD interface are shown in Figures 7.5 and 7.6. Again, on this instrument a similar charged state distribution for multiply charged myoglobin ions is seen. The relative abundance of ions corresponding to the haem group is again higher in the DOD spectrum.

### 7.2.3 Effect of source block temperature and $N_2$ desolvation gas

The Q-ToF mass spectrometer is equipped with a source block heater and a nitrogen curtain gas supply. Curtain gas is emitted from an annular nozzle that surrounds the inlet to the mass spectrometer. It was expected that the block temperature and curtain gas would help to increase desolvation of the droplets and thereby improve the sensitivity of the interface.

A sample of azoxystrobin was prepared as described in Section 7.1.2 at a concentration of 1 ng/μL and placed in the reservoir of the DOD device. Initially the block temperature was set to 100°C with the curtain gas switched off. The abundance of the fragment ion m/z 372 {MH-CH3OH]+ was recorded as a function of time, in single ion monitoring mode, and is displayed in Figure 7.7. As can be seen, the ion abundance approximately doubles when the curtain gas was switched on, then, as the block temperature is reduced a gradual decrease in the signal is observed. Clearly the block temperature and the presence of nitrogen curtain gas are important for desolvation of the droplets.

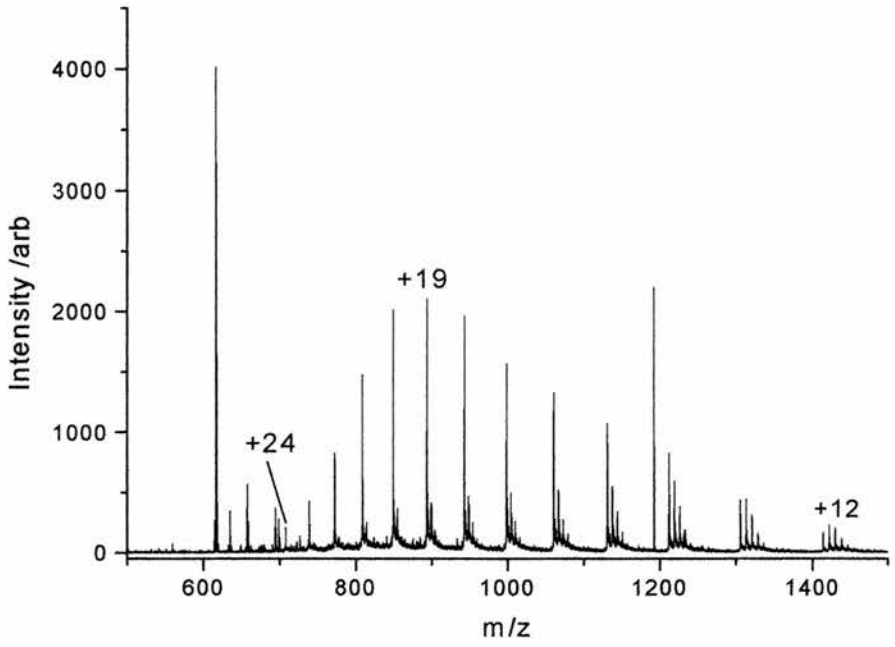


Figure 7-5 DOD MS spectrum for myoglobin (0.01mg/mL) acquired on Q-ToF.

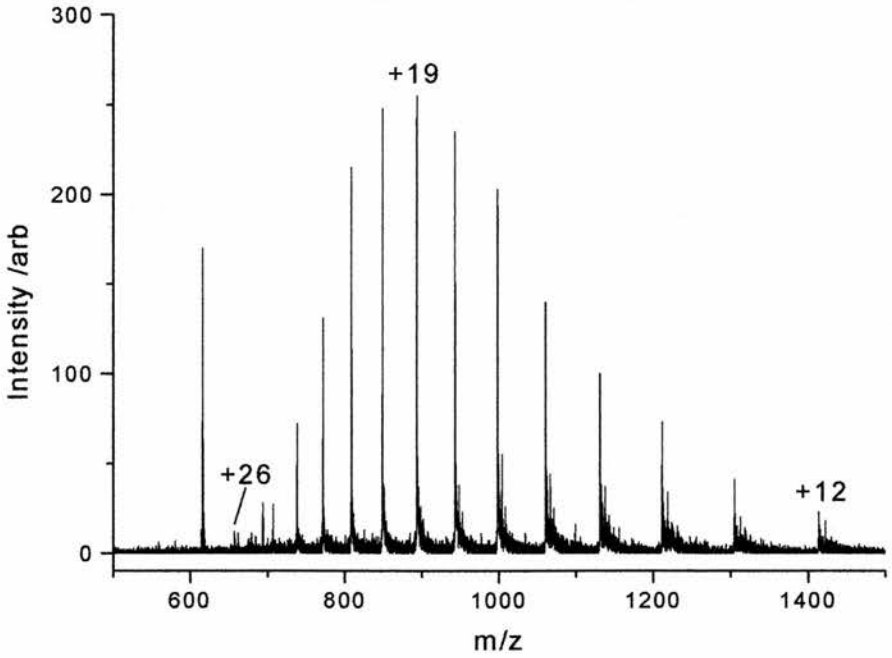


Figure 7-6 nESI MS spectrum for myoglobin (0.01 mg/mL) acquired on Q-ToF.

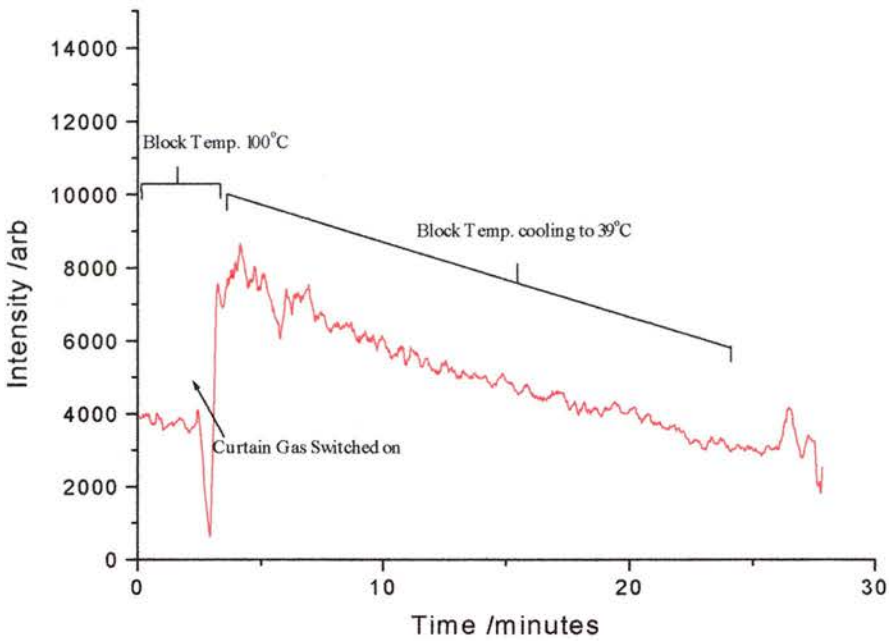


Figure 7-7 DOD SIM signal for m/z 372 fragment ion of azoxystrobin, illustrating effect of $N_2$ desolvation gas and source block temperature.

### 7.3 The Orbitrap

The DOD interface was also installed on a prototype ion trap mass spectrometer [216,217]. The Orbitrap is a novel mass spectrometer, utilising an ion trap first described by Kingdom [218]. It offers potential advantages over many conventional mass spectrometers including high resolution (up to 100,000), increased space charge capacity at higher masses, high mass accuracy and upper mass limit. The trap consists of an outer barrel-like electrode and a central spindle-like electrode along the axis. Ions are formed externally to the trap, and stored in a trapping quadrupole, before being ejected and transported to the trap (Figure 7.8). A series of electrostatic lenses is used to accelerate and focus the ion beam. After the transfer lenses the ion beam pasess through a conductivity restrictor, designed to separate the internal trap volume from the exterior. The ions beam is then deflected and enters the trap through a narrow ion injection channel tangentially to the outer electrode. A further electrode acts as a field compensator to minimise three-dimensional field distortion introduced by the ion injection channel. Ions entering the trap are prevented from hitting the outer electrode by the application of a monotonically increasing electric field, created by applying a voltage to the central electrode. This squeezes them closer to the centre of the trap. The length of time over which this voltage is applied, increases as the mass of the ions to be trapped increases, usually for 20-100 μs. This voltage is removed as soon as there is no risk of the ions colliding with the electrode. Ions orbit around the central electrode, combined with oscillations along the axis, resulting in an intricate spiral motion, as illustrated in Figure 7.8. Excitation of the ions is achieved by off-equator tangential injection (excitation by injection). The mass-to-charge ratio of the ions is derived from the frequency of the axial harmonic ion oscillations. Detection begins as soon as the voltage applied to the central electrode reaches a steady state and is achieved by recording the induced transient image current on the detection plates, followed by fast Fourier transformation (FFT). The axial frequency is used as opposed to radial frequency as only the axial frequency is independent of the energy and spatial spread of the ions.

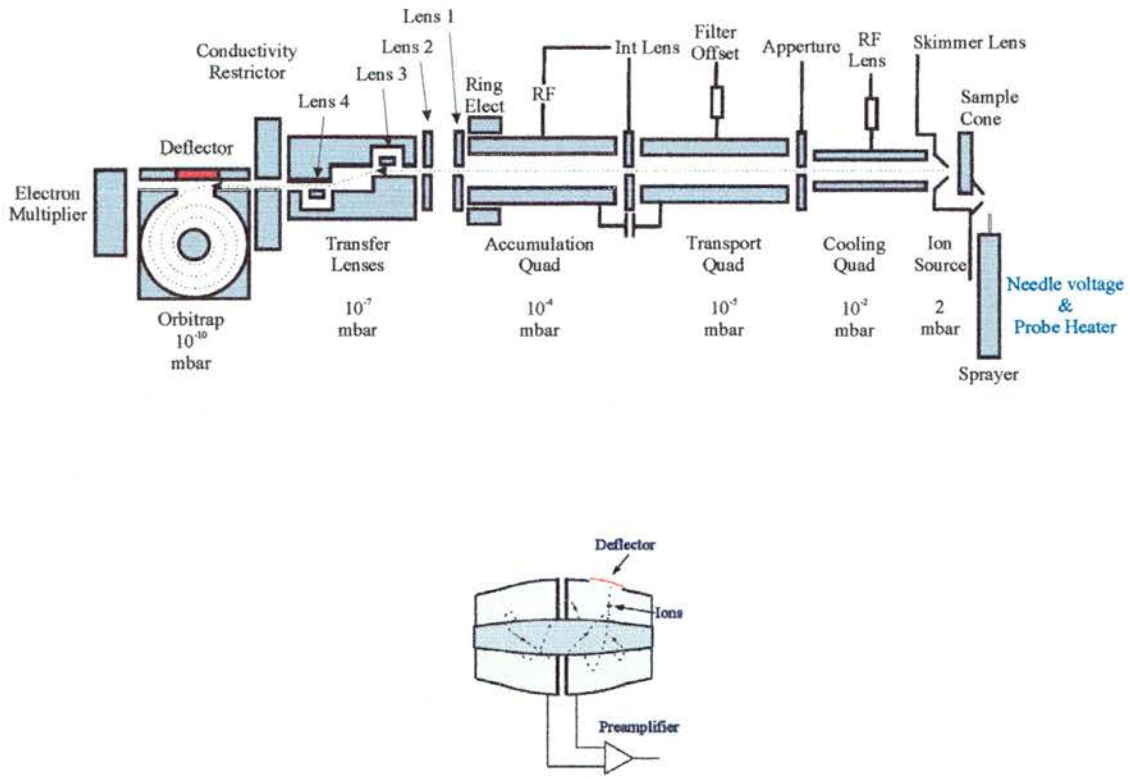


Figure 7-8 Schematic diagram of Orbitrap mass spectrometer.

### 7.3.1 Determining the optimum settings for the Orbitrap

The ESI source on the Orbitrap mass spectrometer (Figure 7.10) provided a constant flow of analyte suitable for tuning the instrument. Reserpine was prepared as described in Section 7.1.2 at a concentration of 5 ng/μL. Sample desolvation was assisted by an electrospray capillary heater and by the application of axial desolvation gas. An electrospray voltage of 4.5 kV was applied to the capillary. A typical ESI spectrum for reserpine is shown in Figure 7.9. The most abundant peak corresponds to protonated reserpine, with the $^{13}C$ isotope clearly resolved. The mass resolution (m/2Δm) is approximately 40,000.

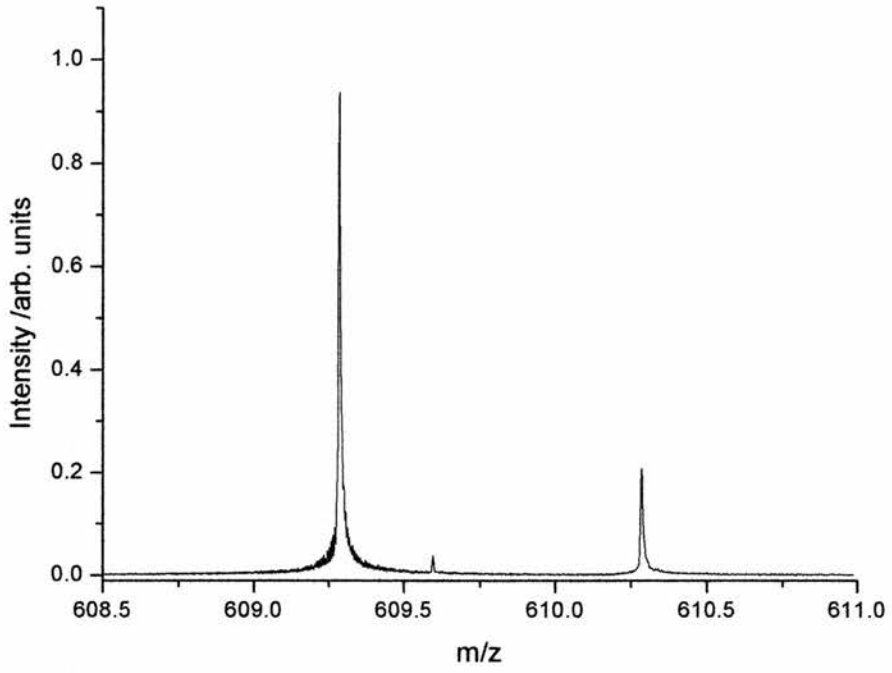


Figure 7-9 ESI spectrum for reserpine. m/z 609.3 $[M+H]^+$ acquired on the Orbitrap.

### 7.3.2 Droplet on demand and the Orbitrap

The limit of detection that could be achieved using the interface was demonstrated using a sample of reserpine at a concentration of 1 ng/μL. Droplet production was synchronised with ion accumulation in the trapping quadrupole. The number of droplets dispensed per scan was gradually reduced as the tuning of the instrument was improved. Increasing the source temperature and the use of curtain gas are two modifications that appeared to improve desolvation and sensitivity. Under these conditions, it was possible to detect a signal due to protonated reserpine from a single droplet, with at good signal-to-noise ratio, as shown in Figure 7.11. The volume of the droplet dispensed was 56 pL and it therefore contained 108 amol. The resulting peak at m/z 609.3 has a mass resolution of 81780 calculated at full width half maximum (FWHM).

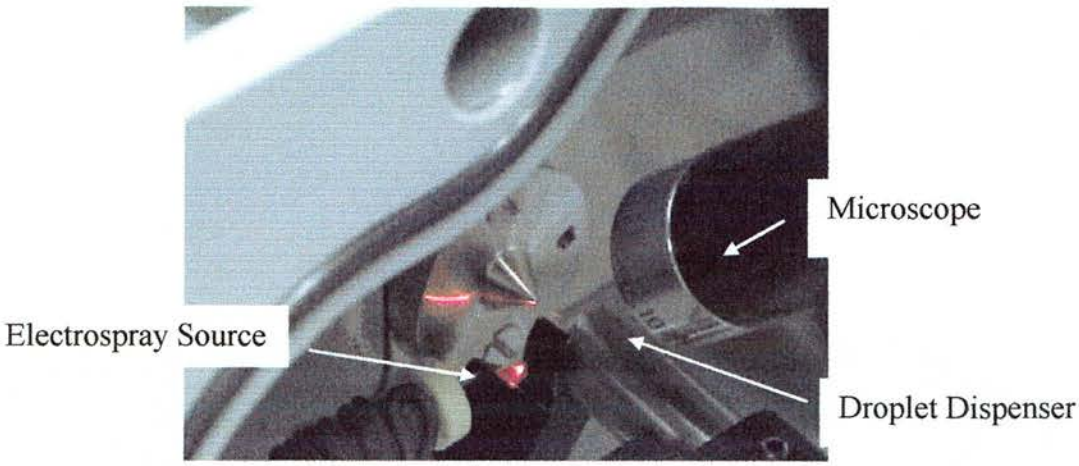


Figure 7-10 Photograph of Orbitrap source highlighting ESI and DOD interfaces.

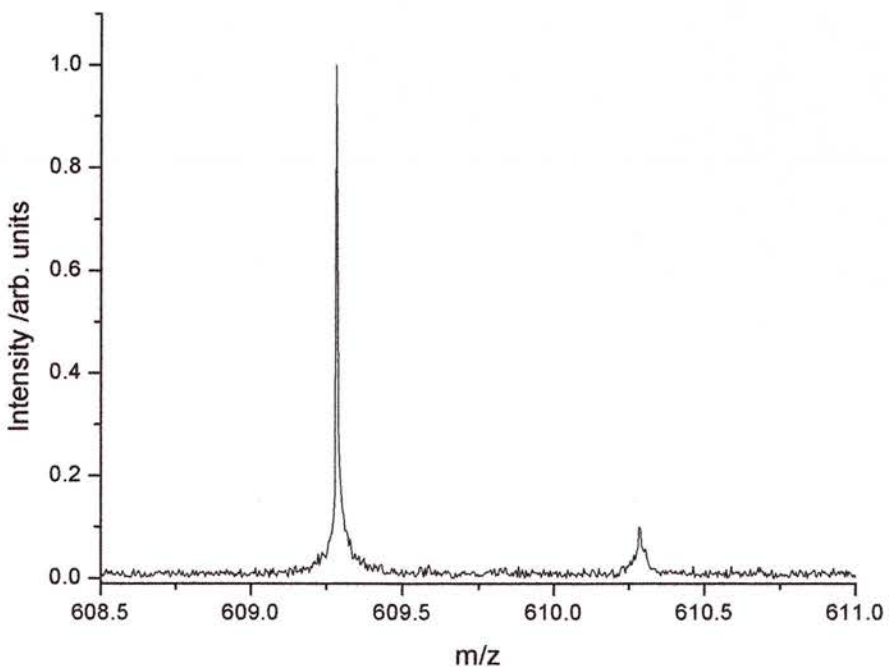


Figure 7-11 DOD mass spectrum recorded for reserpine m/z 609.3 $[M+H]^+$ acquired on the Orbitrap. (1 droplet per scan, 108 amol per drop, resolution 81780).

The Orbitrap, as described in Section 7.2, detects the transient ion image current on the detection plates caused by the decay of the axial frequency of the ions present in the trap. An example of such an image current transient is shown in Figure 7.12.

A PXI based data system (National Instrument, USA) [219] running a custom Lab View (National Instruments, USA) program was used to convert the amplitude/time signal into an amplitude/frequency signal (Figure 7.13) by means of an FFT algorithm. If further information is required, a good review can be found in reference [220]. The axial frequency of an ion within the Orbitrap is inversely proportional to the mass-to-charge (m/z) ratio. Ions with higher axial frequency will have lower m/z values. This can be seen in Figure 7.13 where the transformed image current spectrum is displayed in the frequency domain.


Figure 7-12 Image current transient from ions of reserpine, corresponding to transformed mass spectrum shown in Figure 7.11.

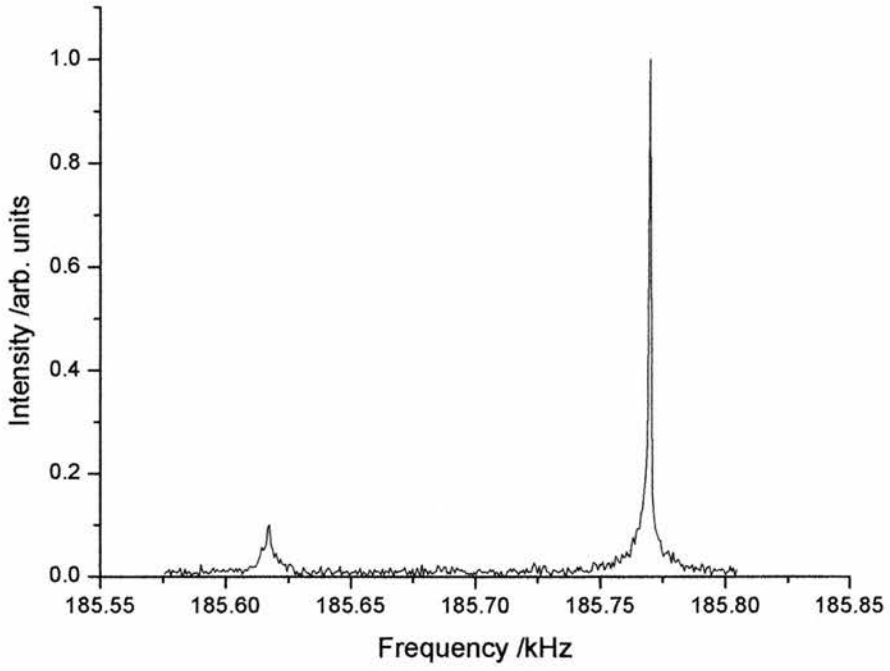


Figure 7-13 DOD frequency domain spectrum for reserpine.

### 7.4 Dynamic range of the droplet on demand interface

A key advantage of the DOD interface is that the number of droplets can be selected to compensate for the concentration of the sample used, thereby increasing the effective dynamic range. The number of droplets dispensed per external trigger event can be adjusted from individual droplets to one thousand. It is also possible to adjust the time delay between the dispensing of each droplet; typically set to 300μs.

To demonstrate the dynamic range of the interface, a sample of bovine insulin B chain was prepared as described in Section 7.1.2 at a concentration of 1 ng/μL. The number of droplets dispensed was varied from one to ten per spectra scan. The signal-to-noise ratio for a single droplet was below detectable levels.

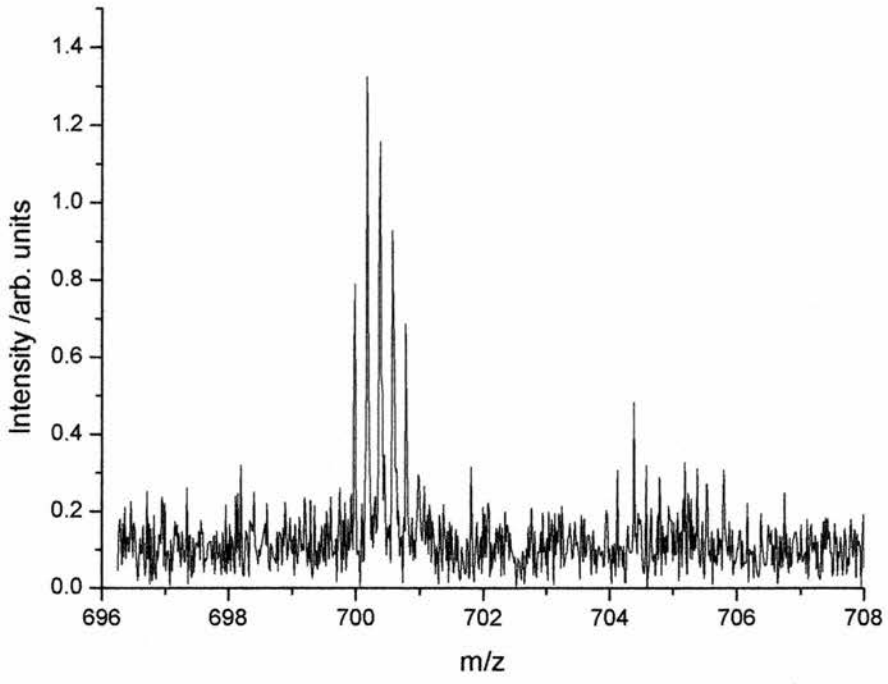


Figure 7-14 DOD mass spectrum for bovine insulin (B chain) m/z 699.7 $[M+5H]^{5+}$ acquired on the Orbitrap. (2 droplets per scan, 1 ng/μL, resolution 81780).

The mass spectrum acquired from 2 droplets of this solution of bovine insulin B chain is shown in Figure 7.14. The $^{13}C$ isotope envelope can clearly be resolved. The signal-to-noise ratio although low, is satisfactory. Figure 7.15 shows a similar mass spectrum acquired from 10 droplets. It can be seen that the signal-to-noise ratio is greatly improved. The signal due to the corresponding sodium adduct is also now visible in the spectrum. Both spectra were collected during the same experiment, using identical Orbitrap operating parameters; the only adjustment was the number of droplets dispensed. The mass resolution of the +5 charge state envelope for bovine insulin B chain in Figure 7.15 is 66700. The difference in signal quality between the spectra shown in Figure 7.14 and 7.15 demonstrates the utility of the DOD interface in being able to adjust the volume of sample analysed, and is highlighted in Figure 7.16 by a direct comparison of the two spectra.

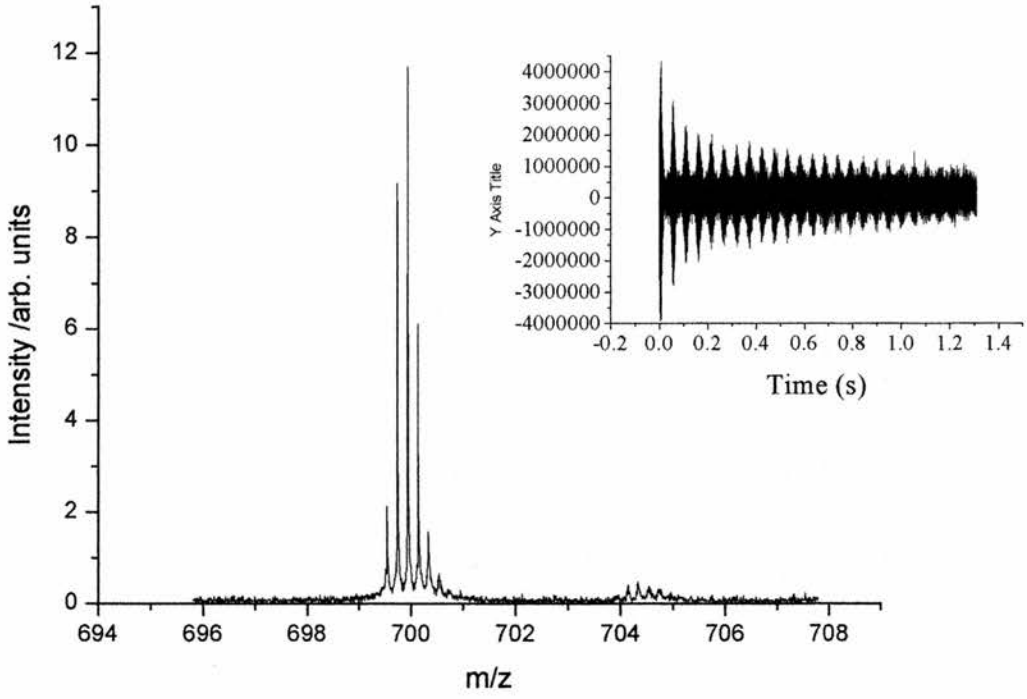


Figure 7-15 DOD mass spectrum for bovine insulin (B chain) m/z 699.7 $[M+5H]^{5+}$ acquired on the Orbitrap. (10 drops per mass analysis, 1 ng/μL,) Insert: corresponding ion current transient

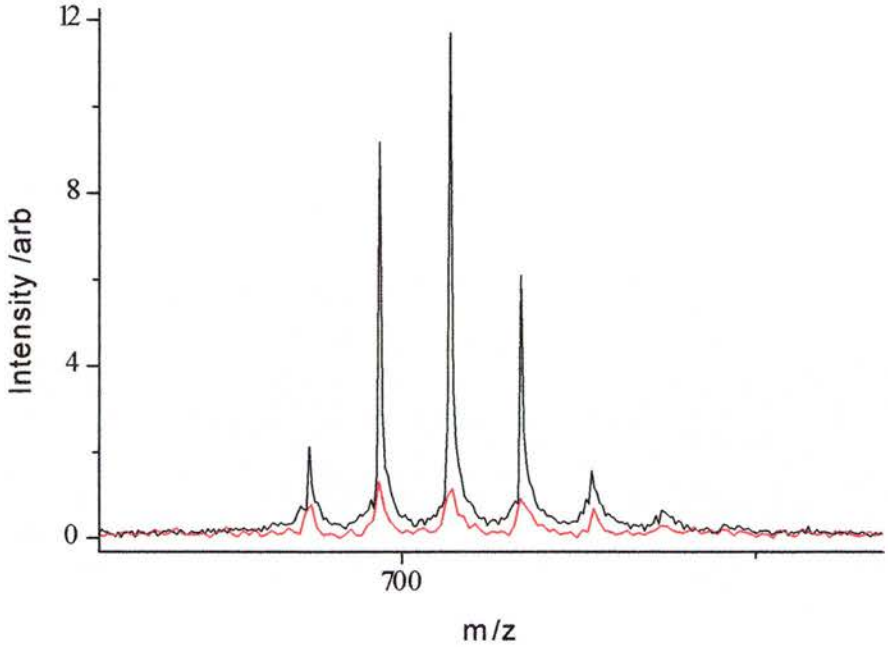


Figure 7-16 Comparison of DOD mass spectra for bovine insulin (B chain). m/z 699.7 $[M+5H]^{5+}$ acquired from 1 droplet (red spectrum) and 10 droplets (black spectrum).

The prototype Orbitrap mass spectrometer was the first beta version built and incorporated several hardware components from other instruments. The principal limitation at present is that the transmission efficiency of ions of high m/z values is limited by the current quadrupole transfer optics.

To demonstrate the upper mass limit of the instrument, a sample of bovine insulin full chain (Sigma Aldrich, UK) and myoglobin (Sigma Aldrich, UK) were prepared, as described in Section 7.1.2, at a concentration of 50 ng/μL. The number of droplets dispensed per mass spectral scan was varied from a single droplet to five droplets per scan, with a delay of 300 μs between dispensing events. A typical mass spectrum for bovine insulin acquired from a single droplet is shown in Figure 7.17.

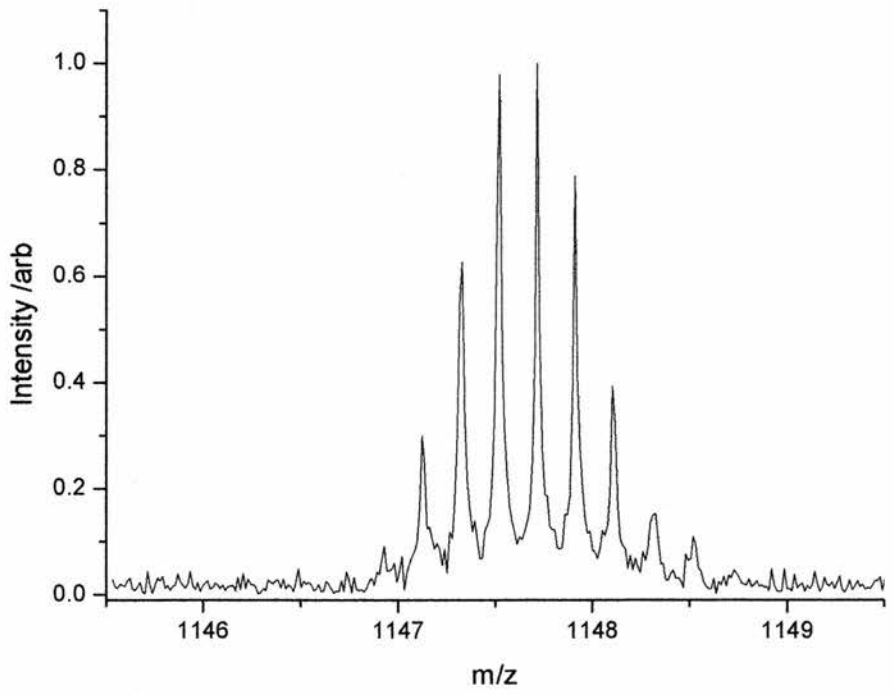


Figure 7-17 DOD mass spectrum for bovine insulin (full chain) m/z 1146.9 $[M+5H]^{5+}$ acquired on the Orbitrap. (1 droplet per scan, 50 ng/μL or 565 amol per scan).

It can be seen from the spectrum that the isotope envelope for the +5 charge state of bovine insulin (full chain) could be detected with good signal-to-noise ratio from a single droplet, containing 565 amol. The mass resolution for isotope envelope of the +5 charge state in the above spectrum is 47500 at FWHM.

It was not possible to detect a signal for myoglobin in any charge state. As myoglobin has been demonstrated to be a reliable standard and was detected using both the LCQ and Q-ToF instruments, it is clear that the problem in detecting ions at high mass is caused by the transfer optics of the Orbitrap and not the DOD interface.

### 7.5 Charged droplet disruption of trapped ions

In order to compare the performance achieved with the DOD interface on the Orbitrap experiments were attempted with the DOD interface installed on a Bruker Daltonics Apex II 3 Tesla Fourier transform ion cyclotron resonance mass spectrometer (Figure 7.18). Again, it was possible to externally trigger droplet production using a TTL pulse controlled by the FT-ICR software.

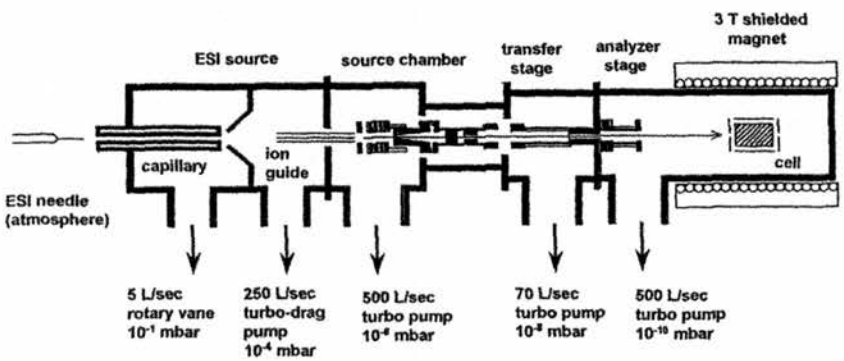


Figure 7-18 Schematic diagram of Bruker Daltonics Apex II FT-ICR mass spectrometer.

While the DOD interface was successfully used to replace the ESI interfaces on the LCQ, Q-ToF and Orbitrap, it proved impossible to detect any signal using the FT-ICR mass spectrometer. Experiments were carried out with reserpine, azoxystrobin and myoglobin at varying concentrations but no ion signals were detected. However, a steep pressure rise in the FT-ICR cell was observed following droplet production. The pressure was seen to rise from $10^{-10}$ to $10^{-6}$ mBar, indicating that a considerable number of molecules were passing into the high-pressure region of the instrument. This observation led to the following hypothesis. One important distinction between the FT-ICR instrument and the others is the absence of a convoluted source region (Figure 7.19). It is likely that the large, charged droplet produced by the dispenser does not completely evaporate. In fact, it is unlikely to reach its first Rayleigh limit [221], which could be as long as 550 ms [222,223] before the charge density of the droplets causes Coulombic fission at ambient pressures and temperature. This time would be considerably longer in the conditions experienced within the mass spectrometer. In fact it is expected that the surface of the droplet would quickly freeze, preventing Coulombic fission. This charged droplet could then continue down the length of the instrument, and any gas phase ions that it encounters will be displaced and lost. In instruments with convoluted source regions (Figure 7.19), the droplet will collide with the source wall and will not be transmitted into the instrument. Therefore this effect would not be observed.

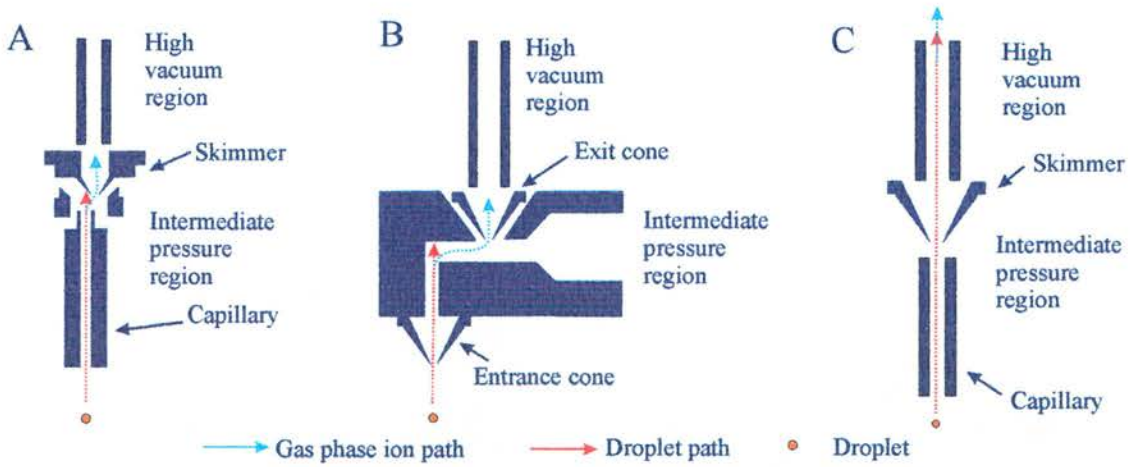


Figure 7-19 Schematics of (A) LCQ API stack, showing the skimmer cone is offset with regard to the heated capillary. (B) Orbitrap (and Q-ToF) showing orthogonal source region. (C) FT-ICR line-of-sight source.

### 7.5.1 Droplet charging

In order to characterise the effect of such a large charged particle passing through the mass spectrometer, it was necessary to calculate the charge present on the droplet. Previously reported methods for determining the number of fundamental charges present on a droplet have used an electrodynamic balance (Figure 7.20) [222,223]. The balance was composed of two ring electrodes formed from 1.7 mm copper wire and aligned parallel at a separation of 4.6 mm. The charged droplet was introduced into the center of the device and held there by the application of a 60 Hz line voltage amplified to 1300 V.

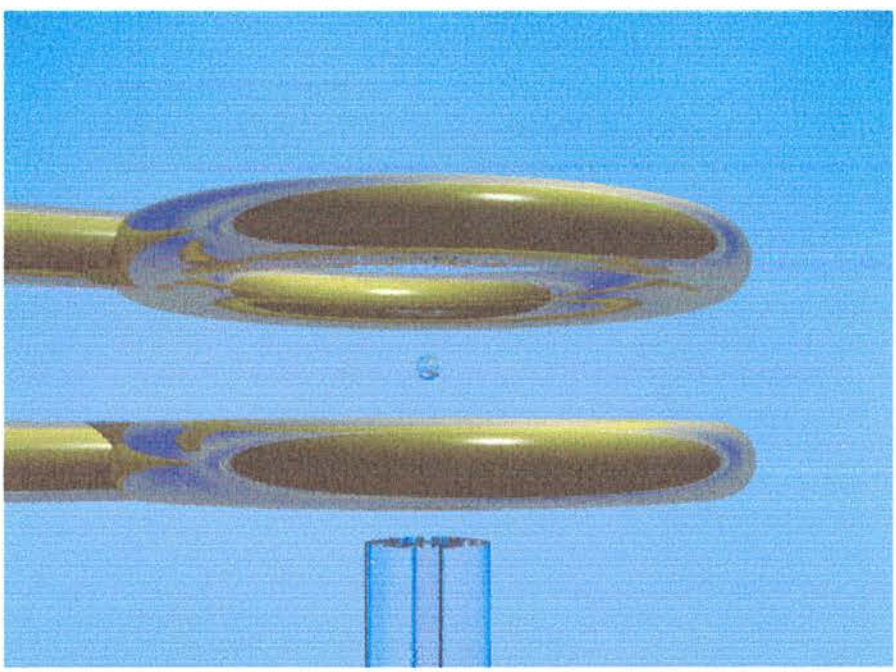

Figure 7-20 Diagram of the electrostatic balance.

A modified version of the Rayleigh equation (equation 7.1) [221] was used:

$$(qe)^2 = 64\pi^2 \varepsilon_o \gamma r_c^3 \qquad \text{Equation 7.1}$$

where $\varepsilon_0$ is the permittivity of free space, $\gamma$ is the surface tension of the droplet and $r_c$ is its radius. This equation describes the relationship between the maximum charge that can be contained on a sphere and its radius.

The diameter of the droplet at the Coulomb limit was estimated using the following equation which, under diffusion-limited evaporation, relates the radius of a droplet, $r$, at a time, $t$, to the original droplet radius, $r_0$.

$$r^2 = r_o^2 - \frac{2Dp^o M}{p_L RT}(\Delta t) \qquad \text{Equation 7.2}$$

$D$ is the diffusion coefficient of the solvent vapour, $p^0$ the vapour pressure of the evaporating species, $M$ the molecular weight, $p_L$ the solvent density, $R$ is the ideal gas constant and $T$ is the temperature.

Single droplets were observed in the trap and the time between its dispensation and the first Coulomb explosion was measured using a stopwatch. In these experiments, the time was of the order of 550 ms. With this information, and knowing the original droplet radius, the radius of the droplet at the Coulomb limit can be calculated (Equation 7.2) and hence the number of charges on the original droplet (Equation 7.1).

This method of calculating the number of fundamental charges contains a number of approximations, summarised in Table 7.2, which could introduce errors into the results. For these reasons it was decided to develop a simpler and more direct method to calculate the number of fundamental charges present on the droplet.

Table 7.2 Possible sources of experimental error

| Estimated Coefficient | Equation | Source of Error |
|---|---|---|
| $\gamma$ | Equation 7.1 | Surface tension of small spheres is reduced due to high curvature [224] |
| t | Equation 7.2 | Time was measured with a hand/stopwatch |
| T | Equation 7.2 | Temperature of the evaporation drop is lower than the ambient temperature [225] |
| $p^0$ | Equation 7.2 | Average vapor pressure is lower than equilibrium. |

### 7.5.2 A direct method for the measurement of droplet charging

In this method, the charged droplets were fired at a target. The voltage produced as the droplets discharged through the target was detected and recorded on a digital storage oscilloscope (DSO). Charge was applied to the droplets by an electrode placed in the liquid reservoir. A 1MΩ resistor was used to convert the current to a potential across the resistor and recorded on the DSO (Figure 7.21). The sample response curves recorded on the DSO were plotted for a range of typical charging potential (Figure 7.22).

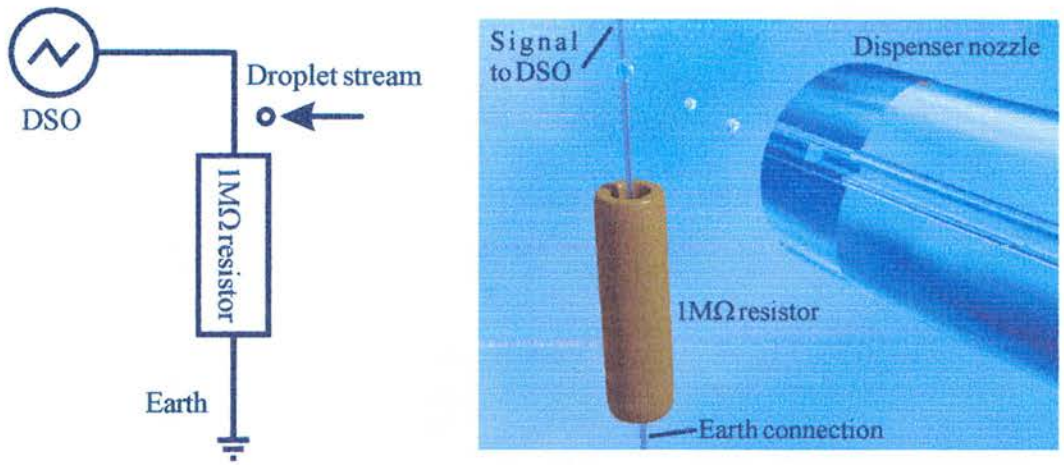


Figure 7-21 Diagram of apparatus used to measure charge on droplets.

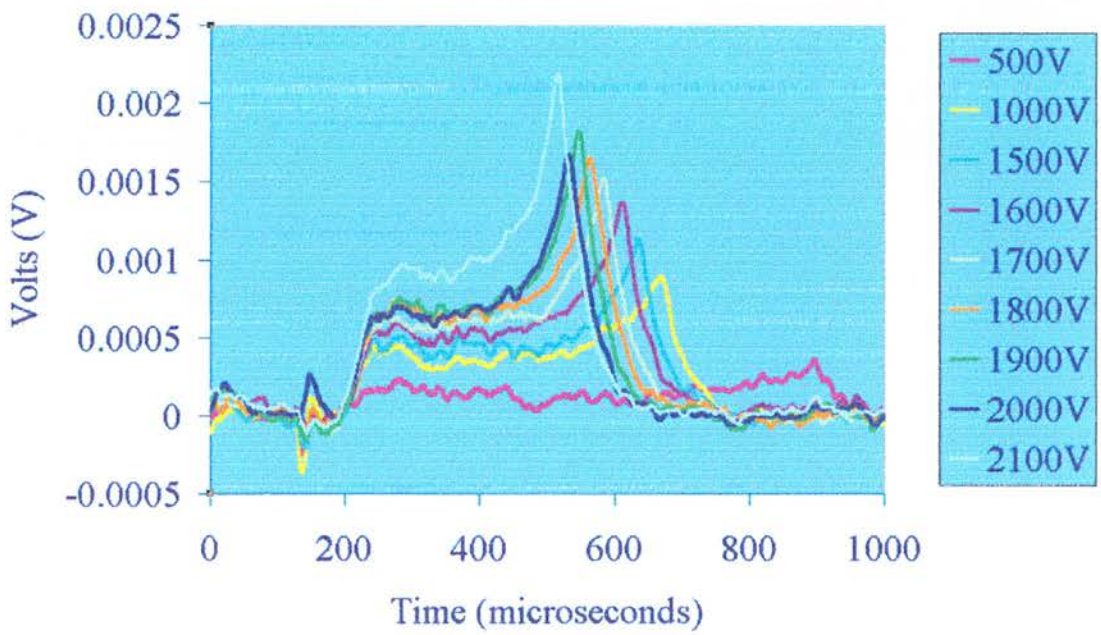


Figure 7-22 Sample response curves recorded on the DSO, for a range of charging potentials.

The number of fundamental charges per droplet, $n$, can be calculated using the equation below, which sums the number of charges associated with each of the $\tau$ data points that define the detected peak,

$$n = \int_0^{\tau} \left( \frac{LtV}{FR} \right) \qquad \text{Equation 7.3}$$

where $L$ is Avogadro's number, $t$ is the reciprocal of the sampling rate of the DSO, $V$ is the voltage at each sampling point, $F$ is the Faraday constant and $R$ is the resistance of the resistor. The number of fundamental charges measured on the droplets, as determined by the method described above, is shown in Figure 7.23 for a number of typical electrospray voltages.

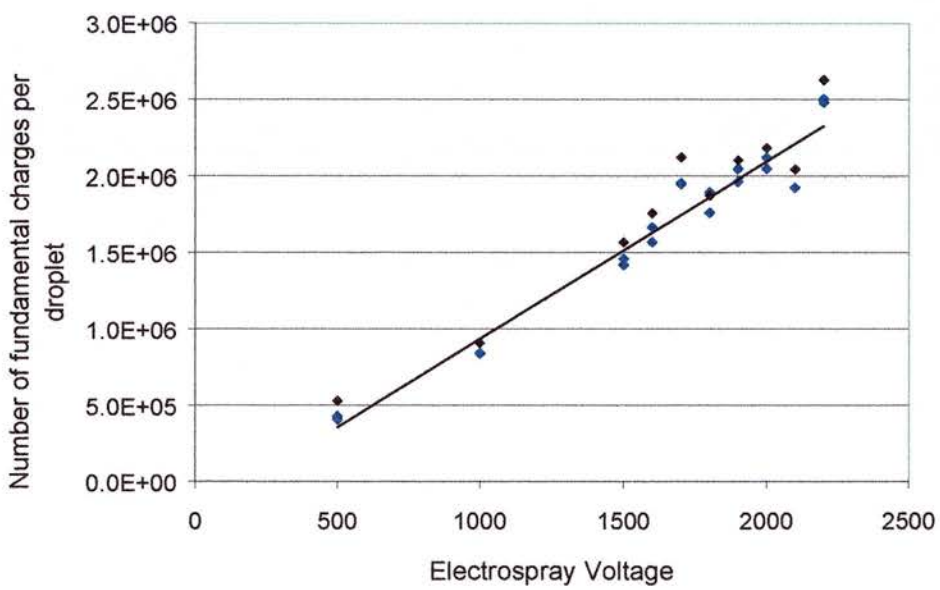


Figure 7-23 Plot of number of fundamental charges per droplet as a function of electrospray voltage.

It can be seen that the number of fundament charges per droplet when using an electrospray potential of 1 kV was of the order of $10^6$. From this, the mass-to-charge ratio of the droplets can be estimated to be of the order of $10^9$ Thomson. The effect of any electrostatic acceleration will therefore be low and the velocity of the droplet within the mass spectrometer will be close to its original velocity (~2 $ms^{-1}$). Therefore, it could take up to 0.5 s to reach the trapping cell on the FT-ICR mass spectrometer.

### 7.5.3 Simion simulation of electrostatic disruption

In addition to the physical disruption, caused by the droplet passing through the instrument, it is hypothesised that the charged droplet would exert an electrostatic disruption on any trapped ions. The electrical potential on the droplet is produced by a charge, Q, acting at a point in space and is given by:

$$V = {}^{kQ}/_{r} \qquad \text{Equation 7.4}$$

where $k$ is Coulomb's constant ($8.98 \times 10^9$ $Nm^2/c^2$), r is the radius of the droplet and $Q$ is the charge that can be calculated as

$$Q = ne \qquad \text{Equation 7.5}$$

where $n$ is the number of charges (~$1 \times 10^6$) and $e$ is the charge of an electron ($1.6 \times 10^{-19}$C)

Using the equations above it is estimated that there would be a potential of 71 V near the surface of the droplet, although it may reach 1000 V if the droplet adopted a non-spherical conformation. A simple example of the effect the droplet may have on any ions trapped in a quadrupole was modeled with Simion (SIS, USA) [226]. The potential on the droplet was set to a number of values and its effect on a population of ions was simulated (Figure 7.24). The mass of the trapped ions was set to 3000 Da, single positive charge, with a kinetic energy of 1 eV.

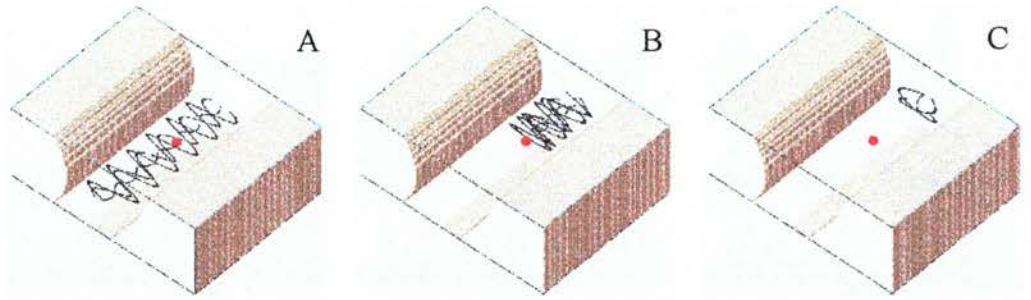


Figure 7-24 Simion simulation of the motion of ions in a quadrupolar field. Voltage on droplet (•): (A) 0V, (B) 0.5 V, (C) 60 V.

The simulation could be improved by the use of hyperbolic instead of circular cross section rods, but it is clear that the droplet would cause significant disruption even at low potentials.

### 7.6 Concluding remarks

A DOD interface for mass spectrometry based on a piezo electric dispenser has been developed. It was shown to have a number of advantages A comparison of the various strengths and weaknesses of the DOD interface and conventional ESI and nESI interfaces is given in Table 7.3. The piezo DOD interface could be easily retrofitted to any instrument already equipped with a convoluted ESI source. Mass spectra were recorded at dispensing rates as low as one droplet per spectrum. The interface has demonstrated improved reliability over nano electrospray, and increased sensitivity in terms of concentration over conventional electrospray.

When fitted on instruments with convoluted ion source paths, higher sensitivity was achieved with the DOD interface than with conventional ESI sources. The DOD interface has a far greater range of flow rates (three orders of magnitude), which can be easily varied to compensate for a wide range of sample concentrations. The droplet size is reproducible for a particular liquid and should permit quantification. When used with line-of-sight sources, as on the Bruker Daltonics FT-ICR

instrument, the failure to achieve any signal was thought to result from disruption of the gas phase ions by progress of the charged droplet through the instrument. The recent development of FT-ICR instruments equipped with convoluted source regions may resolve this problem.

Table 7.3 Comparison of strengths and weaknesses of various interface techniques

| **Parameter** | **Droplet on demand** | **Electrospray** | **Nanospray** |
|---|---|---|---|
| Sample Volume per Scan | 50 pL–60 nL | 33 nL-3μL | 160 pL |
| Flow Rate* | 15–18 nL | 10 μL–1 mL/ min | 50 nL / min |
| Control of Flow Rate | Exact ±1% | Exact ±1% | Uncontrollable |
| Quantifiable | Yes | Yes | No |
| Sensitivity for Reserpine | 100 amol/ scan | 500 amol/ scan** | 100 zmol/ scan** |

* During constant data acquisition.

** Calculated for a 200 ms ion accumulation time.

The mechanism responsible for the formation of gas phase ions from the droplet is unclear. It was seen that the droplet dispenser is an on-demand interface, that is, when the piezo is not firing, no signal can be seen. However, it was also possible to detect a signal when the droplet path was directed to the side of the inlet apertures on the LCQ, Q-ToF and Orbitrap. This suggested that the initial droplet might be forming satellite droplets invisible to the CCD cameras.

The droplet formation process occurs when the piezo actuator creates a pressure pulse in the liquid inside the capillary. When this pulse reaches the capillary tip, it is

transduced into a highly accelerated motion that expels liquid out of the tip. As the piezo relaxes, surface tension pulls the liquid back into the glass capillary. At this point, a neck forms in the liquid that quickly constricts to leave a droplet. In the image shown in Figure 7.25, it can be seen that a large satellite droplet is formed.

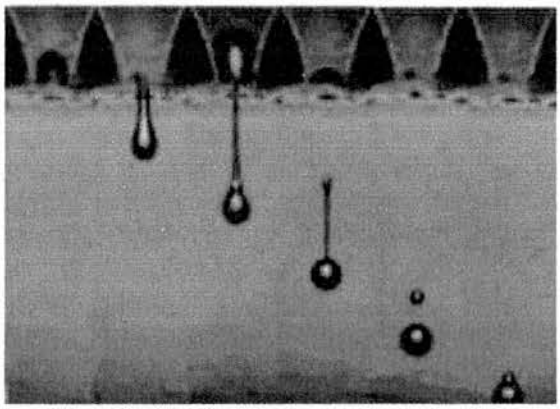

Figure 7-25 Piezo droplet formation. Reproduced from reference [216].

It is possible that any small satellite droplets formed were desolvated to form gas phase ions by the same mechanism as electrospray. It is also possible that since an electrospray potential was applied to the dispenser, piezo assisted Taylor cone electrospray might occur. It may be possible to visualise these events with the use of a high speed, high magnification camera.

# 8 Conclusion

Single cell sampling and analysis have been the focus of sporadic research since the early 1950's. These techniques allow the chemical composition of specific cells within a heterogeneous population to be examined, and hold considerable promise for studies in many fields of biological research, particularly in medicine where the origin of a disease could be a single cell. The ability to profile the intra-cellular concentrations of molecules with biological significance within specific individual cells will offer clear advantages to cellular biologists.

The focus of this research was to develop a technique capable of sampling and quantifying the compounds present in ultra-low volume samples extracted from fungal cells. The research presented in this thesis can be divided into three distinct components:

- development of a novel microsampling and analysis technique for fungal cells, which incorporated capillary electrophoresis (CE) and electrospray ionisation (ESI) mass spectrometry (MS).

- demonstration of the technique by investigation of the endogenous levels of disaccharides within fungal cells of *Neurospora crassa* and the accumulation of a commercially important fungicide within topically treated cells.

- development of novel instrumentation applicable to the analysis of ultra-low volume samples, such as those derived from single cells.

In Chapter 4, a novel technique was described for single cell sampling and analysis (SiCSA) of ultra-low volume samples derived from the fungi *Neurospora crassa*. A modified plant pressure probe was used to aspirate and transfer cell extract into a fused silica capillary, through which separation was achieved by capillary electrophoresis (CE) using an adapted Isco electropherograph. The CE capillary was directly connected to a Q-ToF mass spectrometer using an electrospray ionisation (ESI) interface.

The plant pressure probe, originally developed as a device to measure the turgor pressure of plant cells, was used as a microsampling device, and permitted a wide range of volumes (10-1000 pL) to be aspirated. CE was chosen as a separation and desalting technique since it is particularly applicable to the analysis of complex biological samples. It is an open-tube technique and therefore does not suffer from blockages caused by the large structures present in the cell extract, such as membranes and sub cellular organelles. Flushing with weak sodium hydroxide solution was found to quickly remove molecules adhering to the capillary surface, which would have affected any packed column separation method. The separation capillary also functioned as a convenient transfer device. Aspirated samples of cell cytoplasm could be loaded directly under oil into the separation capillary, and transported to the mass spectrometer avoiding exposure to the environment.

Mass spectrometry was chosen as the detection strategy. Although the sensitivity is somewhat lower compared with electrochemical or laser induced fluorescence detection techniques, mass spectrometric detection has the added benefit that unknown molecules can be identified based on their mass-to-charge ratio and characteristic fragment ions. The use of a sheath flow ESI interface while not providing the ultimate detection limits, did offer a good compromise between sensitivity, ease of use and reliability.

The experiments described in Chapter 5 involved the application of the SiCSA CE-MS instrumentation to measure the concentration of disaccharide within cells of the model fungi, Neurospora crassa. A mutant strain, Hex-1, was used allowing volumes larger than a single cell compartment to be aspirated, reducing the risk of contamination from the extra-cellular matrix. Identification of the disaccharides was confirmed by comparison of CE elution times, MS-TOF and MS/MS-TOF spectra of disaccharide standards with those for aspirated samples. Potential causes of contamination during microsampling and sample transfer by material present in the extra-cellular matrix were investigated. A rhodamine B isothiocyanate-dextran fluorescent dye was added as an extra-cellular marker for contamination. Samples in which contamination was present were identified by laser induced fluorescence

(LIF). An internal standard, angiotensin I, was used to correct for any instability of the CE-MS interface.

The detected concentration of disaccharides in the aspirated cell samples was found to be 1.2 ± 0.1 mM. This value agrees well with previously reported levels of trehalose, which is the predominant disaccharide in cells of *Neurospora crassa* and other fungi. The SiCSA CE-MS technique offers an increase in detection sensitivity of two orders of magnitude over previously reported methods, which are based on information derived from bulk cell samples. In this work, it was not possible to conclusively differentiate between individual disaccharide isomers that were present, although it is likely that the predominant isomer is trehalose. The MS/MS-TOF spectra recorded bore a closer similarity to that expected for trehalose. This disaccharide is synthesised within the cells as a stress response, and has been recorded at levels as high as 15% of the dry weight of the cell. Maltose is actively taken up by the cells but is present at much reduced levels. Therefore, although the measured intra-cellular concentration is the combined level of the predominant disaccharides present, the majority will be trehalose. The results demonstrate the potential of SiCSA techniques to provide quantifiable information from ultra-low volume cell samples.

In the experimental work described in Chapter 6, the SiCSA CE-MS instrumentation was used to measure the amount of azoxystrobin, an important commercially available fungicide, taken up by cells of the Hex-1 mutant of *Neurospora crassa* following topical application. The molecule is highly hydrophobic, with saturation constant in water of 6 mg/L. It has been reported that the molecule enters the cells by simple diffusion, halting respiration within 13 seconds. In an experimental protocol similar to that used for the analysis of disaccharides, angiotensin 1 was used as an internal calibrant and rhodamine B isothiocyanate-dextran as a marker for contamination from the extra-cellular matrix.

After treatment with the fungicide, the cells were incubated for 5 minutes, and then washed three times with a 2% maltose solution. The external calibrant was then added and the sample aspirated. For cells treated with azoxystrobin at a

concentration of 14.8 μM (the saturation concentration of azoxystrobin in water), the intra-cellular concentration was shown to reach 9.9 μM within 5 minutes. The level of disaccharide (principally trehalose) in the treated cells was also measured, and was found to be slightly elevated.

Chapter 7 describes the research carried out to develop a novel droplet on demand (DOD) interface for mass spectrometry that would be applicable to the analysis of ultra-low volume samples. It was hoped that this interface would offer benefits over conventional ESI and nESI in terms of reliability and quantification. The interface was based on a commercially available piezo electric droplet dispenser and offered the facility to synchronise droplet production with the external ion accumulation of the mass spectrometer. The interface was tested on several commercially available mass spectrometers (LCQ, ThermoFinnigan; Q-ToF Micromass), as well as a prototype Kingdom ion trap (Orbitrap), and compared against electrospray ionisation interfaces. On the Orbitrap spectra were acquired at dispensing rates as low as one droplet per scan and a limit of detection of 108 amol was achieved for reserpine, a drug used to treat hypertension.

## 8.1 Current limitations

The limited number of results for the quantitation of the concentration of disaccharides and fungicide in aspirated cell extracts reflects the complexity of the technique. Each of the four steps (sampling, transfer, separation and analysis) requires a high level of expertise for success, even when performed as isolated experiments. This problem is multiplied when the steps need to be performed in series. The published literature reflects this. A large number of references exist describing the use of CE-MS for the analysis of a very diverse range of analytes. There are also a large number of references describing the use of CE for the analysis of single cells. However, there have been very few reported studies describing the use of CE-MS for the analysis of single cells.

## 8.2 Future work

Based on the current limitations of the SiCSA CE-MS technique developed here, future work should be directed towards modifications that will improve the reliability

and simplicity of the procedure. In the majority of cases, the reason for an experiment to fail was a break in the electrical continuity of the separation capillary. The use of a CE instrument with the facility to lightly pressurise the inlet reservoir would provide a marked increase in reliability. In the research presented, single ion monitoring was used for the quantification of intra-cellular concentrations. The use of MS/MS would improve the technique, reducing noise and minimising the possible risk of isobaric molecules affecting future measurements.

Further development of a DOD interface appropriate for CE-MS would also lead to a notable increase in sensitivity and reliability. To achieve a satisfactory level of reliability, a commercially available sheath flow interface was used. As a consequence of the dilution of the eluting analyte there is a corresponding reduction in sensitivity. The use of a piezo droplet on demand interface might alleviate the requirement for sheath flow, and by synchronising droplet production with acquisition of mass spectrometric data, maximise the efficiency of detection.

The experimental technique for SiCSA CE-MS developed here, although suffering from problems associated with reliability of the instrumentation, was successfully used to identify and quantify the intra-cellular concentration of a number of biologically relevant molecules. It is hoped that this technique could be used to further investigate the complex chemical environment present within single cells.

[1] Tomos AD and Sharrock RA, *J. Exp. Biol.*, **2001**, 52, 623

[2] Zabzdyr JL and Lillard SJ, *Trends Anal. Chem.*, **2001**, 20, 467

[3] de Lang RPJ and van Minnen J, *J. Neurosci.*, **1997**, 78, 289

[4] McFadden GI, *Plant Cell Biology- A Practical Approach*, Harris N and Oparka KJ (Ed.), **IRL Press**, Oxford, **1994**

[5] Oparka KJ and Read ND, *Plant Cell Biology- A Practical Approach*, Harris N and Oparka KJ (Ed.), **IRL Press**, Oxford, **1994**

[6] Miller AJ, *Plant Cell Biology- A Practical Approach*, Harris N and Oparka KJ (Ed.), **IRL Press**, Oxford, **1994**

[7] van Steveninck RFM and van Steveninck ME, *Electron Microscopy of Plant Cells*, Hall JL and Hawes CR (Ed.), **Academic Press**, London, **1991**

[8] Harris N, *Plant Cell Biology- A Practical Approach*, Harris N and Oparka KJ (Ed.), **IRL Press**, Oxford, **1994**

[9] Verscht J, Kaluche B, Köhler J, Kockenberger W, Metzler A, Haase A, and Komor E, *Planta*, **1998**, 205, 139

[10] Whittal RM, Keller BO, and Li L, *Anal. Chem.*, **2003**, 70, 5344

[11] Edström JE, *Nature*, **1953**, 172, 809

[12] Smith JD and Markham R, *Biochem. J.*, **1950**, 46, 509

[13] Tomos AD, Hinde P, Richardson P, Pritchard J, and Fricke W, *Plant Cell Biology: A Practical Approach*, Harris N and Oparka KJ (Ed.), **IRL Press**, Oxford, **1994**

[14] Matioli GT and Niewisch HB, *Science*, **1965**, 150, 1824

[15] Matioli GT, Brody S, and Thorell B, *Acta Haematol.*, **1962**, 28, 73

[16] Kennedy RT, Oates MD, Cooper BR, Nickerson B, and Jorgenson JW, *Science*, **1989**, 246, 57

[17] Kennedy RT, St.Clair RL, White JG, and Jorgenson JW, *Mikrochim. Acta.*, **1987**, 2, 37

[18] Kennedy RT and Jorgenson JW, *Anal. Chem.*, **1989**, 61, 436

[19] Govindaraju K and Lloyd DK, *J. Chromatogr. B*, **2000**, 745, 127

[20] Swanek FD, Ferris SS, and Ewing AG, *Handbook of Capillary Electrophoresis*, Landers JP (Ed.), **CRC**, **1997**

[21] Olefirowicz TM and Ewing AG, *Chimia*, **1991**, 45, 106

[22] Olefirowicz TM and Ewing AG, *Anal. Chem.*, **1990**, 62, 1872

[23] Fuhr GR and Reichle C, *Micro Total Analysis Systems*, **2000**, 261

[24] Sims CE, Meredith GD, Krasieva TB, Berns MW, Tromberg BJ, and Allbritton NL, *Anal. Chem.*, **2003**, 70, 4570

[25] Wheeler AR, Morishima K, Arnold DW, Rossi AB, and Zare RN, *Micro Total Analysis Systems*, **2000**, 25

[26] Chiu DT, Hsiao A, Gaggar A, Garza-Lopez RA, Orwar O, and Zare RN, *Anal. Chem.*, **1997**, 69, 1801

[27] Xue Q and Yeung ES, *J. Chromatogr. B: Biomed. Appl.*, **1996**, 677, 233

[28] Shaner, LM and Brown, PR, *J. Cap. Electrophoresis*, **2000**, 23, 975

[29] Olefirowicz TM and Ewing AG, *Anal. Chem.*, **1990**, 51, 1872

[30] Olefirowicz TM and Ewing AG, *J. Neurosci. Methods*, **1990**, 34, 11

[31] Chiu DT, Lillard SJ, Scheller RH, Zare RN, Rodriguez-Cruz SE, Williams ER, Orwar O, Sandberg M, and Lundqvist JA, *Science*, **1998**, 279, 1190

[32] Govindaraju K and Lloyd DK, *J. Chromatogr. B*, **2000**, 745, 126

[33] Bazzanella A, Lochmann H, Tomos AD, and Bächmann K, *J. Chromatogr. A*, **1998**, 809, 231

[34] Bächmann K, Lochmann H, and Bazzanella A, *Anal. Chem.*, **1998**, 645A

[35] Swanek FD, Chen G, and Ewing AG, *Anal. Chem.*, **1996**, 68, 3912

[36] Zhang Z, Krylov S, Arriaga EA, Polakowski R, and Dovichi NJ, *Anal. Chem.*, **2000**, 72, 318

[37] Gilman SD and Ewing AG, *Anal. Chem.*, **2003**, 67, 58

[38] Chen S and Lillard SJ, *Anal. Chem.*, **2003**, 73, 111

[39] Tong W and Yeung ES, *J. Chromatogr. B*, **1996**, 685, 35

[40] Hofstadler SA, Swanek, FD, Gale, DC, Ewing AG, and Smith, RD, *Anal. Chem.*, **15-4-1995**, 67, 1477

[41] Li L, Garden RW, and Sweedler JV, *TIBTECH*, **2003**, 18, 151

[42] Lynn EC, Chung MS, Tsai WC, Hann CC, *Rapid Commun. Mass Spectrom.*, **2003**, 2022

[43] Holland RD, Williams ER, Rafii F, Sutherland JB, Persons CC, Voorhes KJ, and Lay JO Jr, *Rapid Commun. Mass Spectrom.*, **1996**, 10, 1227

[44] Krishnamurthy T and Ross PL, *Rapid Commun. Mass Spectrom.*, **1996**, 10, 1992

[45] Arnold RJ and Reilley JP, *Rapid Commun. Mass Spectrom.*, **1998**, 12, 630

[46] Krishnamurthy T, Ross PL, and Rajamani U, *Rapid Commun. Mass Spectrom.*, **1996**, 10, 883

[47] Haag AM, Taylor SN, Johnston KH, and Cole RB, *J. Mass Spectrom.*, **1998**, 33, 750

[48] Chong BE, Lubman DM, Miller FR, and Rosenspire A, *Rapid Commun. Mass Spectrom.*, **1999**, 13, 1808

[49] Caprioli RM, Farmer TB, and Gile J, *Anal. Chem.*, **1997**, 69, 4751

[50] Further information available at **www.cellpix.com** (12-5-2003)

[51] Garden RW, Moroz LL, Moroz TP, Shippy SA, and Sweedler JV, *J. Mass Spectrom.*, **1996**, 31, 1130

[52] Garden RW, Shippy SA, Li L, Moroz TP, and Sweedler JV, *Proc. Natl. Acad. Sci. USA*, **1998**, 95, 3972

[53] Floyd PD, Li L, Rubakhin SS, Sweedler JV, Horn CC, Kupfermann I, Alexeeva VY, Ellis TA, Dembrow NC, Weiss KR, and Vilim FS, *J. Neurosci.*, **1999**, 19, 7732

[54] van Strien FJC, Jespersen S, van der Greef J, Jenks BG., and Roubos EW, *FEBS Lett.*, **1996**, 379, 165

[55] Jespersen S, Malagon MM, van Strien FJ, Jespersen S, van der Greef J, Roubos EW, and Gracia-Navarro F, *Anal. Chem.*, **1999**, 71, 660

[56] Chaurand P, Stoeckli M, and Caprioli RM, *Anal. Chem.*, **1999**, 71, 5263

[57] Bergquist J, *Chromatographia*, **1999**, 49, S41

[58] Page JS, Rubakhin SS, and Sweedler JV, *Anal. Chem.*, **2002**, 74, 497

[59] Kennedy RT, Oates MD, Cooper BR, Nickerson B, and Jorgenson JW, *Science*, **1989**, 246, 57

[60] Wallingford RA and Ewing AG, *Anal. Chem.*, **1988**, 60, 1972

[61] Kristensen HK, Lau YY, and Ewing AG, *J. Neurosci. Methods*, **1994**, 51, 183

[62] Further information available at **http://www.mc.vanderbilt.edu/histo/blood/erythrocytes.html** (1995)

[63] Hogan BL and Yeung ES, *Anal. Chem.*, **1992**, 64, 2841

[64] Honda S, Naitoh-Ohta Y, Togashi, K, and Taga A, *Anal. Sci.*, **1997**, 13, 557

[65] Kristensen HK, Lau YY, and Ewing AG, *J. Neurosci. Methods*, **1984**, 51, 183

[66] Lochmann H, Bazzanella A, and Bächmann K, *J. Chromatogr. A*, **1998**, 817, 337

[67] Tagliaro F, Manetto G, Crivellente, and Smith FP, *Forensic Sci. Int.*, **1998**, 92, 75

[68] Michaelis L, *Biochem. Zeit.*, **1909**, 16, 81

[69] Gaal O, Medgyesi GA, and Verecykey L, *Electrophoresis in the Separation of Biological Macromolecules*, (Ed.), **Wiley-Interscience**, Chichester, **1980**

[70] Sargent JR and George SG, *Methods in Zone Electrophoresis*, (Ed.), **BDH**, Poole, **2003**

[71] Weiland T and Fischer E, *Naturwiss*, **1950**, 37, 25

[72] Synge RLM, *Biochem. J.*, **1950**, 46, xli

[73] Condsen R, Gordon AM, and Martin AJP, *Biochem. J.*, **1946**, 40, 29

[74] Jorgenson JW and Lukacs KD, *Anal. Chem.*, **1981**, 53, 1298

[75] Jorgenson JW and Lukacs KD, *Science*, **1983**, 222, 266

[76] PhD Thesis, Grant IH, University of Edinburgh, **1990**.

[77] Shaw, *Colloid and Surface Chemistry*, (Ed.), **Butterworth-Heinmann**, Oxford, **1992**

[78] Kosmulski M, Hartikainen R, Maczka E, Janusz W, and Rosenholm JB, *Anal. Chem.*, **2002**, 74, 253

[79] Gouy M, *J. Phys.*, **1910**, 9, 457

[80] Chapman DL, *Phil. Mag.*, **1913**, 25, 475

[81] Stern O, *Zeit. Elektrochem. Angew. Phys. Chem.*, **1924**, 30 , 508

[82] Rice CL and Whitehead R, *J. Phys. Chem.*, **1965**, 69, 4017

[83] Knox JH and Grant IH, *Chromatographia*, **1987**, 24, 135

[84] Knox JH, *Chromatographia*, **1988**, 26, 329

[85] Grushka E, Snyder LR, and Knox JH, *J. Chromatogr.*, **1975**, 13, 25

[86] Grushka E, *Anal. Chem.*, **1970**, 42, 1142

[87] Martin AJP and Synge RLM, *Biochem. J.*, **1941**, 35, 1358

[88] Giddings JC, *Sep. Sci.*, **1969**, 4, 181

[89] Further information available at **http://gc.discussing.info/gs/b_theory/column_efficiency.html#TheoreticalPlates** (3-6-2003)

[90] Burgi DS and Chein RL, *Anal. Chem.*, **1991**, 2042

[91] Further information available at **http://www.chem.vt.edu/chem-ed/sep/theory/resolut1.html** (3-6-2003)

[92] Nogare SD and Chiu J, *Anal. Chem.*, **1962**, 34, 890

[93] Hieftje G, *Anal. Chem.*, **2000**, 309

[94] Abian J, *J. Mass Spectrom.* , **1999**, 34, 157

[95] Mcfadden WH, *J. Chromatogr. Sci.*, **1979**, 17, 2

[96] Barber M, Bordoli RS, Sedgewick RD, and Tyler AN, *J. Chem. Soc. Commun.*, **1981**, 325

[97] Chapman JR, *Practical Organic Mass Spectrometry- A Guide for Chemical and Biochemical Analysis*, Chapman JR (Ed.), **John Wiley and Sons Ltd.**, Chichester, **1993**

[98] Ito Y, Takeuchi T, Ishii D, and Goto M, *J. Chromatogr.*, **1985**, 346, 161

[99] Caprioli RM, Fan T, and Cotterell JS, *Anal. Chem.*, **1986**, 58, 2949

[100] Caprioli RM, *Anal. Chem.*, **1990**, 62, 477A

[101] Dole M, Mack LL, Hines RL, Moberly RC, Ferguson LD, and Alice MB, *J. Chem. Phys.*, **1968**, 49, 2240

[102] Yamashita M and Fenn JB, *J. Phys. Chem.*, **1984**, 71, 4451

[103] Yamashita M and Fenn JB, *J. Phys. Chem.*, **1984**, 88, 4671

[104] Further information available at **www.newobjectives.com** (2003)

[105] Gaskell SJ, *J. Mass Spectrom.*, **1997**, 32, 677

[106] Cole RB, *J. Mass Spectrom.*, **2000**, 35, 763

[107] Dole M, Hines RL, Mack LL, Mobley LD, Ferguson LD, and Alice MB, *Macromol*, **1968** , 1, 96

[108] Dole M, Mack LL, Hines RL, Mobley LD, Ferguson LD, and Alice MB, *J. Chem. Phys.*, **1968**, 49, 2240

[109] Rollgen FW, Bramer-Wagner E, and Buttering L, *J. Phys. Colloq.*, **1984**, 45, C9

[110] Iribarne JV and Thomson BA, *J. Chem. Phys.*, **1976**, 64, 2287

[111] Siu KWM, Guevremont R, Le Blanc JC, O'Brien RT, and Berman SS, *Org. Mass Spectrom.*, **1993**, 28, 579

[112] Gamero-Catano M and de la Mora JF, *Anal. Chimica Acta*, **2000**, 406, 67

[113] Wilm MS and Mann M, *Int. J. Mass Spectrom. Ion Proc.*, **1994**, 136, 167

[114] Juraschek R, Dülcks T, and Karas M, *J. Am. Soc. Mass Spectrom.*, **1999**, 10, 300

[115] Hager DB, Dovichi NJ, Klassen J, and Kebarle P, *Anal. Chem.*, **1994**, 66, 3944

[116] Wollnik, H, *J. Mass Spectrom.*, **1999**, 34, 991

[117] March RE, *J. Mass Spectrom.*, **1997**, 32, 351

[118] Further information available at **http://www.lcgceurope.com/lcgceurope/data/articlestandard/lcgceurope/052002/8133/article.pdf** (21-7-2003)

[119] Wiley WC and McLaren IH, *Rev. Sci. Instr.*, **1955**, 26, 1150

[120] PhD Thesis, Simpson DC, University of Edinburgh, **2002**.

[121] Chernushevich IV, Ens W, and Standing KG, *Anal. Chem.*, **1999**, 71, A452

[122] Cotter RJ, *Anal. Chem.*, **1992**, 64, A1027

[123] Mamyrin BA, Karataev VI, Shmikk DV, and Zagulin VA, *Sov. Phys. Jetp.*, **1973**, 37, 45

[124] Further information available at **http://www.waters.com/WatersDivision/pdfs%5Cms%20primer.pdf?ref=JDRS-5LTGBX** (21-7-0003)

[125] Guilhaus M, Selby D, and Mlynski V, *Mass Spectrom. Rev.*, **2000**, 19, 65

[126] Liu, Hongbin, Lin, Dayin, and Yates, *Biotechniques*, **2002**, 32, 898

[127] Le Catelier HL, *Annales des Mines*, **1888**, 13, 157

[128] Further information available at **www.nikon.com** (29-5-0003)

[129] Further information available at **www.jvc.com** (29-5-2003)

[130] Further information available at **www.sony.com** (29-5-2003)

[131] Further information available at **www.adobe.com** (29-5-2003)

[132] Lin P and Clarke HJ, *Mol. Reprod. Dev.*, **1966**, 44, 185

[133] Metka M, Haromy T, and Huber J, *Gynakol. Rundsch.*, **1985**, 25, 96

[134] Ng SC, Ratnam SS, Bongso A, Goh HH, Wong PC, Chan LK, Hagglund L, and Hamilton M, *Ann. Acad. Med. Singapore*, **1988**, 17, 607

[135] Further information available at **www.narishige.co.jp** (29-5-2003)

[136] Knoblauch M, Hibberd JM, Julian M, Gray JC, van Bel AJE, and Aart JE, *Nat. Biotechnol.*, **1999**, 17, 906

[137] PhD Thesis, Goodwin RJA, University of Edinburgh, **to be submitted**.

[138] Further information available at **www.wpi-europe.com** (29-6-2003)

[139] Tomos AD, *Biotechnol. Lett.*, **2000**, 22, 437

[140] Blackstock, WP. and Weir, MP., *TIBTECH*, **1999**, 17, 121

[141] Green PB, *Plant Physiol.*, **1968**, 43, 1169

[142] Zimmermann U and Steudle E, *Adv. Bot. Res.*, **1978**, 6, 45

[143] Malone M, Leigh RA, and Tomos AD, *Plant Cell Environ.*, **1989**, 12, 919

[144] Tomos AD and Leigh RA, *Annu. Rev. Plant Physiol. Plant Mol. Biol.*, **1999**, 50, 447

[145] Further information available at **www.sge.com** (29-5-2003)

[146] Further information available at **www.druck.com** (29-5-2003)

[147] Ling G and Gerard RW, *J. Cell. Comp. Physiol*, **1949**, 34, 383

[148] Brown KT and Flaming DG, *Neuroscience*, **1977**, 2, 813

[149] Lux D, *Z. Zellforsch. Mikrosk. Anat.*, **1960**, 143, 451

[150] Further information available at **www.sutter.com** (1-6-2003)

[151] Tsuda T, Sweedler JV, and Zare RN, *Anal. Chem.*, **1990**, 62, 2149

[152] Cifuentes A and Poppe H, *Electrophoresis*, **1995**, 16, 2051

[153] Michalske TA and Freiman SW, *Nature*, **1982**, 295, 511

[154] Baeuml F and Welsch T, *J. Chromatogr. A*, **2002**, 961, 35

[155] Further information available at **http://www.crystran.co.uk/sio2data.htm, http://sgquarts.com/downloads/fused%20Quarts%20&%20Fused%20Silica%20Data%20Sheet.pdf** (12-4-2003)

[156] Landers JP, *Handbook of Capillary Electrophoresis*, **CRC**, London, **199**

[157] Severs JC and Smith RD, *Electrospray Ionisation Mass Spectrometry: Capillary Electrophorsis Electrospray Ionisation Mass Spectrometry*, (Ed.), **Wiley**, New York, **1997**

[158] Cai J and Henion J, *J. Chromatogr.*, **1995**, 703, 667

[159] Olivares JA, Nguyen NT, Yonker CR, Clement R, and Smith RD, *Anal. Chem.*, **1988**, 59, 1230

[160] Wahl JH, Goodlett DR, Udseth HR, and Smith RD, *Anal. Chem.*, **1992**, 64, 3194

[161] Further information available at **http://www.micromass.co.uk** (2003)

[162] Deacon JW, *Modern Mycology*, **Blackwell Science**, London, **1997**

[163] Read ND, *Shape and Form in Plants and Fungi*, **Academic Press**, London, **1994**

[164] Wessels JGH and Meinhardt F, *The Mycota. I. Growth, Differentiation and Sexuality*, **Springer-Verlag**, Berlin, **1994**

[165] Read ND, *Linnean Society Symposium Series,* **Academic Press**, London, **1994**

[166] Beadle G and Tatum E, *Proc. Natl. Acad. Sci. USA*, **2003**, 27, 499

[167] Horowitz NH, *Ann. N Y Acad. Sci.*, **1991**, 325, 252

[168] Perkins DD and Davis RH, *Fungal Genet. Biol.*, **2000**, 3, 153

[169] Galagan JE, Calvo SE, Borkovich KA, Selker EU, Read ND, Jaffe D, FitzHugh W, and Birren B, *Nature*, **2003**, 422, 859

[170] Woronin M, *Abh. Senkenbo. Naturforsch.*, **1864**, 5, 333

[171] Markham R and Collinge AJ, *FEMS Microbiol. Rev.*, **1987**, 46, 1

[172] Garrison RG, Lane JW, and Field MF, *J. Bacteriol.*, **1970**, 101, 628

[173] Colling AJ and Markham P, *Exp. Mycol.*, **1985**, 9, 80

[174] Bazzanella, A, Lochmann, H, Tomos AD, and Bachmann, K, *J. Chromatogr. A*, **1998**, 809, 231

[175] Markham P and Collinge AJ, *FEMS Microbiol. Rev.*, **1987**, 46, 1

[176] Hoch HC and Maxwell DP, *Can. J. Microbiol.*, **1974**, 20, 1029

[177] Tenney K, Hunt I, Sweigard J, Pounder JI, McClain C, Bowman EJ, and Bowman BJ, *Fungal Genet. Biol.*, **2000**, 31, 205

[178] Jedd G and Chua NH, *Nature Cell Biol.*, **2000**, 2, 226

[179] Bartnicki-Garcia S and Lippman E, *J. Gen. Microbiol.*, **1972**, 73, 487

[180] Davis RH, *Neurospora*, **2003**

[181] Hill EP and Sussnman AS, *J. Bacteriol.*, **1964**, 88, 1556

[182] Marzluf GA and Matzenberg RL, *Arch. Biochem. Biophys.*, **1967**, 120, 487

[183] Davis RH, *Neurospora crassa and Saccharomyces cerevisiae. Microbiol. Revs.*, **1986**, 50, 280

[184] Elbein AD, *Adv. Carbohydr. Chem. Biochem.*, **1974**, 30, 327

[185] Hottinger T, De Virgilio C, Hall MN, Boller, and Weimken A, *Eur. J. Biochem.*, **1994**, 219, 193

[186] Attfield PV, *Nat. Biotechnol.*, **1997**, 15, 1351

[187] Nwaka S and Holzer H, *Prog. Nucleic Acid Res. Mol. Biol. .*, **1998**, 58, 197

[188] Killick KA, *Carbohydr. Res.*, **1980**, 82, 1

[189] Sweeley CC, Bentley R, Makita M, and Wells WW, *J. Am. Chem. Soc.*, **1963**, 85, 2497

[190] Cabib E and Leloir BE, *J. Biol. Chem.*, **1958**, 231, 259

[191] Neves MJ, Jorge JA, Francois JM, and Terenzi HF, *FEBS*, **1991**, 283, 19

[192] Hanks DL and Sussman AS, *Am. J. Bot.*, **1969**, 56, 1152

[193] Thevein JM, *Microbiol. Rev.*, **1984**, 48, 42

[194] Panek AD, *J. Biotechnol.*, **1985**, 3, 121

[195] Sargent D and Wright BE, *J. Biol. Chem.*, **1971**, 246, 5340

[196] Yeung ES, *J. Chromatogr. A*, **1999**, 830, 243

[197] Further information available at **http://www.probes.com** (2003)

[198] Ferguson IA, Xian C, Barati E, and Rush RA, *J. Neurosci. Methods*, **2001**, 109, 81

[199] Schmued L, Kyriakidis K, and Heimer L, *Brain Res.*, **1990**, 526, 127

[200] Dose EV and Guiochon G, *Anal. Chem.*, **1992**, 64, 123

[201] Clough JM, Anthony VM, de Fraine PJ, Fraser TEM, Godfrey CRA, Godwin JR, and Youle D, *Eighth International Congress of Pesticide Chemistry: Options 2000*, **1999**, 59

[202] Clough JM and Godfrey CRA, *Fungicidal Activity*, Hutson, DH and Miyamoto, J (Ed.), **John Wiley: London**, **1998**

[203] Baldwin BC., Clough JM, Godfrey CRA, Godwin JR., and Wiggins TE., *Modern Fungicides and Antifungal Compounds*, **1996**, 105

[204] Clough JM, *Nat. Prod. Reports*, **1993**, 10, 565

[205] Further information available at **http://www.cas.muohio.edu/~wilsonkg/Bot203/mitochondria/diagram/diagram.htm** (30-6-2003)

[206] Brant U, Schagger H, and van Jagow G, *Eur. J. Biochem.*, **1988**, 173, 499

[207] Heaney SP, Hall AA, Davies SA, and Olaya G, *Resistance of Fungicides in QolSTAR Cross-Resistance Group: current Perspectives*, **2000**

[208] Tomlin CDS, *The Pesticide Manual*, **BCPC**, UK, **2000**

[209] Jennings DH, *The Physiology of Fungal Nutrition*, **Cambridge University Press**, Cambridge, **1995**

[210] Burgstaller W, *Crit. Rev. Microbiol.*, **1997**, 23, 1

[211] Serrano R, *Genome Dynamics, Protein Synthesis, and Energetics*, **Cold Spring Harbour Laboratory press**, New York, **1991**

[212] West IC, *The Biochemistry of Membrane Transport*, **Chapman and Hall**, London, **1983**

[213] PhD Thesis, Swift S, University of Edinburgh, **to be submitted.**

[214] Butcher CPG, Dyson PJ, Johnson BFG, Langridge-Smith PRR, McIndoe JS, and Whyte C, *Rapid Commun. Mass Spectrom.*, **2002**, 16, 1595

[215] Further information available at **http://www.microdrop.de** (30-6-2003)

[216] Hardman M and Makarov AA, *Anal. Chem.*, **2003**, 75, 1699

[217] Makarov AA, *Anal. Chem.*, **2000**, 75, 1156

[218] Kingdom KH, *Phys. Rev.*, **1923**, 21, 408

[219] Further information available at **http://www.ni.com** (2003)

[220] Marshall AG, Hendrickson CL, and Jackson GS, *Mass Spectrom. Rev.*, **1998**, 17, 1

[221] Rayleigh L, *Phil. Mag.*, **1882**, 14, 184

[222] Feng X and Agnes GR, *J. Am. Soc. Mass Spectrom.*, **2000**, 11, 393

[223] Feng X, Bogan MJ, and Agnes GR, *Anal. Chem.*, **2001**, 73, 4499

[224] Taflin DC, Ward TL, and Davis EJ, *Langmuir*, **1989**, 5, 376

[225] Davies CN, *Evaporation of Airborne Droplets*, **Wiley**, New York, **1978**

[226] Further information available at **http://www.sisweb.com** (2003)

## Appendix: courses and conferences

### External conferences and meetings attended

*24th Annual Meeting of the British Mass Spectrometry Society*, University of Reading, 12th - 15th September 1999

*MicroTAS 2000*, Enschede, Netherlands, 14th - 18th May 2000.

*15th International Mass Spectrometry Conference*, Palacio de Congresos, Fira de Barcelona, Spain, 27th August - 1st September 2000

*Pharmaceutical Analysis- Lab on a Chip (Part of the 2000 British Pharmaceutical Conference and held in conjunction with the Joint Pharmaceutical Analysis Group)*, International Convention Center, Birmingham, 11th September 2000.

*The Miniaturisation Revolution- Second British Mass Spectrometry Society Meeting on Miniaturisation- Current and Future Trends in Miniaturised Sample Handling, Separation and Detection Strategies*, SmithKline Beecham Pharmaceutical, Harlow, 13th September 2000.

*14th Sanibel Conference on Mass Spectrometry, Front-End Sample Handling Technologies for Analyses by Mass Spectrometry*, Sundial Beach & Tennis Resort, Sanibel Island, Florida, 25th - 29th January 2002

*4th North American FT-ICR Conference*, Marconi Conference Center, Marshall, California, USA, 3rd - 6th April 2003

## Courses attended

In accordance with the regulations of the School of Chemistry, University of Edinburgh, I have attended the following courses during my period of study:

*Mass Spectrometry* (Lecture Course), Autumn Term 2000; 5 hours in duration as 1 hour lectures.

*Light Microscopy* (Lecture Course), Summer Term 2002; 24 hours in duration as 3 day lectures.

Furthermore, I have attended and participated in Physical Section colloquia and informal meetings, both in Edinburgh and at Firbush Point Field Center, Loch Tay. I have also, in addition, attended and arranged regular group meetings and coordinated two successful study weekends held at Gairloch and Fort William.